IRE
Transactions
on Microwave Theory and Techniques

Volume MTT-6 **JULY, 1958** Number 3

In This Issue

For complete Table of Contents, see page 247.

PUBLISHED BY THE
Professional Group on Microwave Theory and Techniques

IRE PROFESSIONAL GROUP ON MICROWAVE THEORY AND TECHNIQUES

The Professional Group on Microwave Theory and Techniques is an association of IRE members with professional interest in the field of Microwave Theory and Techniques. All IRE members are eligible for membership and will receive all Group publications upon payment of the prescribed annual fee of $3.00. Members of the American Physical Society and the Institution of Electrical Engineers of Great Britain may become affiliated with PGMTT and receive all Group publications upon payment of the Affiliate fee of $7.50 per year.

IRE TRANSACTIONS®

on Microwave Theory and Techniques

Published by the Institute of Radio Engineers, Inc., for the Professional Group on Microwave Theory and Techniques, at 1 East 79th Street, New York 21, New York. Responsibility for the contents rests upon the authors, and not upon the IRE, the Group, or its members. Price per copy: IRE PGMTT members, $2.00; IRE members, $3.00, nonmembers, $6.00. Annual subscription price: IRE members, $8.50; colleges and public libraries, $12.75; nonmembers, $17.00.

Address all manuscripts to K. Tomiyasu, PGMTT Editor, General Electric Microwave Laboratory, 601 California Ave., Palo Alto, Calif. Submission of three copies of manuscripts, including figures, will expedite the review.

IRE Transactions on Microwave Theory and Techniques

Volume MTT-6 JULY, 1958 Number 3

TABLE OF CONTENTS

Message from the Editor

Beginning with this issue, the members of the Editorial Board of the IRE TRANSACTIONS ON MICROWAVE THEORY AND TECHNIQUES will be listed on the Table of Contents page. Since last October our Editorial Board has been increased and the new members who have generously accepted these responsibilities are the following:

John C. Cacheris
Robert E. Collin
H. Heffner
Peter D. Lacy
Theodore Moreno
John M. Richardson
Richard F. Schwartz
Peter D. Strum
Eric Strumwasser
Romayne F. Whitmer
F. K. Willenbrock

—K. TOMIYASU

Lan Jen Chu

Lan Jen Chu was born on August 24, 1913 in Hweiying, Kiangsu, China. He graduated from Chiao Tung University, Shanghai, China with the B.S. degree in electrical power in 1934. He received the S.M. degree in 1935 and the Sc.D. in electrical engineering from M.I.T. in 1938.

Dr. Chu served as a consultant to the Radiation Laboratory and the Radio Research Laboratory on various electromagnetic problems. He joined the staff of the Radiation Laboratory of M.I.T. in 1942 and during the last years of the war he supervised research and design of many special antennas for radar and communication applications. In 1945 he served as an expert consultant to the Secretary of War and was sent to China to head the Advisory Specialist Group to the U. S. Armed Forces in China. In 1948 he received the Certificate of Merit for his accomplishments during World War II.

Dr. Chu is Professor of electrical engineering at the Massachusetts Institute of Technology and a staff member of the Research Laboratory of Electronics. He is a member of Sigma Xi and a Fellow of the Institute of Radio Engineers and the American Physical Society.

Education for Electrical Engineering

LAN JEN CHU†

Thirty years ago an underduate program in electrical engineering consisted chiefly of studying the design and operation of the electrical devices—then relatively few—that were in use at the time. The program included subjects on generators, motors, transmission systems, telephone and telegraph systems, radio, and electric batteries. An average graduate was considered to be adequately equipped to serve society in the entire electrical field. Whenever a new invention was reduced to practical use another subject was merely added to the curriculum. When the curriculum became too crowded for a student to finish it in four years, the concept of options was introduced. Under that concept the undergraduate specialized in one branch of electrical engineering. At graduation he was equipped to serve society in his own field, but was usually not well informed in other fields. He had a tendency to shy away from the other branches of electrical engineering. In more recent years there have been proposals to subdivide undergraduate options into even finer structures in an attempt to supply the needs of vastly diversified electrical industries.

Is this a wise move for the future of engineering education? The danger of the trend to further subdivision lies in the inevitable degeneration of engineering education into vocational training of highly specialized technicians. In a rapidly expanding and changing industry, the rate of obsolescence of specialization is rather high. An educational program of specialization is destined to be short-lived. The effects on both the faculty and the graduate will be undesirable, if not detrimental.

In the Department of Electrical Engineering at the Massachusetts Institute of Technology, under the leadership of Dr. Gordon S. Brown, we are experimenting with a curriculum based upon a different concept of electrical engineering for the undergraduate. In the complex electrical engineering industry we recognize that education for a qualified engineer is a continuing process that extends far beyond graduation. There are formal opportunities in the graduate schools of universities and in advanced industrial training programs. (For specialization, perhaps there is no better way than to work with the industries, where the demands and environment for such specialization exist.) The role of undergraduate electrical engineering education is, we believe, to provide the foundation and discipline necessary for advanced study and specialization in postgraduate years. It has been traditional to emphasize design and operation of devices. Principles and techniques have been introduced only to the extent that the problems required. Our new curriculum puts the primary emphasis on the principles and techniques that make the present devices possible and that will be needed in the future development of the electrical industries. Devices are treated only as illustrations of the principles and techniques.

Nowadays, there are a few terms that are important in almost every subject of electrical engineering. These are time, space, frequency, signal, energy, force, order and disorder, structure, and material. On a sound foundation of the physical sciences and the humanities, we are building a series of courses that deal with the roles and the interplay of these terms in the engineering world. If we are to learn the design and operation of existing devices, we must have a thorough understanding of these terms. Devices will become obsolete. The fundamental principles and techniques that govern them will be more enduring.

Our program has been in operation for several years. It is still too early to make a fair appraisal of the results from the students' point of view. The impact on the faculty has been astounding and gratifying. The revised program is providing us with an opportunity to re-educate ourselves in the fundamentals of electrical engineering. It is helping us to initiate new research which in the past we have left to the physicists. Perhaps it will influence our graduates in the same way. They will then be better equipped to meet the challenge of our ever-changing and expanding profession.

† Dept. Elec. Eng. and Res. Lab. of Electronics, Mass. Inst. Tech., Cambridge 39, Mass.

Report of Advances in Microwave Theory and Techniques—1957*

ROBERT E. BEAM†

THIS report is devoted to advances in theory, experiment, and application of microwave sources, amplifiers, circuits and circuit elements, transmission lines, and detectors. The radiation, propagation, and reception of microwaves are mentioned only indirectly. An attempt is made to provide coverage of foreign as well as domestic advances.

Advances in 1957 continue to be dominated by extensions in the use of gyromagnetic media. Recent developments include the ferromagnetic amplifier and various nonlinear devices. Much attention has been given to such devices as the nonreciprocal phase shifter, the resonance isolator, the field displacement isolator, and circulators which depend upon the Faraday rotation phenomenon. This attention has been directed towards increasing the operation power level of the devices and the operating bandwidth. Ferrites with narrow resonance line widths are needed for both linear and nonlinear devices.

Sources of microwave energy continue to receive considerable study. Advances in this area include extensions in the use of direct stimulation of radiation emission from uncharged matter for amplifiers and sources of microwave energy. Three and four-level solid-state masers appear to be especially noteworthy because they amplify in a continuous manner and because their high permissible spin concentration leads to large gain-bandwidth products. Extensions of traveling-wave-type tubes in various ways, however, have dominated the activity in the realm of microwave sources. The introduction of a crossed-field type of amplifier or oscillator which utilizes a reentrant electron flow and a non-reentrant and nonresonant interaction circuit is noteworthy.

Transmission lines *per se* continue to be important. Activity seems to be dominated by such needs as wider operating bandwidths, higher power handling capabilities, lower attenuation, and miniature size, and by more esoteric considerations of a military or an application nature. Strip and planar transmission lines have continued to be of interest because of their compactness and broad-band transmission characteristics. Interest in large, circular hollow pipes as transmission lines of low attenuation has been sustained. Much of the interest is in maintaining purity of the TE_{01} mode and elimination or control of coupling of this mode with other TE modes and with the TM_{11} mode in curved sections and serpentine bends. Surface waveguides and miscellaneous types of uniform and nonuniform lines or waveguides account for much activity in tota. Foreign interest in surface waveguides appears to be greater than domestic.

Almost all phases of microwave theory and techniques have advanced. In most phases, the advances have been in the nature of refinements and extensions of developments of the past.

The individual work on the subjects mentioned above is listed in three sections: I. Sources and Detectors, II. Transmission Lines, and III. Measurements. Ferrite and other microwave component developments are listed under the various headings.

I. Sources and Detectors

The portion of the microwave spectrum which is usable is determined by the sources and detectors available. Sources continue to be the principal limitation. Activity in the field of sources of microwave energy has been great. Most of the well-established types have been improved, altered, extended, and combined in sundry ways. In addition, the direct interaction of electromagnetic energy with matter as a source of microwave energy is increasing in importance.

Much of the activity has been stimulated by practical needs for:

1) Higher output powers,
2) Wider tuning ranges,
3) Better frequency stability,
4) Higher operating frequencies,
5) Greater ease of tuning,
6) Higher signal-to-noise ratios,
7) Improved mechanical features from the operational and/or manufacturing point of view.

Molecular types of sources will be reviewed first because they are recent in origin. They are promising as sources with low noise levels.

Molecular Types

Microwave fields can interact with the molecules in uncharged matter. In such interactions the internal energy of molecules is directly converted into microwave energy. This conversion is induced by placing the molecules in a microwave field. The emission induced is phase-related to the inducing field.

One of the methods of inducing emission of internal molecular energy is by use of masers (microwave amplifiers by stimulated emission of radiation). Masers may

* Manuscript received by the PGMTT, April 16, 1958.
† Dept. of Elec. Eng., Northwestern University, Evanston, Ill.

be of a molecular-beam type in which a beam of ammonia molecules is separated into upper and lower energy-state beams by utilizing a quadratic Stark effect. If the upper energy beam is passed through an appropriate resonant cavity, the basis for a microwave amplifier of very narrow bandwidth results. By adequately increasing the beam density the power emitted by the molecules may exceed the losses in the walls and load. In this case oscillations build up until saturation effects produce equilibrium. As an oscillator, such a maser produces microwave energy of high spectral purity; as an amplifier, it yields a very narrow bandwidth.

The basic physical properties of molecular amplifiers and several types of amplifiers are described in the following paper which serves as an excellent general introduction to the subject:

[1] J. P. Wittke, "Molecular amplification and generation of microwaves," PROC. IRE, vol. 45, pp. 291–316; March, 1957.

Solids as well as gases may yield molecular amplification. Three- and four-level solid-state masers were proposed last year.

[2] N. Bloembergen, "Proposal for a new type solid state maser," *Phys. Rev.*, vol. 104, pp. 324–327; October, 1956.
[3] M. W. P. Strandberg, "Quantum mechanical amplifiers," PROC. IRE, vol. 45, pp. 92–93; January, 1957.
[4] A. Javan, "Theory of a three level maser," *Phys. Rev.*, vol. 106, pp. 1579–1589; September, 1957.
[5] W. V. Smith, "Microwave amplification by maser techniques," *IBM J. Res. Dev.*, vol. 1, pp. 232–238; July, 1957.
[6] G. Feher and H. E. D. Scovil, "Electron spin relaxation times in gadolinium ethyl sulphate," *Phys. Rev.*, vol. 105, pp. 760–762; January, 1957.
[7] H. E. D. Scovil, G. Feher, and H. Seidel, "Operation of a solid state maser," *Phys. Rev.*, vol. 105, pp. 762–763; January, 1957.
[8] H. Heffner, "The maximum efficiency of the solid-state maser," PROC. IRE, vol. 45, p. 1289; September, 1957.
[9] K. D. Bowers and W. B. Mims, "Three level maser without a magnetic field," paper presented at Conference on Electronic Tube Research, Berkeley, Calif.; June, 1957.
[10] P. F. Chester and D. I. Bolef, "Super-regenerative masers," PROC. IRE, vol. 45, pp. 1287–1289; September, 1957.

Under certain conditions of operation a three-level system appears to be closely related to a parametric-type amplifier. Parametric amplifiers utilize the negative resistance introduced into a circuit by a nonlinear reactance which is driven by a strong high-frequency field. Parametric amplifiers were treated theoretically.

[11] J. P. Wittke, "New approaches to the amplification of microwaves," *RCA Rev.*, vol. 18, pp. 441–457; December, 1957.
[12] S. Bloom and K. K. N. Chang, "Theory of parametric amplification using nonlinear reactances," *RCA Rev.*, vol. 18, pp. 578–593; December, 1957.
[13] B. Salzberg, "Masers and reactance amplifiers—basic power relations," PROC. IRE, vol. 45, pp. 1544–1545; November, 1957.
[14] M. T. Weiss, "Quantum derivation of energy relations analogous to those for nonlinear reactances," PROC. IRE, vol. 45, pp. 1012–1013; July, 1957.

Ferromagnetic amplifiers were proposed for the microwave range and were later operated at 4500 mc. Such amplifiers consist of a cavity which contains a ferrite sample and which can support two resonant modes. A local oscillator excites the cavity in one of the resonant modes and causes the magnetization of the ferrite to precess uniformly. This precession results in a time-varying coupling between the two modes. If the local oscillator frequency is equal to the sum of the resonant frequencies, the local oscillator power is converted through nonlinear effects to signal frequency power.

[15] H. Suhl, "Proposal for a ferromagnetic amplifier in the microwave range," *Phys. Rev.*, vol. 106, p. 384; April, 1957.
[16] M. T. Weiss, "A solid-state microwave amplifier and oscillator using ferrites," *Phys. Rev.*, vol. 107, p. 317; July, 1957.
[17] J. Itoh, "Proposal for a solid-state radio-frequency maser," *J. Phys. Soc. Japan*, vol. 12, p. 1053; September, 1957.

Interest in maser and parametric types of amplifiers initially stems from their promise as low noise devices. Noise figures as low as 1.0 db have been reported for masers. Their limitations include: low power-handling capability, narrow bandwidth, and tuning difficulties. It should be noted, however, that the solid-state microwave amplifiers can be expected to offer advantages with respect to power output, tunability, bandwidth, and simplicity when compared with gaseous types.

[18] J. P. Gordon and L. D. White, "Experimental determination of the noise figure of an ammonia maser," *Phys. Rev.*, vol. 107, p. 1728; September, 1957.
[19] R. V. Pound, "Spontaneous emission and noise figure of maser amplifiers," *Ann. Phys.*, vol. 1, pp. 24–32; April, 1957.
[20] M. W. P. Strandberg, "Inherent noise of quantum-mechanical amplifiers," *Phys. Rev.*, vol. 106, pp. 617–620; May, 1957.
[21] K. Shimoda, H. Takahasi, and C. H. Townes, "Fluctuations in amplification of quanta with application to maser amplifiers," *J. Phys. Soc. Japan*, vol. 12, pp. 686–700; June, 1957.
[22] L. E. Alsop, J. A. Giordmaine, C. H. Townes, and T. C. Wang, "Measurement of noise in a maser amplifier," *Phys. Rev.*, vol. 107, pp. 1450–1451; September, 1957.
[23] M. W. Muller, "Noise in a molecular amplifier," *Phys. Rev.*, vol. 106, pp. 8–12; April, 1957.
[24] A. E. Siegman, "Gain, bandwidth and noise in maser amplifiers," PROC. IRE, vol. 45, pp. 1737–1738; December, 1957.
[25] M. L. Stitch, "Maser characteristics for one and two iris cavities," 1957 IRE WESCON CONVENTION RECORD, pt. 3, pp. 175–181.

Work closely related to that on masers was reported.

[26] L. E. Norton, "Coherent spontaneous microwave emission by pulsed resonance excitation," IRE TRANS. ON MICROWAVE THEORY AND TECHNIQUES, vol. MTT-5, pp. 262–265; October, 1957.

Self-induced coherent emission was found to continue to 10 μsec after removal of a 1-μsec excitation pulse.

Related to the work on molecular amplifiers and oscillators is that on the use of ferrites for frequency multiplication, mixing, detection, and amplitude modulation. As an indication of the possibilities, if second-order effects are included in treating the behavior of the magnetic moments of unbalanced electron spins in ferromagnetic materials under the action of an RF field, the possibility of using ferrites to detect an amplitude-modulated microwave signal becomes apparent.

[27] D. Jaffe, J. C. Cacheris, and N. Karayianis, "Ferrite microwave detector," 1957 IRE NATIONAL CONVENTION RECORD, pt. 1, pp. 242–249.

When two microwave signals of different frequencies are applied to a magnetized ferrite in a waveguide, sum and difference frequencies are generated. The sum-frequency output has been found to be quite linear with respect to variations in signal or local oscillator power levels.

[28] P. H. Vartanian and E. N. Skomal, "Mixing in ferrites at microwave frequencies," 1957 IRE WESCON CONVENTION RECORD, pt. 1, pp. 52–57.

At high peak powers it has been concluded that frequency doubling in ferrites can be made more efficient than low-power doubling in crystals. The frequency conversion is sensitive to sample shape and dimensions as well as to position in the waveguide. Frequency multiplication, especially doubling, promises to be a practical means of generating high-frequency microwave power.

[29] J. L. Melchor, W. P. Ayres and P. H. Vartanian, "Microwave frequency doubling from 9 to 18 kmc in ferrites," PROC. IRE, vol. 45, pp. 643–646; May, 1957.
[30] H. Suhl, "The theory of ferromagnetic resonance at high signal powers," *J. Phys. Chem. Solids*, vol. 1, pp. 209–227; January, 1957.

By inserting a tube of ferrite of low saturation level over the center conductor of a coaxial cable, a high modulation percentage over an 8 per cent bandwidth at *L* band has been achieved by alternately biasing the ferrite into and away from gyromagnetic resonance.

[31] B. Vafiades and B. J. Duncan, "An L-band ferrite coaxial line modulator," 1957 IRE NATIONAL CONVENTION RECORD, pt. 1, pp. 235–241.

Microwave single-sideband modulators using ferrites have received further consideration.

[32] G. Kemanis, "On the Cotton-Mouton effect in ferrites," PROC. IRE, vol. 45, pp. 687–688; May, 1957.
[33] K. I. Khoury, "On the use of ferrites for microwave single-sideband modulators," PROC. IRE, vol. 45, p. 1418; October, 1957.

Gaseous discharges also show promise as sources and detectors. It has been found that in a microwave discharge, the frequencies contained in the output are integral multiples of the applied field frequency. The possibility of utilizing this new phenomenon for developing a high-power and high-efficiency frequency multiplier for the sub-millimeter-wave region has been discussed.

[34] M. Uenohara, M. Uenohara, T. Masutani, and K. Inada, "A new high-power frequency multiplier," PROC. IRE, vol. 45, pp. 1419–1420; October, 1957.

Other investigations of the effect of microwaves on gaseous conductors and of the spectral distribution of the thermal noise of such conductors were reported. Among the results reported were the effects of incident microwave power on the various parts of a hydrogen glow discharge. When incident on the positive column or upon the region adjacent to the cathode, the discharge current increased slightly. When incident on the Faraday dark space, a large decrease in discharge current was noted.

[35] B. J. Udelson, "Effect of microwave signals incident upon different regions of a dc hydrogen glow discharge," *J. Appl. Phys.*, vol. 28, pp. 380–381; March, 1957.
[36] B. J. Udelson, J. E. Creedon, and J. C. French, "Microwave measurements of the properties of a dc hydrogen discharge," *J. Appl. Phys.*, vol. 28, pp. 717–723; June, 1957.
[37] M. Bayet, J. L. Delcroix, and J. F. Denisse, "Theory of the interaction between two electromagnetic waves in an ionized gas," *Ann. Télécomm.*, vol. 12, pp. 140–141; May, 1957.
[38] S. M. Bergmann, "Spectral distribution of thermal noise in a gas discharge," IRE TRANS. ON MICROWAVE THEORY AND TECHNIQUES, vol. MTT-5, pp. 237–238; October, 1957.

Crystals as harmonic generators, mixers, and detectors continue to receive attention. The noise figures obtainable from low-noise mixer crystals approach fundamental theoretical limits. The desire for better noise figures has led to physical cooling of the mixer crystal.

[39] J. M. Richardson and R. B. Riley, "Performance of three-millimeter harmonic generators and crystal detectors," IRE TRANS. ON MICROWAVE THEORY AND TECHNIQUES, vol. MTT-5, pp. 131–135; April, 1957.
[40] A. C. Macpherson, "An analysis of the diode mixer consisting of nonlinear capacitance and conductance and ohmic spreading resistance," IRE TRANS. ON MICROWAVE THEORY AND TECHNIQUES, vol. MTT-5, pp. 43–51; January, 1957.
[41] J. M. Richardson and J. J. Faris, "Excess noise in microwave crystal diodes used as rectifiers and harmonic generators," IRE TRANS. ON MICROWAVE THEORY AND TECHNIQUES, vol. MTT-5, pp. 208–212; July, 1957.
[42] G. C. Messenger, "Cooling of microwave crystal mixers and antennas," IRE TRANS. ON MICROWAVE THEORY AND TECHNIQUES, vol. MTT-5, pp. 62–63; January, 1957.

Traveling-Wave Devices

Traveling-wave tubes are emerging from the laboratory to become elements of microwave systems. However, many improvements and refinements are desirable. Their great promise for practical application has caused studies of traveling-wave devices to dominate the activity in the field of microwave sources. The results of many such studies are frequently applicable, of course, to other types of microwave sources.

Traveling-wave tubes were reviewed from the point of view of the user and procedures in selecting the proper operating performance and circuit design most suited for his application were discussed.

[43] A. H. Nielsen and N. W. Hansen, "The selection and application of traveling wave tubes," 1957 IRE NATIONAL CONVENTION RECORD, pt. 3, pp. 49–56.

A new microwave repeater system which uses a traveling-wave tube for the combined purpose of power amplification and local oscillator action was developed. No automatic frequency control was required.

[44] H. Kurokawa, I. Someya, and M. Morita, "New microwave repeater system using a single traveling-wave tube as both amplifier and local oscillator," PROC. IRE, vol. 45, pp. 1604–1611; December, 1957.

One of the needed improvements for practical application of traveling-wave tubes is that of smaller size. A description was given of a 100-mw, all metal, *S*-band tube which had a minimum gain of 25 db, a weight of less than 3 pounds including solenoid, a maximum solenoid diameter of 2 inches, and a length under 1 foot.

[45] J. O. Bramick, "A light-weight, low-level traveling-wave tube for S-band," 1957 IRE NATIONAL CONVENTION RECORD, pt. 3, pp. 66–70.

Another metal tube of rugged design for use with a compact solenoid or with periodic focusing was described.

[46] R. McClure, "A high-gain traveling-wave tube for *X*-band," 1957 IRE WESCON CONVENTION RECORD, pt. 3, pp. 143–149.

Traveling-wave tubes as tunable oscillators with external feedback and as limiting amplifiers were studied.

[47] V. G. Price and C. T. Anderson, "*X*-band traveling wave tube feedback oscillator," 1957 IRE NATIONAL CONVENTION RECORD, pt. 3, pp. 57–65.
[48] F. B. Fank and G. Wade, "Traveling-wave tube limiters," IRE TRANS. ON ELECTRON DEVICES, vol. ED-4, pp. 148–152; April, 1957.

The power output of a one-watt tube was held constant with $\pm\frac{1}{2}$ db for a 20-db range of input power.

Power and gain considerations were of interest in the medium and high power class of traveling-wave tubes. A pulsed power output of 3 megawatts at an efficiency of 34 per cent was among the results reported.

[49] J. F. Gittins, N. H. Rock, and A. B. J. Sullivan, "An experimental high power pulsed travelling wave tube," *J. Electronics Control*, vol. 3, pp. 267–286; September, 1957.
[50] M. Chodorow and R. A. Craig, "Some new circuits for high-power traveling-wave tubes," PROC. IRE, vol. 45, pp. 1106–1118; August, 1957.
[51] C. W. Barnes, "Power and gain limitations of helix-type travelling wave tubes," *Vide*, vol. 12, pp. 43–48; January–February, 1957.
[52] P. K. Tien and J. E. Rowe, "The backward-traveling power in the high power traveling-wave amplifiers," PROC. IRE, vol. 45, pp. 87–88; January, 1957.
[53] J. L. Putz and G. C. Van Hoven, "Use of multiple helix circuits in 100-watt cw traveling wave amplifiers," 1957 IRE WESCON CONVENTION RECORD, pt. 3, pp. 138–142.
[54] L. W. Holmboe and M. Ettenberg, "Development of a medium power L-band traveling-wave amplifier," IRE TRANS. ON ELECTRON DEVICES, vol. ED-4, pp. 78–81; January, 1957.

Backward-wave amplifiers have a very narrow pass band characteristic which can be shifted over a wide range of frequencies by varying the beam voltage; hence these types of tubes may be used as electronically tunable band-pass amplifiers. Gain fluctuations are being minimized so that practical application of backward-wave amplifiers is feasible.

[55] M. R. Currie and D. C. Forster, "The gain bandwidth characteristics of backward-wave amplifiers," IRE TRANS. ON ELECTRON DEVICES, vol. ED-4, pp. 24–34; January, 1957.

As local oscillators, backward-wave oscillators show promise even at millimeter wavelengths.

[56] J. A. Noland and R. E. Lepic, "Backward-wave oscillators for the 17 to 41 kmc band," *Sylvania Technologist*, vol. 10, pp. 13–16; January, 1957.
[57] A. Karp, "Backward-wave oscillator experiments at 100 to 200 kilomegacycles," PROC. IRE, vol. 45, pp. 496–503; April, 1957.
[58] C. F. Hempstead and A. R. Strnad, "A versatile source of millimeter waves," *Bell Labs. Record*, vol. 35, pp. 241–245; July, 1957.
[59] F. L. Vernon, "The behavior of a backward-wave oscillator with external feedback," 1957 IRE NATIONAL CONVENTION RECORD, pt. 3, pp. 91–102.
[60] R. D. Weglein, "Backward-wave oscillator starting conditions," IRE TRANS. ON ELECTRON DEVICES, vol. ED-4, pp. 177–179; April, 1957.
[61] H. R. Johnson and R. D. Weglein, "Backward-wave oscillators for the 8000–18,000-megacycle band," IRE TRANS. ON ELECTRON DEVICES, vol. ED-4, pp. 180–184; April, 1957.
[62] R. Olivier, "Use of an O-type carcinotron as a uhf generator for wide-band measurements," *Onde Élect.*, vol. 36, pp. 992–996; November, 1956.
[63] P. Palluel, "Experimental study of the characteristics of O-carcinotrons with interdigital lines," *Onde Élect.*, vol. 36, pp. 962–965; November, 1956.

For frequencies below 500 mc, a major design problem is that of obtaining a tube of reasonably small size. Hollow electron beams were used in preference to solid beams for uhf tubes because the size of the tube can be reduced by permitting operation at a lower voltage and greater gain per wavelength for a specified beam power.

[64] D. A. Dunn, "Traveling-wave amplifiers and backward-wave oscillators for uhf," IRE TRANS. ON ELECTRON DEVICES, vol. ED-4, pp. 246–264; July, 1957.

Microwave frequency mixing and frequency division have been accomplished in traveling-wave tubes by employing the nonlinearities of an overmodulated beam. Frequency conversion to microwave intermediate frequencies as well as to frequencies as low as 30 mc with conversion gains as high as 30 db were attained.

[65] R. W. DeGrasse, D. A. Dunn, R. W. Grow, and G. Wade, "Microwave frequency mixing and frequency division with beam-type tubes," 1957 IRE WESCON CONVENTION RECORD, pt. 3, pp. 163–168.
[66] R. W. DeGrasse and G. Wade, "Microwave mixing and frequency dividing," PROC. IRE, vol. 45, pp. 1013–1015; July, 1957.

A traveling-wave tube which employs two helices in cascade to produce frequency multiplication as high as forty was described. Output powers in the range of 20 to 100 mw for beam powers of 2 to 4 watts at output frequencies between 2 and 4 kmc were obtained.

[67] D. J. Bates and E. L. Ginzton, "A traveling-wave frequency multiplier," PROC. IRE, vol. 45, pp. 938–944; July, 1957.
[68] G. Mourier, "Contribution to the large-signal theory of traveling-wave tubes," *Onde Élect.*, vol. 36, pp. 929–936; November, 1956.

Crossed-field devices such as the traveling-wave magnetrons received attention. Small- and large-signal theories and space-charge-effect studies were dominant.

[69] J. Feinstein and G. S. Kino, "The large signal behavior of crossed-field traveling-wave devices," PROC. IRE, vol. 45, pp. 1364–1373; October, 1957.
[70] B. Epsztein, "Effects of space charge in crossed-field tubes," *Compt. Rend. Acad. Sci., Paris*, vol. 244, pp. 2902–2905; June 12, 1957.
[71] R. W. Gould, "Space-charge effects in beam-type magnetrons," *J. Appl. Phys.*, vol. 28, pp. 599–605; May, 1957.
[72] H. A. Haus and D. L. Bobrooff, "Small-signal power theorem for electron beams," *J. Appl. Phys.*, vol. 28, pp. 694–704; June, 1957.
[73] O. Bunemann, "A small-amplitude theory for magnetrons," *J. Electronics Control*, vol. 3, pp. 1–50; July, 1957.
[74] L. Gold, "Space charge in the relativistic magnetron," *J. Electronics Control*, vol. 3, pp. 87–96; July, 1957.

The theory of noise in traveling-wave and related tubes and the practical realization of high signal-to-noise ratios continue to stimulate much activity.

[75] R. Knechtli and W. R. Beam, "Validity of traveling-wave-tube noise theory," *RCA Rev.*, vol. 18, pp. 24–38; March, 1957.
[76] J. Labus, R. Liebscher, and K. Pöschl, "Condition for minimum noise factor of traveling-wave tubes," *Arch. Elekt. Übertragung*, vol. 10, pp. 486–490; November, 1956.
[77] W. W. Rigrod, "Noise spectrum of electron beam in longitudinal magnetic field. I. The growing noise phenomenon," *Bell Sys. Tech. J.*, vol. 36, pp. 831–853; July, 1957.
[78] W. W. Rigrod, "Noise spectrum of electron beam in longitudinal magnetic field. II. The u.h.f. noise spectrum," *Bell Sys. Tech. J.*, vol. 36, pp. 855–878; July, 1957.
[79] H. D. Allen and J. M. Winwood, "A low noise travelling-wave tube amplifier for the 4000 mc/s communications band," *J. Brit. IRE*, vol. 17, pp. 75–85; January, 1957.
[80] F. B. Fank and F. M. Schumacher, "Development and operation of broad-band low noise traveling wave tubes for *X*- and *C*-bands," 1957 IRE WESCON CONVENTION RECORD, pt. 3, pp. 150–155.
[81] J. C. Twombly, "Shot noise amplification in beams beyond critical perveance," 1957 IRE WESCON CONVENTION RECORD, pt. 3, pp. 156–162.
[82] W. R. Beam, "Noise wave excitation at the cathode of a microwave beam amplifier," IRE TRANS. ON ELECTRON DEVICES, vol. ED-4, pp. 226–234; July, 1957.
[83] L. D. Buchmuller, R. W. DeGrasse, and G. Wade, "Design and calculation procedures for low-noise traveling-wave tubes," IRE TRANS. ON ELECTRON DEVICES, vol. ED-4, pp. 234–242; July, 1957.
[84] M. R. Currie and D. C. Forster, "Experiments on noise reduction in backward-wave amplifiers," PROC. IRE, vol. 45, p. 690; May, 1957.

The size and weight of focusing structures for traveling-wave tubes have been limiting factors on the application of traveling-wave tubes. Periodic systems and light-weight permanent magnets as focusing structures were studied and some design procedures were outlined.

[85] M. S. Glass, "Straight-field permanent magnets of minimum weight for twt focusing—design and graphic aids in design," PROC. IRE, vol. 45, pp. 1100–1105; August, 1957.
[86] F. Sterzer and W. W. Siekanowicz, "The design of periodic permanent magnets for focusing of electron beams," *RCA Rev.*, vol. 18, pp. 39–59; March, 1957.
[87] K. K. N. Chang, "Confined electron flow in periodic electrostatic fields of very short periods," PROC. IRE, vol. 45, pp. 66–73; January, 1957.
[88] K. K. N. Chang, "Biperiodic electrostatic focusing for high-density electron beams," PROC. IRE, vol. 45, pp. 1522–1527; November, 1957.
[89] J. L. Palmer and C. Süsskind, "Injection of convergent beams focused by periodic magnetic fields," 1957 IRE WESCON CONVENTION RECORD, pt. 3, pp. 130–137.
[90] J. Labus, "Space charge waves along magnetically focused electron beams," PROC. IRE, vol. 45, pp. 854–861; June, 1957.
[91] D. C. Buck, "Stability of a cylindrical electron beam in non-sinusoidal periodic magnetic-focusing fields," IRE TRANS. ON ELECTRON DEVICES, vol. ED-4, pp. 44–49; January, 1957.
[92] J. S. Cook, R. Kompfner, and W. H. Yocum, "Slalom focusing," PROC. IRE, vol. 45, pp. 1517–1527; November, 1957.

Electron beam phenomena, including such topics as gun design and characteristics, oscillations in beams, and interaction of beams with electromagnetic waves, have received much attention.

[93] L. E. S. Mathias and P. G. R. King, "On the performance of high perveance electron guns," IRE TRANS. ON ELECTRON DEVICES, vol. ED-4, pp. 280–286; July, 1957.
[94] O. L. Hoch and D. A. Watkins, "A gun and focusing system for crossed-field traveling-wave tubes," 1957 IRE WESCON CONVENTION RECORD, pt. 3, pp. 122–129.
[95] K. Fujisawa and T. Kaneko, "Design of electron gun for strip beams," *J. Inst. Elec. Comm. Engrs. Japan*, vol. 39, pp. 942–947; November, 1956.
[96] S. E. Webber, "Electron bunching and energy exchange in a traveling-wave tube," IRE TRANS. ON ELECTRON DEVICES, vol. ED-4, pp. 87–91; January, 1957.
[97] C. C. Wang, "Linear beam tube theory," IRE TRANS. ON ELECTRON DEVICES, vol. ED-4, pp. 92–106; January, 1957.
[98] G. R. Brewer and C. K. Birdsall, "Traveling-wave tube propagation constants," IRE TRANS. ON ELECTRON DEVICES, vol. ED-4, pp. 140–144; April, 1957.
[99] J. A. Mullen, "A power series solution of the traveling-wave tube equations," IRE TRANS. ON ELECTRON DEVICES, vol. ED-4, pp. 159–160; April, 1957.
[100] N. Rynn, "Analysis of coupled-structure traveling-wave tubes," IRE TRANS. ON ELECTRON DEVICES, vol. ED-4, pp. 172–177; April, 1957.
[101] V. N. Schevchik, "An analysis of the energy interchange between an electron stream and an electromagnetic wave," *Radiotekhnika i Elektronika*, vol. 2, pp. 104–110; January, 1957.
[102] P. V. Bliokh, "High frequency oscillations in electron beams with a periodically varying velocity," *Radiotekhnika i Elektronica*, vol. 2, pp. 92–103; January, 1957.
[103] R. L. Jepsen, "Ion oscillations in electron beam tubes; ion motion and energy transfer," PROC. IRE, vol. 45, pp. 1069–1080; August, 1957.
[104] N. C. Barford, "Space-charge neutralization by ions in linear-flow electron beams," *J. Electronics Control*, vol. 3, pp. 63–86; July, 1957.
[105] G. R. Brewer, "Some characteristics of a cylindrical electron stream in immersed flow," IRE TRANS. ON ELECTRON DEVICES, vol. ED-4, pp. 134–140; April, 1957.
[106] D. A. Dunn and W. R. Luebke, "Beam perturbations in confined flow electron beams with planar symmetry," IRE TRANS. ON ELECTRON DEVICES, vol. ED-4, pp. 265–270; July, 1957.

Reports of investigations of helices and other slow-wave structures for traveling-wave tube applications were given.

[107] G. Landauer, "The helix with a cylindrical coaxial attenuator," *Arch. Elekt. Übertragung*, vol. 11, pp. 267–277; July, 1957.
[108] P. Lapostolle, "Helices for traveling-wave tubes. Influence of the supports-attenuation-parasitic modes," *Ann. Télécomm.*, vol. 12, pp. 34–59; February, 1957.
[109] F. Paschke, "The reciprocity of coupling in traveling-wave tubes," *Arch. Elekt. Übertragung*, vol. 11, pp. 137–145; April, 1957.
[110] G. Al'tshuler, A. S. Tatarenko, and S. V. Gerchikov, "Design of a retarding system with double tandem rods," *Radiotekhnika i Elektronika*, vol. 2, pp. 609–617; May, 1957.
[111] K. Morita, M. Kawamura, and Y. Suematsu, "Slow-wave circuit of cascaded annular disks," *J. Inst. Elec. Comm. Engrs. Japan*, vol. 40, pp. 454–460; April, 1957.
[112] J. C. Walling, "Interdigital and other slow wave structures," *J. Electronics Control*, vol. 3, pp. 239–258; September, 1957.

Klystrons

Velocity modulation tubes are of great practical importance. This fact motivates study of methods of improving such tubes. Greater operating bandwidths, higher efficiencies and output powers, lower noise levels, and better modulation methods are representative areas of improvement. One report indicated that efficiencies of 50 per cent for high-power klystrons are attainable. Another report indicated procedures by which the useful bandwidth of a high-power klystron can be doubled and that the maximum bandwidth obtained thus far was 5 per cent.

[113] W. J. Dodds, T. Moreno, and W. J. McBride, Jr., "Methods of increasing bandwidth of high power microwave amplifiers," 1957 IRE WESCON CONVENTION RECORD, pt. 3, pp. 101–110.
[114] W. L. Beaver, R. L. Jepsen, and R. L. Walter, "Wide band klystron amplifiers," 1957 IRE WESCON CONVENTION RECORD, pt. 3, pp. 111–114.
[115] K. H. Kreuchen, B. A. Auld, and N. E. Dixon, "A study of broadband frequency response of the multicavity klystron amplifier," *J. Electronics*, vol. 2, pp. 529–567; May, 1957.
[116] S. V. Yadavalli, "Application of the potential analog in multicavity klystron design and operation," PROC. IRE, vol. 45, pp. 1286–1287; September, 1957.
[117] M. S. Neiman, "Some basic relations in power klystron amplifiers," *Radiotekhnika*, vol. 12, pp. 3–12; April, 1957.
[118] E. D. Naumenko, "Wide-band reflex klystrons for millimeter waves," *Radiotekhnika i Electronika*, vol. 2, pp. 618–621; May, 1957.

The effect of reflector voltage, cavity voltage, reflector spacing, and loading on the output power and frequency of a klystron were discussed in detail.

[119] M. Kenmoku and S. Shitara, "Output control of reflex klystrons," *Onde Élect.*, vol. 37, pp. 102–115; February, 1957.

More detailed analyses of space-charge waves and methods of measuring and exciting them were made. It was shown that analyses restricted to the lowest order space-charge wave leads to incorrect results for optimum drift distances and other parameters.

[120] A. H. Beck, "Excitation of space-charge waves in drift tubes," *J. Appl. Phys.*, vol. 28, pp. 140–141; January, 1957.
[121] W. E. Walters, "Space-charge effects in klystrons," IRE TRANS. ON ELECTRON DEVICES, vol. ED-4, pp. 49–58; January, 1957.
[122] A. H. W. Beck, "High order space charge waves in klystrons," *J. Electronics*, vol. 2, pp. 489–509; March, 1957.
[123] D. Walsh, "The measurement of space charge wavelength in an electron beam," *J. Electronics*, vol. 2, pp. 436–440; March, 1957.

The mode of operation of multireflection klystrons was described and conditions for maximum efficiency established.

[124] B. Meltzer, "Notes on the multi-reflection klystron," *Electronic Radio Engr.*, vol. 34, pp. 109–112; March, 1957.

An investigation of noise in a high-power klystron indicated that the principal source of noise was in the tuning mechanism.

[125] R. A. LaPlante and G. A. Espersen, "A low-noise klystron with high power output," *Philips Tech. Rev.*, vol. 18, no. 12, pp. 361–368; 1956–1957.

A three-resonator, pulsed-grid klystron amplifier was described which could reliably produce a very narrow frequency spectrum. Another method of modulation used a modulating anode.

[126] J. D. Swearingen and C. M. Veronda, "The SAL-89 a grid controlled pulsed klystron amplifier," 1957 IRE WESCON Convention Record, pt. 3, pp. 115–121.
[127] G. M. W. Badger, "A new method for modulating electron beams for pulse applications and linear amplitude modulation systems," 1957 IRE National Convention Record, pt. 3, pp. 82–90.

An investigation of a klystron in which the electron transit angle through the resonator is large indicated that efficiencies which are greater by a factor of two or three than those of conventional klystrons were possible.

[128] V. N. Shevchik, S. A. Suslov, and Y. D. Zharkov, "Investigation of a special type of reflex klystron," *Zh. Tekh. Fiz.*, vol. 27, pp. 377–386; February, 1957.

A klystron design which yields a wide frequency range of operation for constant reflector voltage was described.

[129] M. Kenmoku, "Constant-reflector-voltage klystron," *J. Inst. Elec. Comm. Engrs. Japan*, vol. 40, pp. 981–988; September, 1957.

The nonlinear behavior of klystrons was studied. A nonlinear space-charge-wave equation was derived and by using third-order successive approximations was split into three simultaneous linear equations which were solved for klystrons. Equations for gain and efficiency of two cavity klystrons were given.

[130] F. Paschke, "On the nonlinear behavior of electron beam devices," *RCA Rev.*, pp. 221–242; June, 1957.
[131] K. Fukisawa, T. Kaneko, and T. Namekawa, "General treatment of millimeter-wave klystron cavities," *J. Inst. Elec. Comm. Engrs. Japan*, vol. 40, pp. 556–563; May, 1957.

Magnetrons

Work on magnetrons was quite limited compared with that on traveling-wave tubes. A number of the de-developments listed under traveling-wave devices might have been listed under klystrons or magnetrons. This is especially true of some of the developments in crossed-field traveling-wave devices.

A new microwave device of the crossed-field type known as the "platinotron" which might have been reported under traveling-wave devices is reported here. This device looks like a magnetron. It has a reentrant beam as does the magnetron but a nonreentrant interaction network which is matched at both ends over the frequency band of interest. Power outputs of almost 2 megawatts at 69 per cent efficiency, and 10 per cent bandwidths at efficiencies greater than 50 per cent were obtained.

[132] W. C. Brown, "Description and operating characteristics of the platinotron—a new microwave device," Proc. IRE, vol. 45, pp. 1209–1222; September, 1957.
[133] W. C. Brown, "Platinotron increases search radar range," *Electronics*, vol. 30, pp. 164–168; August, 1957.

Work reported on magnetrons *per se* seemed to emphasize high power, high efficiency, better tunability characteristics, and better performance under pulsed conditions.

[134] J. Ninerailles, B. Vallantin, and P. Stern, "Power magnetrons, MC 1053 and MCV 1053," *Onde Élect.*, vol. 37, pp. 274–281; March, 1957.
[135] Z. Fraenkel, "The development of a tunable cw magnetron in the *K*-band region," IRE Trans. on Electron Devices, vol. ED-4, pp. 271–280; July, 1957.
[136] T. R. Bristol and G. J. Griffin, Jr., "Voltage-tuned magnetron for f-m applications," *Electronics*, vol. 30, pp. 162–163; May, 1957.
[137] E. Petrasco and I. I. Vasilesco, "A frequency-modulated magnetron," *Compt. Rend. Acad. Sci., Paris*, vol. 244, pp. 2296–2298; April 29, 1957.
[138] E. C. Okress, C. H. Gleason, R. A. White, and W. H. Hayter, "Design and performance of a high power pulsed magnetron," IRE Trans. on Electron Devices, vol. ED-4, pp. 161–171; April, 1957.

For certain cylinder voltages when a beam of electrons is injected tangentially into the space between two coaxial cylinders, it was reported that the electrons describe circular paths without a magnetic field being necessary. Power outputs of some tens of milliwatts were obtained at operating wavelengths in the 70–130 cm range.

[139] A. Wersnel, "Magnetless magnetron," *Vide*, vol. 13, pp. 59–63; January–February, 1957.

The effect of cathode eccentricity, space charge theory, and signal theory of magnetrons are other topics which were discussed.

[140] G. E. Becker, "Dependence of magnetron operation on the radial centering of the cathode," IRE Trans. on Electron Devices, vol. ED-4, pp. 126–131; April, 1957.
[141] L. Gold, "Kinetic theory of space charge: part 1—Cut-off character of the static magnetron," *J. Electronics Control*, vol. 3, pp. 97–102; July, 1957.
[142] R. W. Gould, "Space charge effects in beam-type magnetrons," *J. Appl. Phys.*, vol. 28, pp. 599–605; May, 1957.
[143] L. Gold, "Space-charge in the relativistic magnetron," *J. Electronics Control*, vol. 3, pp. 87–96; July, 1957.
[144] O. Bunemann, "A small amplitude theory for magnetrons," *J. Electronics Control*, vol. 3, pp. 1–50; July, 1957.

II. Transmission Lines

In accord with IRE standards, the definition of transmission lines is here considered to encompass ordinary transmission lines, hollow waveguides, and surface-wave structures. Developments in microwave circuit components based on the various types of transmission lines are reviewed after transmission line developments.

TEM Lines

The inherently broad bandwidth characteristics, small size, light weight, and mechanical simplicity of many types of TEM lines continued to stimulate considerable efforts to improve their performance. The interest in filters and other microwave components was sustained by the trend to broad-band systems.

Various aspects of the several types of strip or planar lines were treated theoretically and design methods were further developed.

Higher order mode limitations on the dimensions of symmetrical strip line were used to derive the permissible dimensions at any given frequency and characteristic impedance. Conclusions were reached regarding the best ratio of strip thickness to ground-plane spacing.

[145] K. S. Packard, "Optimum impedance and dimensions for strip transmission lines," IRE Trans. on Microwave Theory and Techniques, vol. MTT-5, pp. 244–247; October, 1957.

A theoretical method was given for computing the capacitance of certain electrostatic-field geometries which previously has proved intractable because the determination of such fields required the evaluation of hyperelliptic integrals. The method was applied to the calculation of the characteristic impedance of a strip line.

[146] J. D. Horgan, "Coupled strip transmission line with rectangular inner conductor," IRE Trans. on Microwave Theory and Techniques, vol. MTT-5, pp. 92–99; April, 1957.

A procedure involving successive approximations to determine the current distribution was applied to a microstrip line to determine the fields associated with the lowest order mode.

[147] T. T. Wu, "Theory of the microstrip," *J. Appl. Phys.*, vol. 28, pp. 299–302; March, 1957.

Unidirectional strip lines utilizing ferrite elements with magnetic fields applied in a transverse sense relative to the direction of a propagation to produce resonance or field displacement were described. Such circuits are useful for phase shifters, modulators, switches, etc.

[148] S. Yoshido, "Microwave transverse magnetic type unidirectional strip circuits," *J. Inst. Elec. Comm. Engrs. Japan*, vol. 40, pp. 30–33; January, 1957.

Several aspects of coaxial and open-wire transmission lines were studied. In one study it was found that it was advantageous to disperse the supporting beads for the inner conductor of a coaxial cable according to a progressive dispersal formula which was derived.

[149] D. Dettinger, "The optimum spacing of bead supports in coaxial line at microwave frequencies," 1957 IRE National Convention Record, pt. 1, pp. 250–253.

Related studies were concerned with random spacing of discontinuities and with statistical prediction of voltage standing-wave ratios for many randomly spaced discontinuities.

[150] R. K. Moore, "The effect of reflections from randomly spaced discontinuities in transmission lines," IRE Trans. on Microwave Theory and Techniques, vol. MTT-5, pp. 121–126; April, 1957.

[151] J. A. Mullen and W. L. Pritchard, "The statistical prediction of voltage standing-wave ratio," IRE Trans. on Microwave Theory and Techniques, vol. MTT-5, pp. 127–130; April, 1957.

Singly and multiply braided outer conductors of coaxial cables were investigated experimentally. It was reported that the studies led to the use of large interweaving angles and thin wires for the braids. Ferromagnetic intermediate layers were tried and were found to introduce practical difficulties.

[152] L. Krugel, "Multiple screening of flexible coaxial cables," *Telefunken Ztg.*, vol. 30, pp. 207–214; September, 1957.

The problem of distortion of waveforms of durations of the order of a millimicrosecond by the high frequency loss in a coaxial cable was analyzed. Generalized curves were presented by which the response of any length of coaxial cable can be predicted if one point on the attenuation vs frequency curve is known.

[153] R. L. Wigington and N. S. Nahman, "Transient analysis of coaxial cables considering skin effect," Proc. IRE, vol. 45, pp. 166–174; February, 1957.

The theory of exponential and other nonuniform lines was the subject of several reports.

[154] R. Codelupi, "Theory of nonuniform lines," *Alta Frequenza*, vol. 26, pp. 226–282; August, 1957.

[155] B. G. Kazansky, "Outline of a theory of non-uniform transmission lines," *Proc. IEE*, Monogram 261R; October, 1957.

[156] Laszlo Solymar, "On higher order approximations to the solution of nonuniform transmission lines," Proc. IRE, vol. 45, pp. 1547–1548; November, 1957.

[157] E. F. Bolinder, "Study of the exponential line by the isometric circle method and hyperbolic geometry," *Acta Polytech.*, Elec. Eng. Ser., vol. 7, no. 8; 1957.

The coupling of a multilayer laminated transmission line to other lines was discussed and the problem of minimizing losses caused by mode conversion was investigated.

[158] H. E. Martin, "Mode-conversion phenomena in multi-layer transmission lines and their effects on transmission along singly and tandem-connected lines," *Arch. Elekt. Übertragung*, vol. 11, pp. 7–16, 81–96; January/February, 1957.

Tape ladder lines of the single-ridge, double-ridge, single T-section, and double T-section types in which the rungs of the ladder are thin tapes were studied. Dispersion curves and coupling impedances were calculated.

[159] P. N. Butcher, "A theoretical study of propagation along tape ladder lines," *Proc. IEE*, vol. 104, pt. B, pp. 169–176; March, 1957.

[160] P. N. Butcher, "The coupling impedance of tape structures," *Proc. IEE*, vol. 104, pt. B, pp. 177–186; March, 1957.

Hollow Waveguides

The high power-handling capacity, wide bandwidth, and low attenuation characteristics of large hollow pipes, excited in the circular TE_{01} mode, continue to attract considerable attention directed towards the eventual practical utilization of such waveguides.

Transmission through straight sections of aluminum tubing manufactured and installed to British commercial tolerances for standard-production, solid ground tubes resulted in attenuations which were 30 per cent above the theoretical value and stable conditions of propagation.

[161] H. E. M. Barlow and E. G. Effemey, "Propagation characteristics of low-loss-tubular waveguides," *Proc. IEE*, vol. 104, pt. B, pp. 254–260; May, 1957.

Bends and curves in TE_{01}-mode waveguides cause mode conversion. Several analyses of such mode conver-

sions were made and methods of preventing or reducing them were proposed.

[162] S. P. Morgan, "Theory of curved circular waveguide containing an inhomogeneous dielectric," *Bell Sys. Tech. J.*, vol. 36, pp. 1209–1252; September, 1957.
[163] H. E. M. Barlow, "Propagation of the circular H_{01} low-loss wave mode around bends in tubular metal waveguide," *Proc. IEE*, vol. 104, pt. B, pp. 402–409; July, 1957.
[164] H. G. Unger, "Circular electric wave transmission in a dielectric coated waveguide," *Bell Sys. Tech. J.*, vol. 36, pp. 1253–1278; September, 1957.
[165] H. G. Unger, "Circular electric wave transmission through serpentine bends," *Bell Sys. Tech. J.*, vol. 36, pp. 1279–1291; September, 1957.
[166] H. G. Unger, "Normal node bends for circular electric waves," *Bell Sys. Tech. J.*, vol. 36, pp. 1292–1307; September, 1957.
[167] S. Kumagai, Nobuaki Kumagai and Hirotaro Ohba, "Mode conversion losses in transmission of TE_{01} modes through conically tapered waveguides," *J. Inst. Elec. Comm. Engrs. Japan*, vol. 40, pp. 1203–1209; November, 1957.
[168] Shin-ichi Iiguchi, "Mode conversion in transmitting TE_{01} wave through a slightly tilted guide," *J. Inst. Elec. Comm. Engrs. Japan*, vol. 40, pp. 870–876; August, 1957.
[169] Shin-ichi Iiguchi, "Mode conversion in transmission of TE_{01} wave through a slight off-set of the guide," *J. Inst. Elec. Comm. Engrs. Japan*, vol. 40, pp. 1095–1102; October, 1957.
[170] M. V. Persikov, "Directional coupler for the H_{01} wave in a waveguide with circularly cross-section," *Radiotekhnika i Electronica*, vol. 2, pp. 65–74; January, 1957.
[171] B. Z. Katsenelenbaun, "Long symmetrical waveguide junction for H_{01} waves," *Radiotekhnika i Electronika*, vol. 2, pp. 531–546; May, 1957.

The TE_{01}-mode losses in a waveguide with walls of alternate rings of conducting and insulating material and in one with walls of helically wound wire were studied.

[172] G. Comte, F. de Carfort, A Ponthus, and J. M. Paris, "Utilization of circular waveguides for the long distance transmission of centimeter and millimeter waves," *Cables and Transmission*, vol. 11, pp. 342–355; October, 1957.

High-power waveguide systems of rectangular cross section have been studied. Results show that multimegawatt power levels bring with them adverse effects of harmonics.

[173] M. P. Forrer and K. Tomiyasu, "Effects and measurement of harmonics in high-power waveguide systems," 1957 IRE National Convention Record, pt. 1, pp. 263–269.

Rectangular waveguides with slight deformations into hexagonal shape have been analyzed by variational methods to determine suitability of such a structure as an approximation for a rectangular guide. Deflections of a rectangular guide subject to internal pressure were also investigated.

[174] T. Humphreys, "Waveguide design for die-casting," *Electronic Radio Eng.*, vol. 34, pp. 441–447; December, 1957.
[175] L. G. Virgile, "Deflection of waveguide subjected to internal pressure," IRE Trans. on Microwave Theory and Techniques, vol. MTT-5, pp. 247–250; October, 1957.

Miscellaneous types of waveguides which received attention include waveguides wound into a helix, septate waveguides, and ridge waveguides.

[176] R. A. Waldron, "Theory of the helical waveguide of rectangular cross-section," *J. Brit. IRE*, vol. 17, pp. 577–592; October, 1957.
[177] B. Valtersson, "Phase velocity in helical waveguides," *Onde Élect.*, vol. 37, pp. 843–849; October, 1957.
[178] R. G. Mirimanov and G. I. Zhileiko, "Analysis of some types of septate waveguides," *Radiotekhnika i Electronika*, vol. 2, pp. 172–183; February, 1957.
[179] T. S. Chen, "Calculation of the parameters of ridge waveguides," IRE Trans. on Microwave Theory and Techniques, vol. MTT-5, pp. 12–17; January, 1957.
[180] J. van Bladel and O. von Rohr, Jr., "Semicircular ridges in rectangular waveguides," IRE Trans. on Microwave Theory and Techniques, vol. MTT-5, pp. 103–106; April, 1957.

Losses in the walls of waveguides and their effect on propagation have received further study. One approach was similar to that used by Sommerfeld in treating surface waves on a single solid conductor.

[181] A. Turski, "Calculation of losses in smooth walls of circular waveguides on the basis of Maxwell's equations," *Arch. Elektrotech. Warsaw*, vol. 5, pp. 567–568; 1956.

Another approach was a surface-impedance one which was applied to parallel plane, rectangular and circular waveguides.

[182] A. E. Karbowiak, "Waveguide characteristics," *Electronic Radio Engr.*, vol. 34, pp. 379–387; October, 1957.

The effects on losses of parallel semicircular grooves in waveguide walls, of utilizing ferrous materials, and of surface finish were studied.

[183] E. A. Marcatili, "Heat losses in grooved metallic surface," Proc. IRE, vol. 45, pp. 1134–1139; August, 1957.
[184] J. J. Allison, F. A. Benson, and M. S. Seaman, "Characteristics of some ferrous and non-ferrous waveguides at 27 Gc/s." *Proc. IEE*, vol. 104, pt. B, pp. 599–602; November, 1957.
[185] J. Allison and F. A. Benson, "Surface finish and attenuation of aluminum waveguides," *Electronic Eng.*, vol. 29, pp. 36–38; January, 1957.

Transient and pulse propagation characteristics of waveguides were investigated.

[186] A. E. Karbowiak, "Propagation of transients in waveguides," *Proc. IEE*, vol. 104, pt. C, pp. 339–348; February, 1957.
[187] R. S. Elliott, "Pulse waveform degradation due to dispersion in waveguides," IRE Trans. on Microwave Theory and Techniques, vol. MTT-5, pp. 254–257; October, 1957.

A magnetized gyromagnetic medium is birefringent. The effect of birefringence has been studied. It is evident that new methods and techniques of model synthesis are needed when ferrite-loaded structures are considered.

[188] H. Seidel, "The calculation of waveguide modes in gyromagnetic media," *Bell Sys. Tech. J.*, vol. 36, pp. 409–426; March, 1957.
[189] H. Seidel, "Viewpoints on resonance in ideal ferrite slab-loaded rectangular waveguides," 1957 IRE WESCON Convention Record, pt. 1, pp. 58–69.
[190] I. A. Monosov, "Characteristics of the Faraday effect in a cylindrical waveguide with a ferrite rod," *Radiotekhnika i Elektronika*, vol. 2, pp. 547–556; May, 1957.
[191] A. K. Stoliarov, "Use of ferrites in waveguide design," *Electrosviaz*, vol. 1, pp. 34–45; May, 1957.
[192] H. Seidel, "Ferrite slabs in transverse electric mode waveguide," *J. Appl. Phys.*, vol. 28, pp. 218–226; February, 1957.

Tapered transitions and gradual changes of cross section were investigated.

[193] B. J. Migliaro, "Designing tapered waveguide transitions," *Electronics*, vol. 30, pp. 183–185; November, 1957.
[194] D. J. Leonard and J. L. Yen, "Junction of smooth flared waveguides," *J. Appl. Phys.*, vol. 28, pp. 1441–1448; December, 1957.
[195] A. L. Gutman, "The calculation of waveguide with gradual change of section," *Radiotekhnika*, vol. 12, pp. 20–28; August, 1957.
[196] G. Piefke, "Reflection at the transition from rectangular waveguide to sectoral horn," *Arch. Elekt. Übertragung*, vol. 11, pp. 123–135; March, 1957.

Surface-Wave and Periodic Structures

Interest in surface-wave transmission lines of the Goubau type has continued. Additional performance

data have been obtained and aspects of the theory of excitation and propagation have been treated.

[197] G. Goubau and C. E. Sharp, "Investigations with a model surface wave transmission line," IRE Trans. on Antennas and Propagation, vol. AP-5, pp. 222–227; April, 1957.
[198] S. N. Contractor and S. K. Chatterjee, "Propagation of microwaves on a single wire, part 2," *J. Indian Inst. Sci.*, vol. 39, sec. B, pp. 52–67; January, 1957.
[199] T. Berceli, "Surface wave propagation along coated wires," *Acta. Tech. Acad. Sci. Hungary*, vol. 17, pp. 219–251; 1957.
[200] A. L. Cullen, "A note on the excitation of surface waves," *Proc. IEE*, vol. 104, pt. C, pp. 472–474; September, 1957.
[201] O. Zinke, "Cables and radio paths at microwave frequencies," *Nachricht. Z.*, vol. 10, pp. 425–430; September, 1957.
[202] Hiroshi Kikuchi, "Electromagnetic fields on infinite wire of high frequencies above plane earth," *J. Inst. Elec. Comm. Engrs. Japan*, vol. 40, p. 721; June, 1957.
[203] B. Chiron, "The influence of external agents on the propagation of a surface wave," *Cables and Transmission*, vol. 11, pp. 237–244; July, 1957.
[204] C. Jauquet, "Transverse-magnetic surface wave on an infinitely conductive cylinder," *Bull. Acad. Roy. Belgique Cl. Sci.*, vol. 43, pp. 1178–1183; November, 1956.

Closely related to the Goubau line are numerous other "open" or surface wave structures. Among these structures are dielectric rods and cylinders and related maze structures, disk structures, helical wires, and dielectric slabs.

[205] C. Jauquet, "Excitation of a transverse magnetic surface-wave propagated on a dielectric cylinder," *Ann. Télécomm.*, vol. 12, pp. 217–233; June, 1957.
[206] D. D. King and S. P. Schlesinger, "Losses in dielectric image lines," IRE Trans. on Microwave Theory and Techniques, vol. MTT-5, pp. 31–35; January, 1957.
[207] G. Piefke, "Wave propagation in the disk line," *Arch. Elekt. Übertragung*, vol. 11, pp. 49–59; February, 1957.
[208] D. Marcuse, "On a novel surface waveguide with bandpass properties," *Arch. Elekt. Übertragung*, vol. 11, pp. 146–148; April, 1957.
[209] G. Schiefer, "The attenuation constant of the helical-wire conductor," *Arch. Elekt. Übertragung*, vol. 11, pp. 35–40; January, 1957.
[210] R. C. Hansen, "Single slab arbitrary polarization surface wave structure," IRE Trans. on Microwave Theory and Techniques, vol. MTT-5, pp. 115–120; April, 1957.
[211] M. A. Miller and V. I. Talanov, "Electromagnetic surface waves guided by a boundary with small curvature," *Zh. Tekh. Fiz.*, vol. 26, pp. 2755–2765; December, 1956.
[212] R. E. Plummer and R. C. Hansen, "Double-slab arbitrary-polarization surface-wave structure," *Proc. IEE*, vol. 104, pt. C, pp. 465–471; May, 1957.

Junctions

The analysis of a discontinuity or a junction in a transmission line or waveguide is a field problem. The results of the analysis are expressed in an equivalent network form for convenience in dealing with the effect of such a discontinuity or junction on a single mode transmission system.

To solve the field problem of a discontinuity in cross section of a rectangular waveguide, the Wiener-Hopf method for solving a certain class of integral equations was applied in one paper. In another paper the Rayleigh-Ritz method was used to obtain approximations for the eigenfunctions and eigenvalues for a dielectric step in a rectangular waveguide.

[213] W. E. Williams, "Step discontinuities in waveguides," IRE Trans. on Antennas and Propagation, vol. AP-5, pp. 191–197; April, 1957.
[214] R. E. Collin and R. M. Vaillancourt, "Application of Rayleigh-Ritz method to dielectric steps in waveguides," IRE Trans. on Microwave Theory and Techniques, vol. MTT-5, pp. 177–184; July, 1957.

The four-terminal network for the junction of an empty rectangular waveguide with a rectangular waveguide partially filled with a dielectric was developed in another paper.

[215] C. M. Angulo, "Discontinuities in a rectangular waveguide partially filled with dielectric," IRE Trans. on Microwave Theory and Techniques, vol. MTT-5, pp. 68–74; January, 1957.

The determination of equivalent circuit parameters for discontinuities was discussed also in the following paper:

[216] R. E. Collin, "Determination of equivalent circuit parameters," IRE Trans. on Microwave Theory and Techniques, vol. MTT-5, pp. 266–267; October, 1957.

Other papers on linear two-port junctions which were presented include:

[217] G. Deschamps, "A variant in the measurement of two-port junctions," IRE Trans. on Microwave Theory and Techniques, vol. MTT-5, pp. 159–161; April, 1957.
[218] L. Breitenhuber, "The dielectric disk as a four pole transformation network to magnify the node displacement for measuring purposes," *Arch. Elekt. Übertragung*, vol. 11, pp. 223–226; June, 1957.
[219] E. F. Bolinder, "Graphical method of determining the efficiency of two-port networks," Proc. IRE, vol. 45, p. 361; March, 1957.
[220] E. F. Bolinder, "A note on the matrix representation of linear two-port networks," IRE Trans. on Circuit Theory, vol. CT-4, pp. 337–339; December, 1957.
[221] W. P. Ayres, "Broad-band quarter-wave plates," IRE Trans. on Microwave Theory and Techniques, vol. MTT-5, pp. 258–261; October, 1957.

Some papers on both linear and gyromagnetic two-port and multiport microwave components are listed under other headings.

Directional Couplers

Strip-line structures were used as the basis for several directional couplers. One paper described two 3-db strip-line couplers. One of these couplers was a quarter wavelength long at the center of its frequency band and had a variation in coupling of ± 0.3 db over a 2:1 frequency band. The other was three quarters of a wavelength long and had the same coupling variation but over a 4.5:1 band. Good directivity and low standing wave ratios were reported for these couplers.

[222] J. K. Shimizu, "Strip-line 3-db directional couplers," 1957 IRE WESCON Convention Record, pt. 1, pp. 4–15.

Bethe's small-slot coupling formulas were applied to the case of coupling between waveguide and strip line. Compact three and four element binomial-array couplers with flat coupling characteristics, good directivity, and high power-handling capacity were built for L band.

[223] H. Perini and P. Sferrazza, "Rectangular waveguide to strip-transmission-line directional couplers," 1957 IRE WESCON Convention Record, pt. 1, pp. 16–21.

A simple extension of Bethe's small-hole coupling theory for coupling through an aperture containing a ferrite was formulated.

[224] D. C. Stinson, "Coupling through an aperture containing an anisotropic ferrite," IRE Trans. on Microwave Theory and Techniques, vol. MTT-5, pp. 184–191; July, 1957.

The boundary value problem of multiple slot coupling between identical rectangular guides was treated in another theoretical investigation.

[225] J. A. Barkson, "Coupling of rectangular waveguides having a common broad wall which contains uniform transverse slots," 1957 IRE WESCON Convention Record, pt. 1, pp. 30–38.

A new design technique involving two strip transmission lines mounted back to back above the ground plane and coupled through slots which were graded in length was described. In one design an equal power split within 1 db over a frequency band of 2800–4300 mc was obtained.

[226] J. M. C. Dukes, "Broad-band slot-coupled microstrip directional couplers," *Proc. IEE*, Paper 2402R; August, 1957.

A forward-type coupler utilizing a multiplicity of capacitive coupling probes inserted in the base of a waveguide for coupling between a coaxial line and TE_{10} mode waveguide was described.

227] P. P. Lombardini and R. F. Schwartz, "A new type of directional couplers for coupling coaxial line to TE_{10} waveguide," 1957 IRE WESCON Convention Record, pt. 1, pp. 22–29.

The problem of many parallel waveguides with continuous and uniform coupling was solved by the application of normal modes and the solution was extended to an infinite number of lines.

[228] J. P. Shelton, Jr., "Multiple-line directional couplers," 1957 IRE National Convention Record, pt. 1, pp. 254–262.

In another paper, a multi-element directional coupler was considered as a cascaded set of two-element couplers, each of which is perfect in match and directivity at the design frequency.

[229] J. W. Crompton, "A contribution to the design of multi-element directional couplers," *Proc. IEE*, vol. 104, pt. C, pp. 398–402; April, 1957.

Hybrid Junctions

A number of papers have appeared on hybrid junctions. A new form of hybrid junction which utilizes the principle of the branch-waveguide directional coupler was described in one paper. The performance of such a hybrid junction was reported to be superior to that of the hybrid-T and rat-race and to compare favorably with that of the short-slot hybrid.

[230] P. D. Lomer and J. W. Crompton, "A new form of hybrid junction for microwave frequencies," *Proc. IEE*, vol. 104, pt. B, pp. 261–263; May, 1957.

[231] L. Young, P. D. Lomer, and J. W. Crompton, "A new form of hybrid junction for microwave frequencies," *Proc. IEE*, vol. 104, pt. B, p. 586; November, 1957.

The transmission properties of new 5, 6, and 10-arm hybrid rings were described in another paper. These should be useful as power dividers. The possibility of obtaining better conjugacy properties by connecting a five and a four-arm ring tandem was also suggested.

[232] H. T. Budenbom, "Transmission properties of hybrid rings and related annuli," 1957 IRE National Convention Record, pt. 1, pp. 186–190.

The development of a strip-line hybrid which maintains a high degree of isolation over a two to one frequency band was also reported.

[233] H. G. Pascalar, "Strip line hybrid junction," IRE Trans. on Microwave Theory and Techniques, vol. MTT-5, pp. 23–30; January, 1957.

Phase errors in a magic-tee were analyzed mathematically and measurements of linearity made.

[234] R. M. Vaillancourt, "Errors in a magic-tee phase changer," IRE Trans. on Microwave Theory and Techniques, vol. MTT-5, pp. 204–207; July, 1957.

Other papers involving hybrid junctions for specialized purposes are listed in other sections of this report.

Microwave Components

Gyromagnetic devices for use in microwave circuits and the theory and measurement of their characteristics received considerable attention.

An analysis of n-wire, ferrite-loaded transmission line having potential symmetry was given in one paper. The results are valid for thin wires and thin ferrite rods. An eight-wire-line *circulator* was evaluated on the basis of the theory.

[235] H. Boyet and H. Seidel, "Analysis of nonreciprocal effects in an n-wire, ferrite-loaded transmission line," Proc. IRE, vol. 45, pp. 491–495; April, 1957.

Another analytical paper developed the scattering matrices of cascaded two and four-port waveguide structures in terms of the scattering matrices of the component sections. Particular attention was given to ferrite-loaded directional couplers and to the conditions under which multi-element structures may function as circulators.

[236] B. Davison, "Multi-element ferrite devices," 1957 IRE WESCON Convention Record, pt. 1, pp. 39–51.

A high-power circulator and a broad-band circulator were described in two other papers.

[237] P. A. Rizzi, "High-power ferrite circulators," IRE Trans. on Microwave Theory and Techniques, vol. MTT-5, pp. 230–237; October, 1957.

[238] E. A. Ohm, "A broad-band microwave circulator," *Bell Labs. Record*, vol. 35, pp. 293–297; August, 1957.

Circle averaging techniques were suggested for application to the measurement of the scattering parameters of nonreciprocal two-ports.

[239] H. M. Altschuler, "Nonreciprocal two-port measurement based on an averaging technique," Proc. IRE, vol. 45, p. 1293; September, 1957.

Ferrite *isolators*, *phase shifters*, *switches* and *circular polarizers* were described in the following papers:

[240] S. Weisbaum and H. Boyet, "Field displacement isolators at 4, 6, 11, and 24 kmc," IRE Trans. on Microwave Theory and Techniques, vol. MTT-5, pp. 194–198; July, 1957.

[241] S. Hayasi, "Figure of merit of resonance-type isolator," Proc. IRE, vol. 45, pp. 1418–1419; October, 1957.

[242] B. J. Duncan, L. Swern, K. Tomiyasu, and J. Hannwacker, "Design considerations for broad-band ferrite coaxial line isolators," Proc. IRE, vol. 45, pp. 483–490; April, 1957.

[243] M. Sucher and H. J. Carlin, "Coaxial line non-reciprocal phase shifters," *J. Appl. Phys.*, vol. 28, pp. 921–922; August, 1957.

[244] S. Wenglin, "The principle of non-gyromagnetic ferrite phase-shifter," 1957 IRE National Convention Record, pt. 1, pp. 288–290.

[245] F. Reggia and E. G. Spencer, "A new technique in ferrite phase shifting for beam scanning of microwave antennas," Proc. IRE, vol. 45, pp. 1510–1517; November, 1957.

[246] S. Sensiper, "Microwave ferrite phase shifter," Proc. IRE, vol. 45, p. 359; March, 1957.

[247] G. S. Uebele, "High-speed ferrite microwave switch," 1957 IRE National Convention Record, pt. 1, pp. 227–234.
[248] J. P. Vinding, "Ferrite switches in radar duplexers," 1957 IRE WESCON Convention Record, pt. 1, pp. 71–76.
[249] H. S. Kirschbaum and S. Chen, "A method of producing broad-band circular polarization employing an anisotropic dielectric," IRE Trans. on Microwave Theory and Techniques, vol. MTT-5, pp. 199–203; July, 1957.

Fast-acting mechanical switches involving novel features were developed too.

[250] H. H. Weichardt, "Fast acting microwave switch," 1957 IRE National Convention Record, pt. 1, pp. 222–226.
[251] W. E. Fromm, S. H. Klug, and K. S. Packard, "Precision high-speed microwave switch," 1957 IRE National Convention Record, pt. 1, pp. 219–221.

Coaxial cable and waveguide *power dividers* investigations were reported. Broad-band response in a coaxial divider was obtained by making the input reflection coefficient and its derivative equal to zero. Any degree of power split was feasible by the design process which was outlined.

[252] J. Reed and G. Wheeler, "A broadband fixed coaxial power divider," 1957 IRE National Convention Record, pt. 1, pp. 177–181.

Two broad-band, short-slot hybrid junctions were used in a variable-ratio power divider for rectangular waveguides. This device may also be used to couple two frequencies into one output.

[253] W. L. Teeter and K. R. Bushore, "A variable-ratio microwave power divider and multiplexer," IRE Trans. on Microwave Theory and Techniques, vol. MTT-5, pp. 227–229; October, 1957.

A new type of power divider designed for use in antenna feeding systems was reported and four classes of dividers for various division ratios were discussed.

[254] T. G. Hame, "Waveguide power dividers," *Electronic Eng.*, vol. 29, pp. 368–373; August, 1957.

There are three principal types of *duplexers:* 1) branching, 2) polarization twist, and 3) balanced. The balanced type is inherently suited to broad-band use. The operation of balanced duplexers employing hybrid junctions as directional couplers was discussed in the following paper:

[255] C. W. Jones, "Broad-band balanced duplexers," IRE Trans. on Microwave Theory and Techniques, vol. MTT-5, pp. 4–12; January, 1957.

Other duplexers developed include a wide-band slab type and a high-power waveguide type utilizing 3-db directional couplers in cascade.

[256] P. Bouvier, "Wide-band duplexer for decimeter-wave aerials," *Ann. Radioélect.*, vol. 12, pp. 315–329; October, 1957.
[257] L. Milosevic, "High power duplexers," *Vide*, vol. 12, pp. 109–116; January/February, 1957.

Waveguide *loads* for high powers were studied too.

[258] V. Hlubuček, "Theoretical analysis of the design of a waveguide load for high powers," *Slaboproudý Obzor*, vol. 18, pp. 420–425; July, 1957.

Resonators and Filters

A number of papers appeared on the subjects of resonators and filters. The following are representaitve of the papers on resonators and related components.

[259] H. E. Bussey and L. A. Steinert, "An exact solution for a cylindrical cavity containing a gyromagnetic material," Proc. IRE, vol. 45, pp. 693–694; May, 1957.
[260] A. E. Karbowiak, "The concept of heterogeneous surface impedance and its application to cylindrical cavity resonators," *Proc. IEE*, Monogram 246R; June, 1957. Also *Proc. IEE*, vol. 105, pt. C, pp. 1–12; March, 1958.
[261] W. A. Gerard, "Reference cavity design considerations," IRE Trans. on Microwave Theory and Techniques, vol. MTT-5, pp. 148–152; April, 1957.
[262] C. M. Crain and C. E. Williams, "Method of obtaining pressure and temperature insensitive microwave cavity resonators," *Rev. Sci. Instr.*, vol. 28, pp. 620–623; August, 1957.
[263] G. N. Rapoport, "Measurement of the intensity of the electric field in cavity resonators by means of the resonant frequency-shift with insertion of a dielectric probe," *Radiotekhnika*, vol. 12, pp. 51–58; February, 1957.
[264] A. Redhardt, "An iterative process for the calculation of electromagnetic fields," *Arch. Elekt. Übertragung*, vol. 11, pp. 227–229; June, 1957.
[265] R. N. Ghose, "Excitation of higher order modes in spherical cavities," IRE Trans. on Microwave Theory and Techniques, vol. MTT-5, pp. 18–22; January, 1957.
[266] R. N. Ghose, "Exponential transmission lines as resonators and transformers," IRE Trans. on Microwave Theory and Techniques, vol. MTT-5, pp. 213–217; July, 1957.
[267] H. J. Riblet, "General synthesis of quarter-wave impedance transformers," IRE Trans. on Microwave Theory and Techniques, vol. MTT-5, pp. 36–43; January, 1957.

Ring type resonant circuits and re-entrant type filter circuits are increasing in importance. The ring circuit has the interesting capacity to resonate with unidirectional progressive waves when directionally coupled to the main guide. When nondirectionally coupled, the ring behaves like an ordinary cavity with standing waves.

[268] F. J. Tischer, "Resonance properties of ring circuits," IRE Trans. on Microwave Theory and Techniques, vol. MTT-5, pp. 51–56; January, 1957.
[269] K. Tomiyasu, "Effect of a mismatched ring in a traveling-wave resonant circuit," IRE Trans. on Microwave Theory and Techniques, vol. MTT-5, p. 267; October, 1957.
[270] J. M. C. Dukes, "Re-entrant transmission-line filter using printed conductors," *Proc. IEE*, Paper 2444R; November, 1957. Also *Proc. IEE*, vol. 105, pt. B, pp. 173–181; March, 1958.

A number of papers on other microwave filters appeared. The most noteworthy of those reviewed were probably those on circularly polarized microwave cavity filters.

[271] C. E. Nelson, "Circularly polarized microwave cavity filters," IRE Trans. on Microwave Theory and Techniques, vol. MTT-5, pp. 136–147; April, 1957.
[272] C. E. Nelson and W. L. Whirry, "Development of circularly polarized microwave cavity filters," 1957 IRE National Convention Record, pt. 1, pp. 191–196.
[273] H. Seidel, "Synthesis of a class of microwave filters," IRE Trans. on Microwave Theory and Techniques, vol. MTT-5, pp. 107–114; April, 1957.
[274] S. B. Cohn, "Direct-coupled-resonator filters," Proc. IRE, vol. 45, pp. 187–196; February, 1957.
[275] R. Bawer and G. Kefalas, "A modified equal-element band-pass filter," IRE Trans. on Microwave Theory and Techniques, vol. MTT-5, pp. 175–184; July, 1957.
[276] F. Shnurer, "Design of aperture-coupled filters," IRE Trans. on Microwave Theory and Techniques, vol. MTT-5, pp. 238–243; October, 1957.
[277] H. Yanai and J. Hamasaki, "*M*-derived waveguide filter," *J. Inst. Elec. Comm. Engrs. Japan*, vol. 39, pp. 1029–1035; December, 1956.
[278] K. Kuroda, "An experiment on a wide-band coaxial filter," *J. Inst. Elec. Comm. Engrs. Japan*, vol. 40, pp. 805–807; July, 1957.
[279] R. A. Van Patten, "Design of imposed low-pass filters using strip-line structures," 1957 IRE National Convention Record, pt. 1, pp. 197–207.

III. Measurements

Advances in microwave measurements were for the most part refinements and extensions of proven techniques and the application of these techniques to new situations. The areas of greatest advance appear to be those of absolute measurement of microwave power, the measurement of noise power, and the measurement of properties of ferromagnetic materials at microwave frequency.

Power Measurement

The absolute measurement of power was the subject of several studies. A new electron-beam technique for measuring either cw or pulse power flow in waveguides was described. The technique consisted of passing an electron beam transversely through an evacuated section of TE_{10}-mode waveguide. Electron transit time is adjusted so that the gain of energy of the electrons from the microwave field is a maximum. The energy gain is measured by means of a dc stopping potential which can be related to the field. The instrument appears to have considerable value for measuring or monitoring high power levels without disturbing the power being measured.

[280] H. A. Thomas, "Microwave power measurements employing electron beam techniques," Proc. IRE, vol. 45, pp. 205–211; February, 1957.

A similar technique for measuring or monitoring the microwave power in a coaxial structure was reported. Part of a coaxial line forms a diode. When power is fed along the line, the potential difference which is developed between the inner and outer conductors is a measure of the power.

[281] W. J. Hoskins, "Microwave power measurements employing electron beam techniques," Proc. IRE, vol. 45, p. 1285; September, 1957.

A new high-power wattmeter of the calorimetric type was developed. Superiority in accuracy, sensitivity, simplicity of construction, and operation to the conventional water-flow meter was claimed.

[282] A. Macpherson, "An absolute microwave wattmeter," Proc. IRE, vol. 45, pp. 688–689; May, 1957.

An instrument, consisting of a thin metallic rod suspended inside a rectangular TE_{011} cavity, was described for the absolute measurement of low-level microwave power. The oscillating system receives periodic impulses via the electromagnetic field by periodically interrupting the flow of power from the source. An error of less than ± 2 per cent in the 5–100 mw range was claimed.

[283] A. L. Cullen and H. A. French, "An instrument for the absolute measurement of low-level microwave power in the 3-cm band," *Proc. IEE*, vol. 104, pt. C, pp. 454–464; September, 1957.

Bolometers were the object of several studies.

[284] J. A. Lane, "Measurements of efficiency of bolometer and thermistor mounts by impedance methods," *Proc. IEE*, vol. 104, pt. B, pp. 485–486; September, 1957.

[285] E. Archbold, "An evaporated gold bolometer," *J. Sci. Instr.*, vol. 34, pp. 240–242; June, 1957.

[286] A. M. Bonch-Bruevich and Y. A. Imas, "Some problems in the application of semiconductor bolometers," *Radiotekhnika i Elektronika*, vol. 2, pp. 317–322; March, 1957.

[287] H. Rieck and F. Panniger, "A new thermistor power-measuring head for $\lambda = 9$–20 cm," *Nachr. Tech.*, vol. 7, pp. 101–104; March, 1957.

[288] V. N. Bogomolov, Y. V. Ilisavski, M. Kornfel'd, L. S. Sochava, and R. I. Strunin, "Low-inertia germanium bolometers," *Zh. Tekh. Fiz.*, vol. 27, pp. 213–215; January, 1957.

A very interesting combination of a cathode-ray type tube and a traveling-wave type tube to produce a wide-band display device was described. The brightness at the screen is a function of the microwave power input.

[289] D. E. George, "The wamoscope—a microwave display device," *Sylvania Technologist*, vol. 10, pp. 5–7; January, 1957.

A closely related study on high-frequency oscillography was reported in the following paper.

[290] H. Maeda, "Waveform observation of electron current using traveling-wave cathode-ray tubes," *J. Inst. Elec. Comm. Engrs. Japan*, vol. 40, pp. 1171–1177; November, 1957.

The measurement of noise in masers and the spectral distribution of thermal noise in a gas discharge were discussed in the following papers:

[291] J. C. Helmer, "Maser noise measurement," *Phys. Rev.*, vol. 107, pp. 902–903; August 1, 1957.

[292] S. M. Bergmann, "Spectral distribution of thermal noise in a gas discharge," IRE Trans. on Microwave Theory and Techniques, vol. MTT-5, pp. 237–238; October, 1957.

A rapid and simple means of measuring wide range of RF power was described.

[293] J. Swift, "A microwave power monitor," *Proc. IRE Australia*, vol. 17, pp. 424–428; December, 1956.

The radiometer, which is a receiving equipment designed to measure noise power to a high degree of accuracy, was the subject of several papers.

[294] G. R. Nicoll, "The measurement of thermal and similar radiations at millimetre wavelengths," *Proc. IEE*, vol. 104, pt. B, pp. 519–527; September, 1957.

[295] J. C. Greene, "Stability requirements and calibration of radiometers when measuring small noise powers," Proc. IRE, vol. 45, pp. 359–360; March, 1957.

[296] L. D. Strom, "The theoretical sensitivity of the Dicke Radiometer," Proc. IRE, vol. 45, pp. 1291–1292; September, 1957.

[297] R. N. Whitehurst, F. H. Mitchell, and J. Copeland, "A calibration procedure for microwave radiometers," Proc. IRE, vol. 45, pp. 1410–1411; October, 1957.

[298] W. H. Ward, "Two portable thermistor radiometers," *J. Sci. Instr.*, vol. 34, pp. 317–321; August, 1957.

A simple bridge method for the absolute calibration of attenuators at the frequency of operation was outlined. The method uses microwave and electronic apparatus which is usually available in microwave laboratories.

[299] E. Laverick, "The calibration of microwave attenuators by an absolute method," IRE Trans. on Microwave Theory and Techniques, vol. MTT-5, pp. 250–254; October, 1957.

The disadvantages of attenuators with transversely moved vanes and T-network attenuators were also discussed and a rotary attenuator was described which is not frequency sensitive and which has a constant phase shift up to a certain limit.

[300] R. Steinhart, "A microwave attenuator which is not frequency sensitive and has a constant phase shift within very wide limits," *Nachrich. Z.* vol. 10, pp. 294–297; June, 1957.

Impedance and Frequency Measurement

A number of papers appeared on impedance measurement with transmission lines. These papers were of the nature of refinements of established techniques. The following list is representative of those reviewed.

[301] L. Lewin, "A contribution to the theory of probes in waveguides," *Proc. IEE*, Monogram 259R; October, 1957. Also *Proc. IEE*, vol. 105, pt. C, pp. 109–116; March, 1958.
[302] D. R. Frankl, "Resistance of a partially short-circuited conducting slab," PROC. IRE, vol. 45, pp. 877–878; June, 1957.
[303] D. Dettinger, "Advantages of expressing standing-wave-ratio in decibels," IRE TRANS. ON MICROWAVE THEORY AND TECHNIQUES, vol. MTT-5, p. 218; July, 1957.
[304] F. J. Charman, "V. H. F. line measurements," *Electronic Eng.*, vol. 29, pp. 499–503; October, 1957.
[305] E. M. Williams and J. H. Foster, "Standing-wave line for uhf measurements of high-dielectric constant materials," IRE TRANS. ON INSTRUMENTATION, vol. I–6, pp. 210–213; September, 1957.
[306] R. Mittra, "An automatic phase-measuring circuit at microwaves," IRE TRANS. ON INSTRUMENTATION, vol. I–6, pp. 238–240; December, 1957.
[307] R. Müller, "Measurement of the circuit impedance of slow-wave structures," *Onde Electr.*, vol. 37, pp. 128–135; February, 1957.
[308] R. W. Beatty, "An adjustable sliding termination for rectangular waveguide," IRE TRANS. ON MICROWAVE THEORY AND TECHNIQUES, vol. MTT-5, pp. 192–194; July, 1957.

The measurement of the dielectric and/or magnetic properties of ferromagnetic and paramagnetic materials was a subject of considerable interest.

[309] L. A. Ault, E. G. Spencer, and R. C. LeCraw, "Circularly polarized traveling wave cavity for ferrite tensor permeability measurements," 1957 IRE NATIONAL CONVENTION RECORD, pt. 1, pp. 282–287.
[310] W. Von Aulock and J. H. Rowen, "Measurement of dielectric and magnetic properties of ferromagnetic materials at microwave frequencies," *Bell Sys. Tech. J.*, vol. 36, pp. 427–448; March, 1957.
[311] B. M. Bowie, "Microwave dielectric properties of solids for applications at temperatures to 300°F," 1957 IRE NATIONAL CONVENTION RECORD, pt. 1, pp. 270–281.
[312] G. Feher, "Sensitivity considerations in microwave paramagnetic resonance absorption techniques," *Bell Sys. Tech. J.*, vol. 36, pp. 449–484; March, 1957.
[313] H. K. Ruppersberg, "Method of measurement to determine the complex dielectric constant at wavelengths from 8 to 80 cm and temperatures to −150°C," *Z. Angew Phys.*, vol. 9, pp. 9–13; January, 1957.
[314] I. Brady, "Measurement of the complex dielectric constant of very-high-dielectric-constant materials at microwave frequencies," *Commun. and Electronics*, no. 30, pp. 225–228; May, 1957.
[315] A. G. Mungall and J. Hart, "Measurement of the complex dielectric constant of liquids at centimetre and millimetre wavelengths," *Can. J. Phys.*, vol. 35, pp. 995–1003; September, 1957.

Time and frequency measurements, and the frequency stabilization of sources received some attention. The molecular oscillator as a frequency or time standard is probably the most noteworthy development in this area.

[316] C. H. Townes, "Recent developments in measurement of time," *Nuovo Cim.*, vol. 5, supplement, No. 1, pp. 222–229; 1957.
[317] H. P. Raabe, "Measurement of instantaneous frequency with a microwave interferometer," PROC. IRE, vol. 45, pp. 30–38; January, 1957.
[318] R. C. Mackey and W. D. Hershberger, "Measurement and control of microwave frequencies by lower radio frequencies," IRE TRANS. ON MICROWAVE THEORY AND TECHNIQUES, vol. MTT-5, pp. 64–68; January, 1957.
[319] I. Goldstein, "Frequency stabilization of a microwave oscillator with external cavity," IRE TRANS. ON MICROWAVE THEORY AND TECHNIQUES, vol. MTT-5, pp. 57–62; January, 1957.
[320] M. Magid, "Broadband frequency stabilization of a reflex klystron by means of an external high Q cavity," 1957 IRE NATIONAL CONVENTIOON RECORD, pt. 1, pp. 208–218.

IV. Conclusion

In reviewing advances in microwave theory and techniques, one is impressed by the amount and quality of the published works. The field advances by the close interplay of physics with engineering. It is a field in which the lead-time between physical discovery and engineering use has approached zero. A bright and interesting future is the promise for those in this field.

V. Acknowledgment

The assistance of Professor G. Adashko, J. C. Simon, Professor A. A. Oliner, and W. L. Pritchard in the coverage of foreign accomplishments is gratefully acknowledged.

A New Form of High-Power Microwave Duplexer*

P. D. LOMER† AND R. M. O'BRIEN‡

Summary—A new form of microwave duplexer, capable of handling twice as much power as an equivalent balanced duplexer is described. It consists of a microwave bridge circuit and a power-sensitive half-wavelength phase shifter. A simple gas-discharge tube is used in the phase shifter, which changes the length in one arm of the bridge circuit by a half-wavelength for high-power and low-power microwave pulses, respectively.

The performance of one form of phase-shift duplexer has been measured over a frequency range from 8500 mc to 10,000 mc. The vswr is less than 1:2 and the receiver isolation is greater than 30 db over most of the waveband. This is comparable to the performance of a balanced duplexer using the same components. The power handling capacity of the phase-shift duplexer is intrinsically twice as great as that of the balanced duplexer. For example, at a wavelength of 3 cm the phase-shift duplexer will operate unpressurized at a peak power level of 200 kw with a 2:1 safety factor on breakdown, whereas performance of a balanced duplexer at this power level is marginal.

Introduction

THE FUNCTION of a microwave duplexer in a pulsed radar is to switch power, first from transmitter to antenna and then, within a few microseconds, from antenna to receiver. A rapid switching action is generally achieved with gas discharge devices ionized by the microwave power from the transmitter.

Two methods of using TR cells in microwave circuits have been described by Smullin and Montgomery.[1] These are the branched and balanced duplexers. The balanced duplexer has advantages over the branched duplexer with respect to bandwidth and power handling; furthermore, its performance is independent of the transmitter impedance. The power handling capacity of a balanced duplexer is restricted to half that of the waveguide itself. This is due to the large standing wave existing between the gas discharge cells and the hybrid junction.

One method of improving the power handling of this type of duplexer has been described by Jones[2] and is referred to as an A-TR balanced duplexer. Standing-waves in the main waveguides are avoided with this arrangement but the bandwidth is restricted by the relatively high-Q A-TR circuits. Improvements in bandwidth may be achieved by using four or six A-TR cells but the arc loss is then two or three times as great.

The total-coupler duplexer described by Milosevic,[3] is capable of handling high powers but includes nineteen discharge tubes. However, the advantages of this form of duplexer are apparent and improvements in design will no doubt follow.

Another method of improving the power handling without increasing the number of tubes has been sought by using a microwave bridge circuit consisting of two hybrid junctions and a power-sensitive phase shifter.[4]

The principle of this method is illustrated in Fig. 1. The transmitter is connected to arm 1 of the first hybrid junction, so that the power splits equally into arms 3 and 4. If the path lengths from the first to the second junction are equal, then the power will pass into arm 7, which is connected to the antenna. If the total path length from arm 6 to 3 is now increased by one half-wavelength, power entering arm 7 from the antenna, after dividing into arms 5 and 6 will recombine into arm 2, the receiver. A method of increasing the electrical path length for low-power signals with respect to that for high-power signals has been devised. This phase shifter, together with its application in a phase-shift duplexer, is described.

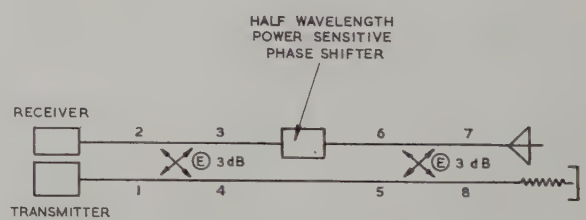

Fig. 1—Principle of the phase-shift duplexer.

The Power-Sensitive Half-Wavelength Phase Shifter

Principle

The power-sensitive half-wavelength phase shifter is a waveguide device which provides path lengths differing by a half-wavelength for high-power and low-power microwave pulses. It consists of a hybrid junction, which is used in conjunction with two gas discharge tubes. Metal shorting plates are placed an effective quarter-wavelength behind these switches. The principle is shown in Fig. 2, where gas discharge tubes are placed across arms 3 and 4 of a hybrid junction. A

* Manuscript received by the PGMTT, July 8, 1957; revised manuscript received, January 17, 1958.

† Services Electronics Res. Lab., Baldock, Herts., Eng.
‡ Watton Eng. Co., Welwyn Garden City, Eng.; formerly with Services Electronics Res. Lab., Baldock, Herts., Eng.

[1] L. D. Smullin and C. G. Montgomery, "Microwave Duplexers," M.I.T. Rad. Lab. Ser., McGraw-Hill Book Co., Inc., New York, N. Y., vol. 14; 1948.

[2] C. W. Jones, "Broadband balanced duplexers," IRE TRANS. ON MICROWAVE THEORY AND TECHNIQUES, vol. MTT-5, pp. 4–12; January, 1957.

[3] L. Milosevic, "Duplexeurs a grande puissance," *Le Vide*, vol. 67, pp. 109–116; January/February, 1957.

[4] C. L. Hogan, "The ferromagnetic Faraday effect at microwave frequencies and its applications—the microwave gyrator," *Bell Sys. Tech. J.*, vol. 31, pp. 1–31; January, 1952. A duplexer is described here which is similar in principle to the phase-shift duplexer; a directional phase-shifter of ferrite is used instead of the half-wavelength power-sensitive phase shifter.

high-power microwave pulse entering at arm 1 is divided equally between arms 3 and 4 by the hybrid junction and ionizes the gas discharge tubes. The pulse is then reflected and if the tubes are placed correctly with respect to the hybrid, all the power will pass into arm 2. Similarly a low-power microwave pulse, insufficient to ionize the discharge tube will be reflected by the metal short circuits and will pass into arm 2. However, the total electrical length of the device will be a half-wavelength longer for a low-power pulse than for a high-power pulse.

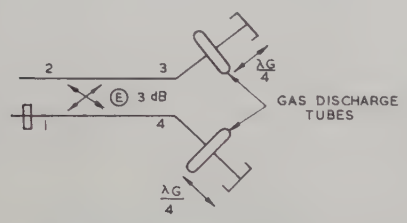

Fig. 2—Principle of the half-wavelength power-sensitive phase shifter.

The Hybrid Junction and Discharge Tube

The principle of the half-wavelength phase shifter has been established experimentally at a wavelength of 3 cm. A 3 db directional coupler, known as a binomial-slot hybrid[5] has been selected as a convenient form of hybrid junction for the phase shifter. It is a branched waveguide directional coupler with five branched waveguides, the voltage coupling coefficients of which are arranged according to the coefficients of a binomial series, as shown in Fig. 3. The voltage coupling is such that power divides equally into arms 3 and 4, there being a 90 degree phase difference between the fields in the two waveguides. Thus if an electrical short circuit is placed across any plane at right angles to arms 3 and 4, all the power entering arm 1 will be reflected into arm 2.

The high-power switching is achieved with a gas discharge tube shown in Fig. 4. This consists of a silica tube containing a gas filling, optimized for low microwave breakdown and arc loss. The tube, which is transparent to low-power microwave pulses, is mounted parallel to the E field across the center of the waveguide. A high-power microwave pulse will ionize the gas in the tube placing an effective short circuit across the waveguide. Loss of power by radiation along the axis of the tube is prevented by means of microwave chokes.

The geometrical configuration of the binomial-slot hybrid is such that a common tube may be used for both arms of the phase-shifter. This is shown in Fig. 5. In this phase shifter a microwave choke is also used to prevent interaction from one waveguide to the other by conduction along the discharge tube.

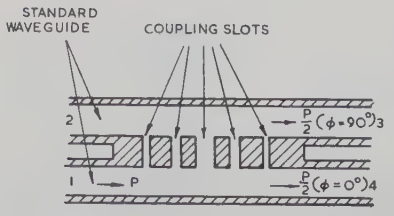

Fig. 3—Binomial-slot hybrid.

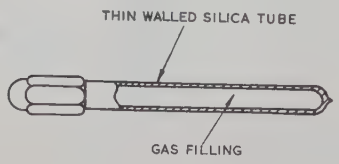

Fig. 4—Gas discharge tube.

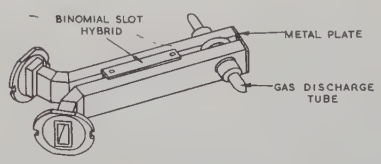

Fig. 5—A power-sensitive phase shifter for the 3-cm waveband.

A Phase-Shift Duplexer for the 3-cm Waveband

Description

One form of phase-shift duplexer has been designed for use at a wavelength of 3 cm. The duplexer, which is composed of four binomial-slot hybrids is shown diagrammatically in Fig. 6. Power from the transmitter, incident on arm 1 of hybrid *A*, divides equally into hybrids *B* and *C*. The former is the phase shifter and the latter a balancing hybrid. From *B* and *C*, the power recombines into the antenna on arm 8 of *D*. On the other hand, incident power from the antenna travels an extra half-wavelength through the phase shifter and hence recombines into the receiver on arm 2 of hybrid *A*. The purpose of the balancing hybrid is to maintain symmetry through the system and hence extend the over-all bandwidth.

One advantage of the binomial-slot hybrid is that it facilitates the use of a common discharge tube for both arms of the phase shifter. This is technically important in that it insures a common position of electrical short circuit for both arms of the phase shifter. Another advantage is that it can be constructed by milling and this enables the whole duplexer to be machined in a single block of metal. A method of doing this is indicated in Fig. 7. Alternatively, the binomial-slot hybrid may be used in conjunction with the short-slot hybrid,[6] in which the narrow walls of the waveguide are adjacent. Power is coupled through a short slot cut in the common walls of the two waveguides. The performance of

[5] P. D. Lomer and J. W. Crompton, "A new form of hybrid junction for microwave frequencies," *Proc. IEE*, vol. 103, pt. B, pp. 261–264; May, 1957.

[6] H. J. Riblet, "The short-slot hybrid junction," Proc. IRE, vol. 40, pp. 180–184; February, 1952.

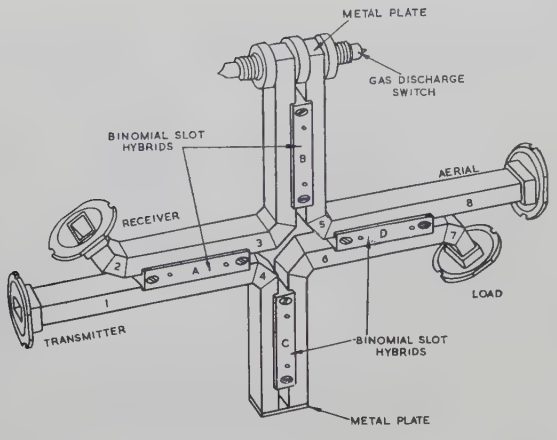

Fig. 6—An experimental phase-shift duplexer for the 3-cm waveband.

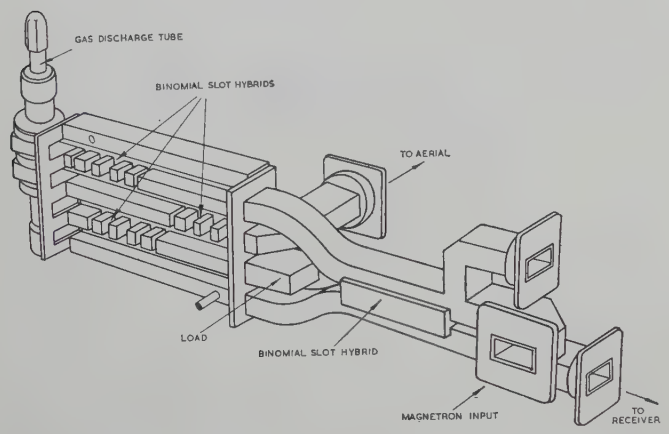

Fig. 7—A phase-shift duplexer milled out of a solid block of metal

this junction is similar to that of the binomial-slot hybrid and the two are in effect complementary. If hybrids *A* and *D* of the duplexer are short-slot hybrids and hybrids *B* and *C* are binomial-slot hybrids, a very compact design may be achieved as shown in Fig. 8.

Performance

Performance data have been obtained from an experimental duplexer in waveguide W.G.16 (0.9×0.4 inch ID) of the type shown in Fig. 6. Measurements were made over a frequency range from 8500 mc to 10,000 mc. The important properties of the duplexer are its impedance in both the transmitting and receiving conditions, the isolation between the transmitter and receiver, and the insertion loss during transmission and reception. Another property, the recovery time, is determined by the characteristics of the gas discharge tube.

The impedance is measured in terms of the voltage standing wave ratio (vswr) which is determined by the reflections from the binomial-slot hybrids and the waveguide corners. The binomial-slot hybrid reflects very little power at the center of the band, from 9000 to 9500 mc and since the waveguide corners are also good over this range the vswr of the complete duplexer is less than 1.1.

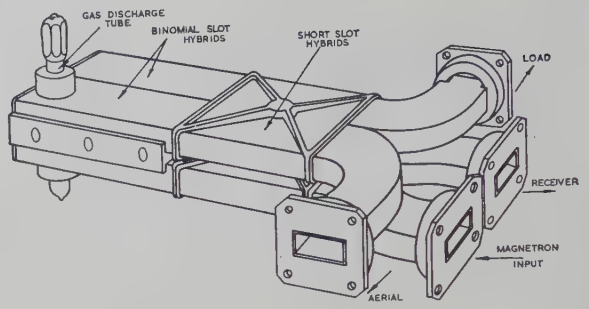

Fig. 8—A phase-shift duplexer using short-slot hybrids and binomial-slot hybrids.

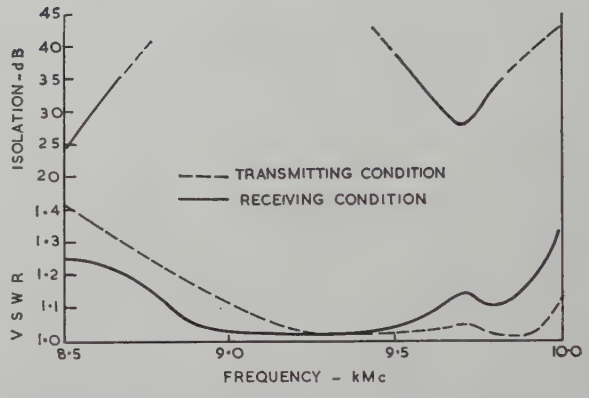

Fig. 9—Performance data for the experimental phase-shift duplexer.

Over most of the 15 per cent frequency band, the vswr is less than 1.2 as shown in Fig. 9.

The isolation between transmitter and receiver is determined by the directivity of the first hybrid *A*. It is modified however by any reflections which enter the receiver arm from the rest of the duplexer. For example, a vswr of 1.1 may limit the receiver isolation to 26 db. The experimental results of isolation against frequency are given in Fig. 9.

Although reflections within the duplexer affect the isolation, reflections from the antenna pass directly into the transmitter arm. In this respect, the phase-shift duplexer differs from the ferrite circulator, in which antenna reflections go into the receiver arm.

The insertion loss of the complete duplexer is less than 0.5 db over the 15 per cent band.

The performance of the duplexer at high power levels has been determined by measurements at a frequency of 9475 mc. The loss in the discharge tube is of the order of 0.2 db. The position of the effective electrical short circuit of the tube is independent of power level so that the performance of the complete duplexer does not depend on the peak power. Measurements on a phase-shifter alone have shown that it will withstand peak power up to 200 kw with the waveguide unpressurized. This corresponds to a power handling of 400 kw for the complete unpressurized phase-shift duplexer. The recovery time of the duplexer is defined as the time after the transmitted pulse for the attenuation between an-

tenna and receiver to drop to 3 db. This is determined by the rate of change of electron temperature and electron density in the afterglow of the discharge. In conventional duplexers, the effect of the afterglow on attenuation is the only important factor, but with the phase-shift duplexer, the phase of the signal is also important. However, measurements have shown that with this gas discharge tube, the recovery time of both phase shift and attenuation are similar. The recovery time of the duplexer is of the order of 5 to 10 μsec to an attenuation of 3 db.

Comparison with a Balanced Duplexer

In order to obtain a direct comparison between the balanced duplexer and phase-shift duplexer, the performance of a balanced duplexer consisting of two binomial-slot hybrids and the same discharge tube has been determined. The arrangement of the balanced duplexer is illustrated in Fig. 10 and its vswr in both the transmitting and receiving conditions is given in Fig. 11. The isolation provided by the second hybrid of the balanced duplexer is given in the same diagram. There is no significant difference in the low-level performance of the two forms of duplexer.

At high-power levels there is a fundamental difference in the leakage power into the receiver arms of the respective duplexers. In the case of the phase-shift duplexer, the leakage is determined by the isolation provided by the first hybrid, modified by any reflections from the phase shifter and the balancing hybrid. In general from 30 db to 50 db isolation may be achieved depending on the bandwidth required. This is equivalent to a peak power leakage of 2 to 200 watts with a 200-kw transmitter. The leakage from the balanced duplexer is a function of the discharge tube and is in the form of a spike and flat leakage.[1] This leakage is reduced by the second hybrid junction but owing to small variations in the formative time of the discharge in the two arms of the duplexer, it is difficult to achieve a greater cancellation than 15 to 20 db. In practice this means that with the duplexer described a spike leakage of about 500 watts peak will enter the receiver arm; thus, in this respect also there is no great advantage in either form of duplexer. In either case it is necessary to use a TR cell or pulsed attenuator to protect the receiver.

The great advantage of the phase-shift duplexer is its power handling ability. The switching system of the phase-shift duplexer is very similar to that of the balanced duplexer but operates at half the input power. The power incident on each section of the discharge tube is only a quarter of the transmitted power, compared to half the transmitted power for a balanced duplexer. Similarly the hybrid used in the phase shifter is handling only half the power. The first and fourth hybrids of the phase-shift duplexer handle the full power but have matched impedances on all arms. It is known that under these conditions a hybrid junction will

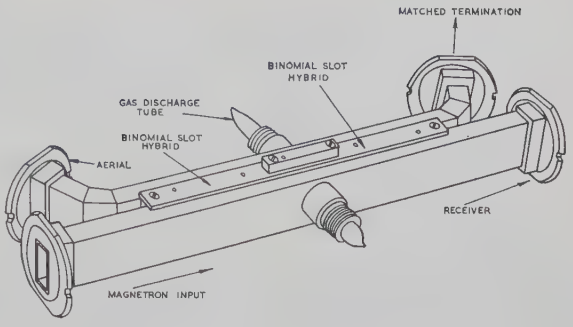

Fig. 10—A balanced duplexer with binomial-slot hybrids and gas discharge tube.

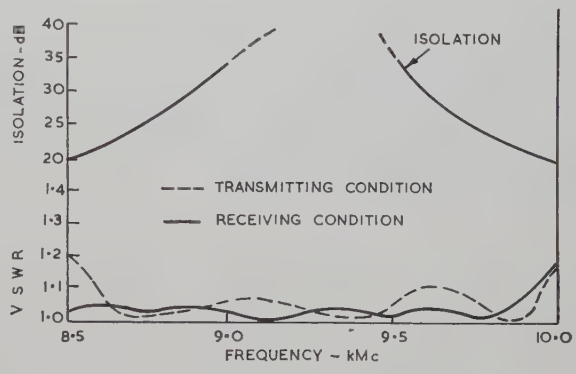

Fig. 11—Performance data for the balanced duplexer.

handle twice as much power as a hybrid with short circuits on two arms. Thus, whether the power handling capacity is limited by the hybrid junction or by the discharge tube, it is intrinsically twice as great for the phase-shift duplexer as for the balanced duplexer.

In general a balanced duplexer operating at 200 kw at a wavelength of 3 cm is working near its maximum power handling capacity and for satisfactory performance in equipment it must be pressurized. The equivalent system using a phase-shift duplexer will operate with a 2:1 safety factor at 200 kw and will not require pressurizing equipment. The advantage of the phase-shift duplexer is as great at higher power levels, since the degree of pressurizing may be reduced, and the life of the discharge tube extended.

Conclusion

The power handling capacity of a phase-shift duplexer is twice that of a balanced duplexer using the same components. The other properties of the two forms of duplexer are similar.

Acknowledgment

The authors wish to thank P. O. Hawkins for his helpful suggestions during the course of this work. Fig. 10 is reproduced by kind permission of the Research Director, Decca Radar Research Laboratories, Tolworth, England, and the paper is published by permission of the British Admiralty.

Radiation from a Rectangular Waveguide Filled with Ferrite*

G. TYRAS† AND G. HELD‡

Summary—This paper presents an approximate analytical solution to the problem of radiation from a ferrite-filled rectangular waveguide. The field distribution at the mouth of the guide is assumed to be unaffected by the termination of the guide. The vector Huygens' principle is applied to find the far-zone radiation field from the determined aperture field.

The solution to the problem is found in this manner for the cases of longitudinal and transverse magnetization of the ferrite. The transverse magnetization case is supplemented with a discussion of a specific numerical example which includes plots of the aperture field distribution and the phase angle as well as plots of the far-zone radiation field. The experimentally known phenomenon of the effect of the applied magnetic field upon the shift of the main lobe[1] is demonstrated and verified analytically.

Introduction

THE low-loss ferrite medium has been actively investigated during the past few years. Polder[2] worked out the effective properties of this medium for plane waves, and Hogan[3] has made various experimental studies of the propagation in a cylindrical guide containing ferrites. Gintsburg,[4] and Suhl and Walker[5] solved the problem of a circular waveguide completely filled with a longitudinally magnetized ferrite medium. Angelakos and Korman[1] made measurements of the radiation pattern from an open-end rectangular waveguide completely filled with a transversely magnetized ferrite.

The nature of propagation of electromagnetic energy through a magnetized ferrite medium is described by the Maxwell's equations which connect the space variations of $\boldsymbol{E}$ and $\boldsymbol{H}$ with the time variations of $\boldsymbol{D}$ and $\boldsymbol{B}$. The relation between the magnetic intensity vector, $\boldsymbol{H}$, and the magnetic induction vector, $\boldsymbol{B}$, in a ferrite medium is characterized in the form $\boldsymbol{B}=(\mu)\boldsymbol{H}$ where (μ) is the permeability tensor. The components of the permeability tensor are derived from the mathematical model which assumes a ferrite sample fully saturated in dc magnetic fields. The other assumptions made are that ac quantities in the equation of motion of the magnetization are small in comparison with the dc quantities, so that their products can be neglected and only linear terms be considered, and also that the ferrite is loss-free.

With these assumptions the permeability tensor is written in the form[2]

$$(\mu) = \begin{bmatrix} \mu & -j\kappa & 0 \\ j\kappa & \mu & 0 \\ 0 & 0 & \mu_0 \end{bmatrix} \tag{1}$$

when the applied magnetic field is along the direction of propagation (z axis) and

$$(\mu) = \begin{bmatrix} \mu & 0 & -j\kappa \\ 0 & \mu_0 & 0 \\ j\kappa & 0 & \mu \end{bmatrix} \tag{2}$$

when the direction of the applied magnetic field is transverse (along the y axis) to the direction of propagation. The components of the permeability tensor are expressed in terms of the applied magnetic field as follows:

$$\mu = \mu_0\left(1 + \frac{p\sigma}{\sigma^2 - 1}\right)$$
$$\kappa = \mu_0\left(\frac{p}{\sigma^2 - 1}\right) \tag{3}$$

where

$$\sigma = \frac{|\gamma| H_0}{\omega}; \qquad p = \frac{|\gamma| M_0}{\mu_0 \omega} \tag{4}$$

and

μ_0 = permeability of free space,
γ = magnetomechanical ratio as classified by Darrow,[6]
H_0 = applied magnetostatic field,
M_0 = dc magnetization (resulting from and directed along H_0).

The notations σ and p have been adopted in an unaltered form from Suhl and Walker.[5] It should be noted at this point that σ represents the ratio of natural precession frequency $|\gamma| H_0/2\pi$ to the carrier frequency and p is the ratio of a frequency $|\gamma| M_0/2\pi\mu_0$, associated with the saturation magnetization M_0, to the carrier

* Manuscript received by the PGMTT, July 19, 1957; revised manuscript received February 10, 1958. Presented at the Joint URSI-IRE Meeting, Washington, D. C., May 22–25, 1957.

† Pilotless Aircraft Div., Boeing Airplane Co., Seattle, Wash.
‡ Dept. of Elect. Eng., University of Washington, Seattle, Wash.

[1] D. J. Angelakos and M. M. Korman, "Radiation from ferrite-filled apertures," PROC. IRE, vol. 44, pp. 1463–1468; October, 1956.
[2] D. Polder, "On the theory of electromagnetic resonance," *Phil. Mag.*, vol. 40, pp. 99–115; January, 1949.
[3] C. L. Hogan, "The ferromagnetic Faraday effect at microwave frequencies and its applications—the microwave gyrator," *Bell Sys. Tech. J.*, vol. 31, pp. 1–31; January, 1952.
[4] A. M. Gintsburg, "Gyrotropic waveguide," *Dokl. Akad. Nauk USSR*, vol. 95, pp. 489–492; 1954.
[5] H. Suhl and L. R. Walker, "Topics in guided-wave propagation through gyromagnetic media, Part I—The completely filled cylindrical guide," *Bell Sys. Tech. J.*, vol. 33, pp. 579–597; May, 1954.
[6] K. K. Darrow, "Magnetic resonance," *Bell Sys. Tech. J.*, vol. 32, pp. 74–99; January, 1953, and pp. 384–405; March, 1953.

frequency. It is important to observe that σ and p always have the same signs; *i.e.*, when H_0 is reversed, so is the saturation magnetization. Furthermore, μ is an even function of the magnetic field whereas κ is an odd function.

Field Components in a Parallel Plane Waveguide

Longitudinal Magnetization

The case of a rectangular waveguide completely filled with a ferrite that is subjected to a steady magnetic field in the direction of propagation has been treated by several authors.[7–9] Chambers used perturbation methods to show the existence of quasi TE and TM modes and he calculated the first term of the power expansion for the fields. Suhl and Walker[8] treated the case of a limit TEM mode in a parallel plane guide. Van Trier[9] discussed the nature of the various modes that can exist in a parallel plane guide.

In this paper we shall derive explicit expressions for the various field components and the propagation constant for the case of a parallel plane waveguide. We begin with the equations derived by Kales[10] from the two Maxwell's curl-equations and the relation of (1)

$$\begin{aligned} \nabla_t^2 E_z + (k_2^2\chi - \beta^2)E_z &= -j\beta\frac{\omega\kappa\mu_0}{\mu} H_z \\ \nabla_t^2 H_z + \left(k_2^2 - \frac{\mu_0}{\mu}\cdot\beta^2\right)H_z &= j\beta\frac{\omega\epsilon\kappa}{\mu} E_z \end{aligned} \tag{5}$$

where

$$k_2 = \omega\sqrt{\epsilon\mu_0}$$

$$\chi = \frac{\mu}{\mu_0}\left(1 - \frac{\kappa^2}{\mu^2}\right)$$

and ϵ=electric inductive capacity[11] for the ferrite. The time and z-dependence of the form $\epsilon^{j(\omega t-\beta z)}$ has been assumed.

It has been shown[7–10] that fields satisfying (5) cannot be separated into the conventional TE, TM, and TEM modes. We shall, therefore, look for any unconventional mode that can propagate under these conditions.

We have to obtain an equation in terms of H_z or E_z only. This can be done by elimination of H_z and $\nabla_t^2 H_z$ or E_z and $\nabla_t^2 E_z$ between the equations of (5). Since it is more convenient to apply the boundary conditions to the electric field, we shall solve (5) for E_z, getting:

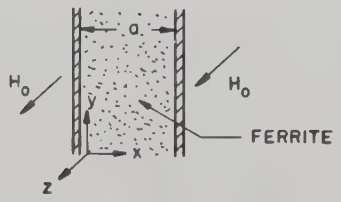

Fig. 1—Geometry of a parallel plane waveguide.

$$\nabla_t^4 E_z + \Psi\nabla_t^2 E_z + \Upsilon^2 E_z = 0 \tag{6}$$

where

$$\Psi = (\chi + 1)k_2^2 - \left(\frac{\mu_0}{\mu} + 1\right)\beta^2 \tag{7}$$

$$\Upsilon = \left[\chi k_2^4 - 2\,k_2^2\beta^2 + \frac{\mu_0}{\mu}\beta^4\right]^{1/2}. \tag{8}$$

Eq. (6) is a fourth-order partial differential equation which cannot be solved in the Cartesian coordinate system by the method of separation of variables. Solution is possible, however, in the case of a parallel plane waveguide where $\partial/\partial y = 0$. In such a case we get

$$\frac{d^4E_z}{dx^4} + \Psi\frac{d^2E_z}{dx^2} + \Upsilon^2 E_z = 0. \tag{9}$$

The other field components can be found to be

$$E_x = j\beta\int E_z dx \tag{10}$$

$$E_y = \frac{\mu}{\beta\kappa}\left[\frac{dE_z}{dx} + M\int E_z dx\right] \tag{11}$$

$$H_x = -\frac{1}{\omega\kappa}\left[\frac{dE_z}{dx} + N\int E_z dx\right] \tag{12}$$

$$H_y = j\omega\epsilon\int E_z dx \tag{13}$$

$$H_z = \frac{j\mu}{\beta\omega\kappa\mu_0}\left[\frac{d^2E_z}{dx^2} + ME_z\right] \tag{14}$$

where

$$M = \chi k_2^2 - \beta^2; \qquad N = \frac{\mu}{\mu_0}k_2^2 - \beta^2. \tag{15}$$

Eq. (9) describes the longitudinal component of the electric field in a longitudinally magnetized ferrite medium between two parallel planes. We shall choose the coordinate system as shown in Fig. 1.

The appropriate boundary conditions are

$$E_z = 0$$

$$\frac{dE_z}{dx} + M\int E_z dx = 0 \tag{16}$$

on the boundaries $x=0$ and $x=a$.

A solution to (9) will depend upon whether the quantity $(\Psi/2)^2 - \Upsilon^2$ is positive or negative. By going

[7] L. G. Chambers, "Propagation in a ferrite-filled waveguide," *Quart. J. Mech. Appl. Math.*, vol. 8, pp. 435–447; December, 1955.

[8] H. Suhl and L. R. Walker, "Topics in guided-wave propagation through gyromagnetic media, Part III—Perturbation theory and miscellaneous results," *Bell Sys. Tech. J.*, vol. 33, pp. 1133–1194; September, 1954.

[9] A. A. Van Trier, "Guided electromagnetic waves in anisotropic media," *Applied Sci. Res.*, sec. B, vol. 3, no. 4, 5; 1953.

[10] M. L. Kales, "Modes in waveguides containing ferrites," *J. Appl. Phys.*, vol. 24, pp. 604–608; May, 1953.

[11] J. A. Stratton, "Electromagnetic Theory," McGraw-Hill Book Co., Inc., New York, N. Y., p. 10, 1941.

back to the original definitions of μ, κ, and χ, it can be shown that

$$\left(\frac{\Psi}{2}\right)^2 - \Upsilon^2 = \frac{p^2}{4(1-\sigma p-\sigma^2)^2} \cdot\left\{[(\sigma+p)k_2^2 - \sigma\beta^2]^2 + 4k_2^2\beta^2\right\}, \quad (17)$$

hence the expression is a positive definite. Therefore we have to consider one case only, namely

$$\left(\frac{\Psi}{2}\right)^2 - \Upsilon^2 > 0.$$

A general solution to (9) can now be written in the form

$$E_z = C_1 \cos \rho_1 x + C_2 \sin \rho_1 x + C_3 \cos \rho_2 x + C_4 \sin \rho_2 x \quad (18)$$

where

$$\rho_{1,2} = \sqrt{\frac{\Psi}{2} \pm \sqrt{\left(\frac{\Psi}{2}\right)^2 - \Upsilon^2}}. \quad (19)$$

After the boundary conditions of (16) are evaluated and the determinant of the coefficients is set equal to zero to obtain a unique solution for the constants C_1 through C_4, the following condition is obtained

$$2\left(\rho_1 - \frac{M}{\rho^1}\right)\left(\rho_2 - \frac{M}{\rho_2}\right)(1 - \cos \rho_1 a \cos \rho_2 a) = \left[\left(\rho_1 - \frac{M}{\rho_1}\right)^2 + \left(\rho_2 - \frac{M}{\rho_2}\right)^2\right] \sin \rho_1 a \sin \rho_2 a. \quad (20)$$

The above relation will be satisfied if we choose ρ_1 and ρ_2 such that

$$\rho_1 = \frac{m\pi}{a}; \qquad \rho_2 = \frac{n\pi}{a} \quad (21)$$

where m and n are two integers,[12] $m \neq n$, both simultaneously odd or even. As a result of this, the constants separate into two independent groups, namely

$$C_3 = -C_1 \quad (22)$$

and

$$C_4 = -\frac{\rho_2}{\rho_1}\left(\frac{\rho_1^2 - M}{\rho_2^2 - M}\right) C_2. \quad (23)$$

Evidently the solution can be written in one of the two ways

$$E_z = C(\cos \rho_1 x - \cos \rho_2 x) e^{j(\omega t - \beta z)} \quad (24)$$

or

$$E_z = C\left(\sin \rho_1 x - \frac{\rho_2(\rho_1^2 - M)}{\rho_1(\rho_2^2 - M)} \sin \rho_2 x\right) e^{j(\omega t - \beta z)}. \quad (25)$$

Since these two solutions are independent of each other, this seems to suggest that the modes in the ferrite can be separated into two independent groups. It will be shown later that the first group represented by (24) goes over to the usual form of TE mode and the second group represented by (25) goes over to the usual form of TM mode when the external magnetostatic field is removed. We shall, therefore, call the first group a quasi TE mode and the second group a quasi TM mode which is in agreement with the conclusions arrived at by other authors.[4,5,7,9]

The remaining field components can now be written as follows:

Quasi TE mode

$$E_x = j\beta C\left\{\frac{\sin \rho_1 x}{\rho_1} - \frac{\sin \rho_2 x}{\rho_2}\right\} \quad (26)$$

$$E_y = -\frac{\mu}{\beta\kappa} C\left\{(\rho_1^2 - M)\frac{\sin \rho_1 x}{\rho_1} - (\rho_2^2 - M)\frac{\sin \rho_2 x}{\rho_2}\right\} \quad (27)$$

$$H_x = \frac{C}{\kappa\omega}\left\{(\rho_1^2 - N)\frac{\sin \rho_1 x}{\rho_1} - (\rho_2^2 - N)\frac{\sin \rho_2 x}{\rho_2}\right\} \quad (28)$$

$$H_y = j\omega\epsilon C\left\{\frac{\sin \rho_1 x}{\rho_1} - \frac{\sin \rho_2 x}{\rho_2}\right\} \quad (29)$$

$$H_z = \frac{\mu C}{j\beta\omega\kappa\mu_0}\left\{(\rho_1^2 - M)\cos \rho_1 x - (\rho_2^2 - M)\cos \rho_2 x\right\}. \quad (30)$$

Quasi TM mode

$$E_x = \frac{j\beta}{\rho_1} C\left\{\cos \rho_1 x - \left(\frac{\rho_1^2 - M}{\rho_2^2 - M}\right)\cos \rho_2 x\right\} \quad (31)$$

$$E_y = \frac{\mu(\rho_1^2 - M)}{\beta\kappa\rho_1} C\left\{\cos \rho_1 x - \cos \rho_2 x\right\} \quad (32)$$

$$H_x = -\frac{(\rho_2^2 - N)}{\omega\kappa\rho_1} C\left\{\left(\frac{\rho_1^2 - N}{\rho_2^2 - N}\right)\cdot \cos \rho_1 x - \left(\frac{\rho_1^2 - M}{\rho_2^2 + M}\right)\cos \rho_2 x\right\} \quad (33)$$

$$H_y = -\frac{j\omega\epsilon}{\rho_1} C\left\{\cos \rho_1 x - \left(\frac{\rho_1^2 - M}{\rho_2^2 - M}\right)\cos \rho_2 x\right\} \quad (34)$$

$$H_z = -\frac{j\mu(\rho_1^2 - M)}{\beta\omega\kappa\mu_0} C\left\{\sin \rho_1 x - \frac{\rho_2}{\rho_1}\sin \rho_2 x\right\}. \quad (35)$$

The propagation constant can be found easily if we notice the following useful relationships:

$$\rho_1\rho_2 = \frac{mn\pi^2}{a^2} = \Upsilon \quad (36)$$

$$\rho_1^2 + \rho_2^2 = (m^2 + n^2)\frac{\pi^2}{a^2} = \Psi. \quad (37)$$

From (37) and (7) it follows immediately that

$$\beta^2 = \frac{1}{1 + \frac{\mu_0}{\mu}}\left\{(\chi+1)k_2^2 - (m^2+n^2)\frac{\pi^2}{a^2}\right\}. \quad (38)$$

A graph of the parameter x is shown in fig. 2.

Until the present time little has been said about the

[12] The same conclusion can be drawn from the relations derived by Van Trier, *op. cit.*, p. 327 (2.57) and (2.58).

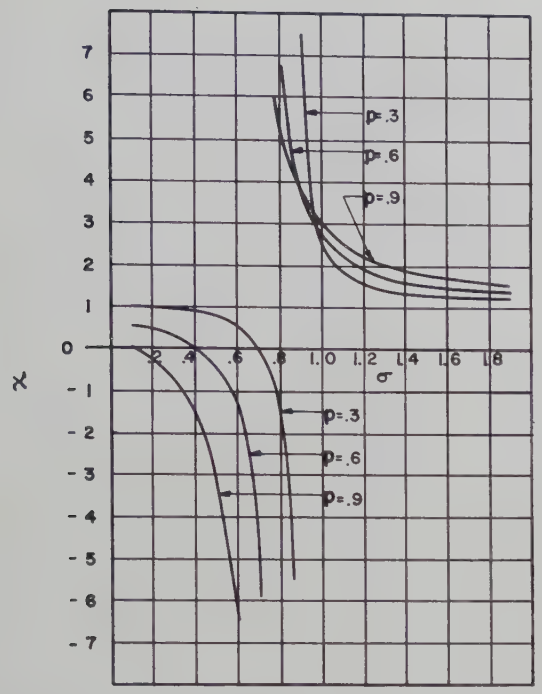

Fig. 2—Relation between χ and σ.

integers m and n except that the boundary conditions impose a restriction that they both be simultaneously odd or even. The other restrictions to be considered are those imposed by the medium itself. They are expressed formally in (36) and (37). Thus, as it could be expected, m and n are not independent; *i.e.*, once one of them is chosen arbitrarily the other one is fixed, and vice versa. The relation connecting the integers m and n can be found if we first eliminate β between (7) and (8) which yields

$$\frac{\Psi}{\omega^2\epsilon\kappa} = -\frac{\kappa}{\mu} \pm \left(1+\frac{\mu_0}{\mu}\right)\sqrt{1+\frac{\mu}{\mu_0}\left(\frac{\Upsilon}{\omega^2\epsilon\kappa}\right)^2}. \tag{39}$$

We can now substitute the relations of (36) and (37) to obtain the desired relationship

$$\rho_2^2 = \left(\frac{\mu^2+\mu_0^2}{2\mu\mu_0}\right)\rho_1^2 - \frac{\omega^2\epsilon\kappa^2}{\mu} \pm \left\{\left(\frac{\mu^2-\mu_0^2}{2\mu\mu_0}\right)^2\rho_1^4 + (\mu+\mu_0)^2\left(\omega^2\epsilon - \frac{\rho_1^2}{\mu_0}\right)\frac{\omega^2\epsilon\kappa^2}{\mu^2}\right\}^{1/2} \tag{40}$$

or

$$n^2 = \left(\frac{\mu^2+\mu_0^2}{2\mu\mu_0}\right)m^2 - \frac{4a^2\epsilon'\kappa^2}{\mu\mu_0\lambda^2} \pm \frac{1}{\mu\mu_0}\left\{\left(\frac{\mu^2-\mu_0^2}{2}\right)^2 m^4 + (\mu+\mu_0)^2\left(\frac{4a^2\epsilon'}{\lambda^2} - m^2\right)\frac{4a^2\epsilon'\kappa^2}{\lambda^2}\right\}^{1/2} \tag{41}$$

where $\epsilon' = \epsilon/\epsilon_0$ and λ is the free space wavelength. Eq. (41) is just about the simplest form of expressing the relation between m and n. It can be solved either graphically or by means of a digital computer.

It is interesting to find out what happens to our solutions as we pass to the limit of zero applied magnetostatic field. When $\sigma = 0$ we can see from (3)

$$\mu = \mu_0$$
$$\kappa = \lim_{p\to 0}(p\mu_0). \tag{42}$$

The propagation constant becomes

$$\beta^2 = \lim_{p\to 0}\left\{k_2^2 - \frac{\rho_1^2+\rho_2^2}{2} - \frac{p^2k_2^2}{2}\right\} \tag{43}$$
$$= k_2^2 - \frac{\rho_1^2+\rho_2^2}{2}.$$

Evidently when $\sigma = 0$, $\rho_1 = \rho_2$ for β to take on the usual form. This can be also shown to be true if we put $\mu = \mu_0$, $\kappa = \lim_{p\to 0}(p\mu_0)$ into (40). We obtain

$$\rho_1^2 - \rho_2^2 = \lim_{p\to 0}\left\{2pk_2\sqrt{k_2^2 - \frac{\rho_1^2+\rho_2^2}{2} - \frac{k_2^2p^2}{4}}\right\} \tag{44}$$

which can also be written as

$$\rho_1^2 - \rho_2^2 = \lim_{p\to 0}\left\{2pk_2\beta\sqrt{1+\frac{k_2^2p^2}{4\beta^2}}\right\} = 0. \tag{45}$$

Thus our propagation constant reduces properly to the form it should have when the external magnetostatic field is removed and the medium becomes isotropic. Next, let us investigate the field components. We can see immediately that when $\rho_1 = \rho_2$ in the quasi TE group then E_z, E_x, and H_y become zero. In the case of the remaining field components we have to exercise a little care going over to the limit since the expressions become indeterminate if we simply put $\rho_1 = \rho_2$ and $\kappa = 0$. If we can imagine a weak enough magnetostatic field such that we can set

$$\frac{\sin\rho_1 x}{\rho_1} \approx \frac{\sin\rho_2 x}{\rho_2}$$
$$\cos\rho_1 x \approx \cos\rho_2 x$$
$$\rho_1^2 \neq \rho_2^2,$$

then we would have for a typical field component, say E_y,

$$E_y = \frac{C}{\beta p\rho_1}(\rho_1^2 - \rho_2^2)\sin\rho_1 x.$$

Substituting for $(\rho_1^2 - \rho_2^2)$ the expression obtained in (45) we get

$$E_y = \frac{2Ck_2}{\rho_1}\sqrt{1+\frac{k_2^2p^2}{4\beta^2}}\sin\rho_1 x.$$

Finally, as we pass to the limit $p = 0$ this becomes simply

$$E_y = K\sin\rho x \tag{46}$$

where K is a constant. The other nonzero field components become

$$H_x = -\frac{\beta}{\omega\mu_0} K \sin \rho x \tag{47}$$

$$H_z = j\frac{\rho}{\omega\mu_0} K \cos \rho x. \tag{48}$$

These equations can be recognized as those describing a TE wave between two parallel planes. Thus our solution in the ferrite medium that we called quasi TE group goes over properly to a TE mode when the external magnetostatic field is removed.

By a similar procedure of going over to the limit of zero magnetostatic field it can be easily shown that the quasi TM group takes on the usual form of TM mode in an isotropic medium.

Transverse Magnetization

The case of a rectangular waveguide containing a ferrite medium subjected to a magnetostatic field transverse in relation to the direction of propagation has been treated by many authors.[9,13–15] Van Trier[9] has solved the case of TE_{n0} mode in a transversely magnetized parallel plane waveguide. Chevalier and Polacco[13] and Epstein[14] also worked on the same problem. Vartanian and Jaynes[15] worked out a solution to the problem of propagation of higher order modes in a transversely magnetized ferrite-filled rectangular waveguide.

In this paper we shall be concerned with a ferrite-filled transversely magnetized parallel plane waveguide that can propagate more than one mode at a time. We shall start with the expressions for the field components and the propagation constant for a single mode guide as found elsewhere[9]

$$E_y = C \sin \nu x \tag{49}$$

$$H_x = -\frac{C}{\omega\mu_0\chi}\left(\frac{\kappa\nu}{\mu}\cos \nu x + \beta \sin \nu x\right) \tag{50}$$

$$H_z = \frac{jC}{\omega\mu_0\chi}(\nu \cos \nu x + \kappa \sin \nu x) \tag{51}$$

$$\beta^2 = k_2{}^2\chi - \nu^2; \qquad \nu = \frac{m\pi}{a}. \tag{52}$$

It is of interest to examine the above equations more carefully. The expression for the electric field is identical with that of a conventional TE_{m0} mode in a rectangular waveguide filled with an isotropic medium. The magnetic field components have additional terms which are functions of the applied magnetostatic field. The propagation constant and the cutoff wavelength deserve special attention. Because of the presence of the parameter χ, the cutoff wavelength (and by the same token the propagation constant) can be adjusted over wide limits. Thus, theoretically, we can make the waveguide "electrically" as large or as small as we please. In Fig. 3 there is a plot of the cutoff wavelength for TE_{10} and TE_{20} modes as a function of the applied magnetostatic field for a standard size waveguide of 0.5×1.0 inch where the dielectric constant of the ferrite has been arbitrarily set equal to one.

In the next section we shall be concerned with one of the possible applications of the electrically adjustable propagation constant, *i.e.*, "electrical scanning." Let us consider waveguide which is terminated with a transversely magnetized ferrite plate as shown in Fig. 4.

We are interested at this moment in the expression for the transverse components of the electric and magnetic fields existing at the mouth of the waveguide. This problem is solved approximately by assuming that the fields at the mouth of the guide are the same as those that would exist were the waveguide not terminated there. To the left of the ferrite plate we assume the existence of the fundamental mode only, *i.e.*, TE_{10} mode. In the ferrite region the waveguide width can be made electrically large by properly adjusting the external magnetostatic field H_0 so that higher order modes can propagate. We assume that some of the incident power is converted into higher order modes at the surface of the ferrite and, since the waveguide is large enough electrically, they may propagate unattenuated. Let l be the thickness of the ferrite plate. The transverse fields at the mouth of the guide can then be written:

$$E_y = C_1 e^{-j\beta_1 l} \sum_{m=1}^{M} \frac{C_m}{C_1} \sin \frac{m\pi x}{a} e^{j\delta_m} \tag{53}$$

$$H_x = -\frac{C_1 e^{j\beta_1 l}}{\omega\mu_0\chi} \sum_{m=1}^{M} \frac{C_m}{C_1}\left(\frac{\kappa}{\mu}\frac{m\pi}{a}\cos\frac{m\pi x}{a} + \beta_m \sin\frac{m\pi x}{a}\right) e^{j\delta_m} \tag{54}$$

where

$$\delta_m = (\beta_1 - \beta_m)\iota. \tag{55}$$

The term C_m/C_1, which is the ratio of the amplitude of the electric field in the mth mode to that in the principal mode, is an unknown. Angelakos and Korman[1] concluded from their experiments with a ferrite-loaded waveguide that some of the incident power is converted into higher order modes upon entering the ferrite region but they made no measurements of the ratio of mode conversion. There is no analytical solution to the problem either. Some of the difficulties connected with obtaining a workable analytical expression have been out-

[13] A. Chevalier and E. Polacco, "Propagation of electromagnetic TE wave in a guide containing ferrites," *C. R. Acad. Sci.*, vol. 239, pp. 692–694; September 20, 1954.

[14] P. S. Epstein, "Wave propagation in a gyromagnetic medium," *Rev. Mod. Phys.*, vol. 28, pp. 3–17; January, 1956.

[15] P. H. Vartanian and E. T. Jaynes, "Propagation in ferrite-filled transversely magnetized waveguide," IRE TRANS. ON MICROWAVE THEORY AND TECHNIQUES, vol. MTT-4, pp. 140–143; July, 1956.

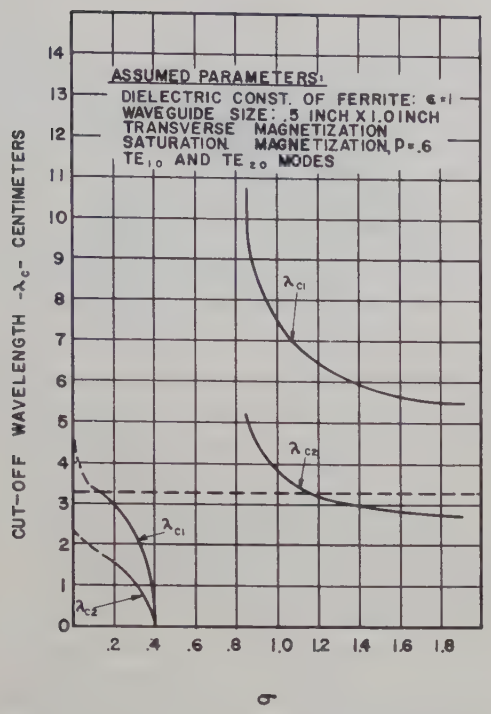

Fig. 3—Cutoff wavelength vs magnetostatic field.

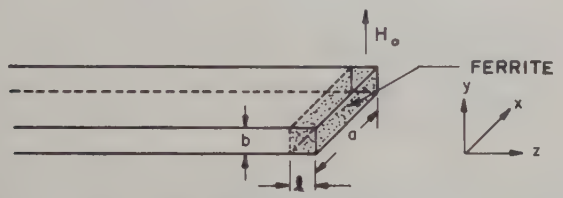

Fig. 4—Waveguide and ferrite plate configuration for solution of the problem of "electrical scanning."

lined by Epstein.[14] In the next section, when computing the radiation field, certain arbitrary values will be chosen for this ratio.

A few words should be mentioned about reciprocity. From (52), it is evident that the system is reciprocal as far as the propagation constant is concerned. Let us, however, examine the wave admittances. We know that in a reciprocal system the wave admittance of the incident wave is equal to that of the reflected wave. Now let us examine the wave admittances for the ferrite. For the incident wave we obtain

$$Y_{yx}^{+} = -\frac{H_x^{+}}{E_y^{+}} = \frac{1}{\omega\mu_0\chi}\sum_{m=1}^{M}\left(\beta_m + \frac{\kappa}{\mu}\frac{m\pi}{a}\cot\frac{m\pi x}{a}\right) \quad (56)$$

and for the reflected wave we obtain

$$Y_{yx}^{-} = \frac{H_x^{-}}{E_y^{-}} = \frac{1}{\omega\mu_0\chi}\sum_{m=1}^{M}\left(\beta_m - \frac{\kappa}{\mu}\frac{m\pi}{a}\cot\frac{m\pi x}{a}\right). \quad (57)$$

Thus, the system is not reciprocal! The forward and backward wave admittances for a waveguide able to propagate two modes are plotted in Fig. 5. It can be seen that these admittances have a mirror symmetry

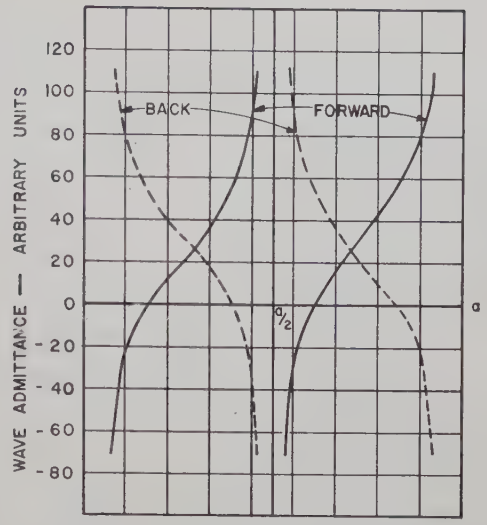

Fig. 5—Aperture forward and back wave admittances.

about the center of the guide. It can be shown that if the direction of the magnetostatic field is changed while the incident wave is being received, the input and output admittances are identical and the reciprocity is restored. The implications of this fact will be considered when discussing the reciprocity of radiation patterns.

Radiation from a Rectangular Waveguide Filled with Ferrite

Introduction to the Problem

The problem of radiation from an open-end waveguide has not, thus far, been solved rigorously. Actually the radiation should be considered to arise from the current distribution on the inside walls of the guide, which is just the current distribution associated with the fields propagated in the interior of the guide, together with the currents flowing from the open end upon the exterior guide surface. Due to this complexity a rigorous solution to the radiation problem has not yet been found. The problem has, however, been solved approximately.[16] In this method the guide opening is assumed to act as an aperture in an infinite screen, and the transverse fields in the aperture are assumed to be the same as those that would exist if the guide did not terminate there. The vector Huygens' formula is applied to obtain the radiation field from the aperture field distribution as discussed by Silver.[17]

We follow this method in the solution of the problem of radiation from an open-end waveguide that is completely filled with ferrite. The expressions for the far-zone fields as derived for a waveguide containing an isotropic medium are modified to suit our purpose. The

[16] L. J. Chu, "Calculation of the radiation properties of hollow pipes and horns," *J. Appl. Phys.*, vol. 11, pp. 603–610; September, 1940.

[17] S. Silver, "Microwave Antenna Theory and Design," McGraw-Hill Book Co., Inc., New York, N. Y., pp. 158–162; 1949.

modified equations are: in the H plane ($\phi=0$)

$$E_\theta = \frac{jke^{-jkR}}{4\pi R}\int_{c.s.}(E_x+\eta\cos\theta H_y)e^{jkx\sin\theta}dS \quad (58)$$

$$E_\phi = \frac{jke^{-jkR}}{4\pi R}\int_{c.s.}(\cos\theta E_y-\eta H_x)e^{jkx\sin\theta}dS, \quad (59)$$

and in the E plane ($\varphi=\pi/2$)

$$E_\theta = \frac{jke^{-jkR}}{4\pi R}\int_{c.s.}(E_y-\eta\cos\theta H_x)e^{jky\sin\theta}dS \quad (60)$$

$$E_\phi = -\frac{jke^{-jkR}}{4\pi R}\int_{c.s.}(\cos\theta E_x+\eta H_y)e^{jky\sin\theta}dS \quad (61)$$

where $k=\omega\sqrt{\mu_0\epsilon_0}$ and $\eta=\sqrt{\mu_0/\epsilon_0}$.

Next, consider the radiation from an open-end waveguide that is completely filled with ferrite which is transversely magnetized. We shall solve this problem for a multimode waveguide, *i.e.*, a waveguide which can propagate more than one mode. The geometry of the problem is shown in Fig. 6. The far-zone electric field patterns are found to be the following: in the H plane ($\phi=0$)

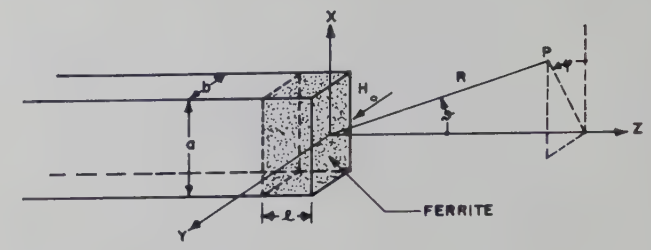

Fig. 6—Geometry of the problem of radiation from an open-end waveguide containing ferrite.

effect of the magnetostatic field H_0 upon the shape and the relative positions of the E_ϕ and E_θ field patterns. To do this we assume the following parameters:

Ferrite saturation magnetization—$p=0.6$
Ferrite dielectric constant[18]—$\epsilon'=1$
Thickness of the ferrite plate—$l=2$ cm
Carrier wavelength—$\lambda=3.2$ cm
Waveguide inside dimensions—$a=2.28$ cm, $b=1.02$ cm
Mode conversion ratio—$C_2/C_1=1$.

$$E_\phi = \frac{j\pi ab}{4\lambda R}C_1e^{-j(kR+\beta_1 l+\xi_1-u)}\sum_{m=1}^{M}\left\{\frac{mC_m}{C_1}\left|\frac{\sin\left(u+\frac{m\pi}{2}\right)}{\left(\frac{m\pi}{2}\right)^2-u^2}\right|\right.$$

$$\left.\text{times}\sqrt{\left(\cos\theta+\frac{\beta_m\lambda}{2\pi\chi}\right)^2+\left(\frac{\lambda}{\pi\chi}\cdot\frac{\kappa}{\mu}\cdot\frac{u}{a}\right)^2}\,e^{j[(\beta_1-\beta_m)l+(\xi-\xi_m)]}\right\}, \quad (62)$$

and in the E plane ($\varphi=\pi/2$)

$$E_\theta = \frac{ab}{\pi\lambda R}C_1\frac{\sin u'}{u'}e^{-j(kR+\beta_1 l-u')}$$

$$\cdot\sum_{m=1}^{M}\frac{C_m}{mC_1}\sin\frac{m\pi}{2}\left(1+\frac{\lambda\beta_m\cos\theta}{2\pi\chi}\right)e^{j(\beta_1-\beta_m)l} \quad (63)$$

where

$$\xi_m = \arctan\left[\left(\frac{\cos\theta+\frac{\lambda\beta_m}{2\pi\chi}}{\frac{\lambda}{\pi\chi}\cdot\frac{\kappa}{\mu}\cdot\frac{u}{a}}\right)^{(-1)^m}\right] \quad (64)$$

$$u=\frac{\pi a}{\lambda}\sin\theta; \qquad u'=\frac{\pi b}{\lambda}\sin\theta. \quad (65)$$

The implications of the above radiation field patterns are not easy to perceive. It will be advantageous at this point to apply these equations to a specific numerical example which would enable us to get a better insight into the situation. Specifically, we are interested in the

It can be seen from Fig. 3 that the TE_{10} mode will propagate through the waveguide when $0.0\leq\sigma<0.15$ and when $\sigma>0.85$ and it will be cut off when $0.15<\sigma<0.85$. The TE_{20} mode will propagate when $0.85<\sigma<1.17$. The TE_{30} mode is cut off completely except for a very small region ($0.85<\sigma<0.90$) which we neglect.

The aperture electric field distribution, E_y, for the two-mode transmission and the phase angle ψ are plotted for several values of the external magnetostatic field H_0 in Fig. 7. It can be seen that the field is shifted to the left-hand side of the guide at $\sigma=0.85$. As the magnetostatic field is increased, the field gradually shifts back to the center of the guide with a decrease in magnitude and it is symmetrical with respect to the center of the guide somewhere between $\sigma=1.05$ and $\sigma=1.10$. As the magnetostatic field is further increased, the electric field shifts to the right-hand side of the guide

[18] It is realized that a dielectric constant of one is not realistic for a ferrite of today since the ferrites produced nowadays have a dielectric constant of about ten. The value of one was introduced here merely to simplify the many numerical calculations that had to be carried out. It is true that when $\epsilon=10$ not only may two modes propagate, but a great many. One may expect, however, that the amplitudes of the higher order modes will be progressively smaller so that their effect may be neglected to the first order of approximation.

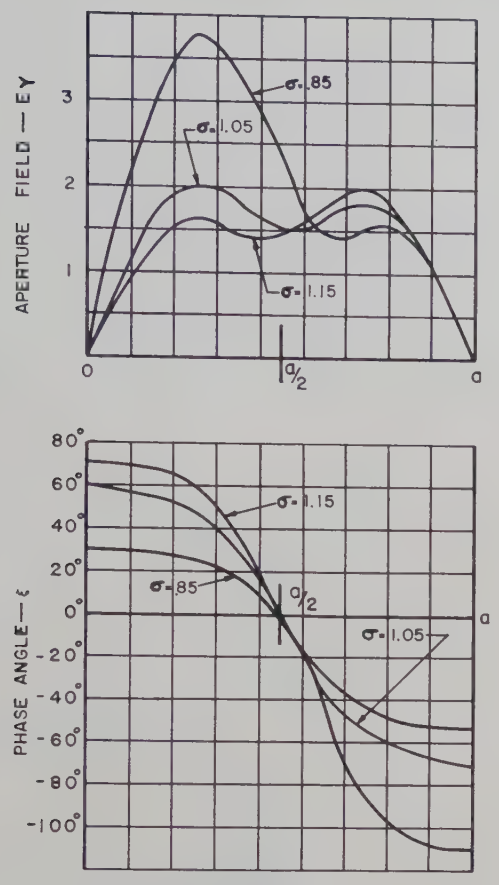

Fig. 7—Aperture electric field and phase angle.

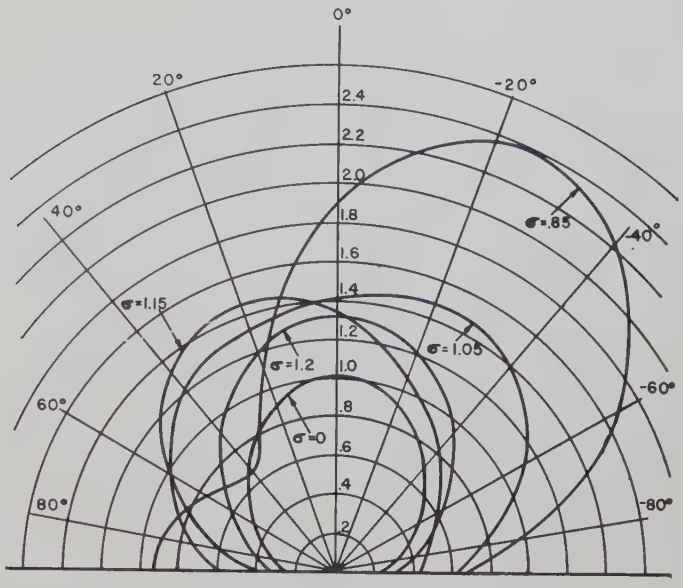

Fig. 8—H-plane electric field pattern.

and at $\sigma = 1.15$ it is exactly opposite with respect to the center of the guide to the position it had at $\sigma = 0.85$.

The electric field pattern in the H plane is plotted in Fig. 8 for a range of magnetostatic field from $\sigma = 0.0$ to $\sigma = 2.0$. Starting with $\sigma = 0.0$ the amplitude of the pattern gradually decreases and it becomes zero at $\sigma = 0.15$, where the propagation constant for the principal mode becomes zero (Fig. 3). There is no radiation between $\sigma = 0.15$ to $\sigma = 0.84$ since all modes in the guide are cut off. At $\sigma = 0.85$ transmission through the guide begins again. Now the waveguide is large enough electrically so that not only the principal mode but also the second-order mode can propagate freely; the radiation pattern is large in magnitude and it reaches its maximum at about -25 degrees off the zero axis. As the magnetostatic field is increased the radiation pattern decreases slightly in amplitude and it shifts farther in the clockwise direction. At the same time, it can be seen, a new sidelobe appears at $+70$ degrees. As the magnetostatic field is further increased, the main lobe remains in the same position as before and the new lobe gradually builds up and moves closer toward the center. This process of contraction of the previous main lobe and the expansion of the new sidelobe on the opposite side goes on until, at $\sigma = 1.15$, a new main lobe is definitely formed at $+20$ degrees. As the magnetostatic field is further increased, the waveguide decreases in size electrically so that the second-order mode is cut off and only the principal one remains. The radiation pattern is now centered again about the zero axis and further increase in the magnetization changes the magnitude only.

The process of pattern formation may be best explained by reference to Fig. 9. The components E_ϕ' and E_ϕ'', corresponding to the radiation patterns of the first and second modes which make up E_ϕ, are plotted there together with the phase angle Γ_2 for a constant value of magnetic field, σ. Since E_ϕ', E_ϕ'', and Γ_2 are all functions of the spherical angle θ and the magnetic field σ, they add in various combinations of magnitudes and phase angle to form the final pattern, E_ϕ.

It may be of interest to estimate the value of error that might have been introduced here due to the assumption that the ratio of mode amplitudes $C_2/C_1 = 1$. The value of this ratio affects the pattern by the way of changing the magnitude of E_ϕ'' in (62). In Fig. 10 three electric field patterns are plotted which correspond to the values of C_2/C_1 of 1, 2, and 0.5. Taking $C_2/C_1 = 1$ pattern as a reference, it may be seen that pattern deviations are significant for values of $C_2/C_1 > 1$, and are relatively small for values of $C_2/C_1 < 1$. However, in each case the pattern is still shifted in the same direction as before. Intuitively, we could say that C_2/C_1 should be smaller than one which concludes that the patterns in Fig. 8 are in no great error, due to the assumption $C_2/C_1 = 1$.

The patterns we have just discussed are transmitting patterns. One may ask whether the same patterns are receiving patterns, too. It was shown in (56) and (57) that the wave admittances of the incident and reflected waves in the aperture are identical except for the sign of κ. It was also shown in Fig. 5 that the input and output wave impedances had a mirror symmetry about the

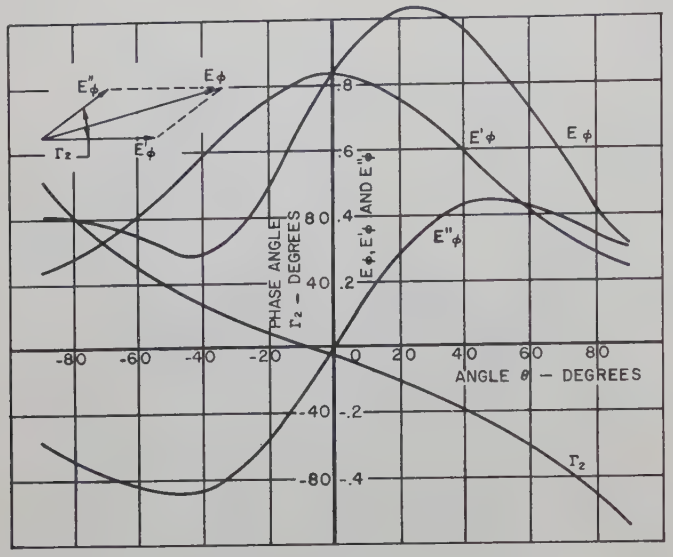

Fig. 9—The mechanics of pattern formation.

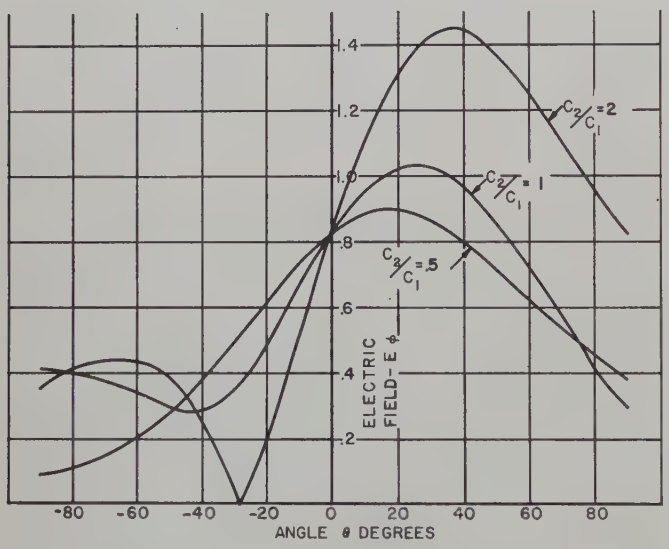

Fig. 10—The effect of the mode conversion ratio C_2/C_1 upon the shape of the pattern.

center of the guide. Thus, from the argument just presented, one may conclude that the transmitting and the receiving patterns, which are functions of the output and input impedance, respectively, will also have a mirror symmetry (see Fig. 11). Also, since the reversal of the direction of the magnetostatic field changes the sign of κ, the receiving and transmitting patterns are interchanged when the magnetostatic field is reversed. These phenomena were demonstrated experimentally by Angelakos and Korman.[1] Their results are reproduced in Fig. 12 for comparison.[19]

The equations for the far-zone radiation fields from an open-end waveguide filled with ferrite magnetized in the direction of propagation are derived in the Appendix.

[19] Angelakos and Korman, *op. cit.*, Fig. 12, p. 1468.

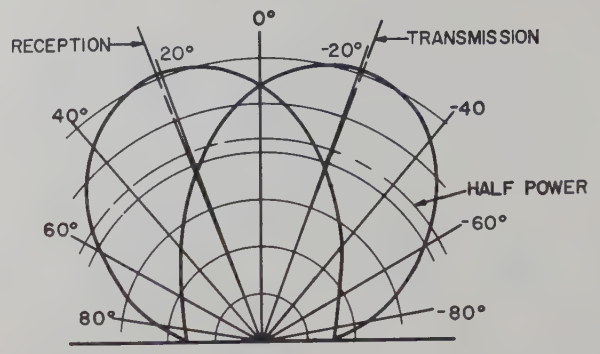

Fig. 11—Nonreciprocity of transmitting and receiving patterns.

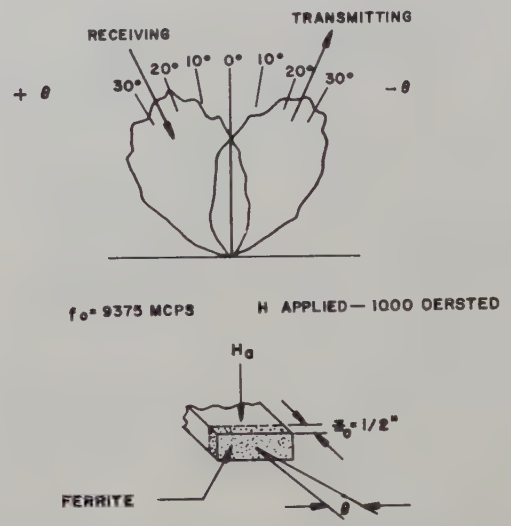

Fig. 12—Experimental patterns of Angelakos and Korman. (Reproduced by permission of the authors.)

Appendix

Radiation from an Open-End Waveguide Filled with Ferrite Longitudinally Magnetized

In this case we restrict ourselves to a waveguide which can propagate a single TE mode only. The geometry of the problem is similar to that of Fig. 6 except that now the direction of the magnetostatic field is in the direction of propagation.

Substituting the expressions for the transverse field components found in (26) through (29) into (58) through (61) and carrying out the integration we obtain: in the H plane ($\phi = 0$)

$$E_\theta = \frac{j^m ab\pi \sin\left(u + \frac{m\pi}{2}\right)}{4\lambda R} \cdot \left\{ \frac{mA_1}{\left(\frac{m\pi}{2}\right)^2 - u^2} - \frac{nA_2}{\left(\frac{n\pi}{2}\right)^2 - u^2} \right\} e^{-j(kR-u)} \tag{66}$$

$$E_\phi = \frac{-j^m ab\pi \sin\left(u + \frac{m\pi}{2}\right)}{4\lambda R}$$

$$\cdot \left\{ \frac{mA_3}{\left(\frac{m\pi}{2}\right)^2 - u^2} - \frac{nA_4}{\left(\frac{n\pi}{2}\right)^2 - u^2} \right\} e^{-j(kR-u)}, \quad (67)$$

and in the E plane ($\phi = \pi/2$)

$$E_\theta = \frac{-j^m \sin\left(\frac{m\pi}{2}\right) ab}{\lambda\pi R} \left\{ \frac{A_5}{m} - \frac{A_6}{n} \right\} \frac{\sin u'}{u'} e^{-j(kR-u')} \quad (68)$$

$$E_\phi = \frac{-j^m \sin\left(\frac{m\pi}{2}\right) ab}{\lambda\pi R} \left\{ \frac{A_7}{m} - \frac{A_8}{n} \right\} \frac{\sin u'}{u'} e^{-j(kR-u')} \quad (69)$$

where

$$A_1 = j \frac{Ca}{m\pi} (\beta + \omega\epsilon\eta \cos\theta) \quad (70)$$

$$A_2 = j \frac{Ca}{n\pi} (\beta + \omega\epsilon\eta \cos\theta) \quad (71)$$

$$A_3 = \frac{Ca}{m\pi\kappa} \left\{ \frac{\eta}{\omega} \left[\left(\frac{m\pi}{2}\right)^2 - N \right] + \frac{\mu \cos\theta}{\beta} \left[\left(\frac{m\pi}{a}\right)^2 - M \right] \right\} \quad (72)$$

$$A_4 = \frac{Ca}{n\pi\kappa} \left\{ \frac{\eta}{\omega} \left[\left(\frac{n\pi}{a}\right)^2 - N \right] + \frac{\mu \cos\theta}{\beta} \left[\left(\frac{n\pi}{a}\right)^2 - M \right] \right\} \quad (73)$$

$$A_5 = \frac{Ca}{m\pi\kappa} \left\{ \frac{\mu}{\beta} \left[\left(\frac{m\pi}{a}\right)^2 - M \right] + \frac{\eta \cos\theta}{\omega} \left[\left(\frac{m\pi}{a}\right)^2 - N \right] \right\} \quad (74)$$

$$A_6 = \frac{Ca}{m\pi\kappa} \left\{ \frac{\mu}{\beta} \left[\left(\frac{n\pi}{a}\right)^2 - M \right] + \frac{\eta \cos\theta}{\omega} \left[\left(\frac{n\pi}{a}\right)^2 - N \right] \right\} \quad (75)$$

$$A_7 = \frac{jCa}{m\pi} (\beta \cos\theta + \eta\omega\epsilon) \quad (76)$$

$$A_8 = \frac{jCa}{n\pi} (\beta \cos\theta + \eta\omega\epsilon). \quad (77)$$

Acknowledgment

Grateful acknowledgment is made to the Boeing Airplane Company for the permission to use the digital computer facilities for most of the computations involved in the text. Thanks are also extended to Carl G. Lindell for computer programming and to K. W. Osborne for lettering and inking the drawings.

Launching Efficiency of Wires and Slots for a Dielectric Rod Waveguide*

R. H. DuHAMEL† and J. W. DUNCAN‡

Summary—This paper describes an experimental investigation of surface wave launching efficiency. Wires, rings, and slots are considered as exciters of the HE_{11} mode on a dielectric rod image line. A formula is derived which relates the efficiency of a launcher to its impedance as a scatterer on the surface waveguide. Efficiency is obtained by using this formula and also by applying Deschamps' method for determining the scattering matrix coefficients of a two-port junction. Graphs are presented which illustrate the variation of efficiency with the dimensions of the launchers and with the parameter λ_g/λ, the ratio of the guide wavelength to the free space wavelength.

* Manuscript received by the PGMTT, August 1, 1957; revised manuscript received January 28, 1958. The work described in this paper was supported by Wright Air Dev. Ctr. under Contract No. AF 33(616)-3220, and is an abstract of Antenna Lab. Tech. Rep. No. 24, Electrical Engineering Research Lab., Engineering Experiment Station, University of Illinois, Urbana, Ill. The paper was presented at the IRE WESCON, Los Angeles, Calif., August 23, 1956.

† Collins Radio Co., Cedar Rapids, Iowa.
‡ Dept. of Elec. Eng., University of Illinois, Urbana, Ill.

Introduction

THE THEORY of wave propagation on dielectric rods has been treated extensively by a number of investigators [1]–[3]. In recent years the dielectric rod waveguide has been employed with considerable success as a dielectric antenna [4], [5]. The mode which is most often used for dielectric rod antennas is the HE_{11} (or dipole) mode. It is the lowest order mode which can propagate on a dielectric rod and has no

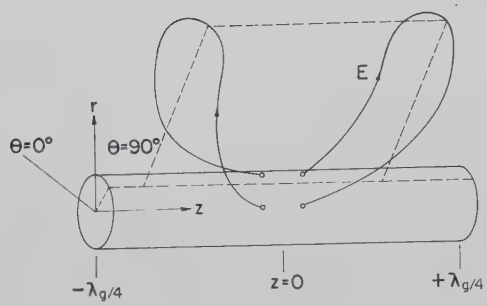

Fig. 1—Typical electric field line of dipole mode on a dielectric rod.

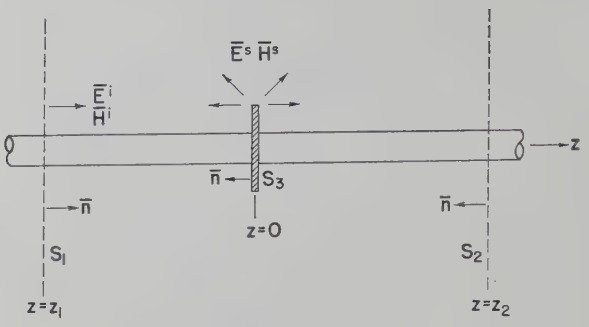

Fig. 2—Surface waveguide and scatterer.

cutoff frequency. Very little information appears in the literature on methods of launching the dipole mode on a rod. The dielectric rod antenna is usually excited from closed metal waveguide or a horn. It appears that the first experimental study of dipole mode launching efficiency was conducted by Margerum at Northwestern University [6]. He measured the launching efficiency of circular metal waveguide which was excited in the TE_{11} mode. Recently, King and Schlesinger measured the radiation loss from a circular aperture in a thin metal sheet placed on a dielectric image line [7]. The purpose of this work was twofold. First, a new method of measuring launching efficiency was investigated and compared with a conventional method. The new method requires a measurement of the impedance that the launcher presents to a surface waveguide when used as a scatterer. The efficiency is simply related to this impedance. With this technique, it is relatively easy to study the variation of launching efficiency with the dimensions of the launcher and the parameter λ_g/λ. Although this method was used only with the dielectric image line, it may be applied to other types of surface waveguides. The second purpose of this work was to investigate various types of simple wire and slot launchers. Curves showing the variation of launching efficiency with launcher dimensions and the parameter λ_g/λ are presented.

The Dielectric Image Line

The characteristics of dielectric rod propagation and the dipole mode will be briefly reviewed. The HE_{11} mode is an asymmetric, hybrid mode which has components of both the electric and magnetic field in the direction of propagation. A typical electric field line outside the rod is shown in Fig. 1 [8]. The cutoff wavelength of a mode is a function of the rod radius b, and free space wavelength λ [3]. For a polystyrene rod with dielectric constant $\epsilon = 2.5$, higher order modes can propagate only when the rod diameter exceeds 0.626λ. The ratio λ_g/λ is a function of the parameter b/λ [3], [5]. As b/λ approaches zero, λ_g/λ approaches unity and most of the power is propagated in the space surrounding the rod. The transverse field distribution of the dipole mode is such that a metal sheet may be passed through the axis of the rod without disturbing the field. A half-round rod mounted on a metal ground plane is the dielectric image line first proposed by King [9], who has developed various circuit components for the dielectric image line and describes a conical horn and parabolic reflector as transitions from image line to closed waveguide [10]. It is possible to measure standing waves along the image line by means of a slotted section in the ground plane [10]; thus, the impedance of a scatterer may be readily determined.[1] In this paper an expression is derived which relates the efficiency of a launcher to its impedance as a scatterer on the surface waveguide.

Launching Efficiency from the Scatterer Impedance

Referring to Fig. 2, consider a cylindrical surface waveguide of arbitrary cross section. The guide is assumed lossless with a surface wave $\bar{E}^i$, $\bar{H}^i$ incident from the left and a perfectly conducting scatterer, denoted as surface S_3, located at $z=0$. The surfaces S_1 and S_2 are infinite transverse planes normal to the z axis located at $z=z_1$ and $z=z_2$, respectively.

The incident surface wave will induce a current on the scatterer which will produce a scattered field that consists of guided waves to the left and right plus a radiation field. An expression for the reflection coefficient, Γ, at the scatterer may be determined by applying the Lorentz reciprocity theorem [11] over the surface of the closed volume defined by S_1, S_2, S_3, and the cylindrical surface of infinite radius between S_1 and S_2. Denoting the scattered field by $\bar{E}^s$, $\bar{H}^s$, we have

$$\iint_{S_1+S_2+S_3} [\bar{E}^s \times \bar{H}^i - \bar{E}^i \times \bar{H}^s] \cdot \bar{n} da = 0 \qquad (1)$$

where the integral over the cylindrical surface of infinite radius vanishes because of exponential decay of the surface wave fields and the radiation condition. Since the scatterer is a perfect conductor $\bar{E}^i = -\bar{E}^s$ on S_3. Thus, the integral over S_3 takes the form

$$\iint_{S_3} [\bar{E}^s \times (\bar{H}^i + \bar{H}^s)] \cdot \bar{n} da \qquad (2)$$

Because of the orthogonality relations [12], [13] between the surface wave modes and the radiation

[1] For details of the dielectric image line and measurement of scatterer impedance, see [5].

field, the only component of the scattered field $\overline{E}^s$, $\overline{H}^s$ which contributes to the integration over S_1 and S_2 is a surface mode of the same type as the incident wave. Moveover, only the transverse components of the surface mode apply in (1), hence we express the transverse components of the incident surface wave in the form

$$\begin{aligned} &\overline{E}_t{}^i e^{-i\zeta z} \\ &\overline{H}_t{}^i e^{-i\zeta z}. \end{aligned} \tag{3}$$

The transverse components of the scattered field propagating in the negative z direction are

$$\begin{aligned} &\Gamma\overline{E}_t{}^i e^{+j\zeta z} \\ &-\Gamma\overline{H}_t{}^i e^{+i\zeta z} \end{aligned} \tag{4}$$

and for the positive z direction are

$$\begin{aligned} &A\overline{E}_t{}^i e^{-i\zeta z} \\ &A\overline{H}_t{}^i e^{-i\zeta z} \end{aligned} \tag{5}$$

where $\overline{E}_t{}^i$, $\overline{H}_t{}^i$ are transverse field vectors normal to the z axis, ζ is the axial propagation constant, Γ is the reflection coefficient for the wave propagating in the negative z direction, and A is a similar coefficient for the positive z direction.

When the field expressions (3) and (5) are substituted into (1) in order to evaluate (1) over the surface S_2, the integrand of (1) is identically zero. Only integration over surfaces S_1 and S_3 contributes to (1). Thus, substituting (3) and (4) into (1), with (2) as the form of (1) over surface S_3, (1) reduces to

$$2\Gamma \iint_{S_1} \overline{E}_t{}^i \times \overline{H}_t{}^i \cdot \bar{n} da = -\iint_{S_3} \overline{E}^s \times (\overline{H}^i + \overline{H}^s) \cdot \bar{n} da.$$

Note that the exponential factors in (3) and (4) vanish in this expression. Hence, the complex reflection coefficient Γ at the scatterer is given by

$$\Gamma = \frac{-\frac{1}{2}\iint_{S_3} \overline{E}^s \times (\overline{H}^i + \overline{H}^s) \cdot \bar{n} da}{\iint_{S_1} \overline{E}_t{}^i \times \overline{H}_t{}^i \cdot \bar{n} da}. \tag{6}$$

The density of current $\overline{J}^s$ on the surface of the scatterer is equal to $\bar{n} \times (\overline{H}^i + \overline{H}^s)$ where $(\overline{H}^i + \overline{H}^s)$ is the *total* magnetic field on S_3. The scattered field produced by this current is $\overline{E}^s$.

We shall now consider the scatterer as a surface wave launcher (*i.e.*, a source). The efficiency of a launcher is defined as

$$\eta = \frac{\text{surface wave power}}{\text{total power input to launcher}} = \frac{P_{sw}}{P_{\text{total}}}. \tag{7}$$

If the current distribution on S_3 as a source is identical to $\overline{J}^s$ of the scatterer, then the field produced by the launcher is identical to the field $\overline{E}^s$ of the scatterer. Thus, the total power input to the launcher is given by

$$P_{\text{total}} = \frac{1}{2} Re \iint_{S_3} \overline{E}^{s*} \times (\overline{H}^i + \overline{H}^s) \cdot \bar{n} da \tag{8}$$

where $\overline{E}^s$ is the field produced by the source current $\overline{J}^s = \bar{n} \times (\overline{H}^i + \overline{H}^s)$ on the imaginary surface S_3 but with the perfectly conducting metal launcher removed. The asterisk (*) denotes the standard operation of taking the conjugate of a complex quantity.

Assuming the field is symmetric about the launcher, the total power in the surface wave propagating in the positive and negative z directions is equal to twice the power in the negative z direction. Thus, we write

$$P_{sw} = 2\left[\frac{1}{2} Re \iint_{S_1} \overline{E}^s \times \overline{H}^{s*} \cdot (-\bar{n}) da\right] \tag{9}$$

where only the surface wave part of the scattered field $\overline{E}^s$, $\overline{H}^s$ applies in (9). As with (1), the form of (9) requires only the transverse components of the field. Substituting (4) into (9) yields

$$P_{sw} = |\Gamma|^2 Re \iint_{S_1} \overline{E}_t{}^i \times \overline{H}_t{}^{i*} \cdot \bar{n} da \tag{10}$$

where the exponential factors of (4) cancel when the complex conjugate of $\overline{H}_t{}^i$ is taken.

Substituting (8) and (10) into (7) gives the expression for launching efficiency as

$$\eta = \frac{|\Gamma|^2 Re \iint_{S_1} \overline{E}_t{}^i \times \overline{H}_t{}^{i*} \cdot \bar{n} da}{\frac{1}{2} Re \iint_{S_3} \overline{E}^{s*} \times (\overline{H}^i \times \overline{H}^s) \cdot \bar{n} da}. \tag{11}$$

We wish to remove the conjugate asterisks (*) appearing in (11). First consider the integral over surface S_1. Since $\overline{E}_t{}^i$ and $\overline{H}_t{}^i$ are in time phase, they may be defined to be real vector functions of the transverse coordinates. Thus, the conjugate sign may be removed from $\overline{H}_t{}^i$ in the integral. Moreover, the integral over S_1 is now a real quantity so the Re sign before the integral may be removed.

Next consider the integral over surface S_3. On S_3, $\overline{E}^s = -\overline{E}^i$. If the axial dimension of the launcher is quite small, then the integration over S_3 may be taken as entirely in the transverse plane. Therefore, only the transverse component of $\overline{E}^s$ contributes to the integral, and the substitution of $-\overline{E}_t{}^i e^{-i\zeta z}$ for $\overline{E}^s$ in (11) is valid. Since $\overline{E}_t{}^i$ is real and $e^{-i\zeta z} \approx 1$ at $z = 0$ for $z/\lambda \ll 1$, the conjugate sign may be removed from $\overline{E}^s$. Hence (11) may be written in the form

$$\eta = \frac{|\Gamma|^2 \iint_{S_1} \overline{E}_t{}^i \times \overline{H}_t{}^i \cdot \bar{n} da}{\frac{1}{2} Re \iint_{S_3} \overline{E}^s \times (\overline{H}^i \times \overline{H}^s) \cdot \bar{n} da}. \tag{12}$$

Comparing (6) and (12) we see that

$$\eta = \frac{|\Gamma|^2}{-Re\ \Gamma}. \tag{13}$$

Note that Γ in this equation is the reflection coefficient at $z=0$ for the *composite* load of the scatterer and the infinite surface waveguide to the right. It is preferable to express efficiency in terms of a measurable parameter which represents just the scatterer and *not* the scatterer plus the infinite surface guide. Consider the particular case of the dielectric image line where one measures the normalized shunt impedance, z, of the scatterer, by placing a short circuit plate an odd multiple of $\lambda_g/4$ to the right of the scatterer [5]. This isolates the scatterer from the dielectric rod to the right of $z=0$ and allows greater accuracy in the standing wave measurements. Therefore, rewriting (13) in terms of the normalized shunt impedance z of the scatterer alone, one obtains

$$\eta = \frac{1}{1 + \left\{\begin{matrix}2\\1\end{matrix}\right\} Re\ z}. \tag{14}$$

Eq. (14) is valid under the following conditions:

[The current distribution on the launcher when used as a source is identical to the current distribution on the launcher when it appears as a scatterer on the surface waveguide.] (15a)

[The axial dimension of the launcher is very small compared to the wavelength.] (15b)

In a similar manner it may be shown that the launching efficiency of a slot or aperture in a perfectly conducting transverse sheet is given by

$$\eta = \frac{1}{1 + \left\{\begin{matrix}2\\1\end{matrix}\right\} Re\ y} \tag{16}$$

where y is the normalized shunt admittance of the slot or aperture. Eq. (16) is valid under the following conditions:

[The electric field distribution in the slot when it is used as a source is identical to the field distribution in the slot when it appears as a scatterer on the surface waveguide.] (17a)

[The axial dimension of the aperture is very small compared to the wavelength.] (17b)

In the above equations, the factor two should be used for bidirectional launching. If a short circuit plate is placed an odd multiple of $\lambda_g/4$ to one side of a wire launcher, or if a cavity is placed on one side of a slot launcher (*i.e.*, unidirectional launching is obtained), then the factor one in (14) and (16) must be used. In all of the results to follow, only unidirectional launching is considered.

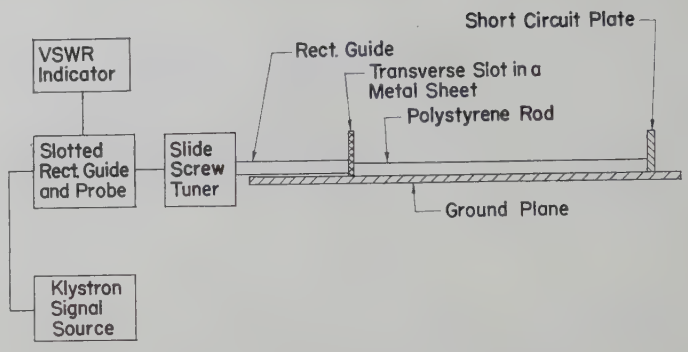

Fig. 3—The equipment used to measure the scattering matrix coefficients of a slot launcher.

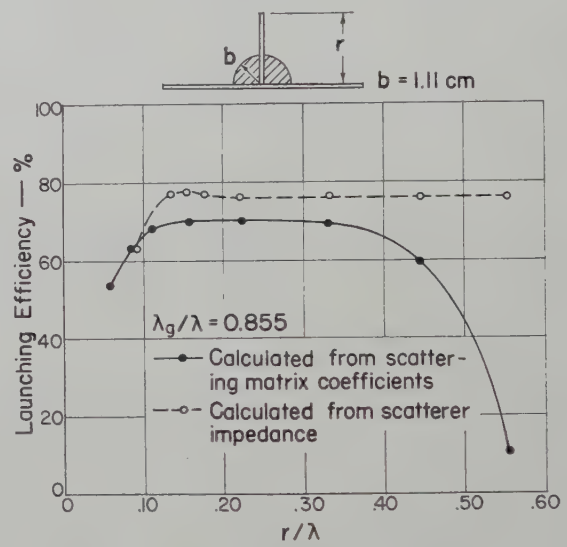

Fig. 4—Launching efficiency of a vertical wire.

Launching Efficiency from Scattering Matrix Coefficients

In several cases a slot or wire launcher was excited from rectangular waveguide and was the source of the surface wave on the image line. For example, excitation of a slot launcher is illustrated in Fig. 3. Efficiency was determined by considering the transition from rectangular waveguide to surface guide through the launcher as a two-port waveguide junction. The scattering matrix coefficients of the launcher were determined by Deschamps' method [14], [15] and the "matched" efficiency was calculated from the coefficients [16]. This method provided a direct measurement of efficiency under operating conditions where the launcher was the source of the surface wave. It was used to check the validity of efficiency as predicted from the scatterer impedance.

A comparison of efficiency by the two methods is illustrated in Fig. 4 for a vertical wire or monopole. The monopole was excited from rectangular waveguide which was mounted below the ground plane. The results agree within 6 per cent for wire lengths less than 0.35λ.

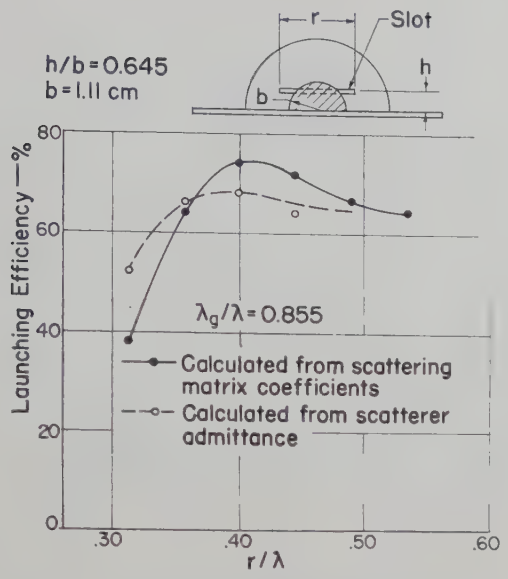

Fig. 5—Launching efficiency of a horizontal slot above the ground plane.

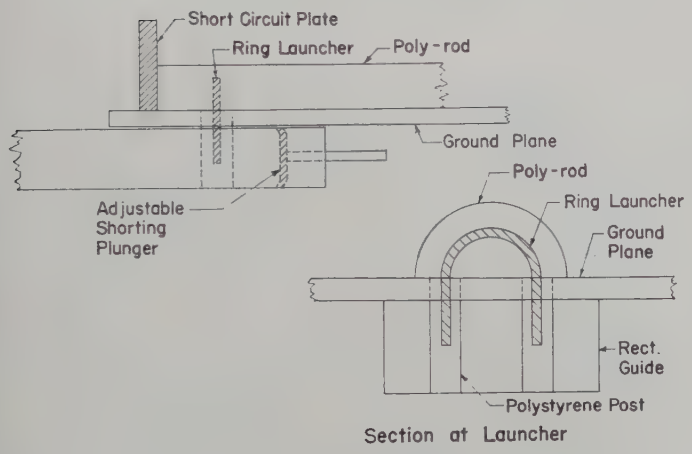

Fig. 6—Excitation of ring launcher from rectangular waveguide.

Efficiency calculated from the scatterer impedance is in serious error for wires longer than 0.35λ. This is because condition (15a) was not satisfied by long wire launchers.

A slot launcher was constructed by milling a narrow slot in a large, thin brass sheet. The slot was above, and parallel to, the ground plane. It was excited from rectangular waveguide as shown in Fig. 3. The variation of launching efficiency with slot length is illustrated in Fig. 5. The two methods yielded results which were within reasonable agreement. If the slot length is small compared to the wavelength, then condition (17a) will usually be satisfied and efficiency calculated from the scatterer admittance should be accurate.

A ring launcher was excited from rectangular guide below the ground plane. Details of this launcher are shown in Fig. 6. A balanced, symmetric excitation of the ring was necessary because the field distribution of the dipole mode requires a current null at the top of the ring. The mean ring radius was 0.715 cm. A comparison of results for this launcher is given in Table I.

TABLE I

λ_g/λ	Frequency mc	Normalized Ring Radius	Per Cent Efficiency Predicted from the Scatterer Impedance	Per Cent Efficiency Measured by Scattering Matrix Method
0.818	7436	0.177	82.3	82
0.897	5928	0.141	80.6	78

Experimental Results

Launching efficiency as a function of launcher dimensions is presented for the vertical monopole, ring, annular slot, and horizontal slot. The efficiency was calculated from the measured scatterer impedance. Unidirectional launching, as well as the satisfaction of conditions (15) or (17), was assumed. The practical problem of obtaining unidirectional launching is discussed in a later section.

Scatterer impedance was measured at six values of λ_g/λ extending from 0.818 to 0.987. Two efficiency curves for each launcher are presented, and they are for λ_g/λ equal to 0.818 and 0.897 which correspond to b/λ equal to 0.275 and 0.22, respectively. Measurements were performed in the frequency range of 5900 to 7400 mc. Surface wave attenuation due to dielectric loss [8] introduced a slight error in the measured impedance of a scatterer. This occurred because of the lossy guide between the measuring probe and scatterer. The effect of the attenuation on efficiency calculations was negligible. In the results presented here, the rod was assumed lossless and no correction was applied to the impedance measurements.

Fig. 7 illustrates the efficiency of a vertical wire or monopole as a function of the normalized wire length. The wire was silver tubing 0.15 cm in diameter and was oriented perpendicular to the ground plane. Fig. 8 shows the launching efficiency of a ring as a function of the normalized ring radius. The ring was positioned concentrically about the rod axis. The radial width of the ring was 0.16 cm and its axial thickness was 0.08 cm. Fig. 9 illustrates the efficiency of an annular slot in a thin metal sheet. The slot was concentric with the rod axis. For this case and all other slot launchers, the slot width was 0.16 cm and the metal sheet thickness was 0.08 cm. Fig. 10 illustrates the launching efficiency of a horizontal slot as a function of the normalized slot length. The slot was located above the ground plane at a normalized height $h/b=0.645$. The manner in which slot height affects the efficiency of a horizontal slot is shown in Fig. 11. Results were obtained only at $\lambda_g/\lambda=0.818$. The data are for resonant slots where the scatterer admittance was a pure conductance. The resonant slot length varied slightly for the different measurements but was always about 14 mm which yields $r/\lambda\approx 0.35$. The normalized slot height h/b appears along the abscissa of the graph. The optimum height was quite critical, and maximum efficiency of 80 per cent was obtained when $h/b=0.72$.

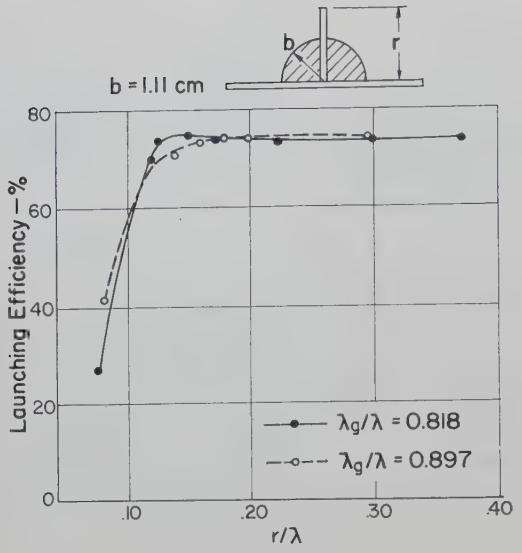

Fig. 7—Launching efficiency of a vertical wire as a function of the normalized wire length.

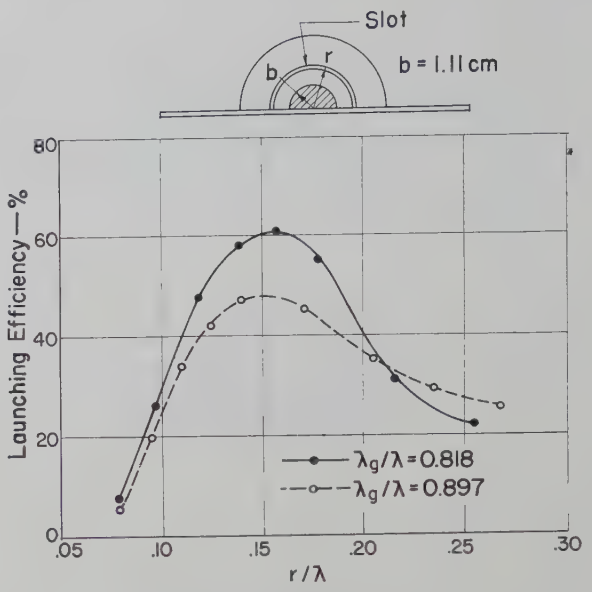

Fig. 9—Launching efficiency of an annular slot as a function of the normalized slot radius.

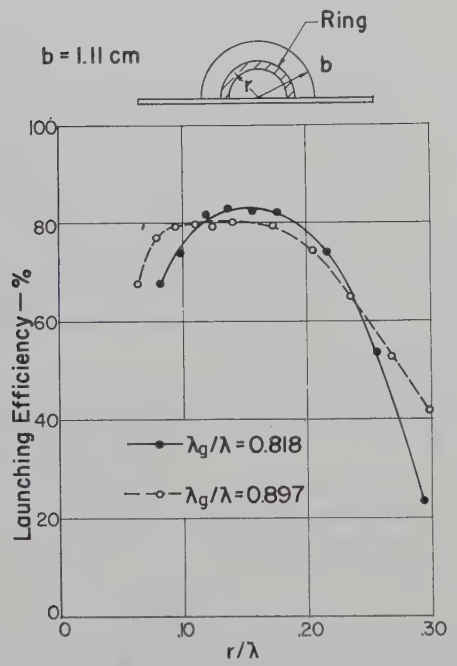

Fig. 8—Launching efficiency of a ring as a function of the normalized ring radius.

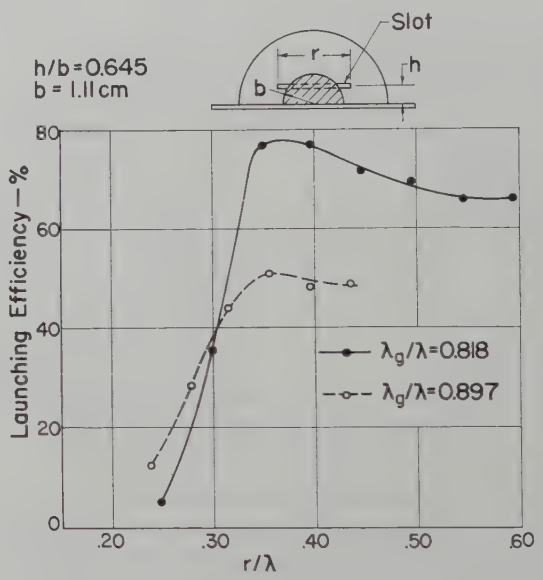

Fig. 10—Launching efficiency of a horizontal slot as a function of the normalized slot length.

The effect of surface wave coupling on launching efficiency is illustrated by the curves of Fig. 12 which show the efficiency of a resonant launcher as a function of λ_g/λ. Efficiency was always calculated when the dimensions of the launcher were such that its impedance or admittance as a scatterer was a real quantity. The largest efficiency was always obtained at the smallest λ_g/λ (largest b/λ). As λ_g/λ approaches unity, the surface wave is only slightly bound to the rod and the efficiency of a source decreases considerably. This effect was particularly evident with the annular slot where the efficiency at $\lambda_g/\lambda = 0.987$ was less than $\frac{1}{2}$ of the value at $\lambda_g/\lambda = 0.818$.

Unidirectional Launching

Unidirectional launching has been assumed in presenting the efficiencies for various types of launchers. For slot type launchers, this is readily accomplished by placing a cavity on one side of the slot or feeding the slot with a waveguide. If the presence of a cavity or waveguide does not disturb the field distribution in the slot (which is usually the case for slot sizes near resonance), then the launching efficiency will be very close to that predicted by the scatterer measurements.

However, for wire launchers it is necessary to place a reflecting device such as a reflecting plate or a parasitic element on one side of the launcher. The problem of required size for a reflecting plate was investigated for the

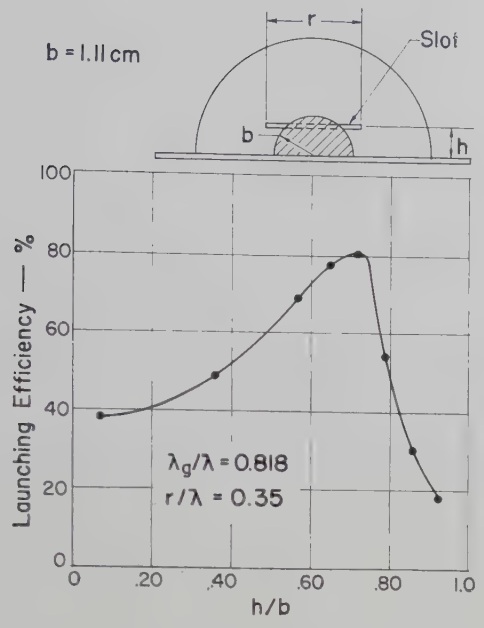

Fig. 11—Launching efficiency of a resonant horizontal slot as a function of the normalized slot height.

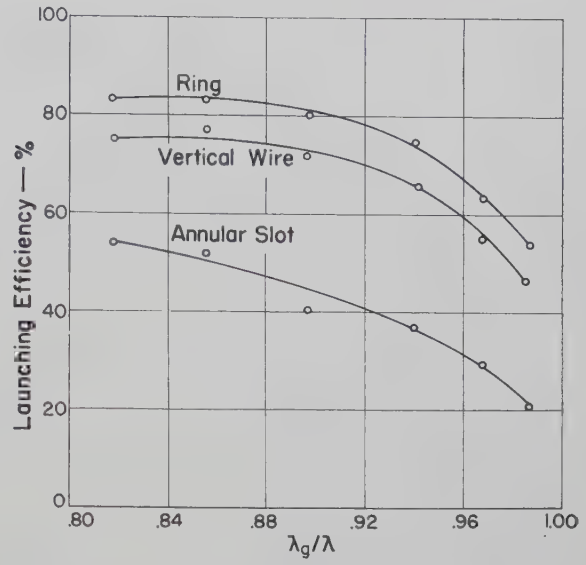

Fig. 12—Launching efficiency of a resonant launcher as a function of the parameter λ_g/λ.

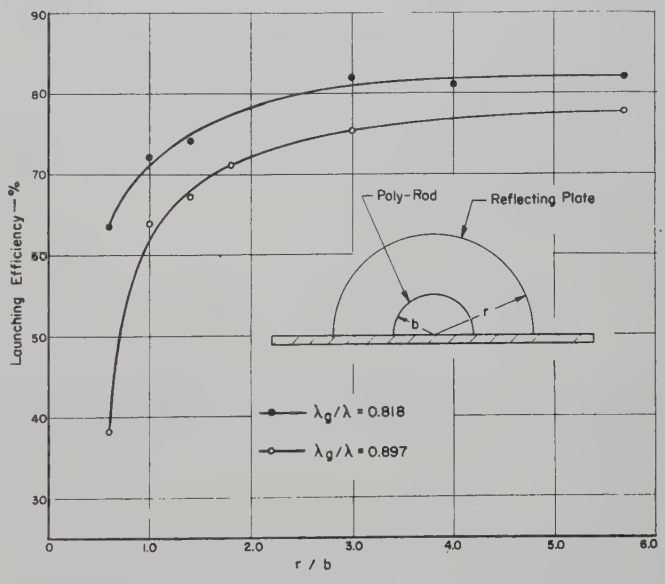

Fig. 13—Launching efficiency of a ring exciter as a function of the normalized reflecting plate radius.

case of a ring launcher at $\lambda_g/\lambda = 0.818$ and 0.897. Scattering matrix measurements of efficiency are shown in Fig. 13. The reflecting plates were very small in axial length, with a thickness of 0.17 cm and were spaced $\lambda_g/4$ from the ring. When the reflecting plate was reduced to the diameter of the rod, the ring efficiency decreased 11 per cent for the case $\lambda_g/\lambda = 0.818$ and 15 per cent for $\lambda_g/\lambda = 0.897$.

The use of a parasitic monopole, as a reflector, placed near a ring launcher was also investigated. For $\lambda_g/\lambda = 0.897$ and the spacing of the monopole from the ring equal to $0.25\lambda_g$, it was found that a monopole length of 0.148λ gave a forward to rear power ratio of 20 db. However, the launching efficiency of the ring decreased from 78 per cent for the case of a plate reflector to 59 per cent for the monopole reflector.

Conclusions

Of the two methods of measuring launching efficiency described, the one making use of the scatterer impedance is by far the most convenient and economical if more than several measurements are needed. The reasons for this are that only one measurement of scatterer impedance is required as compared to four measurements for the scattering matrix method and the fact that it is much easier to construct the scatterer form of a launcher than the actual form. The scatterer impedance may be determined from measurements on the surface waveguide or, if this is not feasible, from measurements in the waveguide feeding the surface waveguide. Of course, in this latter situation, it is necessary to calibrate the junction by some method such as Deschamps'. When a simple launcher is used as a scatterer, the feed terminals are altered; *i.e.*, the terminals of a wire launcher are shorted and the feed terminals of a slot launcher are open circuited. For example, by comparing the ring launcher of Fig. 6 and the ring scatterer of Fig. 8, it is seen that the scatterer form is much easier to fabricate than the actual form of the launcher.

The determination of launching efficiency from the equivalent scattering matrix coefficients is accurate for all types and sizes of launchers whereas the scatterer impedance method is accurate only for simple types of launchers where conditions (15) or (17) are satisfied. Both methods may be applied to other types of surface waveguides.

Launching efficiencies on the image line of 70 to 80 per cent may be obtained from the monopole, ring, and horizontal slot. All are convenient transitions from rec-

tangular waveguide to the image line. Their small size and simplicity may offset the greater efficiency that can be obtained with large and lengthy horns. Alternately, greater efficiencies with the monopoles or rings may be obtained by exciting several of them spaced at half-wavelength intervals along the rod.

Both the monopole and ring maintain good efficiency over a wide frequency range. In this respect they are superior to the horizontal slot.

Acknowledgment

The authors kindly appreciate the support of Wright Air Development Center and wish to thank Nicholas J. Kuhn and Robert L. Jones for assisting with the measurements.

Bibliography

[1] Hondros, D., and Debye, P. "Elektromagnetische Wellen an dielektrischen Drähten," *Annalen der Physik*, Vol. 32 (1910), pp. 465–476.
[2] Carson, J. R., Mead, S. P., and Schelkunoff, S. A. "Hyper-Frequency Wave Guides—Mathematical Theory," *Bell System Technical Journal*, Vol. 15 (April, 1936), pp. 310–333.
[3] Beam, R. E., *et al.* "Final Report on Investigations of Multi-Mode Propagation in Waveguides and Microwave Optics," Army Signal Corps Contract No. W36-039, SC-38240, Microwave Laboratory, Northwestern University, Evanston, Ill., 1950.
[4] Kiely, D. G. *Dielectric Aerials*, "Methuen's Monographs on Physical Subjects," New York: John Wiley and Sons, Inc., 1953.
[5] Duncan, J. W., and DuHamel, R. H. "A Technique for Controlling the Radiation from Dielectric Rod Waveguides," IRE Transactions on Antennas and Propagation, Vol. AP-5 (July, 1957), pp. 284–289.
[6] Margerum, D. L. "The Excitation of Electromagnetic Waves on Dielectric Rods," M.S. Thesis, Department of Electrical Engineering, Northwestern University, Evanston, Ill., 1950.
[7] King, D. D., and Schlesinger, S. P. "Losses in Dielectric Image Lines," IRE Transactions on Microwave Theory and Techniques, Vol. MTT-3 (January, 1957), pp. 31–35.
[8] Elsasser, W. M. "Attenuation in a Dielectric Circular Rod," *Journal of Applied Physics*, Vol. 20 (December, 1949), pp. 1193–1196.
[9] King, D. D. "Properties of Dielectric Image Lines," IRE Transactions on Microwave Theory and Techniques, Vol. MTT-3 (March, 1955), pp. 75–81.
[10] ——. "Circuit Components in Dielectric Image Lines," IRE Transactions on Microwave Theory and Techniques, Vol. MTT-3 (December, 1955), pp. 35–39.
[11] Huxley, L. G. H. *The Principles and Practice of Wave Guides*, New York: The Macmillan Co., 1947, pp. 297–299.
[12] Goubau, G. "On the Excitation of Surface Waves," Proceedings of the IRE, Vol. 40 (July, 1952), pp. 865–868.
[13] Adler, R. B. "Waves on Inhomogeneous Cylindrical Structures," Proceedings of the IRE, Vol. 40 (March, 1952), pp. 339–348.
[14] Deschamps, G. A. "Determination of Reflection Coefficients and Insertion Loss of a Waveguide Junction," *Journal of Applied Physics*, Vol. 24 (August, 1953), pp. 1046–1050.
[15] Storer, J. E., Sheingold, L. S., and Stein, S. "A Simple Graphical Analysis of a Two-Port Waveguide Junction," Proceedings of the IRE, Vol. 41 (August, 1953), pp. 1004–1013.
[16] Altschuler, H. M., and Felsen, L. B. "Network Methods in Microwave Measurements," *Proceedings of Symposium on Modern Advances in Microwave Techniques*, Polytechnic Institute of Brooklyn, Brooklyn, N. Y. (July, 1955), pp. 299–300.
[17] DuHamel, R. H. and Duncan, J. W. "Launching Efficiency of Wires and Slots for a Dielectric Rod Waveguide,"Electrical Engineering Research Laboratory, Engineering Experiment Station, University of Illinois, Urbana, Ill., Antenna Laboratory Technical Report No. 24, August, 1957.

Microwave Switching by Crystal Diodes*

MURRAY R. MILLET†

Summary—**This paper gives the results of an investigation of the use of a microwave crystal as an RF switching element. Variation of a dc bias applied to the crystal will change its impedance, thereby providing an electronic control of microwave power. Empirical data are correlated with the physical structure of the crystal and its equivalent circuit to establish the frequency and power limitations of the switch. A comparison is also made of the switching properties of germanium and silicon crystals. Curves are given for predicting the switching capacity of any diode once its impedance has been normalized with respect to the characteristic impedance of the waveguide. Some methods are suggested for improving the bandwidth and power capacity of the crystal switch.**

Introduction

IN MANY applications the need arises for a fast acting waveguide switch to serve as either an on-off device or RF modulator. The conventional mechanical switch, either rotor or vane type, switches in milliseconds and also has the disadvantage of large size when physical volume is considered. The electronic switch of the ferrite type is smaller in size and has a switching time measured in microseconds. However, large peak powers are required to drive the solenoid, and the problem of holding a large coil current for the duration of a long pulse with fast rise and fall times introduces complexities. This paper describes an RF switch comprised of a crystal rectifier as the switching element. Because of the small time constant of the crystal and its low impedance there is evolved an electronic switch capable of switching in a fraction of a microsecond and requiring low driving power. The crystal switch may also serve as an RF modulator or variable attenuator.

The common use for crystal rectifiers at microwave frequencies is as a mixer or frequency converter in a heterodyne system.[1] When used as such, the local oscil-

* Manuscript received by the PGMTT, October 29, 1957; revised manuscript received, January 23, 1958.
† Philco Corp., Philadelphia, Pa.

[1] H. C. Torrey and C. A. Whitmer, "Crystal Rectifiers," McGraw-Hill Book Co., Inc., New York, N. Y., p. 153; 1948.

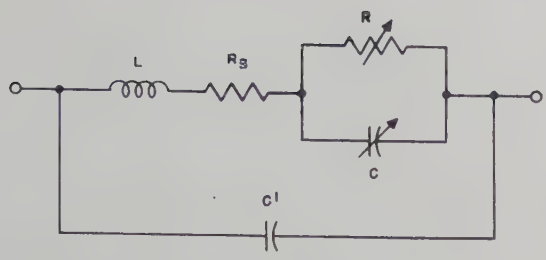

Fig. 1—Equivalent circuit of a crystal rectifier.

lator and signal are both applied to the crystal where, because of the nonlinear element, the two signals are mixed. The result is the generation of new frequencies equal to the sum and difference, and their harmonics, of the original frequencies. In this application the mixing element is localized to the point contact of the crystal where rectification occurs between the semiconductor and the whisker wire. In some cases a bias is applied to the crystal for matching purposes or noise figure improvement.

In addition to use as a mixer, the crystal may serve as a switching device.[2–4] This is accomplished by exploiting the extreme variation of the nonlinear impedance of the crystal with bias. The network representation of the crystal is a resonant circuit composed of nonlinear elements, and thus by changing the bias from a high forward current to a small back current, both the resistive and reactive components of the circuit are radically changed. A large forward bias will decrease the nonlinear resistance and result in a high effective crystal impedance which will absorb little power. On the other hand, a large back bias will result in a low impedance which both absorbs power and causes high reflection. It is this change of impedance which can be used to control power propagated in a transmission line or waveguide.

Equivalent Circuit of the Crystal

For analysis as a switching device, a detailed equivalent circuit is necessary. The complete crystal may be represented as shown in Fig. 1. The whisker presents an inductance, L, which is independent of the applied bias. Considering the whisker as a straight wire, the length of which is small compared to λ, the inductance is calculated by

$$L = 0.002l\left(\ln\frac{4l}{d} - \frac{3}{4} + \frac{d}{2l}\right)$$

where L = inductance in microhenries, l = length in cm, and d = diameter in cm. The permeability is assumed equal to one. In the case of the 1N263 crystal the wire is straight except for very small kinks whose mutual inductance may be neglected. The inductance is calculated to be 3.17 millimicrohenries, resulting in an inductive reactance of 180 ohms at 9.0 kmc.

The spreading resistance of the semiconductor is represented by R_s, a resistance of fixed value, which accounts for the compression of current flow paths at the point of contact. This resistance is a function of the conductivity of the semiconductor and the contact area. If σ denotes the conductivity and r is the radius of an assumed circular area of contact,

$$R_s = \frac{1}{4\sigma r}.$$

Alternatively, the spreading resistance may be taken as the slope of the static I-E curve of the crystal in the region of high forward current. For the average 1N263 the spreading resistance is found to be in the neighborhood of 10 to 20 ohms, while a 1N23C crystal has a spreading resistance of 30 ohms because of the lower conductivity of the silicon. The resistance of the wire is considered negligible.

The resistance R represents the nonlinear resistance of the point contact and semiconductor, or barrier resistance, which varies with the amplitude and polarity of bias. As the current increases in the forward direction, R becomes increasingly small until, in the region of constant slope of the I-E curve, its value is small compared to R_s. In the back bias condition R increases with current, attaining values such that R_s is negligible. This latter value of R may be taken from the I-E curve where the slope is constant in the negative current direction.

The barrier capacitance C is also a function of bias, and accounts for the storage of charge in the boundary layer of the semiconductor. For mixer considerations little error is introduced by assuming C constant.[1] Measured values of the barrier capacitance lie between 0.02 and 1 $\mu\mu$f, which at low frequencies presents a low susceptance in parallel with $1/R$ in the back bias condition. However, at microwave frequencies the susceptance of the barrier capacitance may become large compared to $1/R$ and cause considerable shunting action.

The term C' in the above equivalent circuit includes the parasitic capacitances of the internal studs which support the whisker and semiconductor, and the crystal cartridge itself. There may also be included in this term the reactance contributed by the crystal mount. The capacitance of C' can be easily compensated for by tuning and will henceforth be neglected in the analysis.

Equivalent Circuit as a Switch

When used as an RF switch, the crystal is centered on the waveguide axis in a conventional mount whose backplate has been removed to permit the transmission of power. For switching operation the crystal presents one of two different impedances which are determined by the amplitude and polarity of the applied dc bias. In

[2] M. A. Armistead, E. G. Spencer, and R. D. Hatcher, "Microwave semiconductor switch," Proc. IRE, vol. 44, p. 1875; December, 1956.

[3] F. S. Coale, "A switch detector circuit," IRE Trans. on Microwave Theory and Techniques, vol. MTT-3, pp. 59–61; December, 1955.

[4] D. J. Grace, "A Microwave Switch Employing Germanium Diodes," Applied Electronics Lab., Stanford University, Stanford, Calif., Tech. Rep. No. 26; January 17, 1955.

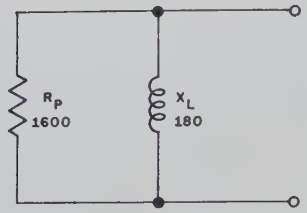

Fig. 2—Equivalent circuit of a crystal under forward bias.

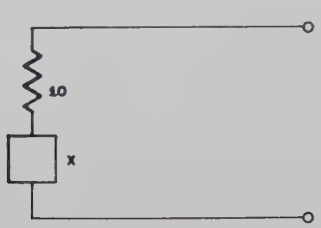

Fig. 3—Circuit of a back-biased crystal in waveguide.

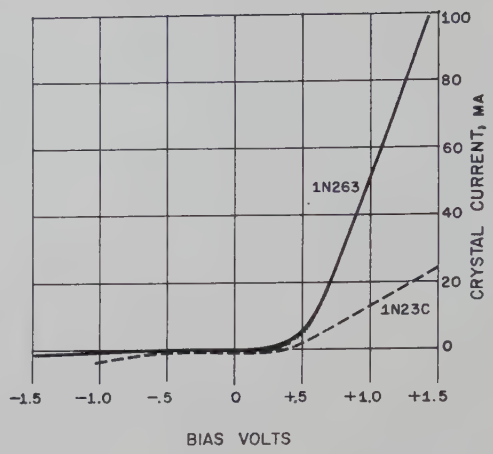

Fig. 4—*I-E* curve of 1N32C and 1N263 crystals.

the passing, or ON condition, a positive bias is applied which results in the nonlinear resistance being small compared to the barrier capacitance, thereby shunting it. The result is a series *R-L* circuit shunted across the waveguide. In the stop, or OFF condition, a back bias is applied which causes the nonlinear resistance to attain high values, and thus be shunted by the barrier capacitance. The crystal is now represented by a series *R-L-C* circuit across the guide. At some frequency the series *L* and *C* will resonate, leaving a very small resistance, the spreading resistance, shunted across the waveguide. It is this change of circuit that achieves the switching action.

Consider the crystal with a high forward bias applied. In this case the value of the nonlinear resistance is approaching that of R_s, assumed to be 10 ohms, and is shunting the barrier capacitance *C*. The resultant circuit is the spreading resistance R_s and a small nonlinear resistance *R*, a total of 20 ohms, in series with the whisker inductive reactance. At 9.0 kmc the circuit is a series *R-L* circuit with a *Q* of 9, and is transformed into the parallel *R-L* circuit of Fig. 2 by

$$R_p = R_s(Q^2 + 1),$$

$$Q = \frac{R_p}{\omega L}.$$

The crystal is in the ON condition, and is now considered in shunt with 0.400×0.900 (RG-52/U) waveguide terminated in a matched load, assumed here to be 400 ohms. When plotted on a Smith chart the admittance of the circuit, normalized with respect to the waveguide, is seen to be 0.25-*j*2. Discounting the reflection loss, under these conditions the power absorbed by the load will be reduced by 20 per cent, or approximately 1 db.

Now consider the crystal with a high back bias applied, resulting in a small back current. The nonlinear resistance is now very large. The barrier capacitance shunts this large resistance and resonates with the whisker inductance or leaves a small residual reactance because of counteraction with it. The resulting circuit is a small resistance, the spreading resistance, in series with a very small (if any) reactance. This circuit is now considered in shunt with the waveguide, as shown in Fig. 3. The result of placing such a circuit across the waveguide is a standing wave ratio of 40 to 1. The power absorbed by the load will be reduced by 97.5 per cent because of absorption by the crystal, together with considerable reflection.

Essentially the same circuit holds for the 1N23C silicon and 1N263 germanium crystals. The silicon crystal, however, is noted to have a higher spreading resistance, and a lower value of nonlinear resistance when biased in the back direction which is attributed to the lower drift mobility[2] of silicon as compared to germanium. The effect of the decreased *R* is less shunting by the barrier capacitance under a negative bias, and thus a higher effective resistance of R_s and *R* placed across the waveguide load, which in turn results in less reflection and more power absorbed by the load. For this reason efforts were centered around the germanium 1N263 as a switching element. However, the silicon diode has been used as a switch but only where the diode is used to shunt a coaxial line.[3] A comparison of average 1N23C and 1N263 *I-E* curves is shown in Fig. 4. A switch using germanium 1N91 diodes to shunt a coaxial line in the 3-kmc range has also been reported.[4]

Switch Operation

The RF admittance presented by the 1N263 crystal, centered in RG-52/U waveguide, is shown in Fig. 5. The admittances shown, which are referred to the center of the crystal, are those of the mounted crystal only, and exclude the admittance of the waveguide load. In the condition of forward bias the admittance is seen to be less than the admittance of the guide, as was shown in the circuit of Fig. 2. The discrepancy between the calculated and measured imaginary parts of the admittance is attributed to the presence of parasitic reactances not accounted for in the calculations. Reversing the bias is seen to result in a crystal admittance which is much larger than the guide admittance, as explained by Fig.

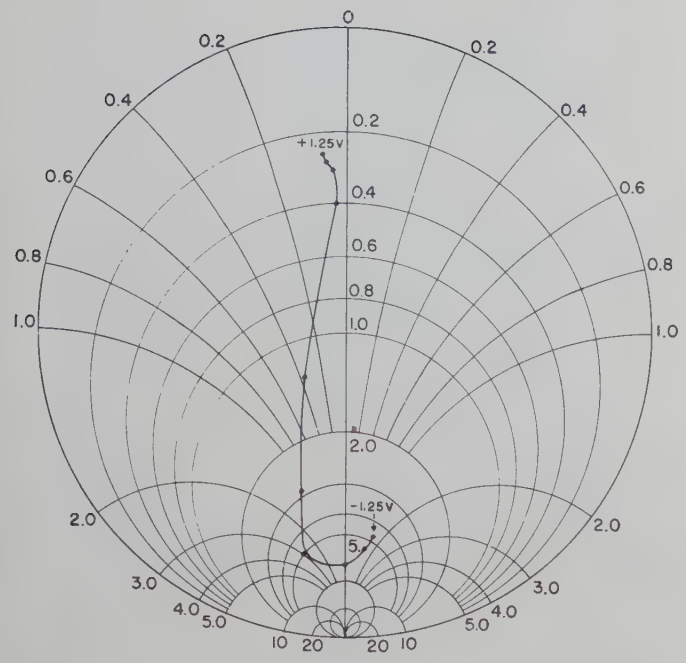

Fig. 5—RF admittance of 1N263 crystal, at 9.2 kmc, 0.5 mw, as a function of bias.

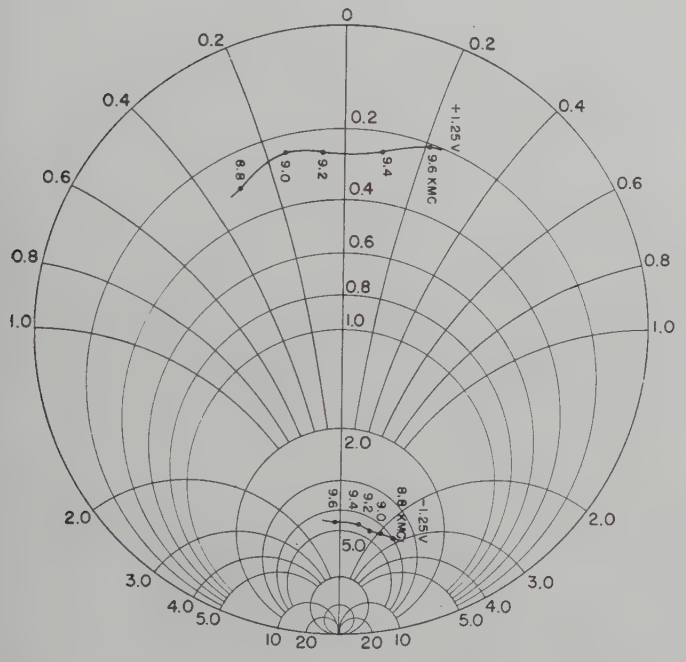

Fig. 6—RF admittance variation with frequency.

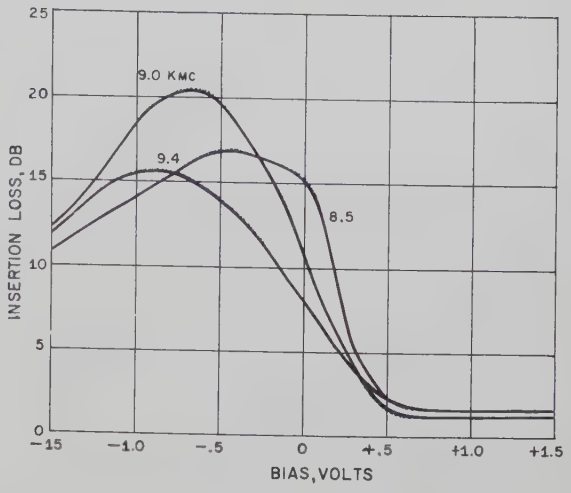

Fig. 7—Insertion loss of crystal switch vs bias.

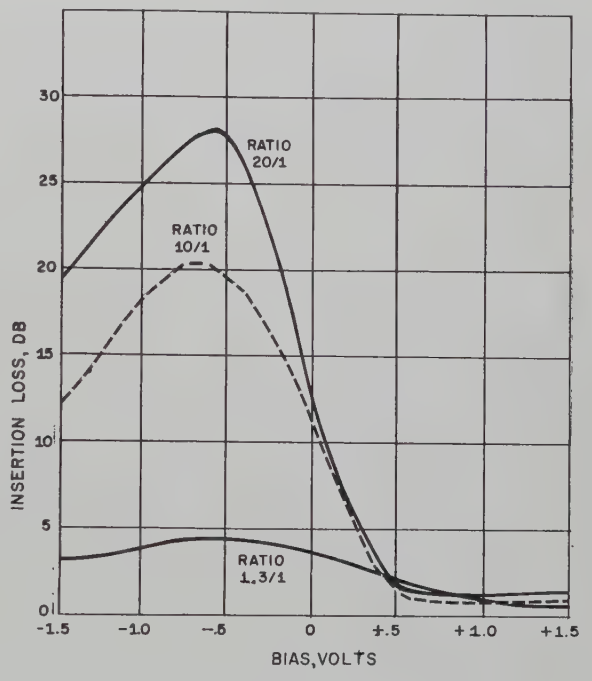

Fig. 8—Variation of switch attenuation with rectifier characteristics.

3. It is seen that with additional increase of back bias the crystal admittance begins to decrease. This is due to the high back bias reaching the Zener voltage of the semiconductor, at which point the current in the back direction begins to increase.

The frequency sensitivity of the crystal is shown in Fig. 6, where the admittances under two opposite biasing conditions are plotted as functions of frequency. At a little over 9.2 kmc the crystal, mounted in its test holder, is resonant in the forward bias condition and the corresponding admittance is a pure conductance. The design frequency of the 1N263, however, is 9.375 kmc. The deviation here from the design resonance is attributed to the fact that the crystal was tested in a mount differing from the one used in the crystal design, and also the differences in measurement technique and production tolerances. Allowing for these external differences the admittances follow closely the equivalent circuits of Figs. 2 and 3. The effect of the back bias circuit being off resonance is illustrated in Fig. 7. These curves were plotted from averaged data taken from randomly selected crystals.

The effect of variation of the rectifier characteristics, or the *I-E* curve, of the crystal is shown in Fig. 8, where a comparison is made between crystals of different front-to-back ratios, all measured at the same frequency. The ratio 10:1 represents the lower limit of the ratios

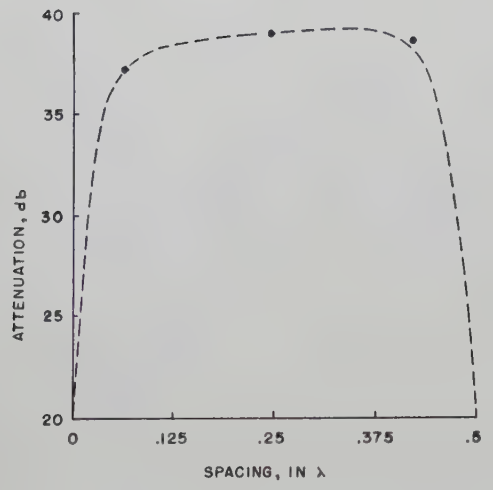

Fig. 9—Insertion loss of two crystal switches vs element spacing.

expected in a production run of crystals. To obtain ratios higher than 15:1 requires hand selection, as was done for the crystal with the 20:1 ratio. The 1.3:1 ratio crystal had been submitted to many previous tests and severely overdriven, both by RF power and direct current.

Limit of Switching

As shown above, the passing and stopping of RF power by the crystal is accomplished by the nonlinear resistance causing either a near match or large mismatch in the guide. The limit of the ratio of passed to stopped power therefore rests entirely in the crystal itself, independent of crystal holder or waveguide tuning. As shown for a 1N263 crystal the pass to stop ratio lies between 25 and 30 db. If, by known means, the stopping limit or isolation of these crystals is to be increased, it appears that this will be only at the expense of correspondingly increased insertion loss in the passing condition.

One method of achieving this is to enclose the crystal in a cavity whose transformer action will increase the impedance of the waveguide as seen by the crystal, and thereby cause a greater mismatch in the stop condition when the crystal impedance is small. However, in the passing condition the impedance is likewise increased by transformer action and will therefore raise the insertion loss. One such model has been built in which the isolation was 40 db, but this was at the expense of the necessary increase of insertion loss to 4.5 db. An alternative method is to increase the guide impedance by narrowing the waveguide in the region of the crystal.

If the length of the over-all switch is no limitation, the crystals may be cascaded, with a spacing between the elements of one-quarter wavelength. The over-all switching attenuation will then be the sum of the individual losses, both in the passing and stopping condition. Fig. 9 shows the isolation vs spacing for two crystals, each of which individually gave 20 db isolation.

Fig. 10 shows the variation of insertion loss as the

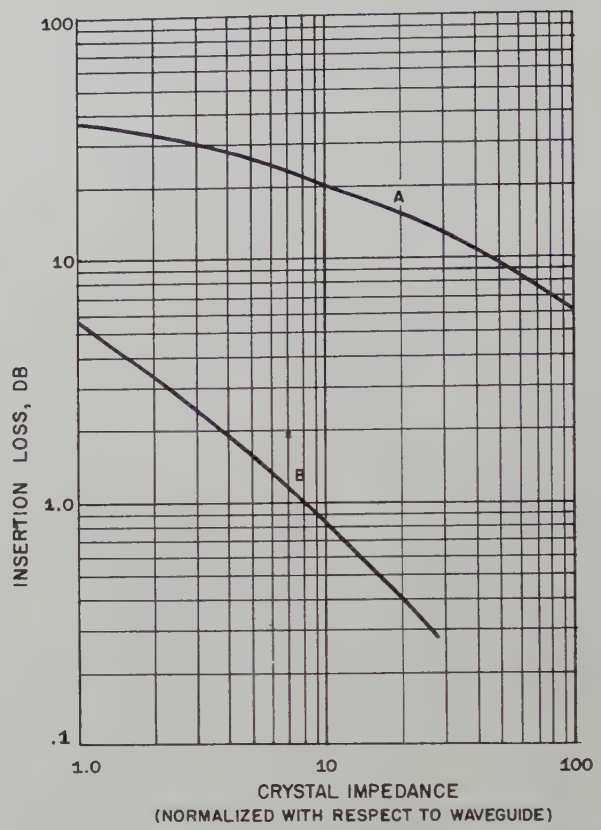

Fig. 10—Insertion loss vs normalized crystal impedance.

crystal impedance, which is normalized to the waveguide impedance, is varied. The curve is normalized so that the insertion loss may be predicted for any crystal, once its front-to-back ratio is known and defined in terms of waveguide impedance. The curve also serves in the reverse case where, with a specified insertion loss, the correct crystal and bias limits may be determined and, if necessary, to what extent the waveguide impedance must be increased.

Switching Time

Assuming the crystal to be in the back bias condition, the whisker inductance and resistance at switching frequencies are considered negligible and the circuit consists essentially of the low barrier capacitance and high barrier resistance, whose average values may be 0.2 $\mu\mu$f and 5000 ohms, respectively. The time constant is then 100×10^{-12} seconds, a small part of a microsecond. During the rise time of a video biasing pulse the nonlinear resistance decreases while the barrier capacitance increases. Thus, the time constant of the circuit is kept fairly constant by the R and C compensating for each other. The same compensation holds for the decreasing portion of the video pulse. The rise and fall times of the video pulse are shortened by the effective nonlinear curve of bias vs time, where the curve is steepened over the positive bias portion, which suggests one of the basic applications of the crystal switch.

Consider the crystal inserted between a pulsed RF source and load. If the crystal is held in a back bias

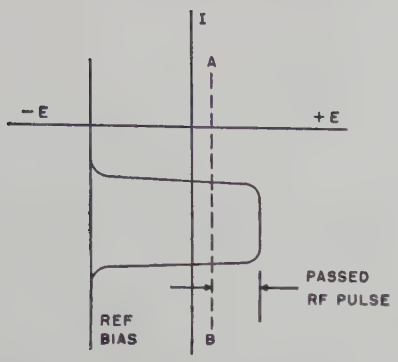

Fig. 11—Pulse shaping by crystal switch.

condition and video pulses of forward bias are applied synchronously with an RF pulse, the transmitted or passed RF pulse will have lower rise and fall times than the incident pulse. Referring to Fig. 11, the passed pulse corresponds to only that portion of the applied video pulse which is to the right of the line *AB* where the slope of the *I-E* curve indicates the nonlinear resistance begins to be small, *i.e.*, a steep slope. Assuming between two and three time constants are needed to arrive at this point from the start of the video pulse, the transmitted RF pulse rise time is only a part of the total rise time, and therefore the passed pulse has a rise time of its own of less than two time constants. Thus it can be seen that RF pulses transmitted through the crystal switch have faster rise and fall times than the original pulse and are also narrower.

Power Limitations

Aside from the power dissipation capacity, the power to be switched is limited by the *I-E* characteristics of the diode. As shown in Fig. 12, the RF signal impinging on the crystal will drive the instantaneous operating point along the curve to voltages corresponding to the peak RF voltage points. In the ON condition the operating point is centered well to the right of the zero bias axis, and must remain on the low resistance portion of the curve for all instantaneous voltages. If the amplitude of the RF signal is such that the operating point is driven into the high resistance portion, the mean impedance of the crystal will increase and thereby increase the insertion loss. Similarly, in the OFF condition the RF signal must be limited to amplitudes such that the operating point is not driven into the low resistance part of the curve, and thereby does not reduce the insertion loss.

In the case of the 1N263 crystal, the *I-E* curve limits the RF peak-to-peak voltage to 2 or 3 volts, which is the case for approximately 1 mw. Fig. 13 shows the effect of increasing the applied RF power. The negative bias was increased in an effort to prevent the operating point from moving into the low resistance part of the *I-E* curve with higher RF power applied. The result was a further decrease of insertion loss because of the instantaneous operating point exceeding the Zener voltage, and an increase of current in the negative direction.

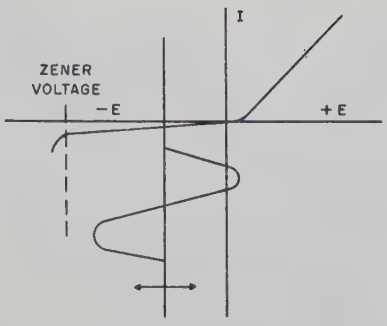

Fig. 12—Operating point on the *I-E* curve due to RF power.

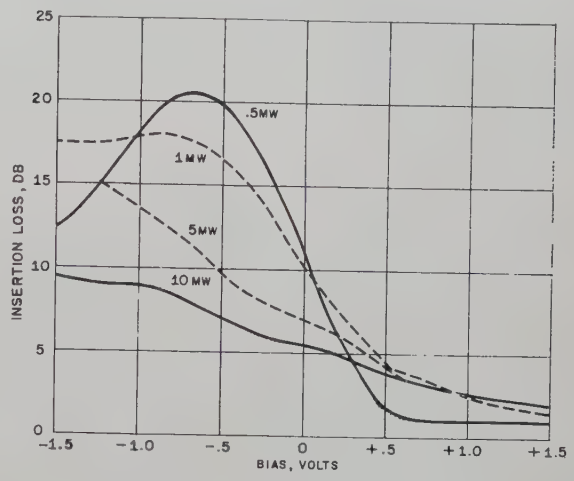

Fig. 13—Insertion loss of 1N263 crystal switch at various power levels.

A method of increasing the power switch capacity of the switch is to cascade the crystals. Though optimum switching is sacrificed in the first crystal, the passed power is sufficiently reduced for optimum operation of the following crystals. What passing insertion loss is tolerable will then determine the number of crystals to be used.

Obviously the switching of higher powers demands a crystal whose *I-E* curve shows a greater Zener voltage and a lower positive slope for the forward bias. By doubling the Zener voltage the RF power to be stopped should more than double, and at the same time the passed power would be increased with higher forward bias. The remaining limitation would be that of heat dissipation.

In an effort to overcome these limitations, existing germanium diodes with higher Zener voltages and higher resistivities than the 1N263 were investigated at *X* band. A 1N34 diode, as packaged by Sylvania, was found to have a Zener voltage indicative of high power switching capacity. The axial leads of the diode were replaced with pins to enable the crystal to be supported in the waveguide mount. The resulting curve of isolation vs bias, at 9.3 kmc, is shown in Fig. 14. The same curve held for all powers up to 15 mw, at which point the excessive current (the sum of the applied dc and rectified RF) caused the point contact to weld into the germanium, after which the diode was no longer a rectifier.

The test was repeated using a Hughes 1N67A. The results showed a limiting power of 5 mw, again only because of the current limitations of the diode. In this case a passing insertion loss of 1 db was attained with a bias of +3 volts and a corresponding current of 300 ma. The maximum insertion loss was 16 db with a negative bias of 125 volts. The 1N67 was supported within a ceramic cartridge for waveguide mounting.

A 1N38 was modified for waveguide mounting in the same fashion as the 1N34. The *I-E* curve and insertion loss vs bias curve at 9.3 kmc are shown in Figs. 15 and 16, respectively. The power switching capacity is seen to follow the prediction of the *I-E* curve. There was no sign of decreased insertion loss at negative biases, or increased insertion loss at positive biases, for all powers up to and including 50 mw. Again the limiting factor was power dissipation.

Conclusions

At present the power limitations of the crystal switch restrict its use to low power applications. However, it has been shown that by utilizing a semiconductor with such characteristics as high Zener voltage and high resistivity, the limit of the power that can be handled can be substantially increased. Experiments are now being conducted toward the development of such semiconductors, and powers of over one watt have been successfully switched.[5] The remaining limitation is that of power dissipation. However, this too can be overcome by proper wafer form factor and semiconductor-to-metal contact area.

In addition, observing the curves for isolation vs bias as a function of frequency, it is seen that the crystal switch is not a broadband device but operates optimumly at the resonant frequency of its whisker inductance and barrier capacitance. In the case of the microwave crystals used the optimum operation was at about 9.3 kmc. However, the fabrication of a crystal to operate at a different frequency should present no problem. By correctly selecting the length of the whisker wire the crystal can be made to operate optimumly at any desired frequency. To broaden the bandwidth of the crystal switch the physical configuration of the crystal must be changed, since both the semiconductor and whisker determine the band over which the crystal will satisfactorily operate. Such a change could be the elimination of the whisker inductance, which would eliminate the resonance of the present crystal. Such a crystal has been described,[6] in which the crystal is matched, RF-wise, up to the point of semiconductor-to-metal contact.

The crystal switch may be compared to the fastest ferrite switches. The latter achieve isolations of 20 db in millimicroseconds, and have capacities of many watts, but demand high driving powers. A crystal switch is seen to give comparable isolation, and more if used in multiple, in comparable switching time with the advantage of low driving power.

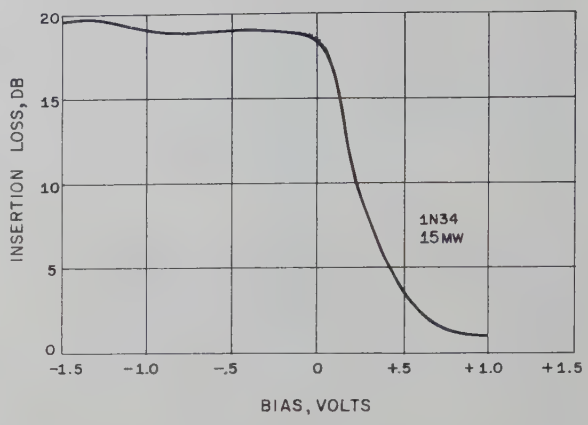

Fig. 14—Insertion loss of a 1N34 germanium diode at 15 mw.

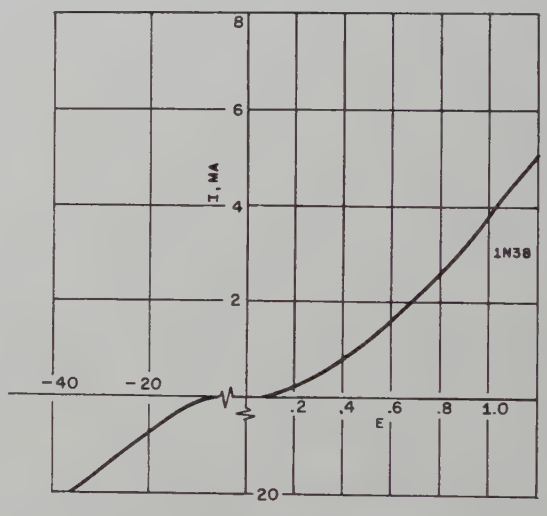

Fig. 15—*I-E* curve of 1N38 diode.

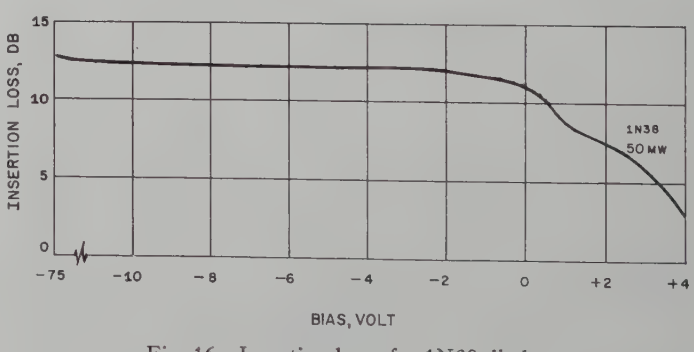

Fig. 16—Insertion loss of a 1N38 diode.

Acknowledgment

Grateful acknowledgment is made to C. T. McCoy for his guidance and helpful suggestions, and for criticisms of H. N. Ringer and R. T. Benware, of the Philco Corporation. There were also discussions with E. G. Spencer of the Diamond Ordnance Fuze Laboratories, Washington 25, D. C.

[5] Personal communication with E. G. Spencer, Diamond Ordnance Fuze Labs., Washington, D. C.

[6] Bell Telephone Labs., "Crystal Rectifiers," Signal Corps Contract No. DA-36-039, Second Interim Rep., January, 1955.

Dielectric Image Lines*

S. P. SCHLESINGER† AND D. D. KING‡

Summary—Some further studies on the dielectric image line are presented. Following a verification of field purity for the conventional image system, the effects of dielectric constant and dielectric geometry on loss, dispersion, and field extent are examined. Results are also discussed for an asymmetric line, *i.e.*, the case of dielectric binding medium partially submerged in an image surface.

Introduction

IT IS the purpose of this paper to report further on the properties of one type of surface wave line, namely the dielectric image line.[1–5]

The axial propagation of electromagnetic energy, radially symmetric about a conducting or dielectric binding medium, has been investigated and reported on by many authors.[6–17] These lines may be thought of as "free" surface wave lines, as contrasted to a transmission line whose electromagnetic field is confined.

* Manuscript received by the PGMTT, November 12, 1957; revised manuscript received, March 17, 1958. The work reported on herein was accomplished at The Johns Hopkins University, supported by AF Cambridge Res. Ctr.

† Dept. of Elec. Eng., Columbia University, New York, N. Y.

‡ Electronic Communications Inc., Timonium, Md.

[1] D. D. King, "Dielectric image line," *J. Appl. Phys.*, vol. 23, pp. 699–700; June, 1952.

[2] ——, "Properties of dielectric image lines," IRE TRANS. ON MICROWAVE THEORY AND TECHNIQUES, vol. MTT-3, pp. 75–81; March, 1955.

[3] ——, "Circuit components in dielectric image lines," IRE TRANS. ON MICROWAVE THEORY AND TECHNIQUES, vol. MTT-3, pp. 35–39; December, 1955.

[4] D. D. King and S. P. Schlesinger, "Losses in dielectric image lines," IRE TRANS. ON MICROWAVE THEORY AND TECHNIQUES, vol. MTT-5, pp. 31–35; January, 1957.

[5] S. P. Schlesinger and D. D. King, "Some Fundamental Properties of Dielectric Image Line," Rad. Lab., The Johns Hopkins University, Baltimore, Md., Final Rep. AFCRC-TN-56-766; December, 1956.

[6] A. Sommerfeld, "Über die fortplanzung Elektrodynamischer Wellen langes eines Drahtes," *Ann. Phys. Chem.*, vol. 67, p. 233; July, 1899.

[7] G. Goubau, "Surface waves and their application to transmission lines," *J. Appl. Phys.*, vol. 21, pp. 1119–1128; November, 1950.

[8] H. M. Barlow and A. E. Karbowiak, "An investigation of the characteristics of cylindrical surface waves," *Proc. IEE*, vol. 100, pt. 3, pp. 321–328; November, 1953.

[9] E. H. Sheibe, B. G. King, and D. L. Van Zeeland, "Loss measurements of surface wave transmission lines," *J. Appl. Phys.*, vol. 25, pp. 790–797; June, 1954.

[10] D. Hondros and P. Debye, "Electromagnetische Wellen in dielektrischen Drahtes," *Ann. Phys.*, vol. 32, pp. 465–476; June, 1910.

[11] H. Ruter and O. Schriever, "Elektromagnetische Wellen an dielektrischen Drahten," *Schrift. Naturalwiss. Ver. Schleswig-Holstein*, vol. 16, pp. 2–60; January, 1915.

[12] J. R. Carson, J. P. Mead, and S. A. Schelkunoff, "Hyperfrequency wave guide mathematical theory," *Bell Sys. Tech. J.*, vol. 15, pp. 310–333; April, 1936.

[13] R. E. Beam, M. M. Astrahan, W. C. Jakes, H. M. Wachowski, and W. L. Firestone, "Dielectric Tube Waveguides," Northwestern University, Evanston, Ill., Rep. ATI 94929, ch. 5; 1949.

[14] C. H. Chandler, "An investigation of dielectric rod as wave guide," *J. Appl. Phys.*, vol. 20, pp. 1188–1193; December, 1949.

[15] W. M. Elsasser, "Attenuation in a dielectric circular rod," *J. Appl. Phys.*, vol. 20, pp. 1193–1200; December, 1949.

[16] P. Mallach, "Untersuchungen an dielektrischen wellenleitern in Stab- und Rohrform," *FTZ*, vol. 1, pp. 8–13; Heft 1, 1955.

[17] H. G. Unger, "Übertragungswerte von Wellen an dielektrischen Leitern," *FTZ*, vol. 8, pp. 438–443; Heft 8, 1955.

To overcome some of the objections of the completely free surface wave lines, one of the authors has developed a modified line which uses a half round dielectric rod mounted on an image plane.[1,2] The boundary conditions dictated by the presence of this plane support the existence of the desirable low-loss, no low frequency cut-off HE_{11} mode, but exclude the higher-loss undesirable modes of the E type. Thus a convenient supporting surface defines, and partially confines, the surrounding field. By choosing a reasonable rod diameter to wavelength ratio, a fairly loosely bound field with attendant low loss may be realized.[4] In addition, the conducting sheet acts as a polarization anchor, and reduces the mode conversion problem. Various circuit components such as bends, junctions, and launchers have been developed for image lines.[3]

Following a verification of field purity, the effect of dielectric constant and guiding surface geometry on the basic properties of the dielectric image line are discussed. These basic properties include loss, field extent, and dispersion. Given a conducting plane upon which a dielectric of some arbitrary cross section may be mounted, one recognizes two general possibilities: the dielectric may be mounted so that the plane is an image in a true sense, or part of the dielectric may be recessed into the conducting plane, producing what may be termed an asymmetrical image system. Both cases will be treated here.

Field Purity

The basic equations for round dielectric rod are reviewed in the Appendix. The characteristic equation involving the radial parameters p and q and evolving out of the application of boundary conditions (3) was solved with $n=m=1$ for a broad range of dielectric constant. These results are shown in Figs. 1 and 2.

The field purity of the HE_{11} mode with a half round dielectric and image surface was substantiated experimentally. Fig. 3 shows a comparison between the radial decrement of axial field component as predicted from the basic equations for the full round rod, and the measured axial field distribution for several half round polystyrene rods mounted on an image surface. The measurements were made at 3 cm in an open resonator[4] with the E-field sensing probe mounted on one end wall and moved normal to the image surface. A thin slot in the end wall so arranged produces no field perturbation since for the HE_{11} mode only H_ϕ is present at $\phi=0$.

Effect of Dielectric Constant

The effect of dielectric constant on loss, field extent, and dispersion has received some attention in the litera-

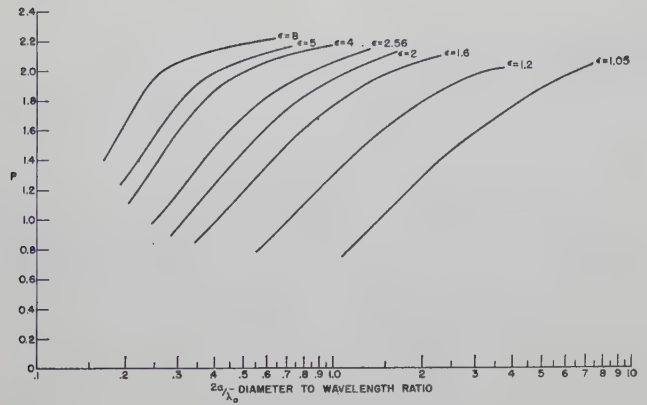

Fig. 1—Radial parameter p as a function of $2a/\lambda_0$ for round rod of dielectric constant ϵ.

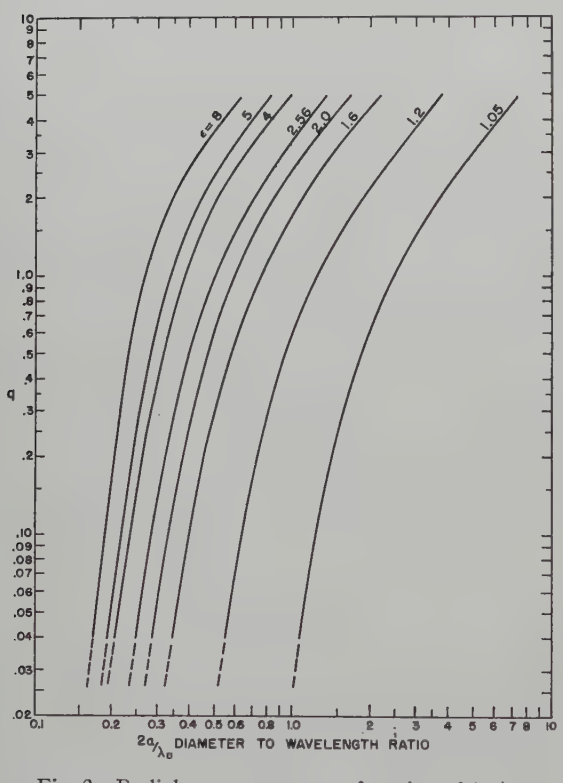

Fig. 2—Radial parameter q as a function of $2a/\lambda_0$ for round rod of dielectric constant ϵ.

ture[16,17] but the range of dielectric constant considered is rather limited, and the results are not presented in a form so as to show the over-all effect of ϵ on field binding and loss in one composite curve. The authors have calculated rod characteristics for a rather broad range of ϵ, based upon the solution of the characteristic equation for the HE_{11} mode.

The effect of dielectric constant on dispersive properties of a dielectric rod propagating the HE_{11} mode may be determined by using in (5) the p, q pairs that satisfy (3). This results in the curves shown in Fig. 4. Note that wavelength approaches asymptotically the value in trinsic in the medium.

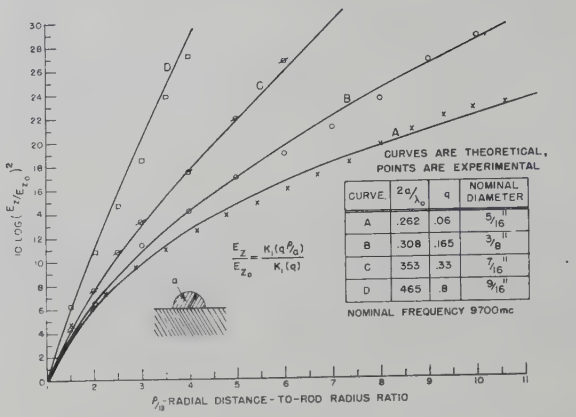

Fig. 3—The radial field distribution at $\phi=0$ showing the predicted and measured decrement of field in db for four samples of half round dielectric rod ($\epsilon=2.56$).

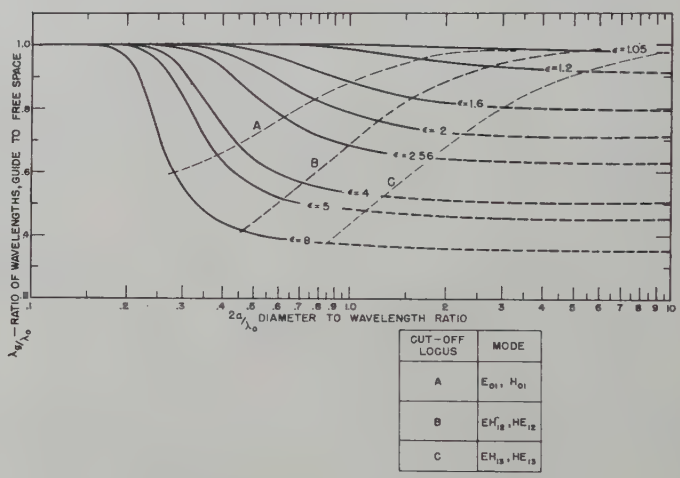

CUT-OFF LOCUS	MODE
A	E_{01}, H_{01}
B	EH_{12}, HE_{12}
C	EH_{13}, HE_{13}

Fig. 4—Effect of dielectric constant on the dispersion characteristics of round rod.

The line loss for a half round dielectric rod on an infinite image surface consists of both dielectric loss and the image plane conduction loss. The authors have derived and experimentally confirmed the expression giving the conduction loss for the dielectric image line propagating the HE_{11} mode.[4] The dielectric loss for the full round rod for this case of $n=m=1$ was determined by Chandler and Elsasser.[14,15] For completeness both of these results are summarized in the Appendix. The loss functions R and R', complex functions of the system parameters, have been calculated for various values of ϵ as shown in Figs. 5 and 6.

Fig. 7 shows a family of curves showing the effect of giving dielectric constant on dielectric loss at 9700 mc and for an assumed loss tangent of 0.001. (The image plane conduction loss, α_c, has been shown to remain an order of magnitude less than α_d for reasonable values of $2a/\lambda_0$ and for wavelengths well into the millimeter region.[4] Fig. 7 shows that α_d tends to peak sharply for high dielectric constant, with no gradual transition toward a maximum. This can be attributed to the short intrinsic wavelength within the rod, which provides very effective binding. As the rod size increases, a lower average field

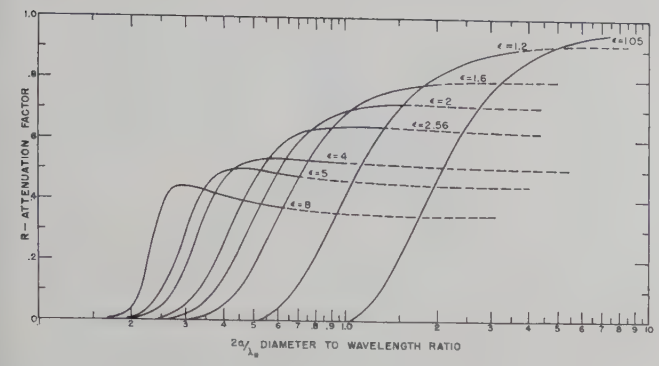

Fig. 5—Dielectric attenuation factor R as a function of $2a/\lambda_0$ for various values of ϵ.

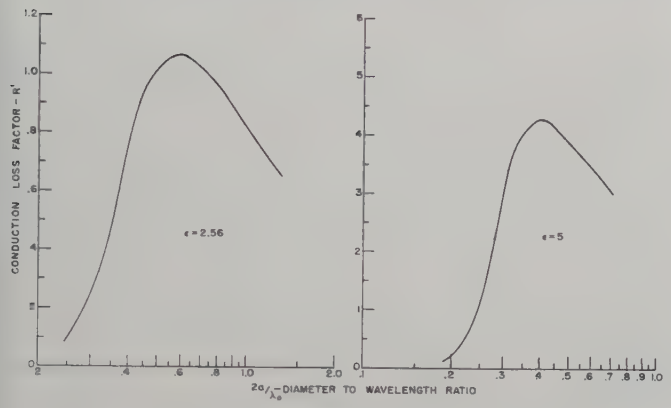

Fig. 6—Conduction attenuation factor R' as a function of $2a/\lambda_0$ for $\epsilon=2.56$, and $\epsilon=5$.

density of the larger cross section reduces the loss.

Since all the pertinent parameters are calculated for the HE_{11} mode and are on hand it would seem valuable to construct a universal plot, showing the combined effect of ϵ on loss, field spread, and rod size, all normalized for frequency and loss tangent. Fig. 8 is such a plot. Here we have a dimensionless loss factor, $\mathfrak{L}=\alpha_d\lambda_0/\phi$ shown as a function of ϵ with field extent ρ_L/λ_0 and rod size $2a/\lambda_0$, as convenient parameters.

The ρ_L of Fig. 8 defines the "extent of field" and is that radius at which the axial field density has decreased by 20 db. This larger value was chosen in preference to the e^{-1} decrease proposed by Mallach[16] since it places less burden on precise measurement of small attenuations.

Fig. 8 shows that for a given size rod and constant λ_0 a greater dielectric constant results in higher loss and closer binding. If we keep field extent constant and increase ϵ, the loss will go down. We note in addition the fact that for high values of ϵ, a change of 0.1 wavelength in diameter will give a much larger increment of loss than at low values of ϵ. This is important for broadband applications.

Effect of Dielectric Rod Configuration

A dielectric image line resonator with provision for axial field and guide wavelength measurement was used

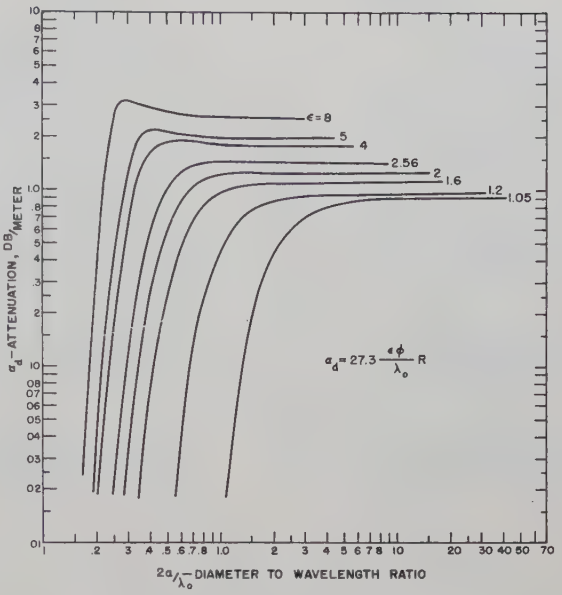

Fig. 7—Attenuation db/meter vs $2a/\lambda_0$ for various values of ϵ at 3 cm.

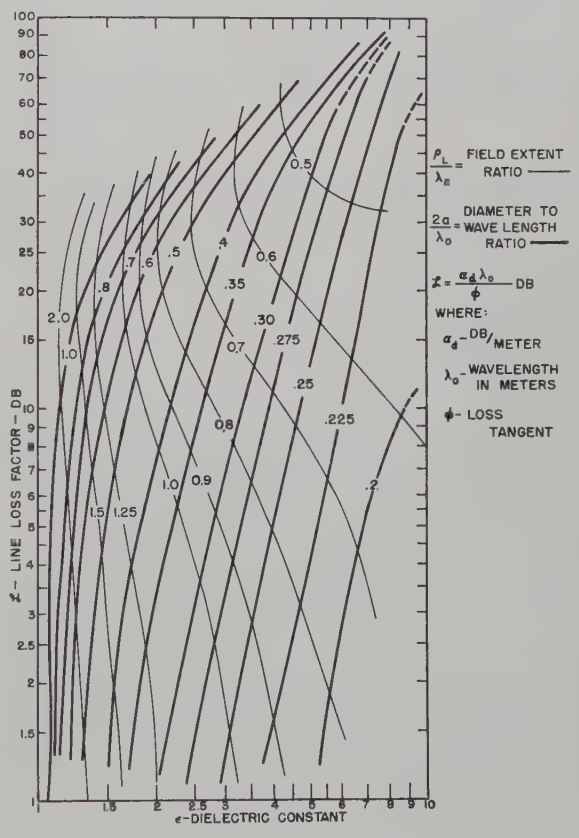

Fig. 8—Normalized line loss factor, $\mathfrak{L}$, as function of ϵ for constant $2a/\lambda_0$ and ρ_L/λ_0.

to measure the characteristics of a variety of dielectric cross sections (Fig. 9). We consider now some experimental data for these various dielectric configurations.

First we consider structures lying on the image plane, and thus the results may be applied to the free space full cross section by the theory of images. Secondly we

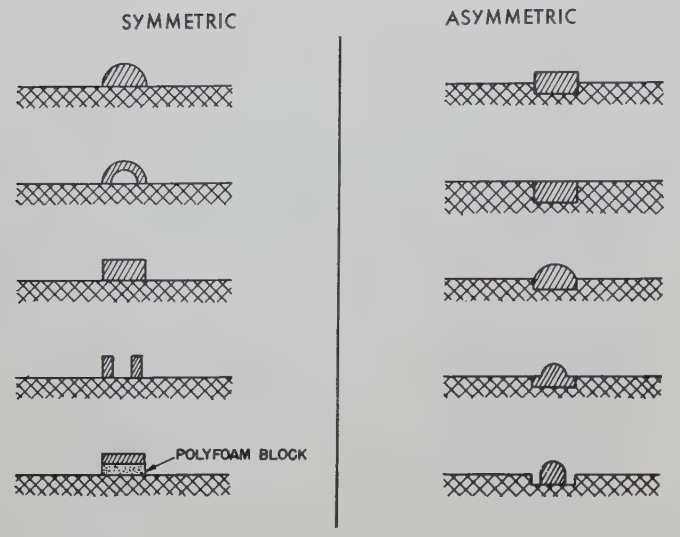

Fig. 9—Configurations of dielectric cross section.

consider the properties of a dielectric strip when partially submerged into a trench in the conducting plane. This produces an "asymmetrical image line"; the conducting sheet serves to perturb the field distribution within the rod because of the new boundary conditions, but no longer acts to mirror truly the configuration of field.

Generally, only field extent and propagation velocity properties are discussed, although the results of two actual measurements of line loss are reported—one for the symmetrical image and the other for the asymmetric or "trench line" case.

The True Image

The properties of the dielectric image line with a half round tube or rod have already been explored in terms of the properties of the full round structure.[13–15] These results may be summarized by noting that the dielectric tube is more attractive than the solid rod from the standpoint of loss and dispersion, but is somewhat less attractive with respect to field spread and ease of fabrication.

In choosing a cross section with which to work, we seek one that is easy to fabricate, lends itself conveniently to the asymmetrical case, and shows promise in binding the field. The rectangular dielectric rod meets these requirements.

The use of some relative field binding index is desirable for an arbitrary cross section. We define a binding effectiveness η_1 as the ratio of the field radius for a half round rod of the same material and cross sectional area as the sample considered to the field radius of that sample. Thus, $\eta_1 > 1$ indicates that the given material and transverse configuration binds closer than the same amount of material in a half round. It is also of interest to establish an index which serves as a guide to loss

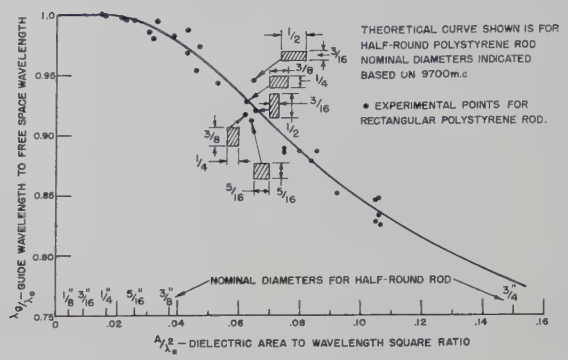

Fig. 10—Dependence of λ_g/λ_0 on the area of dielectric rod. Theoretical curve is for the half round rod; experimental points, for rectangular rod.

properties. We define η_2, the loss index, as the ratio of sample cross sectional area to the area of the half round rod of the same field extent and material.

Rectangular rod: The field extent and guide wavelength characteristics of seventeen samples of rectangular polystyrene rod were measured using the flat plate resonator. In each case the counted number of half-wavelengths yielded a value for λ_g for three or four neighboring resonances, following which a careful measurement was made of the radial distribution of axial electric field component. The latter data when plotted against radial distance-to-sample height ratio gave a 20-db field radius.

Dispersion: The mathematical solution for the circular dielectric as already outlined yields a convenient relation between guide to free space wavelength and the single principal dimension, diameter, provided that the diameter is expressed in number of wavelengths. Thus with a given rod size, the λ_g/λ_0 characteristics may be determined as a function of frequency, or given the frequency the variation with size may be obtained.

Several attempts were made to find a single controlling dimension for the rectangular rod, with the final result based on the intuitively evident fact that the propagation properties should depend on the area of dielectric. Fig. 10 shows how λ_g/λ_0 may be represented as almost a single curve when plotted against the area in square wavelengths. The curve actually drawn is for a half round polystyrene rod. We note that propagation velocity for the rectangular cross section is within about 3 per cent of the value for a half round rod of the same area and dielectric constant. We see further that given a certain area, the orientation has only a slight effect within the approximate 3 per cent.

In the interest of clarity of presentation, the three or four resonances read for each sample are not plotted in the figure, nor is each point identified. The points are not scattered, but if connected keeping either a or b constant, they would produce a closely bunched family of curves.

Fig. 11 shows four of these curves plotted, including

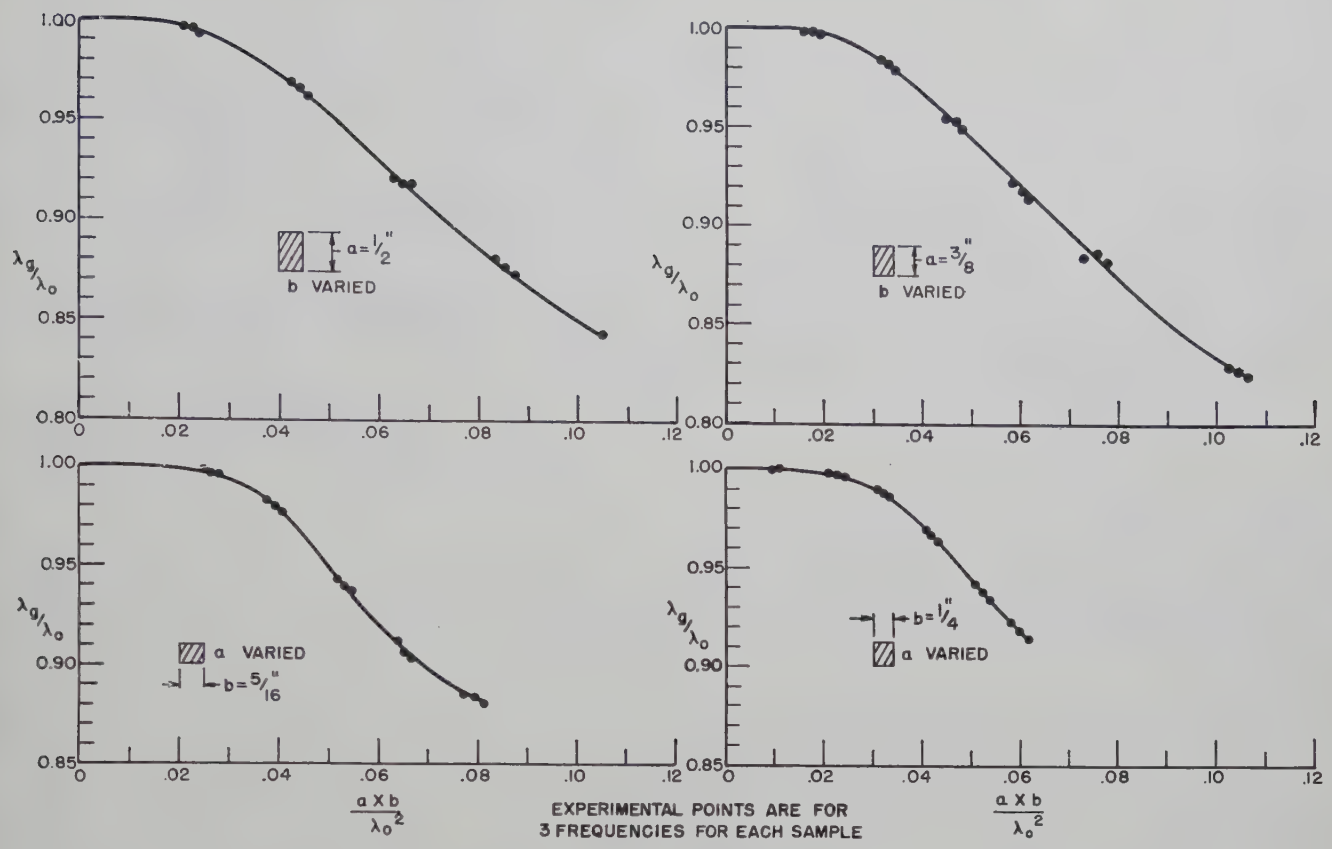

Fig. 11—The variation of λ_g/λ_0 with dielectric area in number of square wavelengths for four sets of rectangular rods.

the neighboring frequency points, indicating that A/λ_0^2 is a good approximation for a normalizing dimensionless ratio.

Field extent: The data representing field extent may be plotted in several different ways to examine the effect of varying each parameter. Attempts to correlate the field extent of rectangular rods with circular rods in terms of equivalent dimensions met with no success. It was noted, however, that the radial field distribution more closely approximated a Hankel function at larger distances, which is what would be expected considering that it is only close to the rectangular boundary that a perturbation on radial symmetry will exist.

The most satisfactory method of showing the results is illustrated in Fig. 12 where the field radius is plotted as a function of sample width for various values of height. There are a few important facts to be gained from this family of curves. The first thing to be noted is the evidence of a resonant effect, resulting in a loosening of the field where the width of sample approaches 3/8 inch ($b/\lambda_0 \approx 0.3$); this dimension very closely approximates the half-wavelength at 9700 mc intrinsic in the medium $\epsilon = 2.56$. This suggests the possibility of a transverse resonance with perhaps a null in the vicinity of $\phi = 0$. The 1/4-inch wide sample shows a particularly close binding.

If we examine the effect of the width dimension on binding quality by plotting the binding effectiveness η_1, we get the curves shown in Fig. 13. In addition to confirming the relatively good binding of the 1/4-inch wide sample, the curves show a surprising regularity considering the rather arbitrary manner of defining the ordinate. To summarize the significance of Fig. 13 we might say that given a sample of dielectric, there exist several sizes of rectangular configuration which are at least as effective in binding as the equivalent half round rod of the same area. The trend of η_2 leads to a similar generalization, as regards a qualitative loss comparison.

Miscellaneous shapes: The main objection to the use of half round dielectric tubing on an image plane lies in the difficulties involved in fabrication and mounting. Perhaps some more convenient transverse arrangement of dielectric mass would simulate physically a hollow tube, thus providing for a low-loss, moderately binding substitute.

In an attempt to realize the above, a pair of long thin rods were erected on the image plane in a manner quite like a pair of tracks. (See Fig. 9.) Measurements were taken on a set of rectangular rods each 3/16-inch high by 1/16-inch thick mounted on the image surface at various distances apart. From all appearances, guide wavelength, and nonradiating field extent, the tracks were propagating an HE_{11}-like mode. Another arrangement was tried whereby a 3/8-inch wide by 1/8-inch

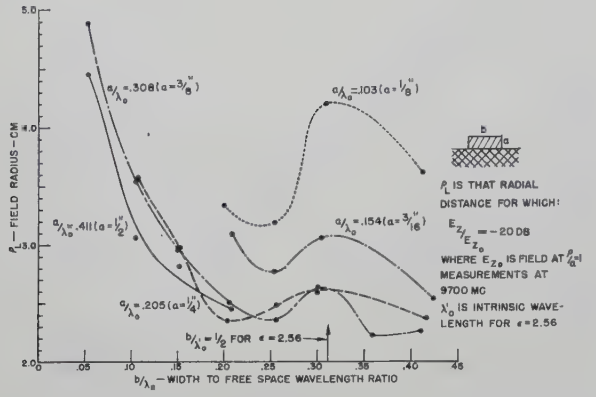

Fig. 12—Field radius, ρ_L vs b/λ_0 for rectangular rod of fixed a/λ_0. $\epsilon=2.5$, $\lambda_0=3.1$ cm.

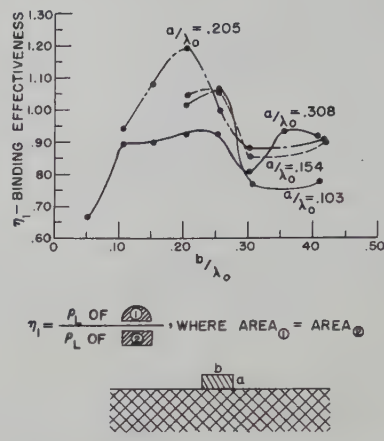

Fig. 13—Binding effectiveness as a function of b/λ_0 for rectangular rod of fixed a/λ_0. $\epsilon=2.5$, $\lambda_0=3$ cm.

thick dielectric slab was mounted above the image surface at various heights supported by polyfoam blocks (Fig. 9). These attempts to improve field binding compared to the same volume of dielectric formed as a tube, were unsuccessful although the dipole mode was easily established.

The properties of these configurations were not investigated further. It does seem that one advantage of a track line would be the ease with which field binding may be controlled. Thus in making slight bends in the horizontal plane one could minimize radiation by bringing the tracks together. This is most applicable at millimeter wavelengths where field spread in terms of many wavelengths is a reasonable value, thus making it possible for one to start with widely spaced strips.

The Asymmetrical Image

The presence of a convenient conducting surface upon which to mount various dielectric samples leads to the consideration of an interesting question. What would be the effect of gradually lowering a dielectric rod of some convenient cross section transmitting with an HE_{11}-like mode, into an axial slot, or trench cut into the conducting surface? Possibly, the change in field configuration brought about by the new boundary conditions within the dielectric, a region of high electric flux density, may result in an improvement in binding or loss for the resulting transmission line. The set of rectangular rods already used may be conveniently utilized for an analysis of this type. Fig. 9 illustrates the various configurations studied.

The dielectric image line resonator was reconstructed to provide a means of mounting the dielectric at various depths. A 3/8-inch wide, 7/16-inch groove was milled down the center of the conductor surface, and by the insertion of suitable long axial inserts, the dimensions of the trench could be varied. Due care was taken to insure conductivity continuity by the application of conducting silver filler to the joints created.

Rectangular rod: Runs were made on three widths of dielectric rectangular rod of various heights, lowered into the image plane to a depth of 1/16, 1/8, and 3/16 inch. In addition, a miscellaneous set of runs was conducted including the odd geometries shown in Fig. 9, plus a few measurements made on the full depth 7/16-inch trough filled with dielectric material. In each case it was possible to set up the HE_{11} mode, although for certain arrangements the binding was too loose to be practical.

Once again there are many ways that the available data could be plotted. One arrangement of these data shows that as a given size rod ($a+d$ is constant) is lowered into the image plane, the field becomes more and more loosely bound. (See Fig. 14 for dimensions a, b, d.) A more interesting consideration might be the following: given a rectangular configuration, what would be the effect on field spread and binding effectiveness of adding a base of ever-increasing depth submerged beneath the image surface?

Fig. 14, showing the field spread for three rectangular rods of different widths, indicates an appreciable tightening of field only for the case of the 3/8-inch rod. Recalling that this width sample operating on the plane showed symptoms of a transverse resonance of 9700 mc, (see Fig. 12), we may explain the apparent improvement in terms of a destroying of this condition for transverse resonance, by the substitution of a short circuit for the open circuit that existed at the side walls of the rod for the completely symmetrical case ($d=0$). This is further substantiated by Fig. 15 which shows an improvement in the binding effectiveness coefficient for the 3/8-inch wide rod sample; however, the coefficient never quite reaches unity.

We observe further from Fig. 14 that a 1/4-inch wide rectangular rod with heights of 1/8 and 3/16 inch does show some decrease in field extent when provided with a submerged base of 1/16-inch depth. The rod with the height of 1/8 inch is perhaps worthy of note since, as shown in Fig. 15, there results a 10 per cent increase in binding effectiveness.

In an effort to check this apparent high efficiency indicated in the latter case, two actual line loss measurements were made by methods described elsewhere,[4] for

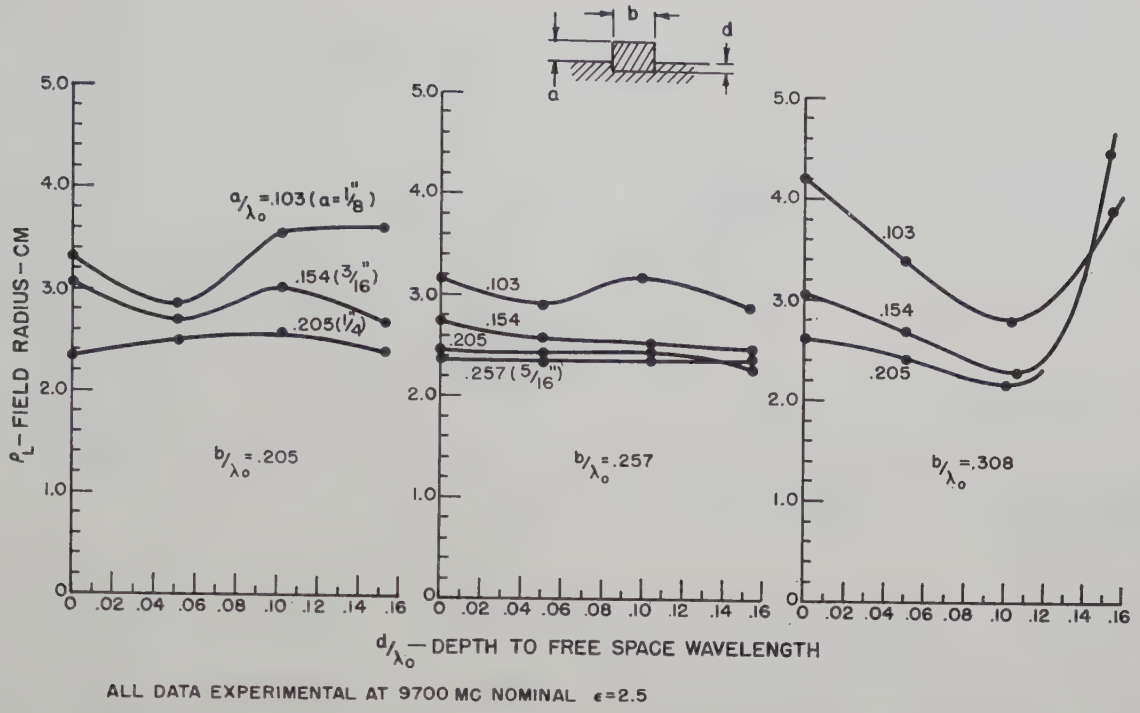

Fig. 14—The variation of field radius ρ_L with depth to free-space wavelength d/λ_0 for rectangular samples of various widths b/λ_0 and heights a/λ_0. $\epsilon = 2.5$, $\lambda_0 = 3.1$ cm.

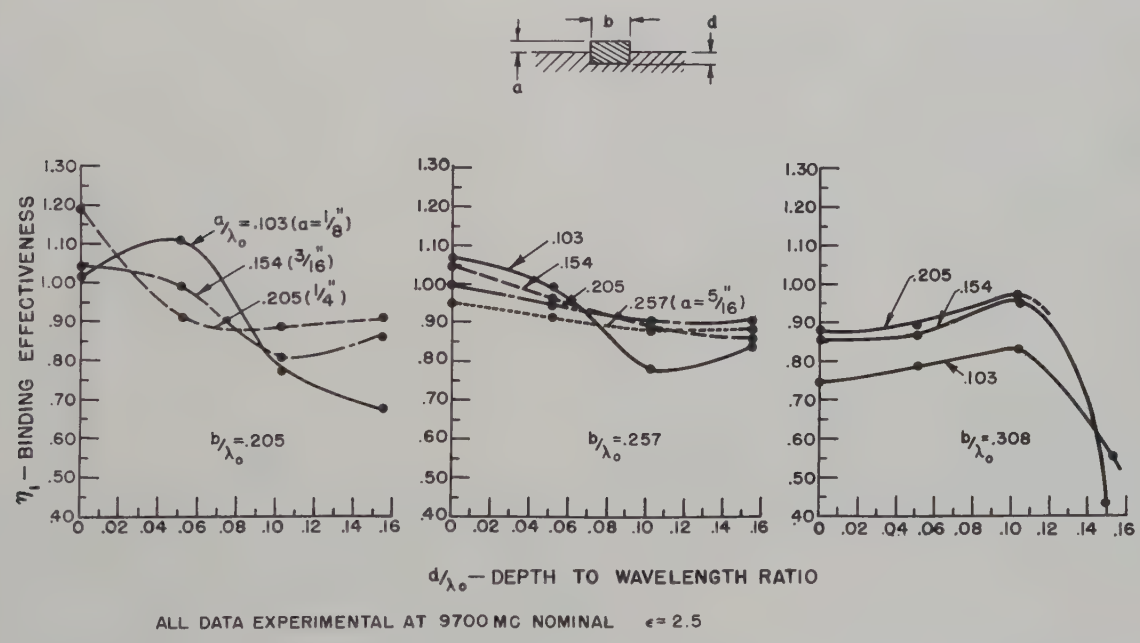

Fig. 15—Binding effectiveness, η_1, as a function of depth, d/λ_0, for various widths b/λ_0 and heights a/λ_0. $\epsilon = 2.5$, $\lambda_0 = 3.1$ cm.

the 1/4×1/8-inch rod, with and without the 1/16-inch submerged floor. The results of this measurement are shown in Fig. 16, where a decrease in loss of some 30 per cent is indicated for the dielectric rod with more mass mounted asymmetrically, compared to the smaller size rod with the same upper configuration mounted on the image surface. In addition we note the surprising fact that the lower loss sample has the more tightly bound field by about 20 per cent (see Fig. 14).

A complete set of curves was made showing the λ_g/λ_0 ratio as a function of area, expressed in number of square wavelengths. These curves are not given here because the results showed in each case that the dispersive properties of the rectangular rod dielectric image trench line remain essentially independent of the depth of penetration into the image plane for binding medium of constant height a. In other words if we plot all the results for the asymmetrical case using directly the set

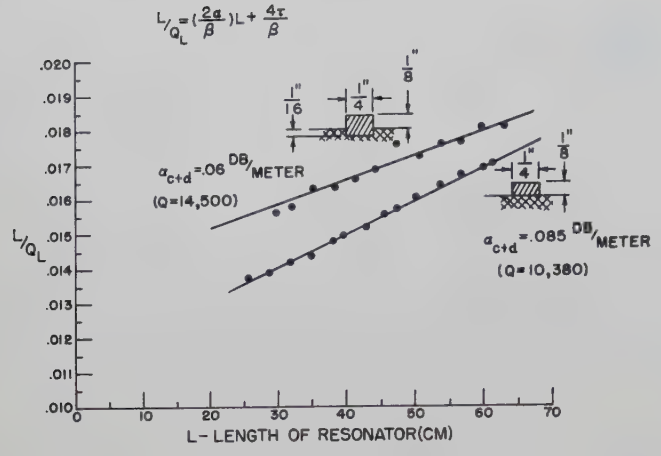

Fig. 16—Experimental curves for separating line loss from miscellaneous end losses, L/Q_L vs L, for a symmetric and an asymmetric dielectric image line with rectangular dielectric as binding medium. $\epsilon=2.56$, $\lambda_0=3.1$ cm.

of axes of Fig. 10 with depth as a parameter, the curves will all lie within the aforementioned 3 per cent of the expected value for a half round rod of equal area. This is true for the 1/4-inch wide samples and holds also to a lesser extent for the 3/8-inch wide samples, even though the added area beneath the surface resulted in a closer field binding.

Miscellaneous shapes: The properties of various odd shapes (Fig. 9) were measured, but the results will not be given in detail since the characteristics followed the same general trend as described in the last section for the rectangular rod asymmetrical image line. For example, the binding properties of a small semicircular rod were not enhanced by the presence of the buried rectangular base, whereas the larger size rods showed some improvement for small bases, but generally the improvement was not spectacular.

The case of a full 7/16-inch deep trench filled with polystyrene rod was investigated.[18] For two widths, 1/4 and 3/8 inch, the simultaneous existence was noted of a closely bound low-Q trench mode of propagation and a high-Q, loosely bound nonradiating HE_{11}-like dipole mode. Taking advantage of the inherently different guide wavelengths, it was a simple matter to utilize the resonator as a mode filter.

Conclusions

The dielectric image line consisting of a half round dielectric rod mounted on a conducting surface of infinite extent propagates the nonradiating HE_{11} mode with a field distribution as predicted from the symmetry of the defining equations and confirmed experimentally, that is, identical to the free-space dielectric transmission line. The presence of the image surface provides for support and limits the contaminating modes to the H type.

[18] F. J. Zucker, "The guiding and radiation of surface waves," *Proc. Symp. on Modern Advances in Microwave Techniques*, Polytechnic Inst. of Brooklyn, Brooklyn, N. Y., vol. 4; 1954.

An evaluation of a loss factor $\mathfrak{L}$ for a broad range of values of the dielectric constant ϵ suggests that low losses and reasonable extent of field may be realized by the fabrication of the binding medium using a material of low dielectric constant. This is particularly desirable at millimeter wavelengths since the increased size of rod for a given set of properties makes handling and fabrication more convenient.

Although there is evidence of a resonance for a transverse dimension approaching intrinsic half wavelength, there are a few sizes of rectangular dielectric rod which may be used as the binding medium for a dielectric image line with resulting increase in binding and loss effectiveness. The guide wavelength for a line with this configuration of cross section is within about 3 per cent of the value for a half round rod of the same area and dielectric constant.

The possibility of efficient surface wave transmission by means of an asymmetrical image system has been examined. The results were not conclusive. For one case, a rectangular "trench line" with the dielectric partially submerged into the image sheet, propagated the HE_{11} mode with lower loss and closer binding than a symmetrical rectangular line with a dielectric having the same area above the plane.

Appendix

Basic Equations for Dielectric Rod

We assume axial field variations in dielectric mediums 1 and 2 as follows:

$$\begin{aligned} E_{z_1} &= AJ_n(p\rho/a)\cos n\phi \\ H_{z_1} &= BJ_n(p\rho/a)\sin n\phi \\ E_{z_2} &= CK_n(q\rho/a)\cos n\phi \\ H_{z_2} &= DK_n(q\rho/a)\sin n\phi \end{aligned} \tag{1}$$

where

$$\begin{aligned} K_{c_1}{}^2 &= (p/a)^2 = \omega^2\mu\epsilon_1 - \beta^2 \\ K_{c_2}{}^2 &= (jq/a)^2 = \omega^2\mu\epsilon_2 - \beta^2. \end{aligned} \tag{2}$$

Determination of the other field components in the usual manner followed by the application of boundary conditions at the rod surface, $\rho=a$, yields finally:

$$(f+g)(\epsilon f+g) - n^2(1/q^2+\epsilon/p^2)(1/p^2+1/q^2) = 0 \tag{3}$$

where

$$f = \frac{J_n'(p)}{pJ_n(p)} \quad \text{and} \quad g = \frac{K_n'(q)}{qK_n(q)}.$$

Two additional expressions may be derived; these are:

$$2a/\lambda_0 = 1/\pi\left(\frac{p^2+q^2}{\epsilon-1}\right)^{1/2} \tag{4}$$

$$\lambda_g/\lambda_0 = \left(\frac{p^2+q^2}{p^2+\epsilon q^2}\right)^{1/2}. \tag{5}$$

Image Line Loss

The total line loss for the dielectric image line in nepers/meter is given as:

$$\alpha' = \frac{1}{2}\,\frac{\sum_{i=1,2} 2R_s \int_{0,a}^{a,\infty} |\hat{n} \times \boldsymbol{H}_i|^2 d\rho \Big|_{\phi=\pi/2} + \sigma_d \int_0^a \int_{-\pi/2}^{\pi/2} |E_1|^2 \rho d\rho d\phi}{\sum_{i=1,2} \int_{0,a}^{a,\infty} \int_{-\pi/2}^{\pi/2} |\boldsymbol{E}_i \times \boldsymbol{H}_i| \, \rho d\rho d\phi}$$

or finally

$$\alpha = 69.5\left(\frac{R_s}{\zeta_2 \lambda_0}\right) R' + 27.3\left(\frac{\epsilon \phi_d}{\lambda_0}\right) R$$

where

α = line loss db/meter,
ϕ_d = loss tangent of dielectric rod,
R_s = image surface resistance,
$\zeta_2 = \sqrt{\mu_2/\epsilon_2} = \sqrt{\mu_0/\epsilon_0}$,
λ_0 = free-space wavelength, meters,
σ_d = conductivity of dielectric rod.

The functions R and R' are defined as:

$$R = \frac{N}{D}$$

$$R' = \frac{1}{\pi \dfrac{2a}{\lambda_0} D}\left[\frac{f(I_1 I_0)}{J_1^2(p)} + \frac{f(H_1 H_0)}{K_1^2(q)}\right]$$

$$N = \left[\frac{\mu\epsilon - 1}{q^2}\left\{\frac{f^2 + \dfrac{1}{p^2} - \dfrac{1}{p^4}}{\dfrac{1}{p^2} + \dfrac{1}{q^2}}\right\} + (\mu V^2 + U^2)X + \frac{4\mu UV}{p^4}\right]$$

$$D = \left[UX(\epsilon + \mu V^2) + UY(1 + V^2) + \frac{2V}{p^4}(\mu\epsilon + U^2) - \frac{2V(1 + U^2)}{q^4}\right]$$

$$U = \frac{\lambda_0}{\lambda_g}$$

$$V = \left[\frac{(\epsilon f + g)}{(\mu f + g)}\right]^{1/2}$$

$$X = f^2 + \frac{(2f + 1)}{p^2} - \frac{1}{p^4}$$

$$Y = -g - \frac{(2g - 1)}{q^2} + \frac{1}{q^4}$$

$$f(I_1 I_0) = \frac{2}{3}\epsilon^2 \frac{S(2S + 3)}{p^3}\{I_1 + J_0(p)J_1(p)\} + I_1 \frac{V^2(\mu\epsilon - 1)}{p(p^2 + q^2)} - \frac{1}{3} I_0 \epsilon^2 \frac{(S^2 - 3)}{p^3} - \frac{1}{3}\epsilon^2 \frac{S^2}{p^4} J_1^2(p)$$

$$f(H_1 H_0) = -\frac{2}{3}\frac{T(2T + 3)}{q^3}\{H_1 + K_0(q)K_1(q)\} + H_1 \frac{V^2(\epsilon - 1)}{q(p^2 + q^2)} - \frac{1}{3} H_0 \frac{(T^2 - 3)}{q^3} - \frac{1}{3}\frac{T^2}{q^4} K_1^2(q)$$

$$S = \left(\frac{UV}{\epsilon} - 1\right)$$

$$T = (UV - 1)$$

$$I_1 = \int_0^p J_1^2(Z)dZ \qquad H_1 = \int_q^\infty K_1^2(Z)dZ$$

$$I_0 = \int_0^p J_0^2(Z)dZ \qquad H_0 = \int_q^\infty K_0^2(Z)dZ.$$

A Fast Ferrite Switch for Use at 70 KMC*

E. H. TURNER†

Summary—A normally open (attenuating) switch using ferrites has been built to operate in the 70-kmc region. It can be operated in 0.5 μsec and can be used with high duty cycles. The attenuation is about one db in the closed position and about 60 db in the open position. Construction and performance of the switch are discussed.

Introduction

ONE of the principal difficulties in fast switching of microwaves by means of ferrites lies in getting high-frequency switching field components to the ferrite without interfering with the microwave transmission path. A number of schemes for accomplishing these ends have been proposed and a summary of these methods and some of the attendant difficulties has been given by Uebele.[1] Many of the microwave problems are removed if one can make a hollow waveguide with a metal wall many skin depths in thickness for the microwave frequency and less than a skin depth in thickness at the highest modulating frequency. Such a construction also makes the design of the coil, which provides the switching field, simpler since the coil is not in the microwave field. A copper wall thickness of 0.0001 inch will reduce the amplitude of a 7.5-mc modulating field component by only 10 per cent but it reduces the amplitude of microwave field components by over 99 per cent for 10 kmc and higher frequencies. Waveguides made with 0.0001 to 0.0002-inch walls have been found to be as good as thick wall guides at 70 kmc and at the same time a square current waveform through a coil around such guides allows switching times of 0.5 μsec.

In order to accomplish the switching with modest currents a Faraday rotation device was used. Here the demagnetizing factor can be quite low (about 0.006 in our case) and if a ferrite with small coercive force is used, the driving field needed to change magnetization of the ferrite is small. The 70-kmc switch described here requires only about 6 oersteds of switching field.

Radio Frequency Operating Principles

The radio frequency elements of the switch are shown schematically in Fig. 1. Power enters through RG98U waveguide at end 1 and goes through a tapered transition to 0.150-inch round waveguide. The polarization of the electric vector is indicated in the chart also on Fig. 1. The electric polarization is normal to the plane of a resistance film 2 and the wave is not affected if this film is made properly (see Appendix). When the switch is closed (transmitting) the ferrite in 3 rotates

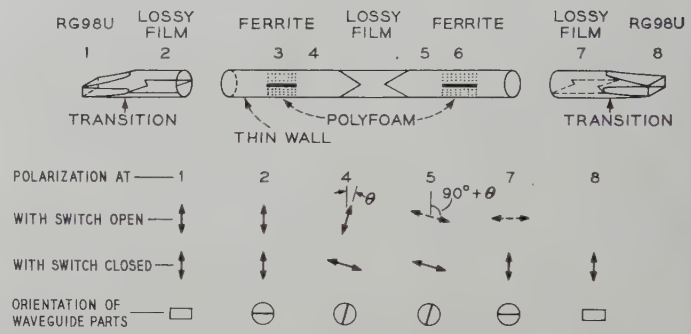

Fig. 1—Schematic of RF switch.

the polarization $(90°+\theta)$ to 4 on the chart. This polarization is normal to the centrally located lossy film and the wave is not affected by the film and is as indicated in 5. The second ferrite 6 rotates the polarization $(90°+\theta)$ in the opposite direction from the earlier rotation. The polarization of the wave is then normal to the lossy film 7 and the wave passes through the round-to-rectangular transition section and out 8 which is again RG98U waveguide. If there is no applied magnetic field the switch will be open (not transmitting), and referring again to Fig. 1 we can trace through the behavior of the switch. Power again enters 1 and is incident on the ferrite loaded section 3 as before. The ferrite will cause a small (at most 5 degrees) rotation of the polarization because of the remanent magnetization of the ferrite. This rotation is indicated by the small angle θ in 4 on the chart of Fig. 1. The lossy film is now parallel to the polarization and absorbs the power from the wave. There are, however, a number of factors which can cause a small amount of power to remain in the ploarization normal to the lossy film. For example, the Faraday rotation is somewhat frequency-sensitive so that θ will depend on frequency. Also, mechanical imperfections can cause the wave polarization to be slightly elliptical. Thus, there will be some power polarized normal to the lossy film and this will be unaffected by the film and will emerge as indicated at 5. The second ferrite loaded section, 6, will rotate this component an amount θ in the opposite sense from the first rotation and the wave will then be polarized as shown in 7. This polarization is in the plane of the lossy film and will be absorbed, so that the double switch section gives higher loss and operates over a wider band.

Design of Rotation Sections and Switching Coils

The magnitude of the driving field required to produce 90 degrees of rotation in the Faraday rotation sections depends on the ferrite used, the radio frequency in-

* Manuscript received by the PGMTT, November 22, 1957; revised manuscript received, March 7, 1958.

† Bell Telephone Labs., Holmdel, N. J.

[1] G. S. Uebele, "High-speed ferrite microwave switch," 1957 IRE National Convention Record, pt. 1, pp. 227–234.

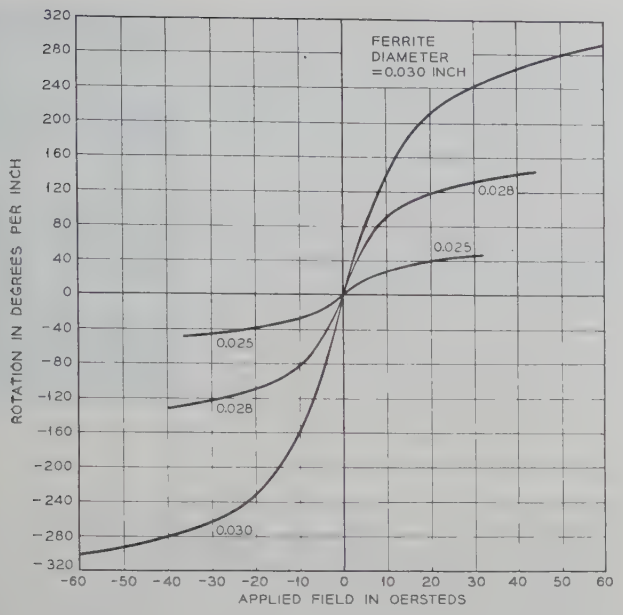

Fig. 2—Rotation of 70-kmc wave in 0.150-inch ID round guide as a function of applied field.

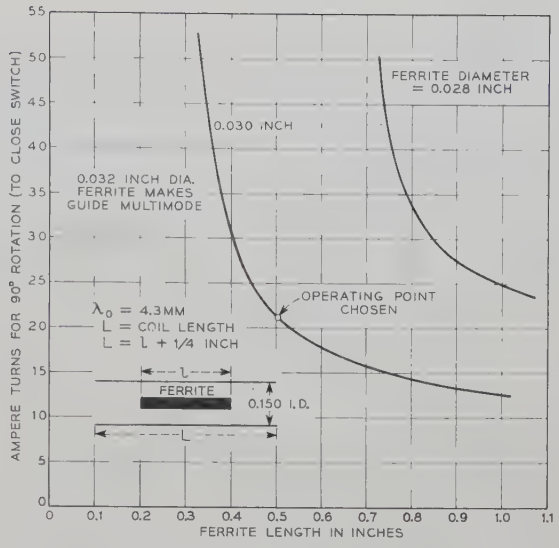

Fig. 3—Ampere-turns needed to close switch.

volved, the guide diameter, and the length and diameter of the ferrite. The ferrite chosen is a nickel zinc ferrite [$Ni_{0.6}Zn_{0.4}Fe_{1.9}Mn_{0.02}O_4$] with the highest saturation magnetization (4900 gauss) available in a material with low coercive force. This provides the maximum effect because of the large magnetization and at the same time the switching fields are small because of the low coercive force. In Fig. 2 the rotation of a 70-kmc wave in degrees per inch of ferrite length is shown as a function of applied field for 0.025, 0.028, and 0.030-inch diameter ferrite rods in 0.150-inch ID round waveguide. The field was varied continuously from a given value in one direction through zero to a given value in the opposite direction and the rotation at zero field was arbitrarily chosen as zero degrees. Ferrite diameters larger than 0.030 inch cause erratic behavior in the rotation vs field plots and we attribute this to generation of higher order modes. The 0.030-inch diameter ferrite does not produce excessive loss or reflection and it was generally used for the switch application because it requires the smallest driving field. (The most serious objection to 0.030-inch diameter ferrite is the frequency sensitivity of the rotation. For applications in which there is no difficulty in providing a field of 25 gauss or more the smaller diameter ferrites are desirable because their rotation vs frequency characteristic is much flatter. A one-inch length of 0.025-inch diameter ferrite is used for the Faraday rotation element in isolators built for the 70-kmc region.)

After the various parameters mentioned above are fixed, it is necessary to decide how long the ferrite rod is to be, and hence how much switching field is required. If the ferrite is made too long, its RF loss is unnecessarily large and the fact that small switching fields are required means also that the switch behavior is affected by stray fields in the vicinity. The coils that provide the switching fields are wound on the outside of the thin wall waveguide and have a diameter small enough to allow the field on the axis of the coil to be calculated approximately from the long solenoid formula for all points not too close to the end of the coil. Accordingly, if the coil projects one-eighth of an inch beyond the ferrite rod at either end it is possible to specify roughly the number of ampere turns required to operate the switch for different ferrite lengths and diameters. This assumes that the ferrite does not appreciably affect the fields in the coil. The assumption is justified in the case of a 0.34-inch diameter coil by the small change in inductance observed when the ferrite is inserted. For coils of 0.20-inch diameter the observed inductance change was large since the ferrite occupies a larger fraction of the coil volume. However, the calculations at least give approximate agreement with our experimental results. In Fig. 3 the number of ampere-turns needed to produce 90 degrees of rotation at 70 kmc is plotted against ferrite length for 0.030-inch and 0.028-inch ferrite diameters in 0.150-inch ID round guide. A length of 0.5 inch of 0.030-inch diameter ferrite in 0.150-inch ID round guide appears to be a natural choice since the ampere-turns required for shorter lengths rises rapidly and the number of ampere turns required for longer lengths is not very much less.

Behavior of Switches

Some switches have been constructed using the electrical principles outlined above. These switches have been tested in two different ways. First, in order to get a good measurement of the loss in the open and closed positions the switches have been tested with direct current through the coils. The attenuation vs current behavior of one of the switches is shown for frequencies of 69.3 kmc, 69.8 kmc, and 71.7 kmc in Fig. 4. Second, in order to test the high-speed switching characteristics of the switches they have been tested with square wave

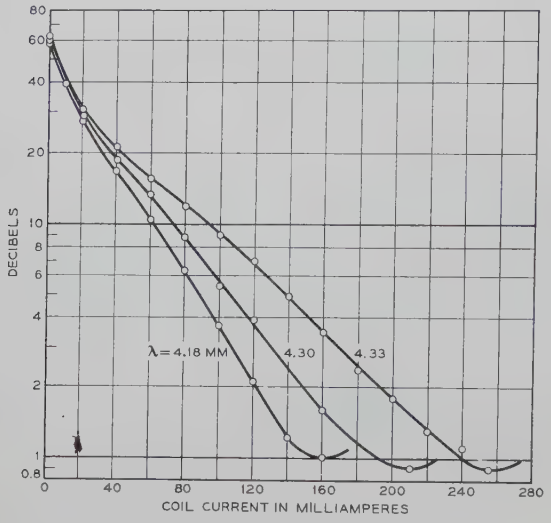

Fig. 4—Attentuation of switch for varying coil current.

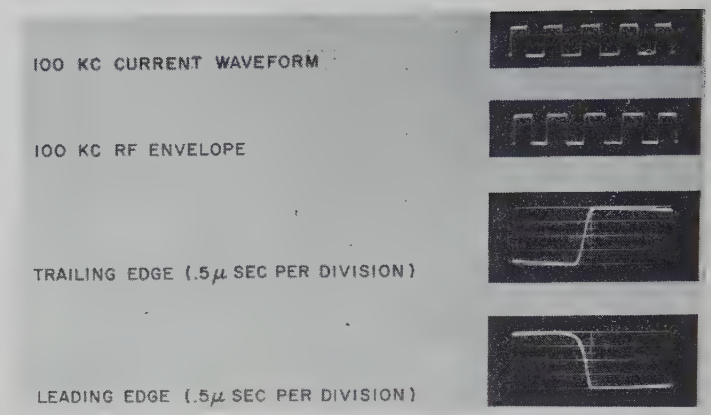

Fig. 5—Response of switch to square current waveform.

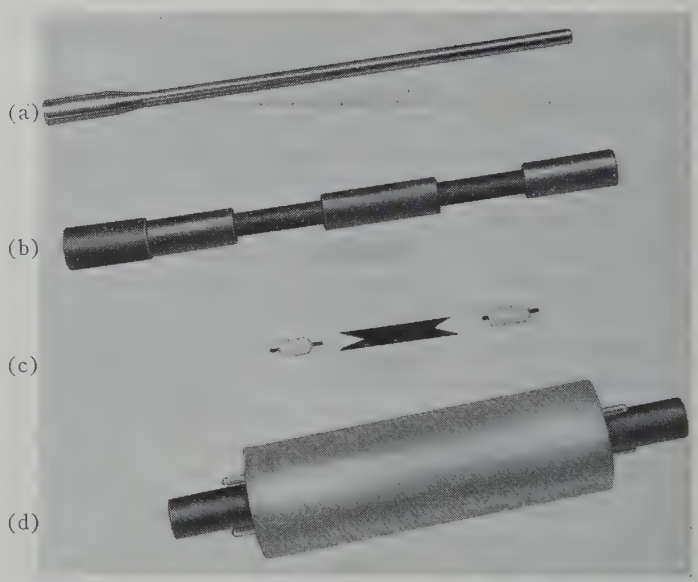

Fig. 6—(a) Stainless steel mandrel. (b) Epoxy resin jacket on thin wall section. (c) Ferrites and central lossy film. (d) Completed switch with coils.

modulation. The detected RF modulation envelope and the current waveform through the driving coils are shown in Fig. 5 for 100-kc square wave modulation. The attenuation vs current characteristic, Fig. 4, is such that even a nonsquare current waveform will produce a fairly square RF envelope. The switches have been driven at up to 250 kc and still produce a recognizable square wave. The coils used overheat if modulating frequencies of a megacycle are used, but with different coils the switches can be made to modulate at a 1-mc rate. It has been reported[2] that such high modulation rates cause the ferrites to heat up because of hysteresis losses to the point where polystyrene supports melt. There has been no such difficulty with this switch construction. Presumably, the fact that the ferrite is switched over only a small portion of the hysteresis loop reduces the energy dissipated per unit volume to a tolerable level. This operating condition is possible, of course, because the ferrite sections used are ample to produce 90 degrees rotation with only small driving fields.

Construction of Switch Unit

Good performance of the switch requires a high quality thin wall waveguide. That is, the inside surface must be uniform and polished and the wall thickness must lie in a range which permits the switching field to penetrate, yet guides the RF field as was indicated earlier. The thin wall is made by electroforming copper on a stainless steel mandrel which is made of AISI Type 303 or 316 stainless steel and is ground and polished to a diameter of 0.150 inch over a four-inch length. The mandrel is shown in Fig. 6(a). A copper coating less than 0.0002 inch thick is deposited on the mandrel from a standard acid copper plating bath. The plating on the ends of the mandrel is built up to about 0.030 inch. This thicker wall is necessary to insure good electrical contact at the ends of the guide, since the RF connections to other guides are butt joints. After washing and drying, the work is then cast in an epoxy resin. The casting mold must be either pliable or made of a material (such as Teflon) to which the casting resin will not adhere; otherwise the casting resin will pull the thin copper plating from the mandrel as the plastic contracts during curing. After the plastic is cured the assembly is turned down as indicated in Fig. 6(b). Finally the mandrel is removed by simply pulling it out at room temperature. The ends of the finished waveguide are then faced off. All that remains is to wind the coils [Fig. 6(d)] and load the guide with a lossy sheet and the ferrite pieces [Fig. 6(c)].

Conclusion

The construction and performance of a normally open ferrite switch operating in the 70-kmc region has been described. Attenuations of about 1 db and 60 db can be obtained in the two switch positions, and the switching time to the 90 per cent points is about 0.5 μsec. The emphasis in the discussion has been placed on this one

[2] W. N. Honeyman and R. S. Cole, "Hysteresis heating of microwave ferrites," Proc. IRE, vol. 45, pp. 1285–1286; September, 1957.

specific switch type but much of the information could be used in designing a normally closed switch or a three-position switch using a cross polarization pick-off to retrieve the power dissipated in resistance sheets. Many of the design principles discussed apply equally to more general types of amplitude modulators.

Appendix

Because of the high frequencies and small sizes involved in the 70-kmc region the ordinary resistance sheet made by evaporating metal film on a dielectric backing sheet causes loss to the wave whose polarization is such that the wave is ordinarily considered to be unaffected. This loss arises in the following fashion. A dielectric sheet stretched across dominant mode waveguide so that its plane is everywhere perpendicular to the plane of the dominant mode electric vector of the empty guide causes components of electric field to occur parallel to the sheet in the altered dominant mode configuration. These field components along the dielectric will cause current flow and hence loss if one or both sides of the dielectric are coated with a metal film. If the sheet is centered on a diametral plane of a round cylindrical waveguide the tangential field components vanish on the diametral plane itself so this is clearly the place to put the evaporated metal film. Accordingly, the resistance sheets used in the switch are made by evaporating metal on one dielectric sheet and covering this with a second dielectric sheet of equal thickness.

The propagation constant of a rectangular waveguide containing a dielectric sheet coated with a film of conductivity σ ohms^{-1} on each side has been obtained by solving the appropriate boundary value problem and this solution indicates the magnitude of the loss expected in the actual circular waveguide. The rectangular guide has a height b, the dielectric thickness is c, and the dielectric center plane lies on the center plane $(b/2)$ of the guide. If the attenuation constant α is small compared to the free space phase constant β_0, and if c is small compared to b, the attenuation constant and phase constant β can be expressed simply:

$$\alpha = 377 \frac{c^2}{2b} \beta_0^2 \sigma \left(\frac{\epsilon_r - 1}{\epsilon_r} \right)^2,$$

$$\beta = \beta_0 \left[1 - \frac{\pi^2}{a^2 \beta_0^2} + \frac{c}{b} \left(\frac{\epsilon_r - 1}{\epsilon_r} \right) \right],$$

where ϵ_r is the relative dielectric constant of the dielectric sheet and a is the width of the waveguide. The attenuation per wavelength becomes appreciable at very high frequencies only because c, the dielectric thickness, cannot be scaled down indefinitely. Experimentally, we have found that a coating of 0.01 ohm^{-1} on a 0.0035-inch piece of Nylar ($\epsilon_r = 3.7$) in 0.150-inch round guide causes a loss of 0.75 db per inch at 70 kmc. The theoretical prediction from the above equation is 0.625 db per inch in 0.148-inch square waveguide. If the conducting film is centered in the dielectric sheet, as mentioned earlier, symmetry requires that there be no conduction loss since the electric field is everywhere normal to the film and the film is much less than a skin depth in thickness. Experimentally, a film constructed in this fashion produces less than 0.1 db per inch of loss in the orthogonally polarized wave.

Theoretical Analysis of the Operation of the Field-Displacement Ferrite Isolator*

KENNETH J. BUTTON†

Summary—**A theoretical analysis of the resistance-sheet isolator is carried out, and numerical solutions are obtained for the forward and reverse propagation constants of the distorted dominant mode in a rectangular waveguide containing a transversely magnetized thick ferrite slab displaced slightly from the side wall. The microwave electric field patterns within the waveguide are plotted for several values of the physical design parameters of the isolator for which experimental performance data have been reported. Field patterns are used to describe the principles of the isolator and to select the optimum values of slab thickness, internal dc magnetic field, ferrite magnetization, and location of the slab in the waveguide for the idealized isolator. Evidence is presented to show that it is necessary to use a comparatively thick ferrite slab located in a very small usable range of distances from the side wall. The appropriate value of internal dc magnetic field is simply related to the magnetization of the ferrite and to the frequency. It has not been necessary to take into account the perturbing effects of the resistance card or matching techniques in order to explain the basic design principles.**

* Manuscript received by the PGMTT, December 16, 1957; revised manuscript received, February 3, 1958. The research reported in this document was supported jointly by the Army, Navy, and Air Force under contract with the Mass. Inst. Tech.

† Lincoln Lab., M.I.T., Lexington, Mass.

Introduction

THE nonreciprocal distortion of the dominant-mode electromagnetic fields in a waveguide containing a magnetized ferrite is now a well-known phenomenon. The different RF electric and magnetic field patterns for forward and reverse propagation in a ferrite-loaded rectangular guide were demonstrated theoretically by Lax, Button, and Roth,[1] and the nonreciprocal field-distortion principle has been used to build resistance-sheet isolators in rectangular guide by Fox, Miller, and Weiss[2] and others,[3] and in a circular guide by Melchor, Ayres, and Vartanian.[4] In each case, isolation was achieved by placing a vane of resistance material in a region of the guide where the RF electric intensity was large for the reverse direction of propagation and small for the forward direction. Recently, Weisbaum and Seidel[5] have reported the experimental performance and a theoretical treatment of a 6200-mc field-displacement isolator consisting of a rectangular waveguide containing a thick ferrite slab transversely magnetized and located nearly against the side wall of the guide. These experimental investigations, particularly the latter,[5] have established that the principal features of the field-displacement isolators are: large reverse-to-forward ratio of attenuation (>150 to 1 in db at 6200 mc), very low loss for the forward direction of propagation (~0.2 db), adequate bandwidth (>8%), low values of applied dc magnetic field (a few hundred oersteds) and moderate, but probably not high, power handling capacity.

The purpose of the present investigation is to establish the theoretical basis for the choice of design parameters for a field-displacement isolator of the type shown in Fig. 1. The notable successes of the laboratory models have depended largely upon the experimenters' ability to visualize the different RF electric field patterns of the dominant mode for the reverse and forward propagation. Additional improvement of performance was obtained by successive variation of parameters. The following exact solutions of the ferrite-loaded waveguide problem will demonstrate the method for finding electric field patterns and will illustrate the patterns in several cases for which experimental performance data have been reported.[5] This paper does not take into account the small perturbations due to the introduction of the resistance card or matching techniques, so that some experimental adjustments will still have to be made.

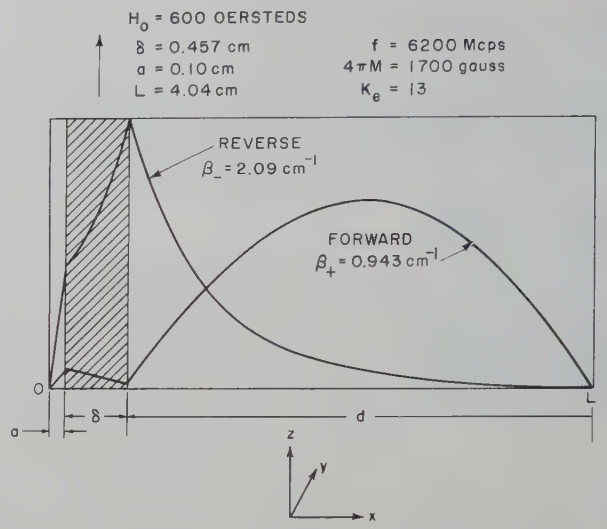

Fig. 1—Transversely magnetized ferrite slab in rectangular waveguide showing the calculated microwave electric field patterns for reverse and forward propagation that are appropriate for a field-displacement isolator. A resistance card may be placed on the right-hand face of the slab to provide attenuation of the reverse wave where the electric intensity is maximum.

Weisbaum and Seidel[5] have already treated thoroughly the theoretical aspects of the shape, location, and resistivity of the resistance card, and they have also discussed the influence of the height of the ferrite slab on performance, matching, and choice of parameters. Furthermore, they have taken into account the possible existence of a longitudinal component of the microwave electric field.

The Boundary Value Problem

The problem of the infinite rectangular waveguide containing a transversely magnetized ferrite slab was formulated by Kales, Chait, and Sakiotis[6] and the procedures for solving the transcendental equations have been fully described by Lax, Button, and Roth[1] in their discussion of the thin-slab ferrite phase shifter. Since the same procedures and notation are used to obtain the following results except in the discussion of the significance of the effective ferrite permeability: $1/\rho = \mu_{eff}/\mu_0$, this paper will be restricted to the presentation and interpretation of results with only the following skeleton description of procedure to bring in the necessary definitions.

The RF electric field for the distorted dominant mode in a rectangular guide containing a transversely magnetized ferrite slab (Fig. 1) may be expressed as

[1] B. Lax, K. J. Button, and L. M. Roth, "Ferrite phase shifters in rectangular waveguide," *J. Appl. Phys.*, vol. 25, pp. 1413–1421; November, 1954.

[2] A. G. Fox, S. E. Miller, and M. T. Weiss, "Behavior and applications of ferrites in the microwave region," *Bell Sys. Tech. J.*, vol. 34, pp. 5–103; January, 1955.

[3] E. H. Turner, "Field displacement isolators at 55 kmc," IRE Trans. on Antennas and Propagation, vol. AP-4, pp. 583–584; July, 1956.

S. Weisbaum and H. Boyet, "A double-slab ferrite field displacement isolator at 11 kmc," Proc. IRE, vol. 44, pp. 554–555; April, 1956.

[4] J. L. Melchor, W. P. Ayres, and P. H. Vartanian, "Energy concentration effects in ferrite loaded wave guides," *J. Appl. Phys.*, vol. 27, pp. 72–77; January, 1956.

[5] S. Weisbaum and H. Seidel, "The field-displacement isolator," *Bell Sys. Tech. J.*, vol. 35, pp. 877–898; July, 1956.

S. Weisbaum and H. Boyet, "Field displacement isolators at 4, 6, 11 and 24 kmc," IRE Trans. on Microwave Theory and Techniques, vol. MTT-5, pp. 194–198; July, 1957.

[6] M. L. Kales, H. N. Chait, and N. G. Sakiotis, "A nonreciprocal microwave component," *J. Appl. Phys.*, vol. 24, pp. 816–817; June, 1953.

$$E_z = (A \sin k_a x) \exp [-j\beta y], \quad \text{region } a$$
$$E_z = [B \sin k_a(L - x)] \exp [-j\beta y], \quad \text{region } d$$
$$E_z = (C \exp [jk_m x] + D \exp [-jkm]) \exp [-j\beta y], \quad \text{region } \delta \quad (1)$$

where β is the propagation constant (the attenuation constant is neglected),[7] $k_a^2 = \omega^2/c^2 - \beta^2$, $k_m^2 = \omega^2 \epsilon \mu_{\text{eff}} - \beta^2$, and $\epsilon/\epsilon_0 = K_e$, the dielectric constant. The transverse wave number in regions a and d is denoted by k_a and in region δ by k_m. The effective permeability

$$\mu_{\text{eff}}/\mu_0 = \frac{(1 + \chi_{xx})^2 + \chi_{xy}^2}{1 + \chi_{xx}} \quad (2)$$

may be positive or negative depending upon the relative magnitudes of χ_{xx}, the diagonal component of the susceptibility tensor, and χ_{xy}, the off-diagonal component.[8] The E fields of (1) are substituted into Maxwell's equations to obtain the components of the RF magnetic field h_x and h_y in each region and the boundary conditions are then applied to obtain four homogeneous simultaneous linear equations for the amplitude coefficients A, B, C, and D whose secular determinant must vanish. B is taken equal to unity for convenience. The determinantal equation which must be solved exactly by numerical methods has the form[1]

$$a = \frac{L - \delta}{2} - \frac{1}{2k_a} \cos^{-1} [P(\pm\beta)] \quad (3)$$

where $P(\pm\beta)$ is given in the Appendix. The solution was accomplished by substituting trial values of β into $P(\pm\beta)$ and computing separate values for the location of the slab, a, for each sign of β.

Location of the Ferrite Slab

The numerical solutions of (3) yield a graph of $\beta_\pm$ vs a for constant values of all other physical parameters. β_+ and β_- are the phase constants for forward and reverse propagation, respectively. Solutions for three different values of the internal dc magnetic field, H_0, are shown in Fig. 2. It is possible to visualize the RF electric field patterns by reading the values of β from Fig. 2 for a particular value of a. For values of β above the horizontal line, k_a is imaginary because β^2 is larger than ω^2/c^2 in the relation $k_a^2 = \omega^2/c^2 - \beta^2$. In that case the mode has a hyperbolic sine dependence in the empty region of the guide and may actually be plotted in region d simply by tracing out the function $\sin k_a(L-x)$. For example, the values of $\beta_\pm$ used in plotting the fields of Fig. 1 were taken from the 600-oersted curves of Fig. 2 for $a = 0.1$ cm. Here k_a^+ is real and k_a^- is imaginary. If k_a^+ were just equal to π/d, the sine curve of Fig. 1 would go to zero at the face of the slab and this is the condition for minimum forward attenuation in the resistance card. To achieve this exactly, the slab must be moved closer to the wall (see Fig. 3) but this would sharply reduce β_- for the reverse direction of propagation and k_a^- would become real. Eventually, for $a < 0.05$ cm, the fields would be nearly identical for both directions of propagation as shown in the inset of Fig. 2 and there would be virtually no isolation. Therefore, although it is easy to define the conditions for which the forward-propagating field goes nearly to zero at the face of the slab, this is not a sufficient condition for an isolator.

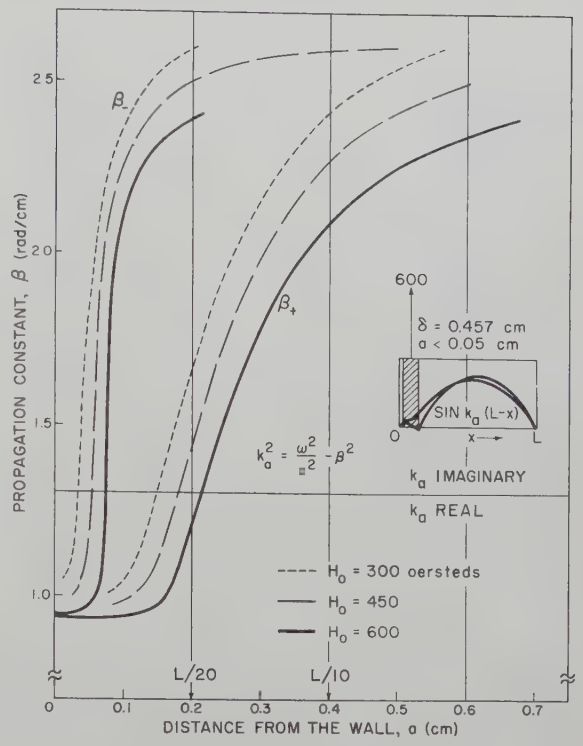

Fig. 2—Solutions of (3) showing the phase constant vs the distance of the slab from the wall with the internal dc magnetic field, H_0, as a parameter. The fields of Fig. 1 were computed by using the values of β from the 600-oersted curves at $a = 0.1$ cm. The fields shown in the inset for very small values of a will not provide sufficient isolation.

The most critical design parameter appears to be the location of the slab. It would be desirable, for example, to place the slab far from the wall to get the largest value of β_- and thus increase the amplitude of the spike in the reverse field pattern. If, however, the slab is placed too far from the wall, β_+ rises sharply for the forward propagation, k_a^+ decreases toward imaginary values, and the electric intensity at the face of the slab rises rapidly, resulting in increased forward attenuation which cannot be tolerated. Even in this relatively large waveguide (4 cm wide) the range of freedom in placing the slab is restricted to about 1 mm in order to satisfy both necessary conditions shown in Fig. 1—a sharp

[7] K. J. Button, "Theory of Ferrites in Rectangular Waveguide," Lincoln Lab., M.I.T., Lexington, Mass., Quart. Prog. Rep. on Solid-State Res., pp. 55–56; November, 1955.

[8] In terms of the Polder permeability tensor components, $1 + \chi_{xx} = \mu$ and $\chi_{xy} = -j\kappa$. See D. Polder, "On the theory of ferromagnetic resonance," *Phil. Mag.*, vol. 40, pp. 99–115; 1949.

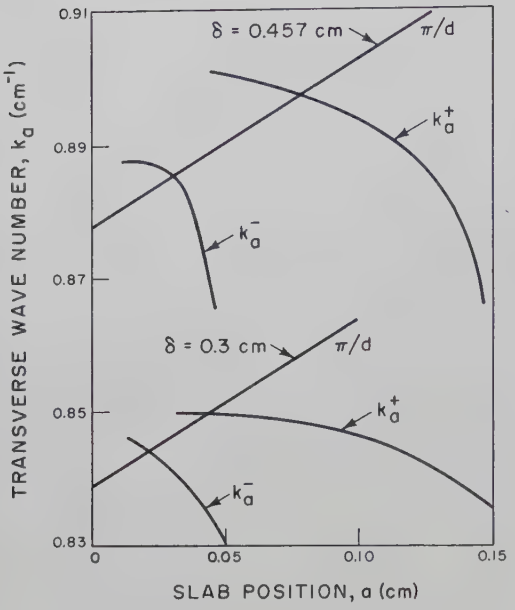

Fig. 3—Plots of the transverse wave number k_a^+ for forward propagation and k_a^- for the reverse direction. The straight lines show the values of π/d for two different slab thicknesses. The intersection of the curves with the straight lines gives the value of a for which the E field goes to zero at the face of the slab. These have been plotted for $H_0=600$ oersteds (negative permeability) because there is no intersection for smaller fields (positive permeability).

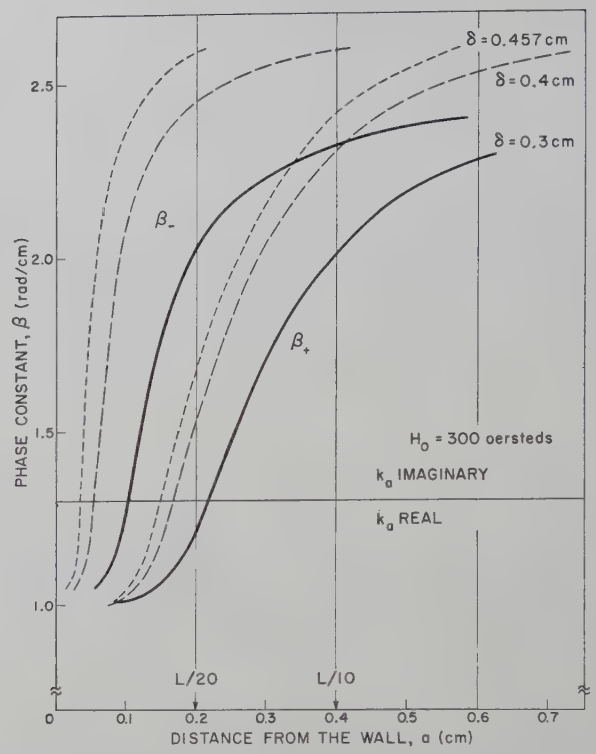

Fig. 4—Solutions of (3) with the slab thickness as a parameter. The result is not sensitive to changes in slab thickness if the slab is sufficiently thick.

hyperbolic spike in the E field for reverse propagation, and a near-zero E field at the face of the slab for forward propagation. The practical range of location is further restricted because β_- should be very large in order both to avoid the steepest portion of the β_- curve (Fig. 2) and to obtain the highest possible spike in the reverse E field.

Slab Thickness

Fig. 4 shows solutions for three different slab thicknesses at an internal dc magnetic field intensity of 300 oersteds. The value of δ is not critical provided that the slab is "thick," that is, about 10 per cent of the waveguide width or greater. The 3-mm case that is shown indicates, however, that curves for thinner slabs fall away rapidly both from high values of β and from small values of a. It is much more difficult to find a value of a for the thinner slab cases where β_+ will be sufficiently small and where β_- will also be very large.

Some selected field patterns are shown in Fig. 5, opposite. The fields of Fig. 5(a) have been plotted for a thick slab with the internal dc magnetic field as a parameter. This shows that the reverse attenuation for the thick slab case is not highly sensitive to changes in magnetic field. If the slab thickness is decreased, however [Fig. 5(b)], the reverse electric field intensity near the ferrite edge begins to collapse. If, in addition, the magnetic field is increased to 600 oersteds within the thin slab, Fig. 5(c) shows that both forward and reverse electric fields become similar and the problem has been reduced to that which has been solved previously for the phase shifter.[1]

DC Magnetic Field and Ferrite Magnetization

An ideal isolator design requires: 1) an hyperbolic sine dependence of the electric field for reverse propagation, and 2) a sinusoidal dependence for forward propagation, which in particular, is near zero at the face of the slab where the resistance card is to be located. The first condition can be assured by using a thick slab slightly spaced from the wall with nearly any convenient dc magnetic field below resonance.

Some care must be taken to achieve the second condition. Weisbaum and Seidel[5] have shown analytically that the forward E field cannot be brought to zero at the face of the slab unless the effective permeability (2) is negative. If the ferrite is completely saturated magnetically and the saturation magnetization is known accurately, then this condition of negative effective permeability may be selected from a plot like that of Fig. 6. When the ferrite is not saturated, the net magnetization is lower than the saturation value and the point of zero permeability shifts to higher fields as indicated by Fig. 6.

The value of a for which the forward E field goes to zero may be found, if desired, by solving (3) and plotting a curve like that of Fig. 2. Alternatively, the condition $k_a=\pi/(L-a-\delta)$ may be imposed on (3) to yield

$$a=\frac{1}{k_a}\tan^{-1}\left[\frac{-k_a\dfrac{\mu_{\text{eff}}}{\mu_0}}{-\dfrac{j\beta}{\theta}+k_m\cot k_m\delta}\right] \tag{4}$$

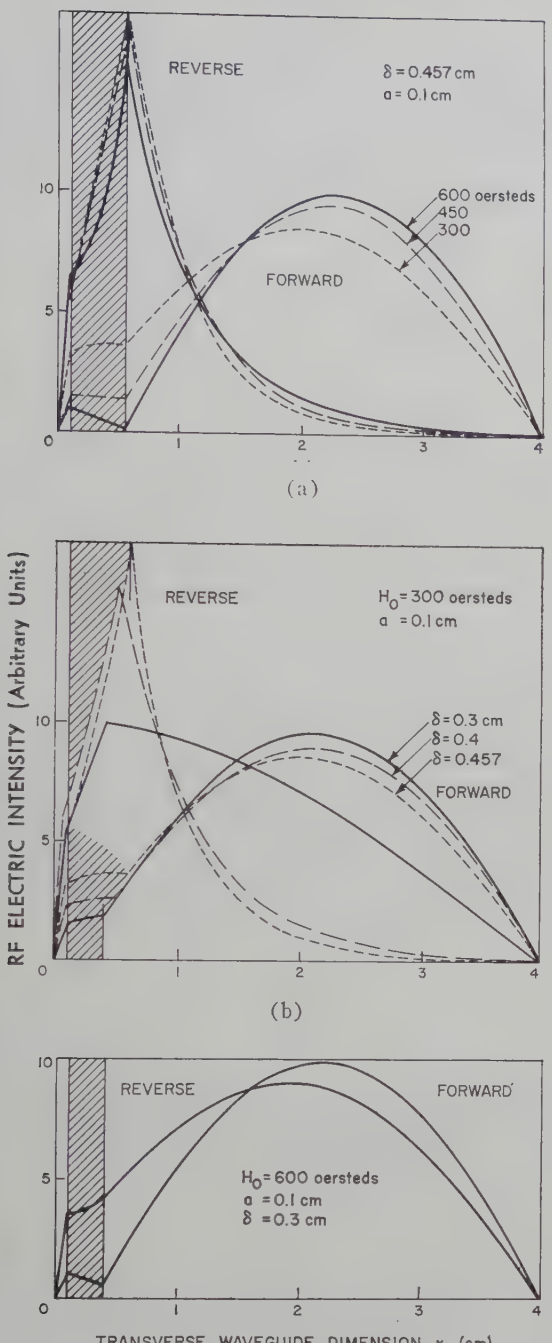

Fig. 5—Selected E-field patterns for (a) three different values of H_0, the internal dc magnetic field intensity, (b) three different slab thicknesses, and (c) a slab that is too thin for effective isolator performance. All calculations have been performed for 6200 mc in standard C-band guide.

where $\theta = (1+\chi_{xx})/\chi_{xy}$. Then this can be solved in the region of negative effective permeability by substituting successive trial values of β until a value of a is obtained which satisfies the relation $L = a+\delta+d$. This latter method has been used successfully in similar problems.[9]

[9] B. Lax and K. J. Button, "Theory of new ferrite modes in rectangular wave guide," *J. Appl. Phys.*, vol. 26, pp. 1184–1185; September, 1955.
K. J. Button and B. Lax, "Theory of ferrites in rectangular waveguides," IRE Trans. on Antennas and Propagation, vol. AP-4, pp. 531–537; July, 1956.

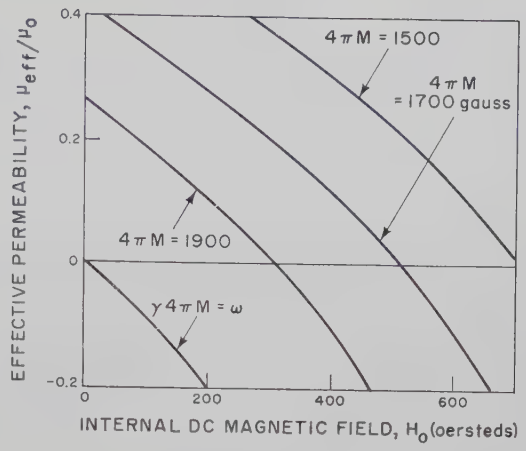

Fig. 6—Effective permeability at 6200 mc vs internal dc field H_0 for several values of magnetization. The magnetization for the lowest curve satisfies the relation $\gamma 4\pi M = \omega$ which may be used as a guide in selecting the appropriate magnetization for a given operating frequency. The curves have been carried back to zero field for comparison purposes but the magnetization would be a function of H at very low fields.

Low-Field Loss

At lower microwave frequencies, the problem of "low-field loss" associated with unsaturated ferrite material is an important consideration and often cannot be avoided. This loss should be nonreciprocal because of the strong energy concentration and rejection effects in field-distortion devices and its influence must be considered at any operating frequency if the applied dc field is small. It may not be assumed from a study of the E fields alone that a great deal of magnetic loss in the ferrite can be tolerated. For the reverse direction of propagation under the conditions shown in Fig. 1, both the electric and magnetic portions of the RF energy are propagated almost entirely within the ferrite so the low-field loss effects should increase the reverse attenuation. If the forward-propagating RF energy were excluded from the ferrite, the performance would be improved by magnetic losses. However, in the forward direction the RF magnetic field is not entirely outside of the ferrite as the electric field is. The transverse component h_x^+ is just β_+ times the E field in the ferrite and is therefore excluded. But the longitudinal component h_y^+ is slightly larger than h_{0y}, the y component of the empty waveguide h field. It is to be expected then, that at very small values of applied dc field, magnetic loss acting on the propagating energy through h_y^+ would moderately increase the forward attenuation. The experimental data[5] show that the loss at very low values of applied field is nonreciprocal, but the magnetization was too small to interpret the effect of low-field loss quantitatively. The designer may be able to turn magnetic losses to his advantage, especially at low microwave frequencies, by choosing the saturation magnetization large enough (Fig. 6) to provide a region of negative effective permeability at small values of applied field where part of the material is not saturated (and the magnetization is less than the saturation value). Negative effective per-

meability makes it possible to minimize the forward-propagating energy within the ferrite which is a necessary condition for minimum forward attenuation both in the ferrite and in the resistance card.

Conclusion

It has been shown that the dominant-mode RF electric field configurations for both directions of propagation may be used to choose the design parameters for the resistance-sheet isolator. It has been concluded that a thick ferrite slab nearly against the side wall operated in a region of negative effective permeability will give the best performance. These are the same conditions used in the laboratory[5] with the possible exception of the condition on effective permeability.

The condition $\gamma 4\pi M \approx \omega$ (from Fig. 6) requires that the ferrite magnetization be known fairly accurately at the temperature and dc field intensity that are to be used. Then a value of internal dc field (corrected for demagnetization) may be chosen for operation in the region of negative effective permeability.

The uncertainties in the values of $4\pi M$ and H_0 will require the experimental adjustment of the applied field in order 1) to operate far enough below resonance, 2) to minimize forward loss over the band, 3) to find a conveniently small applied field, and 4) to nearly saturate the ferrite.

Appendix

The transcendental expression of (3) is somewhat complicated and must be solved numerically. The function $P(\pm\beta)$ from Lax, Button, and Roth[1] is

$$P(\pm\beta) = -\frac{pr \pm q(p^2 + q^2 - r^2)^{1/2}}{p^2 + q^2} \tag{5}$$

where

$$p = \frac{1}{2}\left(\frac{k_a{}^2\mu_{\text{eff}}{}^2}{\mu_0{}^2} + \frac{\beta^2}{\theta^2} - k_m{}^2\right)$$

$$q = j\frac{\beta k_a \mu_{\text{eff}}}{\theta\mu_0}$$

$$r = \frac{1}{2}\left(\frac{k_a{}^2\mu_{\text{eff}}{}^2}{\mu_0{}^2} - \frac{\beta^2}{\theta^2} + k_m{}^2\right)\cos k_a(L-\delta) + k_m \cot(k_m\delta)\frac{k_a\mu_{\text{eff}}}{\mu_0}\sin k_a(L-\delta).$$

Acknowledgment

The author is greatly indebted to Dr. Benjamin Lax for several helpful discussions and for his suggestion of essential points that have been incorporated in this paper. He also wishes to thank Dr. Gerald S. Heller for his criticism of the theory, Richard N. Brown for his assistance with the exploratory computations, and Mrs. Billie H. Houghton for computation of the final data.

Reciprocity Relationships for Gyrotropic Media*

R. F. HARRINGTON† and A. T. VILLENEUVE†

Summary—**Reversal of the dc magnetic field in gyrotropic media transposes the tensor permeability and permittivity. It is shown that this also transposes the impedance, admittance, and scattering matrices of any device. It follows from this that the usual reciprocity statements for isotropic media apply to gyrotropic media if one reverses the dc magnetic field whenever an interchange of source and measurer is made.**

Introduction

FERRITES and gaseous plasma have been called "nonreciprocal" media because the usual reciprocity theorem[1] does not apply to them. However, a modified reciprocity theorem, stated by Rumsey and attributed to M. H. Cohen,[2] applies to such media. A number of useful and interesting interpretations of this reciprocity theorem are presented in this paper.

A ferrite in a dc magnetic field is characterized, insofar as an ac field is concerned, by a tensor permeability $[\mu]$ and a scalar permittivity ϵ.[3] Both $[\mu]$ and ϵ are independent of the amplitude of the ac field so long as it is sufficiently small. The $[\mu]$ is transposed if the dc magnetic field is reversed. A gaseous plasma in a dc magnetic field is characterized, insofar as an ac field is concerned, by a tensor permittivity $[\epsilon]$ and a scalar permeability μ.[4] Both $[\epsilon]$ and μ are independent of the amplitude of the ac field so long as it is sufficiently small. The $[\epsilon]$ is transposed if the dc magnetic field is reversed. The term *gyrotropic* is used to denote a medium characterized by $[\epsilon]$ and $[\mu]$, independent of the amplitude of an

* Manuscript received by the PGMTT, December 23, 1957; revised manuscript received, January 29, 1958.

† Dept. of Elec. Eng., Syracuse University, Syracuse, N. Y.

[1] S. A. Schelkunoff, "Electromagnetic Waves," McGraw-Hill Book Co., Inc., New York, N. Y., p. 478; 1943.

[1] V. H. Rumsey, "The reaction concept in electromagnetic theory," *Phys. Rev.*, vol. 94, pp. 1483–1491; June 15, 1954. Errata, vol. 95, p. 1705; September 15, 1954.

[3] D. Polder, "On the theory of ferromagnetic resonance," *Phil. Mag.*, vol. 40, pp. 99–115; January, 1949.

[4] H. Suhl and L. R. Walker, "Topics in guided wave propagation through gyrotropic media, part I," *Bell Sys. Tech. J.*, vol. 33, pp. 579–659; May, 1954.

ac field, and having the property that $[\epsilon]$ and $[\mu]$ are transposed by reversing the dc magnetic field. Ferrites and plasma are special cases of gyrotropic media. In subsequent discussion, the terminology "when $[\epsilon]$ and $[\mu]$ are transposed" will be frequently used. In ferrites and plasma, this is equivalent to saying "when the dc magnetic field is reversed."

The Reciprocity Theorem

The equations for an ac field in gyrotropic media are

$$\nabla \times \boldsymbol{E} = -j\omega[\mu]\boldsymbol{H}$$
$$\nabla \times \boldsymbol{H} = j\omega[\epsilon]\boldsymbol{E} + \boldsymbol{J} \tag{1}$$

where $\boldsymbol{J}$ represents the electric sources. All dissipation is accounted for in the $[\epsilon]$ and $[\mu]$, including conduction loss. The field from the same sources when $[\epsilon]$ and $[\mu]$ are transposed (indicated by $\sim$) will be denoted by $\widehat{\boldsymbol{E}}$, $\widehat{\boldsymbol{H}}$. Thus, the equations for the careted fields are

$$\nabla \times \widehat{\boldsymbol{E}} = -j\omega[\tilde{\mu}]\widehat{\boldsymbol{H}}$$
$$\nabla \times \widehat{\boldsymbol{H}} = j\omega[\tilde{\epsilon}]\widehat{\boldsymbol{E}} + \boldsymbol{J}. \tag{2}$$

Now consider two sets of sources $\boldsymbol{J}_a$ and $\boldsymbol{J}_b$, producing fields $\boldsymbol{E}_a$, $\boldsymbol{H}_a$ and $\boldsymbol{E}_b$, $\boldsymbol{H}_b$ in the original medium, and fields $\widehat{\boldsymbol{E}}_a$, $\widehat{\boldsymbol{H}}_a$ and $\widehat{\boldsymbol{E}}_b$, $\widehat{\boldsymbol{H}}_b$ in the medium when $[\epsilon]$ and $[\mu]$ are transposed. By scalarly multiplying the second equation of (2) for the a field by $\boldsymbol{E}_b$, and the first equation of (1) for the b field by $\widehat{\boldsymbol{H}}_a$, one obtains

$$\boldsymbol{E}_b \cdot \nabla \times \widehat{\boldsymbol{H}}_a = j\omega \boldsymbol{E}_b \cdot [\tilde{\epsilon}]\widehat{\boldsymbol{E}}_a + \boldsymbol{J}_a \cdot \boldsymbol{E}_b$$
$$\widehat{\boldsymbol{H}}_a \cdot \nabla \times \boldsymbol{E}_b = -j\omega \widehat{\boldsymbol{H}}_a \cdot [\mu]\boldsymbol{H}_b. \tag{3}$$

Subtract the second from the first and apply the identity $\nabla \cdot (\boldsymbol{A} \times \boldsymbol{B}) = \boldsymbol{B} \cdot (\nabla \times \boldsymbol{A}) - \boldsymbol{A} \cdot (\nabla \times \boldsymbol{B})$. This gives

$$\nabla \cdot (\widehat{\boldsymbol{H}}_a \times \boldsymbol{E}_b) = j\omega \boldsymbol{E}_b \cdot [\tilde{\epsilon}]\widehat{\boldsymbol{E}}_a + j\omega \widehat{\boldsymbol{H}}_a \cdot [\mu]\boldsymbol{H}_b + \boldsymbol{J}_a \cdot \boldsymbol{E}_b. \tag{4}$$

A similar manipulation of the second equation of (1) and the first of (2) yields

$$\nabla \cdot (\boldsymbol{H}_b \times \widehat{\boldsymbol{E}}_a) = j\omega \widehat{\boldsymbol{E}}_a \cdot [\epsilon]\boldsymbol{E}_b + j\omega \boldsymbol{H}_b \cdot [\tilde{\mu}]\widehat{\boldsymbol{H}}_a + \boldsymbol{J}_b \cdot \widehat{\boldsymbol{E}}_a. \tag{5}$$

In view of the identity $\boldsymbol{A} \cdot [a]\boldsymbol{B} = \boldsymbol{B} \cdot [\tilde{a}]\boldsymbol{A}$, subtraction of (5) from (4) gives

$$\nabla \cdot (\widehat{\boldsymbol{H}}_a \times \boldsymbol{E}_b - \boldsymbol{H}_b \times \widehat{\boldsymbol{E}}_a) = \boldsymbol{J}_a \cdot \boldsymbol{E}_b - \boldsymbol{J}_b \cdot \widehat{\boldsymbol{E}}_a. \tag{6}$$

Now integrate this throughout a region and apply the divergence theorem to the left-hand side. One now has

$$\iint (\widehat{\boldsymbol{H}}_a \times \boldsymbol{E}_b - \boldsymbol{H}_b \times \widehat{\boldsymbol{E}}_a) \cdot d\boldsymbol{s} = \iiint (\boldsymbol{J}_a \cdot \boldsymbol{E}_b - \boldsymbol{J}_b \cdot \widehat{\boldsymbol{E}}_a) dv \tag{7}$$

where the surface is that bounding the region. Eq. (7) is the general reciprocity formula when all sources are of the electric type. This formula can be extended to include magnetic sources,[2] but these are not necessary for the objectives of this paper.

The left-hand side of (7) vanishes when the surface bounding the region recedes to infinity, or when the surface is covered by a perfect electric conductor. (It also vanishes under other conditions, but these two have the greatest physical significance.) The reciprocity theorem then reduces to

$$\iiint \boldsymbol{J}_a \cdot \boldsymbol{E}_b dv = \iiint \boldsymbol{J}_b \cdot \widehat{\boldsymbol{E}}_a dv. \tag{8}$$

Note that this reduces to the usual reciprocity theorem[1] when $[\epsilon]$ and $[\mu]$ are symmetric tensors, for then $\widehat{\boldsymbol{E}} = \boldsymbol{E}$. Rumsey has defined the quantities appearing in (8) to be *reactions*,[2] and interpreted them as "physical observables." Note that they are *not* power, which would require integrands of the form $\boldsymbol{J}^* \cdot \boldsymbol{E}$ (the * denotes complex conjugate). By defining the reactions

$$\langle a, b \rangle = \iiint \boldsymbol{J}_a \cdot \boldsymbol{E}_b dv$$
$$\langle b, \hat{a} \rangle = \iiint \boldsymbol{J}_b \cdot \widehat{\boldsymbol{E}}_a dv \tag{9}$$

one can write the reciprocity theorem as

$$\langle a, b \rangle = \langle b, \hat{a} \rangle. \tag{10}$$

Thus, in the terminology of the reaction concept, the reciprocity theorem is: *The reaction of one set of sources on another is equal to the reaction of the latter set on the former when* $[\epsilon]$ *and* $[\mu]$ *are transposed.* The interpretation of this should become clearer when we apply it to networks in the next section.

Network Reciprocity

The current source of circuit theory is equivalent to a short filament of electric current applied between a pair of terminals. For this, the reaction becomes

$$\langle a, b \rangle = I_a \int \boldsymbol{E}_b \cdot d\boldsymbol{l}_a = I_a V_{ab} \tag{11}$$

where I_a is the a source and V_{ab} is the voltage due to the b source appearing across the a terminals. Note that this reaction is proportional to V_{ab} (equal to it if $I_a = 1$), and is therefore a measure of V_{ab}. Now consider an N terminal-pair network. The term "network" is used in its general sense, meaning "a configuration of matter." For linear matter, the properties of the network can be expressed in terms of an impedance matrix $[z]$ according to[5]

$$[V] = [z][I] \tag{12}$$

where $[V]$ and $[I]$ are the column matrices of the terminal voltages and currents. If a current I_i is applied to the ith terminal pair, and a current I_j to the jth terminal pair, we have $\langle i, j \rangle = I_i V_{ij}$ from (11). But the source I_j sees all terminals open circuited, so from (12) it follows that $V_{ij} = z_{ij} I_j$, where z_{ij} is the element of $[z]$ in the ith row, jth column. Thus, the elements of the impedance matrix in terms of the reactions are

[5] C. G. Montgomery, R. H. Dicke, E. M. Purcell, "Principles of Microwave Circuits," M.I.T. Rad. Lab. Ser., McGraw-Hill Book Co., Inc., New York, N. Y., vol. 8, p. 87; 1948.

$$z_{ij} = \frac{\langle i, j \rangle}{I_i I_j} \tag{13}$$

valid for all i and j (including $i=j$). The reactions between unit currents are numerically equal to the impedance elements.

Now let the network contain gyrotropic media. Define the impedance matrix for the network with $[\epsilon]$ and $[\mu]$ transposed according to

$$[\hat{V}] = [\hat{z}][I] \tag{14}$$

where $[\hat{V}]$ is the column matrix of the new terminal voltages. Following the same reasoning as for the original network, one has

$$\hat{z}_{ij} = \frac{\langle i, j \rangle}{I_i I_j} . \tag{15}$$

From (10), (13), and (15), it is evident that $z_{ij}=\hat{z}_{ji}$, or

$$[\hat{z}] = [\tilde{z}]. \tag{16}$$

Thus, the network reciprocity theorem is: *The impedance matrix of any network is transposed when* $[\epsilon]$ *and* $[\mu]$ *are transposed.*

Corollaries to this are: *The admittance matrix and the scattering matrix of any network are transposed when* $[\epsilon]$ *and* $[\mu]$ *are transposed.* It is evident that the admittance matrix $[y]$, defined according to[5]

$$[I] = [y][V], \tag{17}$$

is transposed, since $[y]$ is the inverse matrix of $[z]$. The transposition of $[y]$ can also be shown by a procedure analogous to that used to show the transposition of $[z]$. For this, one should extend the reciprocity theorem to magnetic sources, and use the magnetic current equivalent of the circuit voltage source.[6] The scattering matrix $[S]$ is defined according to[7]

$$[V^s] = [S][V^i] \tag{18}$$

where $[V^i]$ is the column matrix of the incident components of terminal voltage and $[V^s]$ is the column matrix of the reflected components. In terms of the impedance matrix, one has[7]

$$[S] = [z - I][z + I]^{-1} \tag{19}$$

where $[I]$ is the unit matrix. The proof that $[S]$ is transposed when $[z]$ is transposed is outlined as follows.

$$\begin{aligned}[\hat{S}] &= [\tilde{z} - I][\tilde{z} + I]^{-1} = \widetilde{[z - I][z + I]^{-1}} \\ &= \widetilde{[z + I]^{-1}[z - I]} = \widetilde{[z - I][z + I]^{-1}} = [\tilde{S}]. \end{aligned} \tag{20}$$

The theorem on the transposition of network matrices applies to microwave networks as well as to the usual circuit theory networks. For example, if the input terminals (or ports) to the network are waveguides, one replaces the current elements used in the previous proof by current sheets across the waveguides. These current sheets are chosen so that only the desired modes are excited. The remainder of the proof is then identical to the preceding one.

[6] R. F. Harrington, "Field equivalence theorems and their circuit analogues," *Elec. Eng.*, vol. 73, pp. 923–927; October, 1954.

[7] Montgomery, Dicke, and Purcell, *op. cit.*, p. 146.

Interpretations of Reciprocity

A few specific interpretations will now be given so that the reader may appreciate the significance of the above reciprocity theorems. These will be stated in terms of reversing the dc magnetic field in gyrotropic media to emphasize the physical interpretation of transposing $[\epsilon]$ and $[\mu]$. Perhaps it should be pointed out that the dc field need not be uniform. Reversal of the dc magnetic field applies to all points, being roughly equivalent to reversing the dc current in a field winding.

1) *The input impedance to any device containing gyrotropic media is unchanged by reversing the dc magnetic field.* The impedance matrix of a two-terminal (one-port) device is of order one (a single element), and thus equal to its transpose.

2) *For a network containing gyrotropic media, the positions of an ac current source and an infinite impedance voltmeter may be interchanged without affecting the voltmeter reading, if at the same time the dc magnetic field is reversed.* This follows from the transposition of $[z]$, since the voltage at terminals i due to a current in terminals j is $V_i=z_{ij}I_j$, all terminals open-circuited.

3) *For a network containing gyrotropic media, the positions of an ac voltage source and an impedanceless ammeter may be interchanged without affecting the ammeter reading, if at the same time the dc magnetic field is reversed.* This follows from the transposition of $[y]$, since the current at terminals i due to a voltage across terminals j is $I_i=y_{ij}V_j$, all terminals short-circuited.

4) *The resonant frequencies of any cavity containing gyrotropic media are unchanged by reversing the dc magnetic field.* This follows from statement 1), since the resonances are infinities of the input impedance.

5) *The transmitting pattern of any antenna containing gyrotropic media is the same as the receiving pattern with the dc magnetic field reversed.* This follows from statement 2) if one considers the given antenna plus a "test" antenna as forming a two-terminal pair device.

6) *The cut-off frequency spectrum of any cylindrical waveguide containing gyrotropic media is unchanged when the dc magnetic field is reversed.* This follows from statement 4), since the cut-off frequencies are the resonances of a two-dimensional cavity.

7) *In any cylindrical waveguide containing gyrotropic media, the propagation constants of positive traveling modes are interchanged with those of negative traveling modes when the dc magnetic field is reversed.* The proof of this follows from statement 2) if one considers the two ends of the guide as ports to a microwave network.

Acknowledgment

This work was supported in part by Office of Ordinance Research, U. S. Army, Contract No. DA-30-115-ORD-861.

Broad-Band Stepped Transformers from Rectangular to Double-Ridged Waveguide*

E. S. HENSPERGER†

Summary—The design of a series of broad-band Tchebycheff-type stepped waveguide transformers from various sizes of standard rectangular waveguides to a double ridged waveguide covering the frequency range of 4750 to 11,000 mc is described. Four separate transformers employing RG-67/U (WR-90), RG-68/U (WR-112), RG-106/U (WR-137), and WR-159 to Airtron ARA-133 double-ridged waveguide have been designed using this technique and cast in aluminum. The complete frequency range is covered by several pairs depending on which sizes of mating rectangular waveguides are desired. The RG-106/U design covers a frequency range of 53 per cent with a maximum VSWR of 1.08, while the other three designs each cover a slightly smaller frequency band with a VSWR not exceeding 1.05. Along with the experimental results obtained, an outline of the design method is given which can be used to design similar transformers between any compatible rectangular and double ridged waveguides.

Introduction

CONSIDERABLE information on the design of stepped single-ridged transformers to rectangular waveguide is available in the literature. However, despite the wide usage of double-ridged waveguides in present day systems, information on the design of well-matched broad-band double-ridged transformers to rectangular waveguide has been noticeably lacking. In this article, the work of Cohn[1] and Hopfer[2] dealing with single-ridged transformers is combined, and suitably modified to yield an accurate design method for double-ridged stepped transformers made between waveguides of arbitrarily selected aspect ratios and cross-sectional dimensions.

General Considerations

The use of stepped impedance sections proportioned to Tchebycheff polynominals will always result in better broad-band results for a given length and bandwidth than the use of tapers or other step functions. The amount of calculation involved in designing Tchebycheff transformers may be somewhat more laborious, but the extra effort is more than justified by the improvement in the end results.

The form of the transformer is shown in Fig. 1. The structure consists of a symmetrical series of steps on the top and bottom of the waveguide with approximately quarter-wavelength spacing between steps. The sections

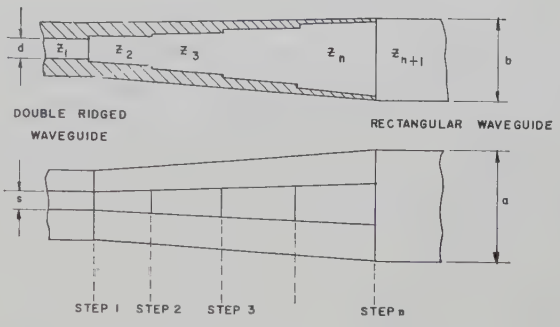

Fig. 1—The double-ridged stepped transformer.

between steps are designated by Z_2, Z_3, etc. Each of these sections is considered to maintain an approximately constant value of impedance throughout its length. For example, if section Z_3 is designed for 215 ohms, the impedance is very close to 215 ohms from one end of section Z_3 to the other end. The symbols d, b, s, and a given in Fig. 1 are intended to cover the gap distance, height of the waveguide, width of the ridges, and width of the waveguide, respectively, at any point throughout the length of the transformer.

As a rule, the rectangular waveguide will be larger in cross section than the ridged waveguide to which it is to be mated. This is due to the large reduction in TE_{10} cutoff wavelength accomplished by the ridge loading. Therefore, for compatible frequency characteristics, the unloaded guide will be considerably larger. The dimensions of the ARA-133 waveguide used in these particular transformer designs are shown in Table IV in a paper by Anderson.[3]

The problem of mating double-ridged waveguide to a rectangular waveguide which is larger in cross section, and still maintaining intermediate sections with constant impedance, can be solved in two ways. The outside dimensions of the waveguides can be blended together by either smooth tapers in both the E and H planes, or by abruptly stepping the waveguide along with the steps in the center ridges. The latter solution is rather impractical from a fabrication standpoint, and more important, the electrical design would be unduly complicated by the large discontinuity susceptances which would have to be compensated. Therefore, the transition is made with smooth tapers in the outside dimensions and in the width of the ridges, thereby main-

* Manuscript received by the PGMTT, January 2, 1958; revised manuscript received, February 10, 1958.

† Airtron, Inc., Linden, N. J.

[1] S. B. Cohn, "Optimum design of stepped transmission-line transformers," IRE TRANS. ON MICROWAVE THEORY AND TECHNIQUES, vol. MTT-3, pp. 16–21; April, 1955.

[2] S. Hopfer, "The design of ridged waveguide," IRE TRANS. ON MICROWAVE THEORY AND TECHNIQUES, vol. MTT-3, pp. 20–29; October, 1955.

[3] T. N. Anderson, "Rectangular and ridge waveguide," IRE TRANS. ON MICROWAVE THEORY AND TECHNIQUES, vol. MTT-4, pp. 201–209; October, 1956.

taining a constant ratio of ridge width to guide width (s/a ratio) throughout the length of the transformer. To complete the necessary requirements for sections with constant impedance, the ratio of the gap between the ridges to the total height of the waveguide (d/b ratio) is calculated for each section by the method given below.

Design Method

The number of steps required for a given maximum VSWR can be roughly calculated by a trial and error solution of (5) in Cohn's article.[4] This equation is given below. Z_1 and Z_{n+1} are the terminating characteristic impedances as defined in Fig. 1. $T_m(x)$ is the Tchebycheff polynomial of mth degree, and

$$S_{\max} = 1 + \frac{\ln\left[\frac{Z_{n+1}}{Z_1}\right]}{T_{n-1}\left[\frac{1}{\cos\phi_1}\right]}.$$

ϕ_1 is the electrical spacing of the steps at the low-frequency end of the band. The equation is derived on the basis of small steps; however, Cohn has shown that the equation holds very well even with fairly large steps. For this type of design where over-all VSWR's of 1.10 or less are desired, it is recommended that at least four or five steps be used to minimize the discontinuity susceptances presented by the steps and the small inherent errors in the design method.

Once the number of steps has been chosen, the Tchebycheff coefficients and the resulting characteristic impedances required for each section are calculated by the methods outlined by either Cohn or Hopfer. As Hopfer points out, use of the impedances at infinite frequency ($Z_{0\infty}$) yields better results than the use of the actual impedances at midband, and this fact has been further substantiated by the results given in this article.

Calculation of the dimensions of the stepped ridge sections according to the prescribed impedances is then undertaken. Since the a and b dimensions of the transition section are tapered, the problem arises as to what specific values of a and b should be used. It has been found from experiment that very good results are obtained by dividing into $(n-1)$ equal parts the differences between the a and b dimensions of the two waveguide sizes used, and then calculating from these values the mean values of a and b in each impedance section. Use of these values for determination of the d/b ratio will yield the mean value of impedance in the section being considered. A slight variation in impedance from one end of the section to the other usually occurs; however, this variation is only about ± 1 ohm if reasonable tapers have been employed, and therefore, the assumption of constant impedance sections is considered to be valid. If the tapers are quite pronounced, the use of the mean values of a and b in each section will introduce objectionable deviations from the mean values of impedance. This can be easily overcome by determining the d/b ratio at each end of the section using the a's and b's at these points instead of the mean values. This method actually yields a much closer approximation to a constant impedance section, and is to be preferred. However, the amount of calculation is doubled, and is only necessary for severe tapers. The actual values of d/b ratio required at each point are determined with the aid of Fig. 2. This is a graph of relative admittance vs d/b ratio taken from information given on Fig. 16 of Hopfer. Hopfer's graph was worked out for single-ridged guide, but since there is no similar graph available for double-ridged guide, it was decided to try these data. Fortunately, actual values of impedance are secondary to relative values in waveguide transformer considerations and excellent results have been achieved using this graph, even though the data apply primarily to single-ridged guide.

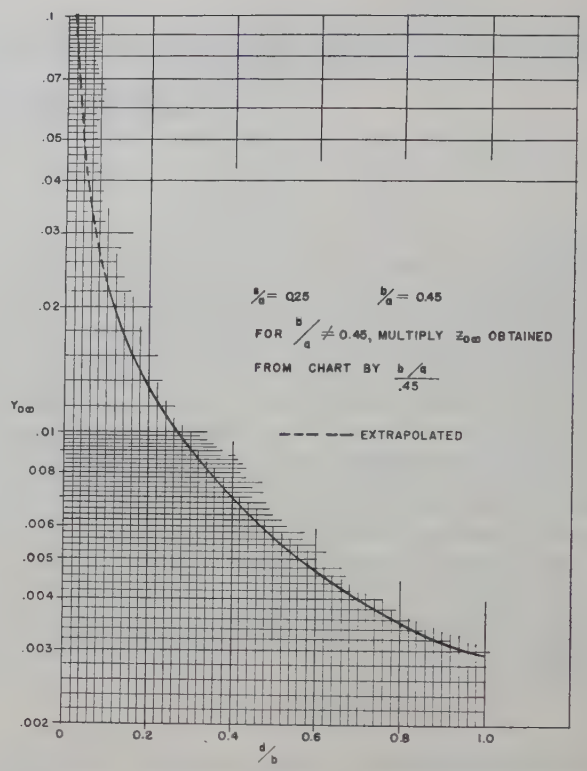

Fig. 2—Relative admittance chart for double-ridged waveguide transformer sections. Plotted from Fig. 16 of Hopfer[2] for constant value of $s/a = 0.25$.

If Fig. 2 is plotted on linear coordinates, it can be seen that the resultant curve is very closely a straight line up to approximately a value of $d/b = 0.8$. After this, the function drops off more and more rapidly from the straight line. This fact is significant because heretofore both double- and single-ridged transformers were designed using a straight line function to determine the relative impedance values between Z_1 and Z_{n+1}.

Fig. 2 is plotted for a constant s/a ratio of 0.25. This value of s/a has been chosen because most double-ridged waveguides are designed with this ratio which

[4] *Op. cit.*, p. 17.

represents the optimum in attenuation and high power handling characteristics. If other s/a ratios are desired, Hopfer's original graph should be used.

The length required for each of the constant impedance sections is then calculated. Since the a and b dimensions vary according to the outside tapers, the cutoff characteristics vary throughout the length of each section, thereby introducing varying λ_g values. To overcome this problem, the TE_{01} mode cutoff frequencies are determined from Hopfer's Fig. 2 for both ends of each section (TE_{20} mode cutoff wavelength should also be checked to be sure that this mode cannot be supported). The mean λ_g at one end of the section under consideration is then calculated from

$$\lambda_{gm} = \frac{2(\lambda_{g1}\lambda_{g2})}{\lambda_{g1} + \lambda_{g2}} .$$

λ_{g1} and λ_{g2} correspond to the guide wavelengths at one end of the section at the low- and high-frequency ends of the design band, respectively. The mean λ_g at the opposite end of the same section is then calculated in the same manner after its TE_{01} mode cutoff frequency has been determined. The actual length of the section (S) is found by combining the λ_{gm} values in the next equation. This procedure is employed for all of the constant impedance sections in the transformer. In general,

$$S = \frac{\lambda_{gm1}\lambda_{gm2}}{2(\lambda_{gm1} + \lambda_{gm2})},$$

all of the section lengths will be different.

Since all of the lengths are different, the original assumption of $(n-1)$ equal length sections for calculation purposes is now slightly in error for constant tapers. However, considerable variation in length can be tolerated since the angles of the tapers are so small that the change in a and b is negligible in most cases. For the transformers designed, except for the WR-159 case, the maximum discrepancy in a and b did not exceed 0.003 inch. If the discrepancies exceed this figure, as in the case of the WR-159 transformer design, the calculations may be easily corrected by using the lengths arrived at in the first approximation to recalculate a new series of d/b ratios and cutoff frequencies with the adjusted a and b dimensions.

Cohn has included in his article a method for compensating the step discontinuity susceptances by decreasing the length of the sections so affected. If four or less steps are used for the transformer, it is suggested that Cohn's procedure for compensation be employed to modify the section lengths. However, if more than four steps are used, the steps are generally small enough for the compensation to become negligible.

Experimental Results

Four transformers from different sizes of standard rectangular waveguide to ARA-133 double-ridged waveguide were designed according to the above principles to cover the frequency range of 4750 to 11,000 mc. Fig. 3 is a tabulation of the pertinent data on these transformer designs. Fig. 4 gives the final VSWR results on a typical RG-68/U aluminum production unit. It can be seen that the VSWR does not exceed 1.05 throughout the frequency range of this unit. The RG-67/U and WR-159 designs yielded comparable results over their respective frequency ranges; however, the RG-106/U design exhibited a maximum VSWR of 1.08. This higher value of VSWR can be attributed to the fact that this design not only covered the entire recommended operating range of RG-106/U, but it extended another 1100 mc below this range as well. A typical production sample of this design is shown in Fig. 5.

No preliminary fabricated design models were made; the designs were calculated and the resulting dimensions were transferred directly through the tools to one-piece castings. None of the designs required further design effort except the WR-159 transformer. The first castings on this unit exhibited the typical Tchebycheff

Waveguide Size	Transformer Frequency Range (mc)	Per cent Bandwidth	Number of Steps	*Length (inches)
RG-67/U	8200–11000	29	5	1.48
RG-68/U	7050–10800	44	6	1.90
RG-106/U	4750– 8200	53	6	3.16
WR-159	4750– 7350	43	7	4.09

* Transformer section only.

Fig. 3—Tabulation of transformers designed to mate with ARA-133 double-ridged waveguide.

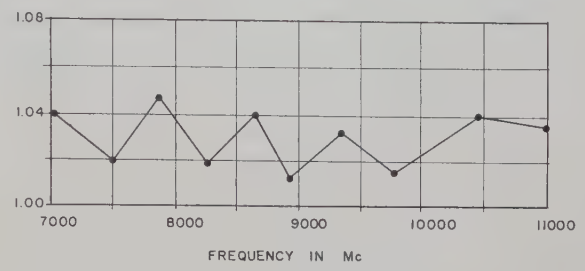

Fig. 4—VSWR vs frequency for RG-68/U to ARA-133 six-step transformer.

Fig. 5

ripple response, but the ripple varied between VSWR's of approximately 1.09 to 1.05. This difficulty was not surprising due to the extreme tapers required in the a and b dimensions, but a maximum VSWR of 1.05 was arrived at fairly easily by trial and error experimentation with the step dimensions.

It is interesting to note that further improvements probably could have been made on these transformer designs, since one of the RG-68/U castings tested did not exceed a maximum VSWR of 1.02 over the 7050 to 10,800-mc range. This outstanding performance can be attributed to the small dimensional variations which occur among many castings of the same design. Obviously, this particular casting possessed exactly the right combination of dimensions. However, for production purposes, a VSWR limit of 1.05 is much more practical since the tolerances which would have to be held to maintain the 1.02 limit are much too tight to be attainable.

Mechanical tolerances on these units presented some problems. In general, it was found that the distance between steps was relatively uncritical, but the height of the steps proved to be quite critical. Tolerances in the order of ± 0.004 inch were found to be adequate for the section lengths, but changes as small as 0.0015 inch in the step heights introduced measurable differences in the VSWR patterns.

Despite the simplifying assumptions and small errors in the design method, the results obtained are very satisfactory, and it is felt that the design method has been proven to be reliable and accurate for this type of waveguide transformer.

A Wide-Band Balun*

J. W. McLAUGHLIN†, D. A. DUNN†, AND R. W. GROW†

Summary—**Experimental results are given for a transformer from an unbalanced 50-ohm coaxial line to a balanced pair of 50-ohm coaxial lines. The design is one proposed by Marchand. The balance, standing wave ratio, and insertion loss are nearly constant over a 13 to 1 frequency range from 650 mc to 8500 mc. The standing wave ratio is less than 2.1 to one and the insertion loss is about 0.5 db over this band of frequencies.**

Introduction

SEVERAL authors[1–4] have presented theoretical analyses of devices suitable for transforming from a balanced to an unbalanced transmission line over a wide frequency range. It is the purpose of this paper to present some experimental results on a balun of the type described by Marchand[1] which provides satisfactory performance over a greater than ten to one band of frequencies extending from 650 to 8500 mc. One use for a balun with this sort of frequency coverage is in connection with microwave oscillators that can tune over frequency ranges of this order of magnitude and that can often be most effectively designed with balanced two-conductor interaction circuits.[5–7] The output of such tubes is in many cases most conveniently brought out of the vacuum envelope by means of two separate coaxial lines having a balanced signal between their center conductors. The balun to be described has been constructed to operate between such a two-coax system and a single coax, but only a slight change of the construction of the balanced output would be required to convert to a balanced shielded pair instead of two separate coaxial lines. Another possible use for a balun of this type would be as a microwave power splitter to obtain two equivalent outputs which differ in time phase by 180°.

Fig. 1 is a photograph of the balun. It transforms an unbalanced input signal supplied to the 50-ohm Hewlett-Packard G-76A receptacle input mounted on the brass cylinder into a balanced output signal appearing between the center conductors of the two 50-ohm RG5/U cables.

Fig. 2 is a schematic diagram of the device as proposed by Marchand.[8] Z_{OC} is the impedance of the unbalanced line C, Z_{OT} is the impedance of the large outer

* Manuscript received by the PGMTT, January 22, 1958; revised manuscript received, April 17, 1958. This work was supported by the U. S. Army Signal Corps.

† Electronics Res. Lab., Stanford University, Stanford, Calif.

[1] N. Marchand, "Transmission line conversion," *Electronics*, vol. 17, pp. 142–145; December, 1944.

[2] E. G. Fubini and P. J. Sutro, "A wide-band transformer from an unbalanced to a balanced line," PROC. IRE, vol. 35, pp. 1153–1155; October, 1947.

[3] Radio Res. Lab. Staff, "Very High Frequency Techniques," McGraw-Hill Book Co., Inc., New York, N. Y., pp. 85–92; 1947.

[4] W. K. Roberts, "A new wide-band balun," PROC. IRE, vol. 45, pp. 1628–1631; December, 1957.

[5] P. K. Tien, "Bifilar helix for backward-wave oscillators," PROC. IRE, vol. 42, pp. 1137–1143; July, 1954.

[6] H. R. Johnson, T. E. Everhart, and A. E. Siegman, "Wave propagation on multifilar helices," IRE TRANS. ON ELECTRON DEVICES, vol. ED-3, pp. 18–24; January, 1956.

[7] D. A. Dunn, "Traveling-wave amplifiers and backward-wave oscillators for VHF," IRE TRANS. ON ELECTRON DEVICES, vol. ED-4, pp. 246–264; July, 1957.

[8] N. Marchand, *op. cit.*, Fig. 10.

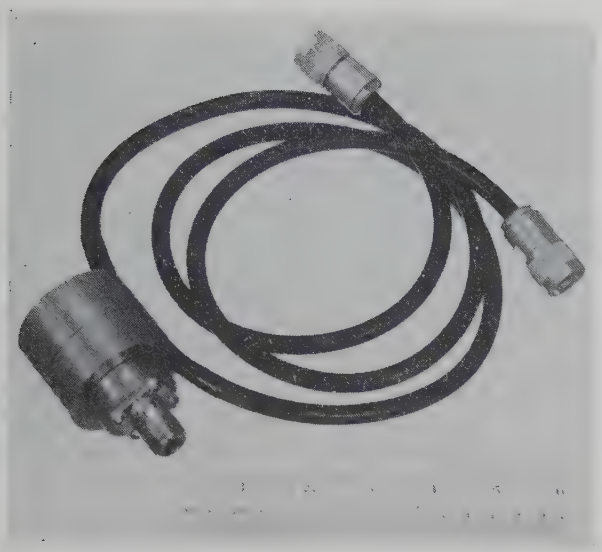

Fig. 1—An unbalanced input fed into the *N*-connector receptacle mounted in the brass cylinder is transformed into a balanced signal appearing between the two center conductors of the pieces of RG5/U cable coming out of the brass cylinder.

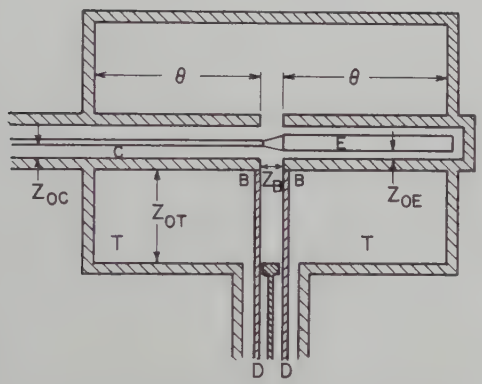

Fig. 2—A schematic drawing of the balun (after Marchand). The unbalanced line *C* drives the balanced line starting at *BB*. Two shorted coaxial stubs *T*, *T* use the outer conductors of coaxial lines *C* and *E* as their center conductors. The balanced line can be split into two separate coaxial lines *D*, *D* as shown, if desired.

shorted stubs *T*, Z_{OE} is the impedance of the small open-circuited stub *E* connecting directly to the unbalanced line, and Z_B is the impedance seen at the internal balanced line terminals, *BB*. Marchand shows that this impedance Z_B seen at the internal balanced terminals can be written in terms of Z_{OC}, Z_{OE}, and Z_{OT} as follows:

$$Z_B = Z_{OC} \frac{1 - j\frac{Z_{OE}}{Z_{OC}} \cot\theta}{1 - j\frac{Z_{OC}}{2Z_{OT}} \cot\theta - \frac{Z_{OE}}{2Z_{OT}} \cot^2\theta} \quad (1)$$

where θ is the electrical length of the shorted stub, as indicated in Fig. 2. The value of θ should be 90 degrees at mid-band and Z_{OE} should be chosen to make

$$Z_{OE} = \frac{(Z_{OC})^2}{2Z_{OT}} . \quad (2)$$

Z_{OT} should be made as large as possible.

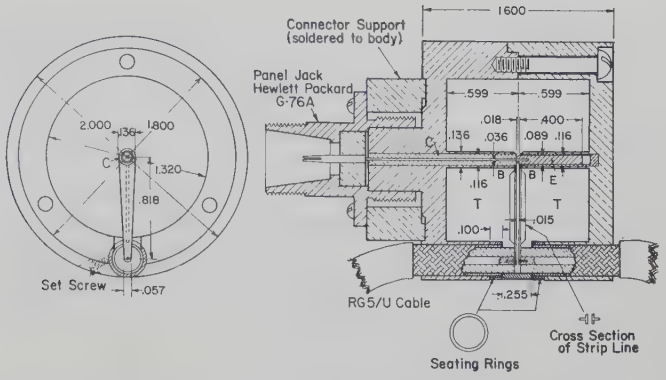

Fig. 3—A scale drawing of the balun shown in Fig. 1.

The design of the balun to be described used

$$Z_{OE} = 10.7 \text{ ohms}$$
$$Z_{OT} = 136 \text{ ohms}$$
$$Z_{OC} = 50 \text{ ohms}$$
$$Z_B = 50 \text{ ohms at 5 kmc.}$$

A tapered balanced strip line section was used to connect the internal balanced terminals to the two external coaxial lines, each of 50-ohms impedance. The tapered section transformed Z_B from 50 to 100 ohms at the connections to the external lines.

The physical arrangement used is shown in Fig. 3. Relevant dimensions are marked in inches and the labeling corresponds to Fig. 2. The internal section of unbalanced line *C* is RG141/U teflon cable with a solid outer conductor 0.010 thick. This outer conductor and the opposing extended stub were machined as integral parts of the main body. Since the two ends of the balanced strip line must be accurately spaced from each other by only 0.015, the two external coax lines must seat precisely in the body of the balun. This was accomplished by soldering the seating rings to the braid of these external lines before assembly. The cables are trimmed to extend the correct amount beyond the seating rings after the rings are soldered. The seating rings are held by set screws and the connections between the strip lines and the coax center conductors are made with flexible pins set into the center conductors.

Experimental Results

The VSWR looking into the unbalanced coax with the balanced coaxial lines terminated is an indication of how well the balun transforms from the 50-ohm unbalanced system to the 50-ohm internal balanced terminals, and also of how well the tapered strip line transforms from the 50-ohm internal balanced terminals to the 100-ohm external balanced terminals. Also included in the VSWR measurements are the effects of reflections from discontinuities in the transmission lines, and imperfections in the terminations. The measured plot of VSWR vs frequency shown in Fig. 4 includes all of these effects. The dotted curve in Fig. 4 shows the calculated

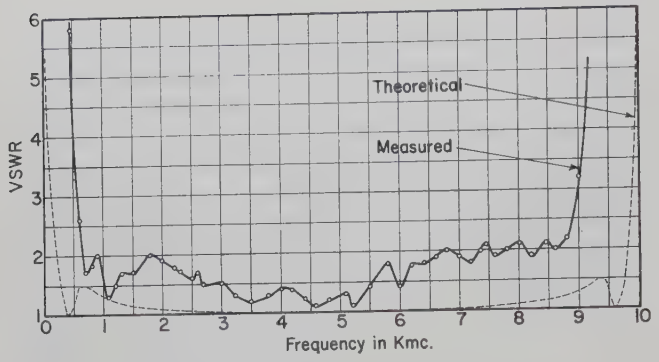

Fig. 4—A plot of standing wave ratio as a function of frequency looking into the unbalanced line C with terminations on both lines D, D. The dashed curve is a theoretical curve.

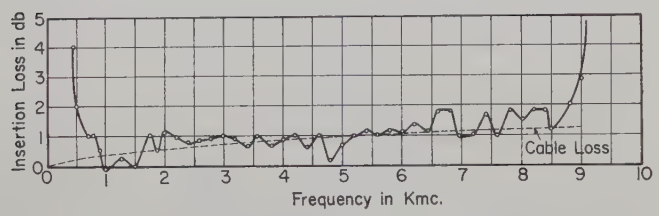

Fig. 5—A plot of insertion loss vs frequency through the balun for a signal fed into the unbalanced line C. The losses in the two RG-5/U cables varied as indicated by the dashed curve. The deviations of the insertion loss above and below the cable loss were caused by the mismatches between the various components used in the system. The actual loss of the balun is probably much less than 0.5 db.

values of VSWR which are theoretically ortainable from this design, neglecting any discontinuities or imperfections in the tapered strip line and terminations. The theoretical curve is obtained from

$$\text{VSWR} = \frac{Z_B}{Z_{OC}} \qquad Z_B > Z_{OC} \tag{3}$$

$$\text{VSWR} = \frac{Z_{OC}}{Z_B} \qquad Z_B < Z_{OC}. \tag{4}$$

Z_{OC} is the 50-ohm impedance of the unbalanced coaxial line. Z_B is the impedance at the internal balanced terminals as given by (1). The measured VSWR is below 2.1 from 0.65 to 8.5 kmc.

The insertion loss characteristics of this balun are plotted in Fig. 5. The measurements were made using the calibrated attenuator of a signal generator to compare the relative amounts of power transmitted to a crystal through a transmission system that first included the balun and then bypassed it. The difference between these two readings is the insertion loss in db. It is important to note that no special effort was made to match the impedances of the various components in either the presence or the absence of the balun. In the frequency range from 2 to 7 kmc a thermistor and power bridge were used to measure the actual power transmitted through the transmission system, first including, and then excluding the balun. The value of insertion loss over the frequency range from 0.65 to 6.5 kmc is less than 1.5 db. From 0.65 to 8.5 kmc the insertion loss is less than 2 db. An important source of loss in this setup was the loss of the two sections of RG5/U cable attached to the balun. Each was 2 feet long, so the cable loss varied from 0.4 db at 1 kmc to 1.2 db at 8 kmc and is indicated in Fig. 5 by the dashed line. The mismatches between the various components account for the deviations of the measured insertion loss above and below the cable loss. The actual total loss of the balun and the cable should be approximately the median value between the excursions of the measured insertion loss. Since it is apparent that the average of the measured curve only slightly exceeds the cable loss of the balun the results of the measurement seem quite reasonable. The deviations then are mainly the result of the mismatches at the various junctions and do not indicate precisely the net loss of the balun itself. It seems reasonable, however, that the actual loss at any frequency is much smaller than the deviations measured. In fact, the loss of the balun itself is probably much less than 0.5 db.

An experiment was performed to obtain some indication of the degree to which the two balanced outputs compared in amplitude and phase. This measurement was performed by applying a signal to the unbalanced input and connecting the two balanced outputs through 10-db coaxial attenuators to a slotted line. In this way the amplitude of the two signals could be compared by measuring the SWR and the phase could be compared by measuring the position of the central minimum. The attenuators differed only slightly so that a high degree of accuracy was possible in measuring the amplitudes. The positions of the attenuators were then reversed so that two different readings could be made and the effect of the attenuators could thereby be separated from the balun unbalance. In the range from 2 to 4 kmc the db difference between the two outputs of the balun was less than 0.38 db, and the average difference was 0.13 db. Over the same frequency range the deviation of the position of the central minimum was also observed. It was determined that the variation of phase shift through the other equipment was so great that it was impossible to obtain data which were truly representative of the small amount of phase shift present in the balun. It may be stated, however, that the phase shift was certainly much less than the peak-to-peak phase shift variation of 0.0012λ which was caused by the 10-db attenuators.

Power-Flow Relations in Lossless Nonlinear Media*

H. A. HAUS†

Summary—**The Manley-Rowe relations, originally derived for nonlinear lumped circuit elements, are generalized to include the power flow in the fields produced in the presence of lossless, nonlinear media. The generalization is carried out first for nonlinear anisotropic media with single-valued relations between the instantaneous $\overline{E}$ and $\overline{P}$, and $\overline{H}$ and $\overline{M}$. The proof is extended to include gyromagnetic media under small-signal excitation at the signal frequency (but large excitation at the pump frequency). The relations are applied to show under what conditions power gain can be achieved with a three-frequency and a four-frequency excitation of a ferrite. The form of the coupling coefficients in the electromagnetic operation of a ferrite amplifier is shown to be a consequence of the generalized Manley-Rowe relations.**

I. Introduction

CONSIDERABLE attention has been given recently to amplifiers that employ nonlinear electromagnetic media, are "pumped" at one frequency, and provide gain at one or more frequencies. Good noise performance at microwave frequencies, and other advantages, can be expected from these "parametric" amplifiers, as they are often called. As a specific example of a parametric amplifier, Manley and Rowe[1] considered the nonlinear capacitor, and proved some general relations among the powers flowing into the capacitor terminals at several frequencies. Their results are also applicable to lossless inductors. It is not obvious however, how their power relations can be applied to electromagnetic problems involving nonlinear anisotropic electric and magnetic media. It is also not clear whether their relations are still applicable to nonlinear, nonreciprocal circuits. Devices containing nonlinear gyromagnetic media have equivalent circuits that exhibit nonreciprocal properties. In the construction of the ferromagnetic microwave amplifier one employs just such nonlinear media. Therefore, it seems necessary to extend the Manley-Rowe relations to include the electromagnetic power flow of fields in lossless nonlinear media, and in media which exhibit gyromagnetic effects.

This paper is divided in four parts. First, we derive two expressions for the power flow density (Poynting vector) in nonlinear media at various frequencies. These expressions are used as the basis of the generalization of the Manley-Rowe relations.

Second, we study the relation between the magnetic field intensity $\overline{H}$ and the magnetization $\overline{M}$ for lossless anisotropic magnetic media under the restriction that $\overline{H}$ be a single-valued function of $\overline{M}$.[2] The same is done for the relation between the electric field intensity $\overline{E}$ and the polarization $\overline{P}$ of a lossless anisotropic dielectric material. These relations are then used in the proof of the Manley-Rowe relations for lossless media with single-valued relations between $\overline{H}$ and $\overline{M}$, and $\overline{E}$ and $\overline{P}$.

Third, we apply the well-known relation between $\overline{H}$ and $\overline{M}$ in a gyromagnetic medium to prove the Manley-Rowe relations for lossless gyromagnetic media under small-signal excitation (but, in general, under large excitation at the pump frequency and its harmonics).

Finally, we apply the generalized Manley-Rowe relations to show under what conditions one can achieve gain in a cavity loaded by a ferrite and resonant at the pumping frequency, the signal frequency, and one "idling" frequency. It is found that gain can only be achieved if the idling frequency and signal frequency are both below the pumping frequency. A similar study, carried out for a device operating at the pumping frequency, signal frequency, and two "idling" frequencies, shows that gain can be achieved at frequencies higher than the pump frequency but less than twice the pump frequency. It is shown that an interrelation exists between the coupling coefficients of the equations for the "electromagnetic operation"[3] of a three-frequency (pump, signal, and idling frequency) ferrite amplifier. This interrelation is a consequence of the generalized Manley-Rowe relations.

II. General Power Relations in Nonlinear Media

Suppose that an excitation at two frequencies, ω_0 and ω_1, is applied to a nonlinear medium. The nonlinear medium produces, in general, fields at all frequencies $m\omega_1+n\omega_0$, where m and n are all positive and negative integers. (Components at negative frequencies have the interpretation that is usual in complex Fourier series expansions.) Thus, the electric field at any point $\bar{r}$ can be expanded in the complex Fourier series,

$$\overline{E}(\bar{r}, t) = \sum_{m,n} \overline{E}_{m,n}(\bar{r}) e^{j(m\omega_1+n\omega_0)t}, \tag{1}$$

where the m's and n's run over all integers from $-\infty$ to $+\infty$. Since $\overline{E}(\bar{r}, t)$ is a real vector, we conclude that

$$\overline{E}_{m,n} = (\overline{E}_{-m,-n})^*. \tag{2}$$

* Manuscript received by the PGMTT, January 28, 1958; revised manuscript received March 31, 1958.

† Res. Lab. of Electronics and Elec. Eng. Dept., M.I.T., Cambridge, Mass.

[1] J. M. Manley and H. E. Rowe, "Some general properties of nonlinear elements—Part I. General energy relations," PROC. IRE, vol. 44, pp. 904–914; July, 1956.

[2] We consider $\overline{H}$ to be a single valued function of $\overline{M}$, if $\overline{H}(\bar{r}, t)$ at the point $\bar{r}$ and the time t depends only upon $\overline{M}(\bar{r}, t)$ at the same point and at the same time. $\overline{H}(\bar{r}, t)$ is not supposed to depend upon the time (or space) derivatives of $\overline{M}$. For a linear medium this restriction is equivalent to the requirement that the reciprocity relation be fulfilled.

[3] H. Suhl, "Theory of the ferromagnetic microwave amplifier," *J. Appl. Phys.*, vol. 28, pp. 1225–1236; November, 1957.

Similar expressions apply to the magnetic field $\overline{H}(\bar{r}, t)$, the polarization $\overline{P}(\bar{r}, t)$, and the magnetization $\overline{M}(\bar{r}, t)$. The time-dependent Maxwell equations can be split into Fourier components (one set of equations for each Fourier component). We have

$$\nabla \times \overline{E}_{m,n} = -j\mu_0(m\omega_1 + n\omega_0)(\overline{H}_{m,n} + \overline{M}_{m,n}) \quad (3)$$

$$\nabla \times \overline{H}_{m,n} = j(m\omega_1 + n\omega_0)(\epsilon_0\overline{E}_{m,n} + \overline{P}_{m,n}). \quad (4)$$

Dot-multiplying (3) by

$$\frac{m\overline{H}_{m,n}^*}{m\omega_1 + n\omega_0},$$

the complex conjugate of (4) by

$$\frac{m\overline{E}_{m,n}}{m\omega_1 + n\omega_0},$$

and subtracting the two resulting equations, we obtain, after adding over all m and n,

$$\nabla \cdot \sum_{m=-\infty}^{\infty} \sum_{n=-\infty}^{\infty} \frac{m\overline{E}_{m,n} \times \overline{H}_{m,n}^*}{m\omega_1 + n\omega_0} = -j \sum_{m=-\infty}^{\infty} \sum_{n=-\infty}^{\infty} m\overline{M}_{m,n} \cdot \overline{H}_{m,n}^* + j \sum_{m=-\infty}^{\infty} \sum_{n=-\infty}^{\infty} m\overline{P}_{m,n}^* \cdot \overline{E}_{m,n}, \quad (5)$$

where the summations over the products $\overline{E}_{m,n} \cdot \overline{E}_{m,n}^*$ and $\overline{H}_{m,n} \cdot \overline{H}_{m,n}^*$ cancel by virtue of (2) and by an analogous relation for the Fourier components of the magnetic field. Eq. (5) is one of the basic relations for the power flow in nonlinear media which we use in deriving the generalization of the Manley-Rowe relations. Indeed, in order to accomplish the generalization, we only have to prove that the summations on the right-hand side of (5) are zero for the lossless media under consideration.

An equation analogous to (5) can be derived by dot-multiplying (3) by

$$\frac{n\overline{H}_{m,n}^*}{m\omega_1 + n\omega_0},$$

and the complex conjugate of (4) by

$$\frac{n\overline{E}_{m,n}}{m\omega_1 + n\omega_0}.$$

Again, subtracting the two resulting equations, and adding over all m and n, we obtain

$$\nabla \cdot \sum_{m=-\infty}^{\infty} \sum_{n=-\infty}^{\infty} \frac{n\overline{E}_{m,n} \times \overline{H}_{m,n}^*}{m\omega_1 + n\omega_0} = -j \sum_{m=-\infty}^{\infty} \sum_{n=-\infty}^{\infty} n\overline{M}_{m,n} \cdot \overline{H}_{m,n}^* + j \sum_{m=-\infty}^{\infty} \sum_{n=-\infty}^{\infty} n\overline{P}_{m,n}^* \cdot \overline{E}_{m,n}. \quad (6)$$

III. Proof of the Manley-Rowe Relations for Lossless "Reciprocal" Media

We call a medium "reciprocal" if a single-valued relation exists between $\overline{H}$ and $\overline{M}$ on the one hand, and $\overline{E}$ and $\overline{P}$ on the other hand. The medium does not have to be isotropic, *i.e.*, $\overline{M}$ does not have to be parallel to $\overline{H}$, and $\overline{E}$ is not necessarily parallel to $\overline{P}$.

Let us study the relation between $\overline{H}$ and $\overline{M}$ that has to hold in order to fulfill the requirement of losslessness. The energy per unit volume supplied to the material in order to produce the magnetization $\overline{M}$ is

$$\int_0^{\overline{M}} \overline{H} \cdot d\overline{M}, \quad (7)$$

where $\overline{H}$ is considered as a function of $\overline{M}$, $\overline{H}(\overline{M})$. Integral (7) has to be single-valued, independent of the "path" in the space of the magnetization vector $\overline{M}$. If $\overline{M}$ is varied, but eventually brought back to its original value, a closed path is described in the space of the magnetization vector $\overline{M}$. The integral over the closed path, $\oint \overline{H} \cdot d\overline{M}$, has to be zero if the medium is lossless and, therefore, no energy is lost in the magnetization. We have

$$\oint \overline{H} \cdot d\overline{M} = 0, \quad (8)$$

for an arbitrary path in the space of the magnetization vector $\overline{M}$. This is possible if, and only if, $\overline{H}$ can be written as the gradient (in the $\overline{M}$ space) of a potential function $U(\overline{M})$:

$$\overline{H} = \nabla_M U(\overline{M}), \quad (9)$$

where

$$\nabla_M = \bar{i}_x \frac{\partial}{\partial M_x} + \bar{i}_y \frac{\partial}{\partial M_y} + \bar{i}_z \frac{\partial}{\partial M_z}.$$

In a similar way, for a lossless anisotropic dielectric medium, we derive

$$\overline{E} = \nabla_P V(\overline{P}), \quad (10)$$

where

$$\nabla_P = \bar{i}_x \frac{\partial}{\partial P_x} + \bar{i}_y \frac{\partial}{\partial P_y} + \bar{i}_z \frac{\partial}{\partial P_z}$$

is the gradient in the space of the polarization vector, $\overline{P}$, in which we may represent $\overline{E}$ as a vector field.

First, let us consider the energy and power relations in a lossless *magnetic* material when two excitations at the angular frequencies ω_0 and ω_1 are applied to the material. The time dependence of the field vectors then contains components at frequencies $m\omega_1 + n\omega_0$, where m and n are (positive or negative) integers. At each point in space we must have, for the magnetization vector,

$$\overline{M} = \sum_{m=-\infty}^{\infty} \sum_{n=-\infty}^{\infty} \overline{M}_{m,n} e^{j(m\xi + n\eta)}, \quad (11)$$

where[1]

$$\xi = \omega_1 t \qquad \omega_1 = 2\pi f_1$$

$$\eta = \omega_0 t \qquad \omega_0 = 2\pi f_0$$

$$\overline{M}_{m,n} = \frac{1}{4\pi^2}\int_0^{2\pi} d\eta \int_0^{2\pi} d\xi \overline{M}(\xi, \eta) e^{-j(m\xi+n\eta)}$$

and

$$\overline{M}_{m,n} = (\overline{M}_{-m,-n})^*.$$

$\overline{M}_{m,n}$ is a complex vector function of ξ and η and of the spatial coordinates $\bar{r}=\bar{r}(x, y, z)$. The variables ξ and η can be considered as independent[1] in some mathematical operations. This means that $\overline{M}$ is considered as a function of ξ and η *in the entire* ξ-η *plane.* If we plot each vector component of $\overline{M}(\xi, \eta)$ as the third coordinate in a Cartesian coordinate system (in which ξ, η are the other two coordinates) we obtain three surfaces above the ξ-η plane, one surface for each component of $\overline{M}$. Let us now study the physical significance of these three surfaces. Consider a physical process with particular fundamental excitation frequencies ω_1 and ω_0. Then consider the cuts of the three surfaces $M_x(\xi, \eta)$, $M_y(\xi, \eta)$, and $M_z(\xi, \eta)$ with a plane perpendicular to the ξ-η plane, passing through the origin with the slope $\xi/\eta=\omega_1/\omega_0$. The curves thus obtained are plots of M_x, M_y, and M_z as functions of time for this particular process. A plane with a different slope $\xi/\eta=\omega_1'/\omega_0'$ produces, in general, different curves. These curves are the plots of M_x, M_y, and M_z as functions of time for another physical process, with the fundamental frequencies ω_1' and ω_0'. This new process has the initial values, $M_x(0, 0)$, $M_y(0, 0)$, and $M_z(0, 0)$ at $t=0$, in common with the original process since $\overline{M}(\xi, \eta)$ is a single-valued function of ξ and η. Thus, when we study $\overline{M}(\xi, \eta)$ as a function of ξ, η over the entire ξ-η plane we are studying an infinite number of physical processes with different fundamental frequencies ω_1 and ω_0. All processes have the initial value $\overline{M}(0, 0)$. The time dependence of any particular process (with the frequencies ω_1 and ω_2) is singled out through a cut by a plane perpendicular to the ξ-η plane and intersecting the ξ-η plane along a line through the origin with a slope $\xi/\eta=\omega_1/\omega_0$. For this reason we shall call the line $\xi/\eta=\omega_1/\omega_0$ the "process line." We make use of this picture, in particular, when we are considering gyromagnetic media. Returning now to the problem at hand, we recall that the relation between $\overline{H}$ and $\overline{M}$ is single-valued, by assumption. Hence

$$\overline{H} = \overline{H}[\overline{M}(\xi, \eta)] = \overline{H}(\xi, \eta). \tag{12}$$

$\overline{H}$ can be expanded in a similar Fourier series as $\overline{M}$:

$$\overline{H} = \sum_{m=-\infty}^{\infty}\sum_{n=-\infty}^{\infty} \overline{H}_{m,n} e^{j(m\xi+n\eta)}, \tag{13}$$

where

$$\overline{H}_{m,n} = (\overline{H}_{-m,-n})^* \tag{14}$$

and

$$\overline{H}_{m,n} = \frac{1}{4\pi^2}\int_0^{2\pi} d\eta \int_0^{2\pi} d\xi \overline{H}(\xi, \eta) e^{-j(m\xi+n\eta)}. \tag{15}$$

Dot-multiplying both sides of the complex conjugate of (15) by $jm\overline{M}_{m,n}$, and adding over all m and n, we obtain

$$\sum_{m=-\infty}^{\infty}\sum_{n=-\infty}^{\infty} jm\overline{H}_{m,n}{}^* \cdot \overline{M}_{m,n} = \frac{1}{4\pi^2}\int_0^{2\pi} d\eta \int_0^{2\pi} d\xi \overline{H}(\xi, \eta) \cdot \sum_{m=-\infty}^{\infty}\sum_{n=-\infty}^{\infty} jm\overline{M}_{m,n} e^{j(m\xi+n\eta)}. \tag{16}$$

The double summation under the integral of (16) can be identified by comparing it with (11):

$$\sum_{m=-\infty}^{\infty}\sum_{n=-\infty}^{\infty} jm\overline{M}_{m,n} e^{j(m\xi+n\eta)} = \frac{\partial \overline{M}}{\partial \xi}.$$

If we introduce this equation into (16), we have

$$\sum_{m=-\infty}^{\infty}\sum_{n=-\infty}^{\infty} jm\overline{H}_{m,n}{}^* \cdot \overline{M}_{m,n} = \frac{1}{4\pi^2}\int_0^{2\pi} d\eta \int_0^{2\pi} d\xi \overline{H}(\xi, \eta) \cdot \frac{\partial \overline{M}}{\partial \xi}. \tag{17}$$

But $d\xi(\partial\overline{M}/\partial\xi)=d\overline{M}$, with η held constant. Furthermore, according to (9),

$$d\overline{M} \cdot \overline{H} = d\overline{M} \cdot \nabla_M U(\overline{M}) = dU(\overline{M})$$

with η held constant. But $\overline{M}$ is a periodic function of ξ, and U is a single-valued function of $\overline{M}$. Therefore,

$$\int_0^{2\pi} d\xi \frac{d\overline{M}}{d\xi} \cdot \overline{H} = \int_{\overline{M}(0,\eta)}^{\overline{M}(2\pi,\eta)} dU = 0.$$

We thus obtain

$$\sum_{m=-\infty}^{\infty}\sum_{n=-\infty}^{\infty} jm\overline{H}_{m,n}{}^* \cdot \overline{M}_{m,n} = 0. \tag{18}$$

In a similar way we obtain

$$\sum_{m=-\infty}^{\infty}\sum_{n=-\infty}^{\infty} jn\overline{H}_{m,n}{}^* \cdot \overline{M}_{m,n} = 0 \tag{19}$$

$$\sum_{m=-\infty}^{\infty}\sum_{n=-\infty}^{\infty} jmP_{m,n}{}^* \cdot \overline{E}_{m,n} = 0 \tag{20}$$

$$\sum_{m=-\infty}^{\infty}\sum_{n=-\infty}^{\infty} jn\overline{P}_{m,n}{}^* \cdot \overline{E}_{m,n} = 0. \tag{21}$$

These equations can now be used to derive the extension of the Manley-Rowe relations. Introducing (18) and (20) into (5),we obtain

$$\nabla \cdot \sum_{m=-\infty}^{\infty}\sum_{n=-\infty}^{\infty} \frac{m\overline{E}_{m,n} \times H_{m,n}{}^*}{m\omega_1 + n\omega_0} = 0. \tag{22}$$

In a similar way, when (19) and (21) are introduced into (6) the result is

$$\nabla \cdot \sum_{m=-\infty}^{\infty} \sum_{n=-\infty}^{\infty} \frac{n\overline{E}_{m,n} \times \overline{H}_{m,n}^*}{m\omega_1 + n\omega_0} = 0. \tag{23}$$

Eqs. (22) and (23) are the generalizations of the Manley-Rowe relations in differential form.

Let us now imagine that the device under consideration is enclosed by a perfect conductor, except for the openings provided by the feeding guides. Number the various propagating modes in all the guides (each mode in every guide is assigned a particular number) 1, 2, $\cdots$, i, $\cdots$, N. Define, in the usual way, a voltage amplitude $V_{m,n,i}$ and current amplitude $I_{m,n,i}$ for each frequency component $m\omega_1+n\omega_0$ of the ith mode. Now, integrating over the entire volume of the device enclosed by the perfect conductor and by the cross-section planes of the guides, from (22) and (23), we obtain

$$\sum_{m=-\infty}^{\infty} \sum_{n=-\infty}^{\infty} \sum_{i=1}^{N} \frac{mV_{m,n,i}I_{m,n,i}}{m\omega_1 + n\omega_0} = 0;$$

$$\sum_{m=-\infty}^{\infty} \sum_{n=-\infty}^{\infty} \sum_{i=1}^{\infty} \frac{nV_{m,n,i}I_{m,n,i}}{m\omega_1 + n\omega_0} = 0.$$

These are the generalizations in equivalent-circuit terminology of the Manley-Rowe relations for microwave devices containing nonlinear anisotropic reciprocal media.

IV. The Small-Signal Manley-Rowe Relations for Gyromagnetic Media

We turn now to the derivation of the Manley-Rowe relations for gyromagnetic media. For this case, only the proof for small-*signal* excitation (but large *pump* excitation) has been found. Since most analyses of gyromagnetic media make use of the small-signal assumptions, publication of the proof at this time seems justified.

The small-signal theory of parametric amplifiers starts with the results of the (in general nonlinear) analysis of the pump excitation in the absence of an applied signal. Let us identify the frequencies ω_1 and ω_0 of Sections II and III with the pump frequency ω_p, and signal frequency ω_s, respectively. The pump excitation produces excitations at the pump frequency ω_p and all its harmonics. A small applied signal produces excitations at the sideband frequencies $m\omega_p+n\omega_s$. Among these, only the sidebands for $n=\pm 1$ are linearly related to the applied signal amplitude. All higher order sidebands, $|n|>2$, contain the applied signal amplitude raised to the nth power and are, therefore, negligible compared to the first order excitation ($|n|=1$) at small applied signal levels.

With this recognition, (6) can be adapted directly to the study of small signal power. Indeed, (6) contains only products of the sideband-excitation amplitudes ($n\neq 0$). If these amplitudes are found from a small-signal analysis to be correct within first order of the applied signal amplitude, the expressions in (6) can be found from them to be correct within second order. All contributions of terms with $|n|>1$ are of higher order than second and can be disregarded in a small-signal analysis. Within the small-signal assumption we thus obtain for (6)

$$\nabla \cdot \sum_{m=-\infty}^{\infty} \sum_{n=\pm 1} \frac{n\overline{E}_{m,n} \times \overline{H}_{m,n}^*}{m\omega_p + n\omega_s} = -j \sum_{m=-\infty}^{\infty} \sum_{n=\pm 1} n\overline{M}_{m,n} \cdot \overline{H}_{m,n}^* + j \sum_{m=-\infty}^{\infty} \sum_{n=\pm 1} n\overline{P}_{m,n}^* \cdot \overline{E}_{m,n}. \tag{24}$$

Eq. (24) is the small-signal counterpart of (6). Any small-signal solution will have to satisfy this equation.

Eq. (5) does not have a small-signal counterpart since it contains cross products of the pumping amplitudes. Small-signal theory disregards the second order changes in these quantities as caused by a small applied signal excitation. However, such second order changes contribute terms of second order to (5). Thus, small-signal theory does not provide the information necessary to use (5) up to second order.

We proceed now to prove the generalized, small-signal Manley-Rowe relations for gyromagnetic media. For this purpose, we must show that the right-hand side of (24) is equal to zero if $\overline{E}$ and $\overline{P}$ on the one hand, and $\overline{H}$ and $\overline{P}$ on the other, fulfill the relations of gyromagnetic media.

We assume that the dielectric characteristics of the material are reciprocal (see Section III for the use of "reciprocal" as applied to nonlinear media). For this case, it has been proved, in general, that

$$\sum_{m=-\infty}^{\infty} \sum_{n=-\infty}^{\infty} jn\overline{P}_{m,n}^* \cdot \overline{E}_{m,n} = 0. \tag{25}$$

For a small applied signal, all terms in (25) with $|n|\neq 1$ are negligible, and thus we have

$$\sum_{m=-\infty}^{\infty} \sum_{n=\pm 1} jn\overline{P}_{m,n}^* \cdot \overline{E}_{m,n} = 0. \tag{26}$$

Having proved that the second term on the right-hand side of (24) is zero, we turn our attention to the first term. We must prove that

$$\sum_{m=-\infty}^{\infty} \sum_{n=\pm 1} jn\overline{M}_{m,n} \cdot \overline{H}_{m,n}^* = 0, \tag{27}$$

subject to the condition that $\overline{M}$ and $\overline{H}$ must satisfy the equation of a gyromagnetic medium. We have

$$\dot{\overline{M}} = -\gamma(\overline{M} \times \overline{H}), \tag{28}$$

where $\overline{M}$ and $\overline{H}$ are the time-dependent magnetization and magnetic field, containing both the large-signal and small-signal parts.

First, consider the magnetization $\overline{M}(t)$. It consists of the large-signal part $\overline{M}_0(t)$ produced by the pumping

excitation. Aside from a time-average component, this part has only Fourier components at ω_p and its harmonics. The small perturbation $\overline{M}_1(t)$ of $\overline{M}(t)$, produced by a small signal at the frequency ω_s, has Fourier components at $m\omega_p \pm \omega_s$.

Thus

$$\overline{M}(t) = \overline{M}_0(t) + \overline{M}_1(t), \tag{29}$$

where

$$\overline{M}_0(t) = \sum_{m=-\infty}^{\infty} \overline{M}_m e^{jm\omega_p t} \tag{30}$$

$$\overline{M}_1(t) = \sum_{m=-\infty}^{\infty} \sum_{n=\pm 1} \overline{M}_{m,n} e^{j(m\omega_p + n\omega_s)t}. \tag{31}$$

With an analogous separation of the magnetic field into a small-signal part and a large-signal part, we obtain for (28)

$$\dot{\overline{M}}_1 = -\gamma(\overline{M}_0 \times \overline{H}_1 + \overline{M}_1 \times \overline{H}_0). \tag{32}$$

Eq. (32) determines $\overline{H}_1$ in terms of $\overline{M}_1$. Note, however, that it does not yield the component of $\overline{H}_1$ parallel to $\overline{M}_0$, $\overline{H}_1^{\parallel}$, since that component cancels when it is cross-multiplied by $\overline{M}_0$. Thus, (32) gives a relation only for $\overline{H}_1^{\perp}$, the component of $\overline{H}_1$ perpendicular to $\overline{M}_0$. The component $\overline{H}_1^{\parallel}$ is entirely independent of $\overline{M}_1$. Let us introduce, again, the variables

$$\xi = \omega_p t; \qquad \eta = \omega_s t. \tag{33}$$

In terms of these variables we may rewrite $\overline{M}_1$ formally as a function of ξ and η:

$$\overline{M}_1 = \overline{M}_1(\xi, \eta) = \sum_{m=-\infty}^{\infty} \sum_{n=\pm 1} \overline{M}_{m,n} e^{j(m\xi + n\eta)}. \tag{34}$$

The time derivative of $\overline{M}_1$ for any particular choice of ω_p and ω_s, *i.e.*, for any particular "process-line" in the ξ-η plane, is

$$\dot{\overline{M}}_1 = \omega_p \frac{\partial \overline{M}_1}{\partial \xi} + \omega_s \frac{\partial \overline{M}_1}{\partial \eta}. \tag{35}$$

We may now introduce (35) into (32), in order to obtain $\overline{H}_1$ as a function of ξ and η. According to (30) and (33),

$$\overline{M}_0 = \sum_{n=-\infty}^{\infty} \overline{M}_m e^{jm\xi} = \overline{M}_0(\xi). \tag{36}$$

Cross-multiplying (32) by $M_0(\xi)$ and expressing H_0 as a function of ξ analogously to (36) we have

$$\overline{H}_1^{\perp}(\xi, \eta) = \frac{1}{\gamma} \frac{1}{M_0^2} \left[\overline{M}_0(\xi) \times \left[\omega_p \frac{\partial \overline{M}_1(\xi, \eta)}{\partial \xi} + \omega_s \frac{\partial \overline{M}_1(\xi, \eta)}{\partial \eta} \right] + \gamma \overline{M}_0(\xi) \times [\overline{M}_1(\xi, \eta) \times \overline{H}_0(\xi)] \right]. \tag{37}$$

Eq. (37) gives the component of the small-signal H field perpendicular to $\overline{M}_0$. Note that $\overline{M}_0^2$ is a constant, independent of ξ. Indeed, from (28), applied to the pumping excitation alone, we have

$$\dot{\overline{M}}_0 = -\gamma(\overline{M}_0 \times \overline{H}_0)$$

or, if we use (36) and a corresponding equation for $\overline{H}_0$, we obtain

$$\omega_p \frac{\partial \overline{M}_0(\xi)}{\partial \xi} = -\gamma(\overline{M}_0(\xi) \times \overline{H}_0(\xi)). \tag{38}$$

Dot-multiplying (38) by $\overline{M}_0$, we have

$$\omega_p \frac{\partial \overline{M}_0(\xi)}{\partial \xi} \cdot \overline{M}_0(\xi) = \frac{1}{2} \omega_p \frac{\partial}{\partial \xi} (\overline{M}_0^2(\xi)) = 0.$$

Thus, $\overline{M}_0^2$ does not depend upon ξ.

The component of $\overline{H}_1$ parallel to $\overline{M}_0$, $\overline{H}_1^{\parallel}$, is independent of $\overline{M}_1$. It can obviously be written as

$$\overline{H}_1^{\parallel}(\xi, \eta) = \overline{M}_0(\xi) f(\xi, \eta) \tag{39}$$

where $f(\xi, \eta)$ is a periodic scalar function of ξ and η.

Having expressed all time functions as function of ξ and η, we are ready now to construct the proof for (27) analogously to the derivation of (17). We have

$$\sum_{m=-\infty}^{\infty} \sum_{n=\pm 1} jn\overline{M}_{m,n} \cdot \overline{H}_{m,n}^* = \frac{1}{4\pi^2} \int_0^{2\pi} d\xi \int_0^{2\pi} d\eta \overline{H}(\xi, \eta) \sum_{m=-\infty}^{\infty} \sum_{n=\pm 1} jn\overline{M}_{m,n} e^{j(m\xi + n\eta)} = \frac{1}{4\pi^2} \int_0^{2\pi} d\xi \int_0^{2\pi} d\eta \frac{\partial \overline{M}_1}{\partial \eta} \cdot \overline{H}_1. \tag{40}$$

If we split $\overline{H}_1(\xi, \eta)$ into its components parallel and perpendicular to $\overline{M}_0$, we can write for the integral on the right-hand side of (40)

$$\frac{1}{4\pi^2} \int_0^{2\pi} d\xi \int_0^{2\pi} d\eta \frac{\partial \overline{M}_1}{\partial \eta} \cdot \overline{H}_1 = \frac{1}{4\pi^2} \int_0^{2\pi} d\xi \int_0^{2\pi} d\eta \frac{\partial \overline{M}_1}{\partial \eta} \cdot \overline{H}_1^{\perp} + \frac{1}{4\pi^2} \int_0^{2\pi} d\xi \int_0^{2\pi} d\eta \frac{\partial \overline{M}_1}{\partial \eta} \cdot \overline{H}_1^{\parallel}. \tag{41}$$

In the appendix, using (37) and (39), the proof is presented that the integrals on the right-hand side of (41) equal zero. This completes the generalization of the Manley-Rowe relations to gyromagnetic media under small-signal excitation. From (24), for these we have

$$\nabla \cdot \sum_{m=-\infty}^{\infty} \sum_{n=\pm 1} \frac{n\overline{E}_{m,n} \times \overline{H}_{m,n}^*}{m\omega_p + n\omega_s} = 0. \tag{42}$$

The integral form of (42) is obtained by interating it over a volume enclosed by the surface S

$$\sum_{m=-\infty}^{\infty} \sum_{n=\pm 1} \oint \frac{n\overline{E}_{m,n} \times \overline{H}_{m,n}^*}{m\omega_p + n\omega_s} \cdot d\overline{S} = 0. \tag{43}$$

V. Application of the Manley-Rowe Relations

The Manley-Rowe relations indicate what devices can be realized either by using nonlinear reciprocal or

gyromagnetic media. Among the devices that are of interest is the parametric amplifier. A particular version of this is a device containing a nonlinear medium to which power is *supplied*[4] at the pump frequency. A signal is applied to it at a frequency ω_s. Other frequencies are not produced directly but only through the nonlinear action of the medium.

Let us study first a particularly simple, but important, case of a parametric amplifier in which the only frequency components with a finite power flow are those of the pump frequency, of the small signal, and of one sideband, the "idling" frequency (either at the frequency $\omega_p+\omega_s$, or at the frequency $\omega_p-\omega_s$). This can be accomplished if the nonlinear medium is inside a cavity that is resonant at ω_p, ω_s and $\omega_p\pm\omega_s$, but not at any other of the frequencies $m\omega_p+n\omega_s$. The small-signal Manley-Rowe relation (43) then reduces to

$$\text{Re} \oint \left[\frac{\overline{E}_{0,1} \times \overline{H}_{0,1}^*}{\omega_s} \pm \frac{\overline{E}_{1,\pm 1} \times \overline{H}_{1,\pm 1}^*}{\omega_p \pm \omega_s} \right] \cdot d\overline{S} = 0, \quad (44)$$

in which the integration is carried over a surface enclosing the nonlinear medium. The surface vector $d\overline{S}$ points outward from the surface. Note that the power flow at the pump frequency does not appear explicitly in the small-signal expression (44).

We are interested in obtaining power gain at the signal frequency with no other power than the pump power *supplied* to the medium. The relation

$$\text{Re} \oint \overline{E}_{1,\pm 1} \times \overline{H}_{1,\pm 1}^* \cdot d\overline{S} \geqq 0 \quad (45)$$

indicates that, at the (idling) frequency $\omega_p\pm\omega_s$, we *extract* power from, rather than supply it to, the medium, Using inequality (45) in (44), we obtain

$$\mp \left[\frac{\omega_p \pm \omega_s}{\omega_s} \right] \text{Re} \oint \overline{E}_{0,1} \times \overline{H}_{0,1}^* \cdot d\overline{S} \geqq 0.$$

Thus, we get power *out* of the medium at the desired frequency, ω_s, provided that 1) $\omega_s<\omega_p$ and 2) the side band at which power is extracted from the medium is a lower sideband at frequency $\omega_p-\omega_s$ (see Fig. 1). However, if $\omega_s>\omega_p$ and/or the other sideband that is used is at $\omega_p+\omega_s$, no power can be extracted from the medium. This proves the following theorem.

Theorem

A small-signal parametric amplifier that uses a "reciprocal" or gyromagnetic medium cannot have power gain at a frequency higher than the pump frequency, if a finite power flow is associated only with three frequencies ω_s, ω_p, $\omega_p\pm\omega_s$. However, this theorem does not entirely exclude the possibility of gain at a signal frequency higher than the pump frequency. Indeed, if we allow for finite amplitudes at *four* frequencies, ω_p, ω_s, $\omega_p+\omega_s$, and $\omega_p-\omega_s$,

[4] In this sense the signal source does not supply any power to the medium, since more power flows out of the medium at the signal frequency than flows into it, if gain is to be obtained.

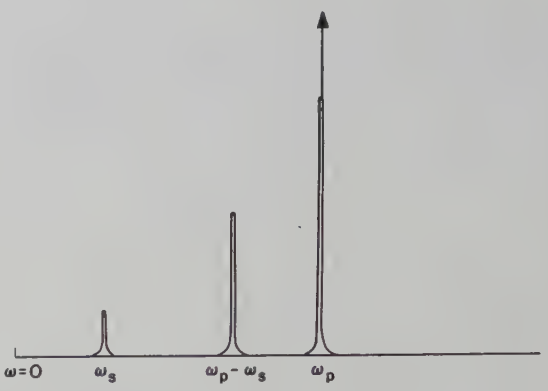

Fig. 1—Spectrum for three-frequency parametric device with possibility of gain.

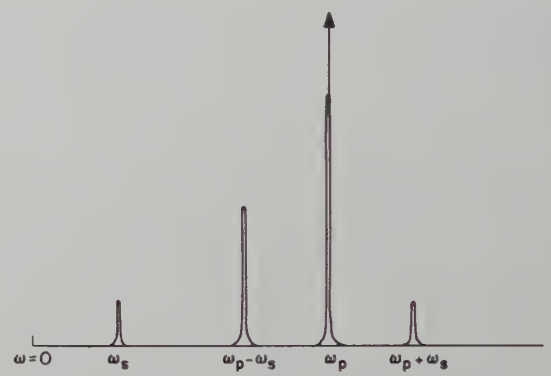

Fig. 2—Spectrum for four-frequency parametric device with gain.

then from (43), we obtain

$$\text{Re} \left[\oint \frac{\overline{E}_{0,1} \times \overline{H}_{0,1}^*}{\omega_s} \cdot d\overline{S} + \oint \frac{\overline{E}_{1,1} \times \overline{H}_{1,1}^*}{\omega_p + \omega_s} \cdot d\overline{S} - \oint \frac{\overline{E}_{1,-1} \times \overline{H}_{1,-1}^*}{\omega_p - \omega_s} \cdot d\overline{S} \right] = 0. \quad (46)$$

Now, if we assume that $\omega_s<\omega_p$, but with $\omega_p+\omega_s$ as the signal frequency, and ω_s and $\omega_p-\omega_s$ as the idling frequencies, we find that extraction of power from the medium at frequency $\omega_p-\omega_s$ permits positive values of the integral Re $\oint \overline{E}\times\overline{H}^*\cdot d\overline{S}$ at both frequencies ω_s and $\omega_p+\omega_s>\omega_p$. Thus, the Manley-Rowe relations do not prohibit power gain at a frequency $\omega_p+\omega_s$. The spectrum of the four frequencies that are employed is shown in Fig. 2.

If, however, $\omega_s>\omega_p$, then not all integrals Re $\oint \overline{E}\times\overline{H}^*\cdot d\overline{S}$ in (46) can be positive. Thus, power gain is impossible at signal frequencies higher than twice the pump frequency. We have thus proved the following theorem.

Theorem

The generalized Manley-Rowe relations permit power gain in a parametric amplifier at a frequency $\omega_p+\omega_s$ *in the range* $\omega_p<\omega_p+\omega_s<2\omega_p$, *if a finite power flow is associated with four frequencies,* ω_s, $\omega_p-\omega_s$, $\omega_p+\omega_s$, and ω_p.

Now we turn to another application of the generalized Manley-Rowe relations. Eq. (43) imposes restrictions

upon the general form of the coupling equations for cavity modes in the presence of ferrites. The limitations on the length of this paper do not permit a detailed derivation. A brief summary of the results obtained should suffice. For this purpose we are going to consider Suhl's analysis[3] as an example. Eqs. (13) and (14) of Suhl[3] give the equations of (weak) coupling produced by a ferrite sample between the amplitudes A_1 and A_2 of the resonant modes of a cavity at the frequencies ω_1 and ω_2, where $\omega_1+\omega_2=\omega_p$. These equations are

$$\left(2\lambda+\frac{\omega_1}{Q_1}\right)A_1=\rho_{12}A_2^*$$

$$\left(2\lambda+\frac{\omega_2}{Q_2}\right)A_2=\rho_{21}A_1^*$$

where λ gives the (slow) time variation of the modes as $\exp(\lambda t)$. It can be shown that (43) imposes on the coupling coefficients ρ_{12} and ρ_{21} the restriction

$$\frac{\rho_{12}}{\omega_1}\int_{\text{cavity}}h_1^2dv=\frac{\rho_{21}}{\omega_2}\int_{\text{cavity}}h_2^2dv \tag{47}$$

where h_1 and h_2 are the normalized fields of the modes 1 and 2. Detailed calculations of the coupling coefficients, as done by Suhl,[3] confirm (47).

VI. Conclusions

It has been found that the electromagnetic Poynting vectors (pertaining to various frequencies) of fields in "reciprocal" media obey (22) and (23). When equivalent circuit terminology is introduced into the field problem, relations result that are very similar in appearance to the Manley-Rowe relations.

A small-signal form of one of the generalized Manley-Rowe relations, (43), has been proved for gyromagnetic media. The relation can be used to determine under what circumstances power gain can be expected from a gyromagnetic medium under parametric excitation. The same relation can also be used to predict the form of the equations for the coupling between cavity modes produced by a "parametrically" excited ferrite. It is worth mentioning that (43) can be used as the basis of a theory of mode coupling produced by a parametrically excited uniform ferrite rod in a uniform microwave structure. This application of (43) is reminiscent of the use of the kinetic power theorem[5] as the basis for the traveling-wave tube analysis.[6]

VII. Appendix

We shall prove that

$$\int_0^{2\pi}d\xi\int_0^{2\pi}d\eta\,\frac{\partial\overline{M}_1}{\partial\eta}\cdot\overline{H}_1{}^{\parallel}=0 \tag{48}$$

and

$$\int_0^{2\pi}d\xi\int_0^{2\pi}d\eta\,\frac{\partial\overline{M}_1}{\partial\eta}\cdot H_1{}^{\perp}=0. \tag{49}$$

Consider, first, the integrand in (49) and use (37). Then we have

$$\frac{\partial\overline{M}_1}{\partial\eta}\cdot H_1{}^{\perp}=\frac{1}{\gamma}\,\frac{1}{\overline{M}_0{}^2}\left\{\omega_p\overline{M}_0(\xi)\times\frac{\partial\overline{M}_1(\xi,\eta)}{\partial\xi}\cdot\frac{\partial\overline{M}_1(\xi,\eta)}{\partial\eta}\right.$$
$$\left.+\,\gamma\overline{M}_0(\xi)\cdot[\overline{M}_1(\xi,\eta)\times\overline{H}_0(\xi)]\times\frac{\partial\overline{M}_1(\xi,\eta)}{\partial\eta}\right\}. \tag{50}$$

A glance at (34) shows that $\overline{M}_1(\xi,\eta)$ can be split into

$$\overline{M}_1(\xi,\eta)=\bar{m}_+(\xi)e^{j\eta}+\bar{m}_-(\xi)e^{-j\eta}, \tag{51}$$

where

$$\bar{m}_+(\xi)=\sum_{m=-\infty}^{\infty}\overline{M}_{m,+1}e^{jm\xi}$$

and

$$\bar{m}_-(\xi)=\sum_{m=-\infty}^{\infty}\overline{M}_{m,-1}e^{jm\xi}.$$

For the sake of brevity, we omit, henceforth, the explicit indication of arguments ξ and η. Let us consider the integral over ξ and η of the first term in (50).

$$I_1=\int_0^{2\pi}d\xi\int_0^{2\pi}d\eta\,\frac{1}{\gamma}\,\frac{1}{\overline{M}_0{}^2}\left(\omega_p\overline{M}_0\times\frac{\partial\overline{M}_1}{\partial\xi}\cdot\frac{\partial\overline{M}_1}{\partial\eta}\right). \tag{52}$$

If we introduce (51) into (52) for $\overline{M}_1$, we note that only products of $\bar{m}_+$ and $\bar{m}_-$ will remain after integration of η over the periodic interval of η.

$$I_1=\int_0^{2\pi}d\xi\,\frac{2\pi j}{\gamma\overline{M}_0{}^2}\omega_p\overline{M}_0\cdot\left(\frac{\partial m_-}{\partial\xi}\times\bar{m}_+-\frac{\partial\bar{m}_+}{\partial\xi}\times\bar{m}_-\right)$$
$$=\int_0^{2\pi}d\xi\,\frac{2\pi j}{\gamma\overline{M}_0{}^2}\omega_p\overline{M}_0\cdot\frac{\partial}{\partial\xi}(\bar{m}_-\times\bar{m}_+). \tag{53}$$

Next, let us look at the integration over η of the second term in (50). We note that

$$\frac{1}{\gamma\overline{M}_0{}^2}\overline{M}_0\cdot(\overline{M}_1\times\overline{H}_0)\times\frac{\partial\overline{M}_1}{\partial\eta}$$
$$=\frac{1}{\gamma\overline{M}_0{}^2}\left[\left(\overline{M}_1\cdot\frac{\partial\overline{M}_1}{\partial\eta}\right)\overline{M}_0\cdot\overline{H}_0-\left(\overline{H}_0\cdot\frac{\partial\overline{M}_1}{\partial\eta}\right)\overline{M}_1\cdot\overline{M}_0\right]. \tag{54}$$

Integrating this term over one period of η, and using a simple vector identity, we obtain

$$I_2=\int_0^{2\pi}d\xi\,\frac{1}{\gamma\overline{M}_0{}^2}\int_0^{2\pi}d\eta\left[\overline{M}_0\cdot(\overline{M}_1\times\overline{H}_0)\times\frac{\partial\overline{M}_1}{\partial\eta}\right]$$
$$=\int_0^{2\pi}d\xi\,\frac{1}{\gamma\overline{M}_0{}^2}\left[(\overline{M}_0\cdot\overline{H}_0)\int_0^{2\pi}\frac{\partial}{\partial\eta}\left(\frac{1}{2}\,\overline{M}_1{}^2\right)d\eta\right.$$
$$\left.+\,2\pi j\overline{H}_0\times(\bar{m}_+\times\bar{m}_-)\cdot\overline{M}_0\right]. \tag{55}$$

[5] L. J. Chu, "A kinetic power theorem," presented at 1951 IRE Conf. on Electron Devices, Durham, N. H.; June, 1951.

[6] J. R. Pierce, "Coupling of modes of propagation," *J. Appl. Phys.*, vol. 24, pp. 179–183; February, 1954.

The first term on the right-hand side of (55) equals zero. Combining (53) and (55), for the integral of (50) we obtain

$$I_1 + I_2 = \int_0^{2\pi} d\xi \int_0^{2\pi} d\eta \, \frac{\partial \overline{M}_1}{\partial \eta} \cdot \overline{H}_1^{\perp}$$

$$= \frac{2\pi j}{\gamma \overline{M}_0^2} \int_0^{2\pi} d\xi \Big[\omega_p \overline{M}_0 \cdot \frac{\partial}{\partial \xi} (\bar{m}_- \times \bar{m}_+) - \gamma (\overline{M}_0 \times \overline{H}_0) \cdot (\bar{m}_- \times \bar{m}_+) \Big]. \quad (56)$$

However, if we use (38), we find that the integrand of (56) reduces to a total differential

$$\omega_p \overline{M}_0 \cdot \frac{\partial}{\partial \xi} (\bar{m}_- \times \bar{m}_+) - \gamma (\overline{M}_0 \times \overline{H}_0) \cdot (\bar{m}_- \times \bar{m}_+) = \omega_p \frac{\partial}{\partial \xi} (\overline{M}_0 \cdot \bar{m}_- \times \bar{m}_+).$$

The integral over one period in ξ of a total derivative with respect to ξ is zero. Thus, we have proved the correctness of (49). Finally, we have to prove (48). First, we note that $\overline{H}_1^{\parallel}$ is parallel to $\overline{M}_0$. Thus it is possible to write $\overline{H}_1^{\parallel}$ in the form

$$\overline{H}_1^{\parallel} = \overline{M}_0(\xi) f(\xi, \eta), \quad (39)$$

where $f(\xi, \eta)$ is an arbitrary scalar function of ξ and η. Thus,

$$\frac{\partial}{\partial \eta} (\overline{M}_1) \cdot \overline{H}_1^{\parallel} = \frac{\partial}{\partial \eta} (\overline{M}_1 \cdot \overline{M}_0) f(\xi, \eta). \quad (57)$$

However, from (32) and (28), we have

$$\dot{\overline{M}}_1 \cdot \overline{M}_0 + \overline{M}_1 \cdot \dot{\overline{M}}_0 = -\gamma (\overline{M}_1 \times \overline{H}_0 + \overline{M}_0 \times \overline{H}_1) \cdot \overline{M}_0 - \gamma (\overline{M}_0 \times \overline{H}_0) \cdot \overline{M}_1 = 0. \quad (58)$$

Thus, for every "process-line" originating at the source of the ξ-η plane, we have

$$\omega_p \frac{\partial}{\partial \xi} (\overline{M}_1 \cdot \overline{M}_0) + \omega_s \frac{\partial}{\partial \eta} (\overline{M}_1 \cdot \overline{M}_0) = 0. \quad (59)$$

Therefore $\overline{M}_1 \cdot \overline{M}_0$ is constant along every process line. At the origin, all process lines have the same value of $\overline{M}_1 \cdot \overline{M}_0$. Hence, $\overline{M}_1 \cdot \overline{M}_0$ is constant throughout the entire ξ-η plane and

$$\frac{\partial (\overline{M}_1 \cdot \overline{M}_0)}{\partial \eta} = 0.$$

Accordingly, (57) equals zero. This proves the correctness of (48).

VIII. Acknowledgment

The author is indebted to Dr. E. Schlömann and D. L. Bobroff, of the Research Division, Raytheon Manufacturing Company, Waltham, Mass., for many useful discussions and criticisms. The author is also grateful to Dr. M. E. Hines, Bell Telephone Laboratories, for having made available his unpublished work on parametric amplifiers. An acknowledgment is due to Dr. M. T. Weiss, Bell Telephone Laboratories, whose quantum-mechanical derivation of the Manley-Rowe relations[7] suggested the existence of the present proofs.

[7] M. T. Weiss, "Quantum derivation of energy relations analogous to those for nonlinear reactances," Proc. IRE, vol. 45, pp. 1012–1013; July, 1957.

One Aspect of Minimum Noise Figure Microwave Mixer Design*

SAUL M. BERGMANN†

Summary—**A theory is derived which enables a direct measurement of the optimum RF impedance for minimum noise figure. This is achieved by an extension of Pound's method for loss measurements. Also, an analysis is made of the relation between minimum noise figure and maximum gain of the mixer represented as a two-port network.**

The procedure consists of first matching the RF signal input terminals with short-circuited IF terminals. Next open-circuited IF terminal conditions are obtained by a circuit used by Pound. Then a reference plane is determined coinciding by preference with the plane of a maximum in the standing wave pattern of VSWR = r. A discontinuity is finally introduced that would have a VSWR of $\rho = \sqrt{r}$ and have its maximum or minimum at the plane of reference.

* Manuscript received by the PGMTT, February 5, 1958; revised manuscript received, April 3, 1958.

† Laboratory for Electronics, Boston, Mass.

Introduction

MICROWAVE mixer performance has been treated in the literature [1]–[3]. In this paper the mixer is represented by a two-port network. It is assumed that the network has been optimized on an image-frequency termination basis. The aspect treated

is that of determining the optimum mismatch value for the RF signal source. This is done by an extension of Pound's analysis of loss measurement. Minimum loss conditions are first determined. The relation between minimum loss and minimum noise figure is then taken up. Finally an outline is given of the determination of optimum mismatch.

Minimum Loss Requirement

Mixer behavior can be represented by a three-terminal pair network. The terminals are the signal input, IF output, and image frequency load. This representation has been confirmed experimentally and is considered adequate for practical purposes. The same nomenclature as with some treatments made elsewhere [4]–[5] will be used throughout.

It can be shown that the expressions [5] for signal source admittance giving minimum loss correspond to the conjugate-image impedances as developed by Roberts [6], and hold for any two-terminal-pair network.

It is advantageous to choose RF and IF terminals so that (111) and (112) in Torrey and Whitmer [5] can be considerably simplified. For this the following conditions must be fulfilled.

1) With the IF terminals short-circuited, the RF input is matched to satisfy

$$Y_{sc} = Y_\alpha = G_{sc} = G_{\alpha\alpha}.$$

2) The capacitor of the IF resonant circuit in Pound's apparatus [7] is adjusted to set up maximum signal reflection. This is equivalent to an addition of a susceptance, b_β to the IF terminals, which resonates out the imaginary part of $Y_{\beta\beta}$. This corresponds to open-circuited IF terminals.

3) With a standing-wave pattern resulting from condition 2 a choice of RF terminals is made so that $Y_\alpha = Y_{oc}$ is real and equal to G_{oc}.

These terminals would lie in a plane of a maximum or a minimum in the standing-wave pattern.

It may be shown that with this choice of RF terminals, $(Y_{\alpha\beta}Y_{\beta\alpha})$ is real and equal to $G_{\alpha\beta\beta\alpha}$.

Further, the loss

$$L = \frac{|Y_{\alpha\beta}|}{|Y_{\beta\alpha}|} \cdot \frac{1 + \sqrt{\frac{G_{oc}}{G_{sc}}}}{1 - \sqrt{\frac{G_{oc}}{G_{sc}}}}. \tag{1}$$

This is the underlying theory of Pound's apparatus for loss measurements.

We now write the value of (111) and (112) of Torrey and Whitmer [5], and (14) of Pound [9] under fulfillment of conditions 1–3. These equations become respectively

$$G_\alpha = G_{\alpha\alpha}\left\{1 - \frac{G_{\alpha\beta\beta\alpha}}{G_{\alpha\alpha}G_{\beta\beta}}\right\}^{1/2} \tag{2}$$

$$G_\beta = \left[G_{\beta\beta}^2 - \frac{G_{\alpha\beta\beta\alpha}G_{\beta\beta}}{G_{\alpha\alpha}}\right]^{1/2} \tag{3}$$

$$Y_\alpha = G_{\alpha\alpha} - \frac{G_{\alpha\beta\beta\alpha}}{y_\beta + G_{\beta\beta}}. \tag{4}$$

If (3) is put into (4) for y_β, the resulting equation becomes equal to (2).

Furthermore, since

$$G_{sc} = G_{\alpha\alpha} = G_o$$

where G_o is the characteristic conductance of the guide,

$$G_{oc} = G_{\alpha\alpha} - \frac{G_{\alpha\beta\beta\alpha}}{G_{\beta\beta}} = G_{sc} - \frac{G_{\alpha\beta\beta\alpha}}{G_{\beta\beta}} \tag{5}$$

$$\sqrt{G_{sc}G_{oc}} = G_{\alpha\alpha}\left[1 - \frac{G_{\alpha\beta\beta\alpha}}{G_{\alpha\alpha}G_{\beta\beta}}\right]^{1/2} \tag{6}$$

which is identical to (2).

Since the network is purely resistive with these proper terminals this result means that (6) is an image impedance of the network looking into the RF side. Thus if an RF signal source of impedance equal to (6) were connected to the network, it would correspond to minimum loss (or maximum gain). For this to be achieved it is seen from (5) that

$$G_{oc} < G_{sc}$$

and $G_{sc}/G_{oc} = r$, where r is the VSWR as measured under condition 2. It follows that G_{oc} corresponds to a plane of maximum in the standing wave pattern.

It is possible to set up an impedance $\sqrt{G_{sc}G_{oc}}$ at the plane corresponding to G_{oc}.

The VSWR ρ corresponding to this impedance is given by

$$\rho = \frac{G_{sc}}{\sqrt{G_{sc} \cdot G_{oc}}} = \sqrt{\frac{G_{sc}}{G_{oc}}} = \sqrt{r}.$$

Thus, in order to satisfy the condition of minimum loss a real impedance of magnitude $\rho = \sqrt{r}$ has to be set up at the plane of G_{oc}. This can be readily done since ρ and the plane of $\sqrt{G_{sc}G_{oc}}$ are given.

Minimum Noise Figure Condition

In an unpublished paper, Haus and Adler [8] have studied the noise behavior of a network whose internal noise contribution can be considered thermal of temperature T.

A relation

$$\frac{F - 1}{1 - \frac{1}{G}} = \frac{T}{T_o}$$

is then found where F is the noise figure of the network, G is the gain of the network, and T_o is the absolute reference temperature, *i.e.*, 290°K.

An analysis of F as a function of G for the case of a passive network shows that F is a monotone decreasing function of G. Therefore it follows that the condition of maximum gain would correspond to that of minimum noise figure of the network. Consequently, if the mixer can be considered as a network whose noise contribution is of thermal nature, one would be interested in minimum loss for minimum noise figure.

Signal-Source Impedance Setup for Minimum Noise Figure

On the basis of the foregoing analysis an outline is given of the experimental setup for minimum noise figure source impedance.

1) General precautions should be taken as outlined by Wheeler and Dettinger [3].
2) The IF output is terminated by Pound's IF circuit [7]. With the switch in the short-circuit position, the VSWR is measured on the RF side and matched.
3) With the switch in the open-circuited position, tune the circuit to provide maximum VSWR $=r$ on the RF side which was previously matched, and measure r.
4) The plane corresponding to a maximum or minimum in the standing wave whose VSWR $=r$ is recorded and ρ is calculated.
5) A discontinuity is introduced in the line to set up a real impedance of magnitude $\rho=\sqrt{r}$ at the recorded plane.

Circumstances did not permit supplementing these considerations with experimental data.

Bibliography

[1] Pound, R. V. *Microwave Mixers*. New York: McGraw-Hill Book Company, Inc. (1948), pp. 61–68.
[2] Strum, P. D. "Some Aspects of Mixer Crystal Performance," Proceedings of the IRE, Vol. 41 (July, 1953), pp. 875–889. See Fig. 4, p. 879.
[3] Wheeler, H. A., and Dettinger, D. *Measuring the Efficiency of a Superheterodyne Converter by the Input Impedance Circle Diagram*. Wheeler Monographs, Wheeler Laboratories, Inc., Great Neck, N. Y., pp. 33–38; March, 1949.
[4] Torrey, H. C., and Whitmer, C. A. *Crystal Rectifiers*. New York: McGraw-Hill Book Company, Inc. (1948), pp. 115–116.
[5] *Ibid.* Eqs. (111) and (112), p. 138.
[6] Roberts, S. "Conjugate-Image Impedances," Proceedings of the IRE, Vol. 34 (April, 1946), pp. 198P–204P.
[7] Torrey and Whitmer, *op. cit.* Fig. 7.5b, p. 208.
[8] Haus, H. A., and Adler, R. B. "Optimum Noise Performance of Linear Amplifiers," to be published.
[9] Pound, *op. cit.* Eq. (14), p. 63.

Acknowledgment

Thanks are extended to Drs. J. Shekel, and H. A. Haus and to P. D. Strum for helpful criticisms and comments. The disclosure by Dr. Haus of part of his unpublished paper is gratefully acknowledged.

A Broad-Band High-Power Vacuum Window for X Band*

H. J. SHAW† and L. M. WINSLOW‡

Summary—**Recent developments in high-power tubes for the 3-cm wavelength region have created a need for waveguide output windows which are capable of transmitting peak power in excess of 1 megw and average power in the neighborhood of 1 kw, and which have frequency bandwidths of about 15 per cent. This paper describes a structure which is designed to meet these electrical requirements, and which also has desirable physical and fabricational properties. A dielectric plug, which forms the vacuum seal, is used as one element of a three-element filter. The design procedure and experimental results are discussed.**

* Manuscript received by the PGMTT, March 13, 1958; revised manuscript received, April 11, 1958. The work described was done under the sponsorship of Signal Corps Contracts DA 36(038)-SC 63189, and DA 36(039)-SC 73178, and Air Force Contract AF 33(600)-27784.

† Microwave Lab., Stanford University, Stanford, Calif.
‡ Raytheon Manufacturing Co., Santa Barbara, Calif.; formerly with Microwave Lab., Stanford University, Stanford, Calif.

Introduction

VACUUM windows present one of the major problems at present in the design of practical high-power microwave tubes. In the 3-cm wavelength region, recent developments[1] in high-power tubes have created a need for output windows which are capable of transmitting peak power in excess of 1 megw and average power in the neighborhood of 1 kw, and which have frequency bandwidths of about 15 per cent. Such windows are used in the output waveguides of high-power tubes to allow transmission of RF power from the

[1] M. Chodorow, E. L. Ginzton, J. Jasberg, J. V. Lebacqz, and H. J. Shaw, "Development of high-power pulsed klystrons for practical applications," to be published.

evacuated output cavities of the tube to a pressurized external circuit.

A dielectric element is employed which can be made transparent to the RF wave by suitable impedance matching. This can be accomplished by shaping the dielectric, as, for example, in tapered cone windows[1–3] and stepped windows[4,5] or by utilizing matching sections separate from the dielectric.[1,6,7] The present design, referred to as a filter window, uses separate matching elements, with the over-all structure designed as a three-element band-pass filter for broad-band operation.

Electrical Design

A half-wavelength dielectric plug of characteristic admittance Y_1 in a waveguide of characteristic admittance Y_0 has the following input admittance.

$$\frac{Y_{in}}{Y_0} = \frac{Y_1}{Y_0}\left(\frac{Y_0 + jY_1 \tan \beta l}{Y_1 + jY_0 \tan \beta l}\right) \tag{1}$$

where

$\beta = 2\pi/\lambda_{g_1}$ = propagation constant in dielectric,
λ_{g_1} = wavelength in dielectric plug in waveguide.
l = length of dielectric plug along the axis of propagation.

At the frequency for which $l = \lambda_{g_1}/2$, Y_{in} is equal to Y_0, and an impedance match results. In the neighborhood of this frequency, the input impedance of the dielectric plug is similar to that of a parallel resonant circuit, and can be described in terms of the resonant frequency and loaded Q. To evaluate the loaded Q, the $\tan \beta l$ in (1) is first expanded about the point $\beta l = \pi$. The resulting equation may be put into the form

$$\frac{Y_{in}}{Y_0} \approx 1 + j4Q_L \frac{\Delta f}{f_0}. \tag{2}$$

This may be recognized as the input admittance of a parallel resonant circuit connected across a waveguide of characteristic admittance Y_0, where f_0 is the resonant frequency and Q_L is the Q of the circuit when loaded on both sides by the characteristic admittance Y_0. In terms of parameters for the dielectric plug, Q_L is found to be

$$Q_L \approx \frac{\pi}{4}\left(\frac{\lambda_{g_0}}{\lambda_{g_1}} - \frac{\lambda_{g_1}}{\lambda_{g_0}}\right)\left[1 - \frac{1}{K}\left(\frac{\lambda}{2a}\right)^2\right]^{-1} \tag{3}$$

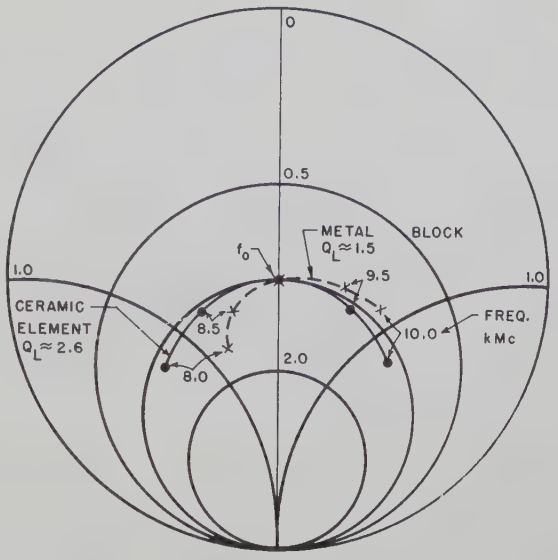

Fig. 1—Smith chart representation of theoretical input admittance of ceramic element and metal block elements.

where

λ_{g_0} = guide wavelength in air-filled guide,
λ_{g_1} = guide wavelength in dielectric-filled guide, and
K = relative dielectric constant.

For rectangular waveguide, we have

$$l_0 = \frac{\lambda_0}{2}\left[K - \left(\frac{\lambda_0}{2a}\right)^2\right]^{-1/2} \tag{4}$$

and

$$\frac{\lambda_{g_0}}{\lambda_{g_1}} = \left[K - \left(\frac{\lambda}{2a}\right)^2\right]^{1/2}\left[1 - \left(\frac{\lambda}{2a}\right)^2\right]^{-1/2} \tag{5}$$

where

λ = free space wavelength,
l_0, λ_0 = resonant values of l, λ, and
a = waveguide width (major axis).

A low value of Q_L is desired for broad-band operation. As can be seen from (4) and (5), Q_L is low for low dielectric constant and for waveguide operating far from cutoff. Fig. 1 illustrates the theoretical resonance properties of the specific commercial ceramic (Wesgo AL300) used in the present windows. It has a dielectric constant of about 9.3. The resonant frequency is 9.0 kmc, and the bandwidth over which the insertion loss is less than 0.1 db (VSWR less than 1.35) is 490 mc. The comparison of theoretical and experimental values of reflection coefficient is shown in Fig. 2.

To obtain greater bandwidth than provided by the resonant dielectric plug alone, the ceramic section is used as one element of a multielement band-pass filter. Filters of the type employed here have approximately the same bandwidth as a single element, when compared at the 3-db insertion-loss points. However, if the insertion loss is to be restricted to lower values, as in the 0.1-db example above, then the multielement filter may have a bandwidth much larger than that of a single ele-

[2] J. E. Shepherd, "Harnessing the Electron," *Sperry Eng. Rev.*, vol. 10, pp. 7–8; March/April, 1957.
[3] L. H. LaForge, "Application of ceramic sections in high-power pulsed klystrons," *Amer. Cer. Soc. Bull.*, vol. 36, pp. 119–120; March, 1956.
[4] L. Ragan, "Microwave Transmission Circuits," M.I.T. Rad. Lab. Ser., McGraw-Hill Book Co., Inc., New York, N. Y., pp. 218–227; 1948.
[5] H. K. Jenney, F. E. Vaccaro, "A step-type, broad-band X-band ceramic waveguide window," IRE Trans. on Electron Devices, vol. ED-3, pp. 30–32; January, 1956.
[6] H. G. Hereward and M. G. N. Hine, "A method of broadbanding waveguide windows," Proc. IRE, vol. 42, pp. 1450–1451; September, 1954.
[7] S. P. Otsuka, "Studies in the design of a broad-band high-power microwave window," Engineer's thesis, Stanford University, Stanford, Calif.; June, 1954.

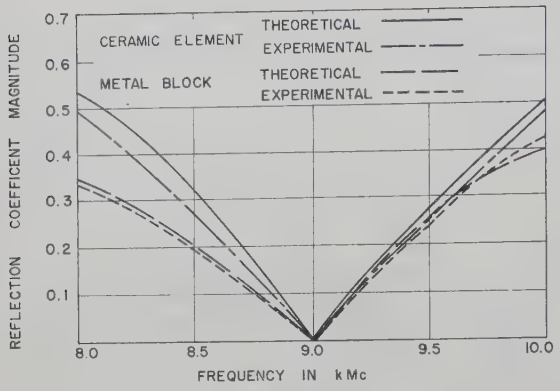

Fig. 2—Reflection coefficient vs frequency for ceramic element and metal block elements.

ment. The present filter is designed as a quarter-wavelength-coupled resonant element filter. The electrical characteristics of quarter-wavelength-coupled filters have been described by Ragan.[8] If all the elements have the same Q_L and resonant frequency, the ratio of incident power P_0 to transmitted power P_L, for n elements, is shown to be

$$\left(\frac{P_0}{P_L}\right)_n = 1 + x^2 U_n^2(kx) \tag{6}$$

where $U_n(kx)$ is the Tchebycheff polynomial of the second kind, k is a frequency-sensitivity correction, and x is the frequency variable. Specifically:

$$\begin{aligned} U_1(kx) &= 1 \\ U_2(kx) &= 2kx \\ U_3(kx) &= 4k^2x^2 - 1 \end{aligned} \tag{7}$$

$$U_{n+1}(kx) = 2kxU_n(kx) - U_{n-1}(kx)$$

$$k = 1 + \frac{\pi}{4Q_L}\left[1 - \left(\frac{\omega_c}{\omega}\right)^2\right]^{-1} \tag{8}$$

$$x \approx 2Q_L \frac{\Delta f}{f} \tag{9}$$

w_c = waveguide cutoff frequency.

The factor k is used to correct for the change in electrical length of the coupling lines between elements as the frequency changes. The power transmission ratios for filters with $Q_L = 2.8$ and $f_0 = 9000$ mc in H-band waveguide are shown in Fig. 3. The uncorrected curves are computed with $k = 1$, while for the corrected curves k is evaluated according to (8). An inspection of the curves shows an increase in bandwidth, for a specified insertion loss, as an advantageous effect of the frequency sensitivity of the coupling lines.

The three-section filter was chosen because of its low insertion loss and adequate pass band for our application. The ceramic is used as one element of the filter. The other elements may be composed of various types of resonant devices, such as waveguide cavities, irises,

[8] *Op. cit.*, pp. 613–716.

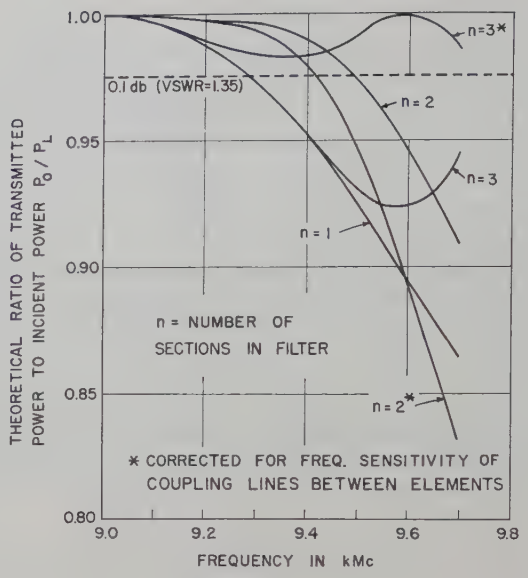

Fig. 3—Filter transmission characteristics for $Q_L = 2.8$.

or capacitive obstacles.[9] The particular element chosen for our application is termed a resonant block, and consists of a metal rectangular parallelepiped placed in the waveguide to periodically change the waveguide impedance. It is in effect a form of capacitively coupled rectangular waveguide cavity. These blocks may take different physical forms, as shown in Fig. 4, while retaining similar electrical properties.

The blocks were chosen as the resonant elements because they lead to a simple assembly and can provide optical shielding of the ceramic, as discussed later. A single centered block used in conjunction with the symmetric blocks may shield the ceramic optically while operating as desired electrically.

In a similar manner, two asymmetric blocks connected to the opposite sides of the waveguide may be used, but local fields between elements have been observed to couple power into undesirable modes in the ceramic section. This effect is detected during cold testing as a narrow peak in the curve of reflected power as a function of frequency. In use, higher mode resonances in a window can cause sparking and power loss. An advantage of the present dielectric geometry is that the resonant frequencies are calculable as functions of the various dimensions.

The blocks have a resonant frequency and an effective loaded Q which are functions of the block and waveguide dimensions. The theoretical properties are shown on a Smith chart in Fig. 1, and a comparison between theory and experiment is shown in Fig. 2, for the particular case of $f_0 = 9.0$ kmc and $Q_L = 1.5$. The electrical properties of the resonant blocks can be found by considering the admittance Y_1 for the waveguide section with the block,

[9] L. M. Winslow, "A wide-band ceramic waveguide window," Engineer's thesis, Stanford University, Stanford, Calif.; August, 1956.

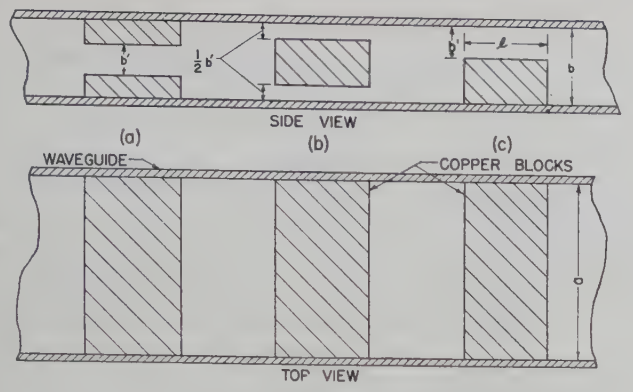

Fig. 4—Resonant block elements. (a) Symmetric block, (b) single centered block, (c) asymmetric block.

$$\frac{Y_1}{Y_0} = \frac{b}{b'} = c \tag{10}$$

where b is the height of the waveguide, and $b-b'$ is the height of an asymmetric block, or twice the height of a symmetric block, as shown in Fig. 4.

The resonant length is

$$l = \frac{\lambda_g}{2\pi} \tan^{-1}\left(\frac{2B_d c}{B_d^2 + 1 - c^2}\right) \tag{11}$$

where B_d=discontinuity susceptance at f_0.

A fair approximation for Q_L may be made for small B_d as follows:

$$Q_L \approx \frac{\pi}{4}\left(c - \frac{1}{c}\right)\left[1 - \left(\frac{\lambda}{\lambda_c}\right)^2\right]^{-1}. \tag{12}$$

The filters discussed thus far have had identical Q_L's. Since the value of the Q limits the bandwidth, it is logical to decrease the Q. This can be done for the matching elements, but it cannot be done for the ceramic element. In the Tchebycheff design of quarter-wave-coupled filters, the end elements are of lower Q than the center elements, in which case the end elements act also as impedance transformers. In the present filter-window case, however, this scheme is not employed, as we desire to confine the matching elements to the vacuum side of the ceramic section, and thus one end element must be the ceramic element. Rather than complete an analytic solution to the problem of staggered Q, as applied to the present case, which would need to include frequency sensitivity of the line and element, the solution was found experimentally, first numerically on a Smith chart and then with a cold-test setup.

The final design for a filter window centered at 9.0 kmc was a structure using two elements with $Q_L=1.5$ and the ceramic element of $Q_L=2.6$. The physical picture is shown in Fig. 5, and the measured electrical properties are given in Fig. 6. The 0.1-db bandwidth is 1430 mc, or 16 per cent.

High-Power Properties

With regard to power handling capacity, both peak power and average power effects must be considered.

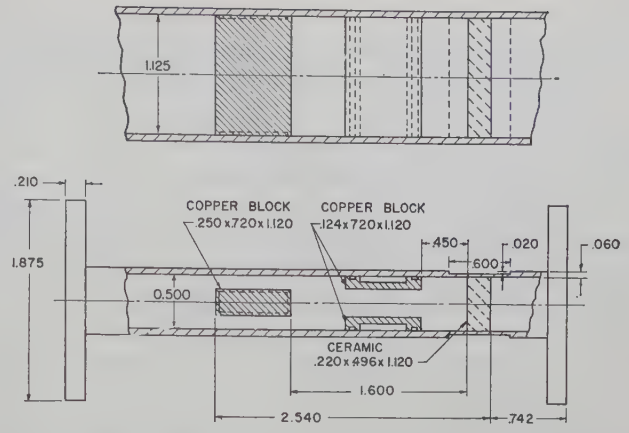

Fig. 5—Filter window in H-band waveguide centered at 9.0 kmc.

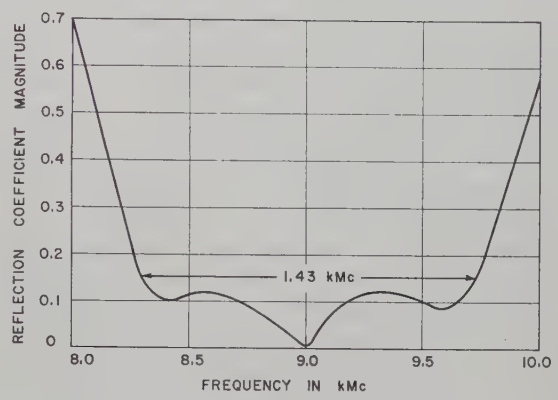

Fig. 6—Measured transmission properties of the filter window of Fig. 5.

Taking first the question of transmitting high peak power, one aspect concerns breakdown due to high RF electric field strength E. In the present design, the dielectric region and the waveguide on the output side of the assembly both have smooth detailed geometry, free of irregularities which can lead to localized regions of high E. Gaps between the interfaces of the ceramic edges and waveguide walls, where large E could be developed, are not difficult to avoid with the present geometry. Sharp edges caused by metallizing or by brazing material on the dielectric face on the output side of the window are avoided during fabrication, as mentioned later. The transmission properties of the dielectric plug are such that E within the dielectric never exceeds that in the output waveguide. Thus, in the dielectric and output waveguide sections, the full power capabilities of normal H-band waveguide should be realizable. The theoretical value of breakdown voltage at atmospheric pressure in uniform H-band waveguide at these frequencies corresponds to a peak power level of 1.77 megw.[10]

On the vacuum side of the dielectric section, breakdown due to high peak power would probably be an unimportant consideration were it not for possibilities of

[10] Ragan, *op. cit.*, p. 191.

multipactor[11,12] discharge. This is a form of secondary electron loading which can dissipate RF energy. It is an electron transit-time phenomenon and could in principle be established, at certain peak-power levels, in the spaces formed by the loading bars.

There is considerable evidence that successful operation of windows at high peak powers requires shielding of the dielectric element from direct optical paths leading to interior of tube. This presumably avoids breakdown resulting from electrons reaching the dielectric. In the present design, the loading bars which provide electrical broadbanding also provide optical shielding.

With regard to average RF power capability, the following statements can be made. The rectangular geometry of the ceramic element has short paths from interior points of the ceramic to the top and bottom walls of the waveguide. This provides for cooling of the interior points, as heat developed within the ceramic due to dielectric RF loss can be effectively carried away through the conductivity of the ceramic. The axial distribution of E within the dielectric is such that it is never larger than in the external waveguide, and E^2 in the axial center of the dielectric is about 10 per cent of its value in the external waveguide. Thus, from the viewpoint of the gross ratio of heat conductance to total internal heat developed, the thick dielectric should be better than a thin one (except possibly in the case of forced convection cooling). This does not take account of the relation between spatial distribution of thermal stress and over-all symmetry of the dielectric which probably is also of importance.

The power handling capabilities of this window have been evaluated in two series of tests. One of these was a laboratory-type experiment in which a model of the window, constructed as described above, was inserted in the output waveguide system of a megawatt klystron, so that the output power of the klystron was transmitted directly through the test window and then to a matched load. To evaluate the window in the correct environment, the section of waveguide leading from the klystron to the test window was evacuated, so that the input section of the window containing the copper filter blocks operated in vacuum as it would if installed directly on a tube. The waveguide leading from the output side of the window to the matched load was pressurized at about three atmospheres. The pressure of three atmospheres was necessary to avoid breakdown in the waveguide circuitry associated with power monitoring apparatus. This was a fixed-frequency experiment with the klystron operating at 9000 mc. No breakdown of any kind was observed while transmitting peak power of 1 megw through the window. The klystron modulator capacity limited the average RF power through the window to 100 watts.

[11] K. Bol, "The multipactor effect in klystrons," 1954 IRE Convention Record, pt. 2, pp. 151–155.

[12] G. Abraham, "Interaction of electrons and fields in cavity resonators," Ph.D. dissertation, Stanford University, Stanford, Calif.; 1950.

A second evaluation, covering both peak and average power, was obtained from operational data on an industrial megawatt X-band klystron developed by General Electric Company, Palo Alto, Calif., on which the output window is an adaptation of the present design. Differences from the present window design consist of various changes in fabrication technique which adapt the window assembly to the particular processes employed for commercial manufacture. The output window on this tube has transmitted peak power on the range of 1 to 2 megw, and average power in the range of 1 to 2 kw, over the frequency range of 8500 to 9600 mc, which is the tuning range of the klystron. The tube was operated into a waveguide system pressurized in the range of one to three atmospheres.

Fabrication

In the models described here, the ceramic block is brazed directly into OFHC copper waveguide by procedures which have been successfully used in other ceramic applications.[3] The waveguide wall thickness is reduced to 0.020 inch in the region of the ceramic, and a molybdenum clamp is placed on the outside of the waveguide in this region to keep the copper from expanding away from the ceramic during brazing. The moly-manganese process is used to metallize the ceramic edges, and a hydrogen furnace braze to the waveguide is made using a Silcoro solder ring placed on the vacuum side of the ceramic. The copper matching blocks are brazed in beforehand using Nicoro solder. Stainless steel jigs are used to hold all internal parts in place during brazing.

No trouble has been experienced in obtaining vacuum-tight seals around the rectangular ceramic block. The simgle rectangular shape is easy to grind to close tolerance. The corners to be brazed are given a slight radius. Final grinding of the broad faces is done after metallizing of the edges; this cleans up any of the metallizing mixture which may have run over onto the faces. The completed window assembly has been subjected to repeated bakeouts at 450°C without trouble.

The thick ceramic block results in a rugged assembly. Forces due to pressurizing of the external waveguide, at several atmospheres if desired, present no problem. Since optical shielding of the ceramic is achieved by means of the matching bars, the assembly can be mounted directly at the output cavity of a klystron or traveling-wave tube, forming a compact output system.

Acknowledgment

The authors are indebted to V. Dryden and J. Snyder for assembly techniques used in the models described here and for assistance in the laboratory testing of the window. Appreciation is expressed to B. G. Ryland, Section Manager, and A. D. LaRue, Project Engineer, of the General Electric Microwave Laboratory, Palo Alto, Calif., for permission to include test results relating to window operation obtained with their 1-megw X-band klystron.

Correspondence

A 5-MM Resonance Isolator*

The rectangular waveguide resonance isolator operating at frequencies from 3000 to 24,000 mc is a simple and compact device since the dc magnetic field requirements are relatively low. In the 5-mm range, however, resonance isolators are not practical if conventional ferrites are used because very high magnetic fields of about 20,000 oersteds are required to obtain resonance at these high frequencies. By using highly oriented Ferroxdure, resonance isolators in the millimeter range become feasible because of the high internal anisotropy field of 17,000 oersteds exhibited by this material.[1] Thus, with Ferroxdure a magnetic field of a few thousand oersteds is sufficient for resonance in the 5-mm region.

Such a 5-mm resonance isolator has been built and is shown in cross section in Fig. 1 and assembled in Fig. 2. A brief description of the assembly of this device might be of interest. A piece of highly oriented Ferroxdure was carefully ground to a thickness of 0.005 inch, a width of 0.021 inch, and a length of 2 inches. This material was then mounted on a strip of 0.020-inch thick laminated polystyrene using carbon tetrachloride and polystyrene as the adhesive. This strip served to space the ferrite from the waveguide wall by the proper amount. In addition, a strip of 0.010-inch thick laminated polystyrene was bonded to the other side of the ferrite in order to help concentrate the RF field in the ferrite.[2] The two strips of polystyrene also reinforced the fragile ferrite so that it could be handled without breakage. This composite sample was then placed in position against one wall of the waveguide and fastened to it, utilizing a long slim hypodermic needle to inject a mixture of carbon tetrachloride and polystyrene in the appropriate places.

The performance of the isolator at three different frequencies is shown in Fig. 3. It can be seen that reverse-to-forward ratios of better than 20 to 1 in db can readily be obtained at a given frequency by a proper choice of dc magnetic field. The VSWR was measured to be less than 1.1 even though no effort was made to match the device.

In order to permit the operation of the isolator over a wide range of frequencies with a high reverse-to-forward ratio, it is evident from Fig. 3 that the dc field must be varied as the frequency is changed. This magnetic field variation is accomplished by means of a variable shunt placed on top of the magnet as shown in Fig. 2. The shunt is varied by means of the screw which permits one to change the field in the gap from 1200 to 4300 oersteds. This unit has been used in test bench setups with at least a 20 to 1 ratio in db over the frequency range from 53 kmc to 58 kmc.

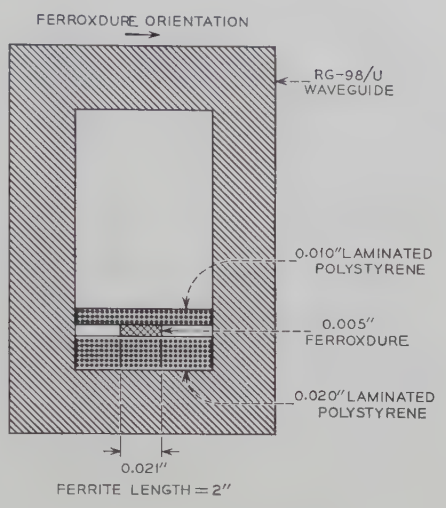

Fig. 1—Cross section of the 5-mm resonance isolator.

Fig. 2—Assembled 5-mm resonance isolator.

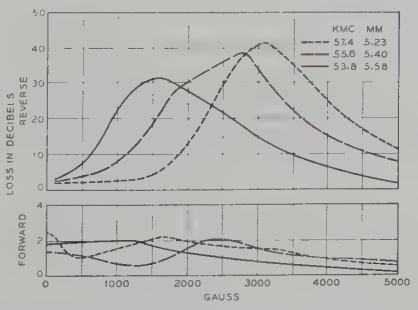

Fig. 3—Reverse and forward loss vs applied field at three frequencies for the 5-mm resonance isolator.

M. T. Weiss
F. A. Dunn
Bell Telephone Labs.
Holmdel, N. J.

* Received by the PGMTT, January 27, 1958.

[1] M. T. Weiss, "The behavior of ferroxdure at microwave frequencies," 1955 IRE Convention Record, pt. 8, pp. 95–99. Also see "Ferromagnetic resonance in ferroxdure," *Phys. Rev.*, vol. 98, pp. 925–926; May, 1955.

[2] M. T. Weiss, "Improved rectangular waveguide resonance isolators," IRE Trans. on Microwave Theory and Techniques, vol. MTT-4, pp. 240–243; October, 1956.

On Riblet's Theorem*

Riblet[1] presented the following theorem which is concerned with the synthesis of a quarter-wave impedance transformer: "The necessary and sufficient conditions that a rational function of p with real coefficients written in the form

$$Z(p) = \frac{m_1(p) - n_1(p)}{m_2(p) - n_2(p)} \tag{1}$$

with m_1 and m_2 odd or even and n_1 and n_2 even or odd, be the input impedance of a cascade of n equal-length transmission line sections terminated in a resistance are: 1) $Z(p)$ must be a positive real function of p, and 2) $m_1(p)m_2(p) - n_1(p)n_2(p) = C(p^2-1)^n$."

These two conditions are surely necessary, but are not sufficient. To illustrate, consider the following function, which meets the two conditions but is not realizable as a circuit of this kind:

$$Z(p) = \frac{m_1(p) + n_1(p)}{m_2(p) + n_2(p)} = \frac{2p^2 + 2p + 4}{3p + 1} \tag{2}$$

where $m_1(p) = 2p^2+4$, $n_1(p) = 2p$, $m_2(p) = 1$, $n_2(p) = 3p$. Clearly, $Z(p)$ is a positive real and

$$\begin{aligned} m_1(p)m_2(p) - n_1(p)n_2(p) &= (2p^2 + 4) - 2p \cdot 3p \\ &= -4(p^2 - 1)^1. \end{aligned}$$

Hence, $Z(p)$ satisfies the two conditions of the theorem. Let us try to realize $Z(p)$ through the use of Richards' theorem as indicated by Riblet.

$$\begin{aligned} Z_c &= Z(1) = 2 \\ Z_1(p) &= Z_c \frac{pZ(p) - Z_c}{-Z(p) + pZ_c} = \frac{1}{2}(p+1) \\ &= \frac{m_1'(p) + n_1'(p)}{m_2'(p) + n_2'(p)} \qquad (3) \\ m_1'(p) &= 1/2, \quad n_1'(p) = p/2 \\ m_2'(p) &= 1, \quad n_2'(p) = 0. \end{aligned}$$

$Z_1(p)$ is positive real and

$$\begin{aligned} m_1'(p)m_2' - n_1'(p)n_2'(p) &= 1/2 = 1/2 \cdot (p^2 - 1)^0. \end{aligned}$$

$Z_1(p)$ meets the two conditions, but cannot be realized as a cascaded network of equal-length transmission line sections terminated in a resistance. This function should be realized as shown in Fig. 1. The total circuit representation of $Z(p)$ in (2) is shown in Fig. 2.

The following restriction must be added: "3) Assuming that the numerator and denominator of $Z(p)$ in (1) are prime to each other, the degrees of both the numerator and denominator must be equal to n."

* Received by the PGMTT, February 28, 1958.

[1] H. J. Riblet, "General synthesis of quarter-wave impedance transformer," IRE Trans. on Microwave Theory and Techniques, vol. MTT-5, pp. 36–43; January, 1957.

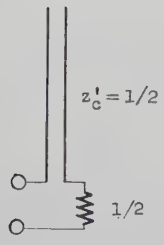

Fig. 1

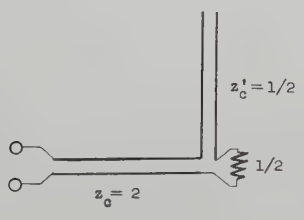

Fig. 2

It is apparent that this third condition is sufficient and mathematical induction will readily prove that it is necessary.

This additional restriction completes the necessary and sufficient conditions. This theorem may also be easily reduced from the writer's theorem 1 presented in anothe publication.[2]

Hiroshi Ozaki
Faculty of Engineering
Osaka University
Osaka, Japan

[2] H. Ozaki and J. Ishii, "Synthesis of transmission-line networks and the design of UHF filters," IRE Trans. on Circuit Theory, vol. CT-2, pp. 325–336; December, 1955. See theorem 1, p. 326.

Ferrite Directional Couplers with Off-Center Apertures*

Introduction

A recent study[1,2] of Bethe's small-hole coupling theory has led to an extension of his work to include the case where the coupling aperture is filled with an anisotropic ferrite. This new theory is applicable to any situation where Bethe's coupling theory is useful and is hindered chiefly by inadequate expressions for the magnetic dipole moments of the ferrite. Fortunately, simple expressions[3] for these magnetic dipole moments are available when the ferrite sample is small compared with the wavelength inside it. Experimental verification of this new coupling theory was obtained with a cross-guide coupler and with a collinear coupler for a centered coupling hole.[4] Since the new theory is equally applicable to situations where the coupling is off center,[5] this paper considers the theoretical and experimental aspects more fully. This seems especially worthwhile since other workers[6,7] have recently considered the case of an off-center aperture. However, their work was performed from either a different viewpoint or else less rigorously. The new coupling theory is quite general and can be used irrespective of waveguide configuration or propagating mode.

In this paper, simple expressions for the coupling and directivity of a cross-guide coupler and a collinear coupler will be presented with some experimental results. In all cases, the ferrite parameters were chosen to obtain a good correspondence between the theoretical and experimental curves of coupled power. Unfortunately, the sample size used was too large to expect exact agreement between theory and experiment.

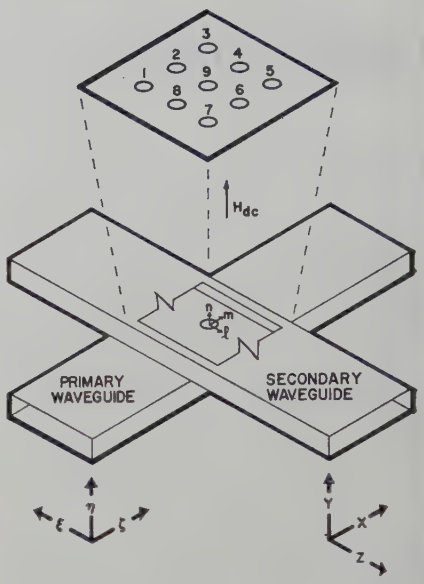

Fig. 1—Cross-guide directional coupler.

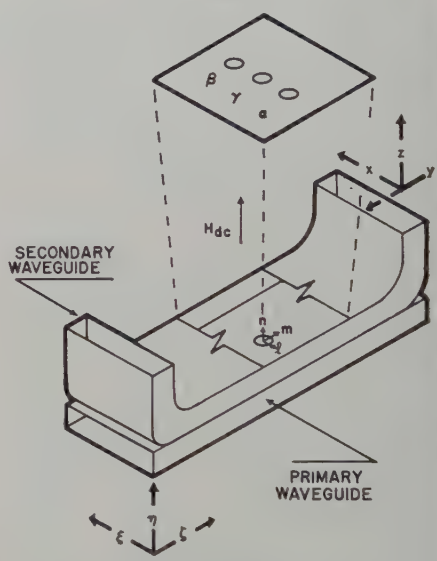

Fig. 2—Collinear directional coupler.

Theoretical Results

The following theoretical expressions for the coupling and the directivity are good approximations when the coupling hole is small compared with wavelength and when the ferrite sample is small compared with the wavelength inside it. No attempt has been made to determine the limits of the validity of the approximate expressions although experiments indicate that the theory governing the behavior of the ferrite is too simplified for many applications.

The amplitudes of the normal modes excited in the secondary waveguide by a unit normal mode in the primary waveguide are given elsewhere for both the cross-guide coupler[8] and the collinear coupler.[9] The expressions we use below for the coupled power are valid only for two identical rectangular waveguides propagating the TE_{10} mode and for a round coupling hole of diameter d. The coupling hole location is given by x and ξ for $0 \leq x \leq a$ and for $0 \leq \xi \leq a$, where a is the width of the waveguide. The orientation of the waveguides and the definition of the three sets of axes are given in Fig. 1.

For the cross-guide coupler, let us consider the expression for the power coupled in both directions in the secondary waveguide when the coupling hole is located at a point of circular polarization; *i.e.*, when

$$\tan \frac{\pi x}{a} = \tan \frac{\pi \xi}{a} = \lambda_g/\lambda_c.$$

For this case, let us choose the frequency so that $\lambda_g = \lambda_c$. Thus, we obtain in db

$$C_{\perp}^{\pm} = C_0 + 20 \log \left| j(1-\chi_{ll})\Upsilon + R\Psi + \chi_{lm}\Omega \right| \quad (1)$$

where

$$\Upsilon = \sin \frac{\pi}{a}(\xi \pm x)$$

$$\Psi = \sin(\pi x)/a \sin(\pi \xi)/a$$

and

$$\Omega = \cos \frac{\pi}{a}(\xi \mp x).$$

The upper and lower signs in the superscript indicate the power coupled in the positive and negative directions, respectively. All of the symbols used are defined elsewhere[10] except R which is defined as $R = QF_EF_H^{-1}$.

For the collinear coupler, the expressions under the same conditions are the following in db:

$$C_{\parallel}^{\pm} = C_0 + 20 \log \left| -(1-\chi_{ll})\Omega + j\chi_{lm}\Upsilon + R\Psi \right| \quad (2)$$

where the orientation of the axes is defined in Fig. 2. Eqs. (1) and (2) are given a further

* Received by the PGMTT, March 24, 1958. Presented at the 1957 Annual PGMTT Meeting, New York, N. Y., May 9, 1957.

[1] D. C. Stinson, "Coupling through an aperture containing ferrites," Ph.D. dissertation, Dept. of Elec. Eng., University of California, Berkeley, Calif.; 1956.

[2] D. C. Stinson, "Coupling through an aperture containing an anisotropic ferrite," IRE Trans. on Microwave Theory and Techniques, vol. MTT-5, pp. 184–191; July, 1957.

[3] *Ibid.*, see Appendix.

[4] *Ibid.*, pp. 188–189.

[5] *Op. cit.*, Ph.D. dissertation, Appendix E.

[6] R. W. Damon, "Magnetically controlled microwave directional coupler," *J. Appl. Phys.*, vol. 26, pp. 1281–1283; October, 1955.

[7] A. D. Berk and E. Strumwasser, "Ferrite directional couplers," Proc. IRE, vol. 44, pp. 1439–1446; October, 1956.

[8] Stinson, *op. cit.*, "Coupling through an aperture containing an anisotropic ferrite," (16).

[9] *Ibid.*, (12).

[10] *Ibid.*, (22) and (28).

TABLE I

Coupling for Various Aperture Locations

Large		Small		Constant	
$C_1^-(+)$	$C_2^{\pm}(+)$	$C_1^-(-)$	$C_2^+(-)$	$C_3^-(\pm)$	$C_1^+(\pm)$
$C_3^+(+)$	$C_4^+(+)$	$C_4^+(-)$	$C_4^-(+)$	$C_\alpha^-(\mp)$	$C_\beta^-(\pm)$
$C_5^-(-)$	$C_6^{\pm}(-)$	$C_3^-(-)$	$C_3^+(+)$		
$C_7^+(-)$	$C_8^+(-)$	$C_\alpha^+(+)$	$C_\beta^+(-)$		
$C_4^-(-)$	$C_3^-(+)$	$C_\gamma^+(+)$	$C_\gamma^-(-)$		
$C_\alpha^+(-)$	$C_\beta^+(+)$				

variation since the susceptibility χ_{lm} is an odd function of the applied magnetostatic field.

The directivity is defined as the ratio in decibels of the power coupled in a particular direction in the secondary arm for an incident wave in the forward and backward directions, respectively, in the primary arm. Thus, we obtain in db

$$D = \left| C^+ - C^- \right| . \qquad (3)$$

The coupling defined here is the negative of the standard definition. This is done so that an increase in coupled power corresponds to an increase in the ordinate of the curve of coupling vs magnetostatic field or frequency.

It is interesting to note, by inspection of (1) or (2), that the power coupled in one direction can be made independent of the magnetic susceptibilities by a proper choice of the hole location. Moreover, the susceptibilities can be made much larger than unity and can be controlled by the applied magnetostatic field. For a spherical ferrite sample, the maximum value of the susceptibility is inversely proportional to the reduced damping constant.[11] For ordinary microwave ferrites, this results in a maximum increase in coupling of about 20 db. The aperture locations in the cross-guide coupler and in the collinear coupler for which the coupling is significantly affected by the magnetostatic field are shown in Figs. 1 and 2, respectively. Information concerning the coupled power for some of the various aperture locations is given in Table I. The notation $C_i^-(+)$ means the coupling in the negative direction, aperture location i, and a positive value of the applied magnetostatic field. Thus, the sense of the magnetostatic field is indicated by the plus or minus sign inside the parentheses.

Experimental Results

Curves of coupling vs the magnitude of the magnetostatic field for the cross-guide coupler, aperture location 1, and a Ferramic R-1 sphere are given in Fig. 3(a). Using (3), the directivity of the coupler for a positive magnetostatic field of 3 kilo-oersteds is 26 db. The coupling is −37 db. Curves of coupling vs the magnitude of the magnetostatic field for the collinear coupler, aperture location α and a Ferramic R-1 sphere are given in Fig. 3(b). The directivity for a negative magnetostatic field of 3 kilo-oersteds is 27 db. The coupling is −37 db. Another aperture location is γ, the centered hole. The coupling curves for this are shown in Fig. 3(c). An interesting characteristic is that the directivity is about 26 db with no applied magnetostatic field which decreases to zero when the magnetostatic field increases to 3 kilo-oersteds. In the cases considered, agreement between theory and experiment is acceptable in a qualitative sense. Unfortunately, the sphere was too large to expect exact quantitative agreement. Coupling curves were also run on a 3-hole coupler using 3 Ferramic R-1 spheres and aperture location α. The center hole was larger than the end holes in order to improve the directivity. The measured coupling curves were similar to those in Fig. 3(b). For a negative applied magnetostatic field of 3 kilo-oersteds, the directivity was 42 db and the coupling was −26 db. For no magnetostatic field, the coupling was −46 db and the directivity was at least 30 db.

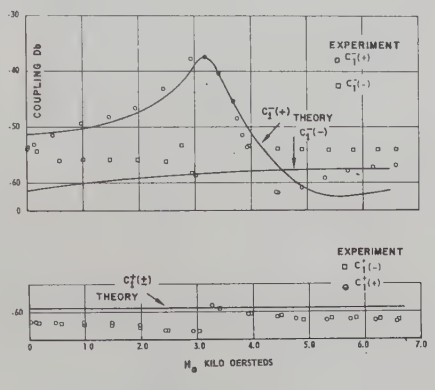

(a)

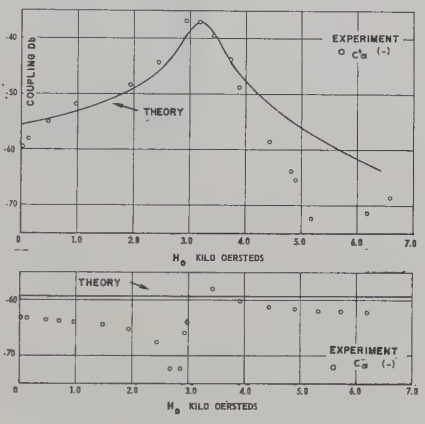

(b)

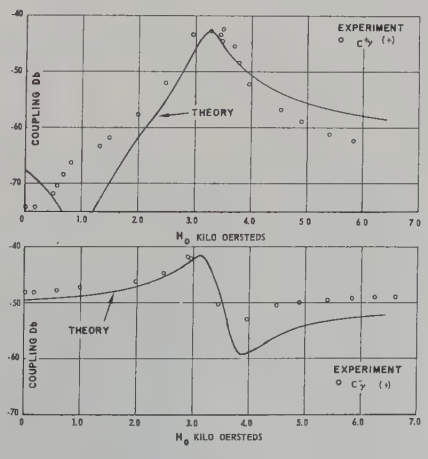

(c)

Fig. 3—Comparison of theory and experiment for coupling with Ferramic R-1 sphere of 0.124-inch diameter. Theoretical values for $\lambda_1 = 0.08$, $R = 1.278$, $E = 0.813$, $C' = 0.816$: (a) cross-guide coupler, aperture location 1; (b) collinear coupler, aperture location α; (c) collinear coupler, aperture location γ.

Conclusions

Ferrite directional couplers display several advantages over normal directional couplers, such as nonreciprocal coupling and the electrical control of coupling. The couplers also permit one to obtain fairly good absolute data and quite good comparative data on the characteristics of ferrite materials. Work in this area will be reported at a later date.

Acknowledgment

The author wishes to thank M. L. Fisher for considerable aid in the measurement program.

Donald C. Stinson
Lockheed Missile Systems Div.
Sunnyvale, Calif.

A Modulator for Microwave Mixers*

A method is described for producing an amplitude modulated wave at an intermediate frequency from the mixing of two cw signals in a coaxial or waveguide system. The method is adaptable to any frequency range in which crystal mixers are used. At least 82 per cent modulation is produced by this method, and the envelope is a square wave. The repetition rate is 0 to 20 kc with presently available commercial components.

One advantage of this system is to provide an ac signal for further amplification. In addition, the frequency and phase of the envelope depends only on the stability of the audio generator and the chopper. This makes the system suitable for use with a phase sensitive detector. Thus, the bandwidth of the detector system can be readily reduced to 1 cps. This system of modulation has been used to replace the swept local oscillator in a microwave attenuation measurement system.

Fig. 1 is a wiring diagram of the modulator. As is well known, the impedance and conversion loss of a crystal depend on the

* Received by the PGMTT, March 19, 1958.

[11] *Ibid.*, see Appendix

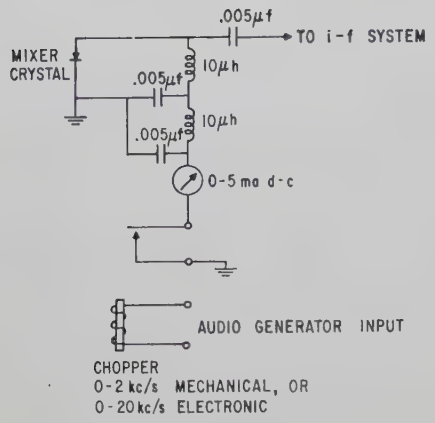

Fig. 1—Circuit diagram of modulator.

amount of rectified current in the crystal. The chopper serves to present alternately a low and a high impedance dc return. This change in crystal current affects the conversion loss to produce a square wave with more than 80 per cent modulation.

The modulator was developed for use in an attenuation measurement system. In this application a primary standard attenuator is in the IF system between the mixer and IF amplifier so that the principal noise source is the input stage of the IF amplifier. The ratio of the fundamental component of signal at 1 kc derived from the chopper modulation to that derived from a swept local oscillator was approximately unity. Thus, in this particular system the signal and noise levels remain unchanged.

In many applications there would be no isolation between the crystal mixer and the IF amplifier. In this type of receiver, the crystal noise is significant. The additional noise introduced by the chopper modulation was measured for 100-cps bandwidth at 1 and 10 kmc. The ratio of noise power with the chopper operating to that produced when the local oscillator was operating cw was 14 db. The ratio of the noise power with the chopper operating to that produced when the local oscillator was swept was 12 db.

The reduction of noise power by use of a phase sensitive detector can be 20 db without materially increasing the time to make an observation. Such a reduction would increase the dynamic range of the attenuation measurement system by 20 db, or increase the sensitivity of a receiver with the IF amplifier connected directly to the crystal by 8 db.

In summary, a method of producing phase-controlled amplitude modulated IF signals from mixing cw signals has been developed for microwave receivers which has been successful in the frequency range 300 mc to 12,000 mc. The principle appears applicable to any frequency range in which crystal mixers are used. For a given signal-to-noise ratio, the dynamic range of a microwave attenuation measurement system can be increased by 20 db through the use of this modulator and a phase sensitive detector without increasing the time constant in the final indicating device.

G. E. Schafer
Natl. Bur. of Standards
Boulder, Colo.

Reciprocal Ferrite Phase Shifters in Rectangular Waveguide*

A recent article by Reggia and Spencer[1] describes a reciprocal ferrite phase shifter for rectangular waveguide. This phase shifter consists of a pencil of ferrite suspended along the central axis of the waveguide by means of a dielectric. The phase is controlled by an applied longitudinal magnetic field. This geometry is shown in Fig. 1. Large amounts of phase shift are produced by this geometry with low insertion loss, and application to antenna beam scanning appears likely, as suggested by Reggia and Spencer.

One of the limitations of the configuration of Fig. 1 is power handling. In this regard it is similar to Faraday rotators in circular waveguide. The ferrite in both instances is suspended by a dielectric in the center of the guide having no contact with the walls. If the ferrite material were to be placed in contact with the waveguide walls, a large amount of heat would be conducted away, thus greatly increasing the power handling ability. In order to investigate this possibility, the configurations shown in Fig. 2 were measured for reciprocal phase shift characteristics. It was found that the geometry used in Fig. 2(a) resulted in a phase advance, while that used in Fig. 2(b) resulted in a phase delay. The results of these measurements taken at 9600 mc are shown in Fig. 3.

A measurement of insertion loss for the three phase shifters showed that the loss of the configuration of Fig. 1 varied from 0.3 db at zero field to about 0.8 db at saturation, while that of Fig. 2(a) stayed constant at a value near 0.1 db for all fields, and that of Fig. 2(b) varied from 0.2 db to 0.6 db at saturation. These loss figures indicate that the figure of merit (degrees of phase shift÷loss) for the design with the ferrites in contact with the narrow walls of the waveguide [Fig. 2(a)] is equal or slightly better than that of the centrally suspended ferrite rod. The amount of phase shift is low for the configuration of Fig. 2(a) when compared to that of Fig. 1. However, additional changes in thickness or height might improve this situation.

The configuration of Fig. 2(a) was subjected to 250 watts of average power resulting in a measured temperature rise at the waveguide wall of only 50°C.

The temperature rise indicated resulted in some additional measurements on the temperature sensitivity of these phase shifters. Measurements were made of phase shift as a function of temperature, and all three designs were found to show large variations. Phase shifts due to temperature variations over the range −20°C to +71°C showed as much change as that due to variation of applied magnetic field. In order to apply these phase shifters to antenna scanning, ovens may have to be utilized to stabilize temperature variations. Another approach that can offer a partial solution relies on controlling the magnetic field in such a way as to compensate for temperature changes.

* Received by the PGMTT, April 2, 1958.
[1] F. Reggia and E. G. Spencer, "A new technique in ferrite phase shifting for beam scanning of microwave antennas," Proc. IRE, vol. 45, pp. 1510–1517; November, 1957.

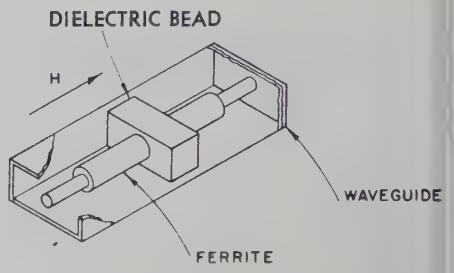

Fig. 1—Phase shifter using a cylindrical rod of ferrite suspended along the axis of a rectangular waveguide.

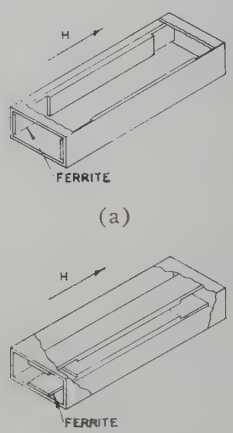

Fig. 2—Reciprocal ferrite phase shifters in rectangular waveguide in which the ferrite is in contact with the waveguide wall.

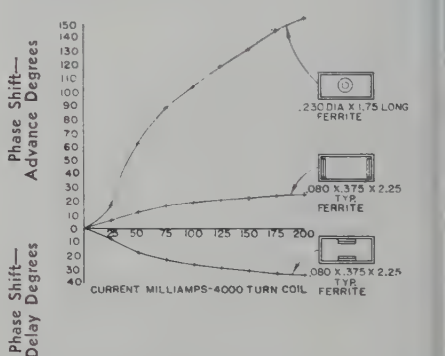

Fig. 3—Reciprocal phase advance and delay of the ferrite phase shifters constructed with R-1 ferrite and utilizing a 2.5-inch long 4000-turn coil of 0.005-inch diameter wire wrapped about the 1 × ½-inch OD rectangular waveguide.

This can be done by employing either an open or closed loop circuit. However, this technique limits the dynamic range of the phase shifter.

In summary, it can be pointed out that the result of attempting to improve the power handling ability of the design of Reggia and Spencer resulted in two new ferrite geometries, one giving a phase advance and the other a phase delay, each with power handling capabilities of at least 250 watts. Additionally, the temperature sensitivity of all three devices may limit their usefulness in antenna beam scanning applications unless they are utilized in a parallel feed system where only relative phase shifts are important, and all the phase shifters have identical geometry.

Alvin Clavin
Rantec Corp.
Calabasas, Calif.

Contributors

Robert E. Beam (S'37–A'41–SM'44–F'56) was born on July 11, 1914, in Cambridge, Ohio. He received the B.E.E. degree from The Ohio State University in 1937 and the Ph.D. degree from Iowa State College in 1940. While at Iowa State he was a part-time teaching and research assistant.

R. E. Beam

During 1940–1941 he was an instructor in electrical engineering at the University of Arkansas. During 1941–1942 he taught at Southern Methodist University. In June, 1942, he joined the faculty of the electrical engineering department of Northwestern University, where he spent much of his time during World War II teaching UHF techniques to Army Signal Corps trainees. After World War II he became technical director of the Microwave Laboratory at Northwestern University, in which capacity he conducted research on such topics as multimode waveguides, dielectric-rod and dielectric-tube waveguides and antennas, coated-conductor waveguides and antennas, and improved shapes of microwave antennas. He has served as an engineering consultant for various companies and is the author or co-author of a number of technical papers and the textbook "Theory and Application of Microwaves." He was one of the group which founded the National Electronics Conference in 1944 and has participated in the activities of this organization since its founding.

Dr. Beam is a member of the AIEE, ASEE, AAUP, Sigma Xi, Tau Beta Pi, Eta Kappa Nu, Phi Kappa Phi, and Pi Mu Epsilon. He has been a full professor of electrical engineering at Northwestern University since 1950.

❖

Saul M. Bergmann, for a photograph and biography, please see page 268 of the October, 1957 issue of these TRANSACTIONS.

❖

Kenneth J. Button was born in Rochester, N. Y. on October 11, 1922. After serving as an electronic technician with the U. S. Army from 1942 to 1946, he received his undergraduate and graduate training in physics and mathematics at the University of Rochester, where, from 1948 through 1950, he worked as an assistant in high energy nuclear physics research at the cyclotron laboratory. From 1950 to 1952, he was a teaching assistant in physics and electronics and received the M.S. degree in physics in 1952. He joined the M.I.T. Lincoln Laboratory in 1952 and became engaged in the study of electromagnetic wave propagation in ferromagnetic and semiconductor materials at microwave and infrared frequencies. He has specialized in resonance phenomena with particular emphasis on the applications to ferrite microwave devices and is currently engaged in the co-authorship of a book on this topic.

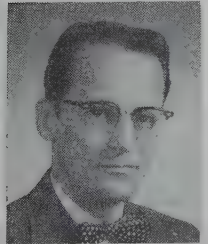

K. J. Button

Mr. Button is a member of the American Physical Society.

❖

Raymond H. DuHamel (A'53–M'57) was born in Tuscola, Ill., on October 11, 1922. He received the B.S. degree from the University of Illinois in 1947, the M.S. degree in 1948, and the Ph.D. degree in 1951, all in electrical engineering. While in graduate school, he held a research assistantship with the Radio Direction Finding Laboratory at the University, where he did research on antennas for rdf systems and on methods of antenna pattern synthesis.

R. H. DuHamel

From 1951 to 1952, he worked on television antennas at RCA Laboratories, Princeton, N. J. From 1952 to 1956, he was a resarch assistant professor in electrical engineeting at the University of Illinois, where he was in charge of the Antenna Laboratory. Since 1956, he has been head of the Antenna Group at Collins Radio Company in Cedar Rapids, Iowa.

Dr. DuHamel is a member of Sigma Xi and Eta Kappa Nu.

❖

James W. Duncan (A'53) was born in Decatur, Ill., on September 15, 1926. He received the B.S. degree from the University of Colorado in 1950 and the M.S. degree from the University of Illinois in 1955.

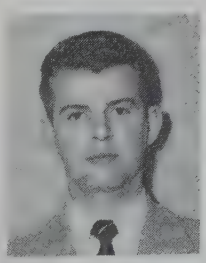

J. W. Duncan

From 1950 to 1953, he worked for Sandia Corporation, Albuquerque, N. M., as a development engineer. Since 1953, he has been a teaching and research assistant at the University of Illinois and is continuing graduate study for a Ph.D. degree in electrical engineering.

Mr. Duncan is a member of Eta Kappa Nu, Tau Beta Pi, Sigma Tau, and Pi Mu Epsilon.

❖

Donald A. Dunn (S'46–A'52–SM'56) was born on December 31, 1925, in Los Angeles, Calif. He received the B.S. degree from California Institute of Technology in 1946, and the M.S. degree in 1947, the degree of Engineer in 1950, the LL.B. degree in 1951, and the Ph.D. degree in 1956, all from Stanford University, Stanford, Calif. He was a research assistant from 1947 to 1950 and has been a research associate from 1951 to the present at Stanford Electronics Laboratories, where he has been doing research on traveling-wave tubes. Since 1953 he has been a group leader and lecturer. From 1951 to 1953 he was associated with the firm of Flehr and Swain as a patent attorney.

D. A. Dunn

Dr. Dunn is a member of the bar of the State of California and has been admitted to practice before the U. S. patent office. He is a member of Sigma Xi.

❖

R. W. Grow was born in Lynndyl, Utah, on October 31, 1925. He received the B.S. and M.S. degrees in electrical engineering from the University of Utah in 1948 and 1949, respectively, and the Ph.D. degree in electrical engineering from Stanford University in 1955. From 1952 to 1953 he was an RCA Fellow in Electronics under the National Research Council.

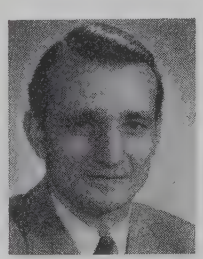

R. W. Grow

From 1949 to 1951, Dr. Grow was employed as an electronic scientist at the U. S. Naval Research Laboratory where he worked successively in the fields of radar countermeasures and nuclear physics, participating in the 1951 Atomic Weapons Tests. Late in 1951 he became associated with the electronics research laboratory at Stanford University where he has been engaged in microwave tube research, specializing in traveling-wave tubes, backward-wave oscillators, and traveling-wave tube mixers. At present he is a research associate at the Stanford Electronics Laboratories.

Dr. Grow is a member of Sigma Xi, Tau Beta Pi, Phi Kappa Phi, and Phi Eta Sigma.

Roger F. Harrington (S'48–A'53) was born in Buffalo, N. Y., on December 24, 1925. He received the B.E.E. degree in 1948 and the M.E.E. degree in 1950, both from Syracuse University, Syracuse, N. Y., and the Ph.D. degree in 1952 from The Ohio State University, Columbus, Ohio.

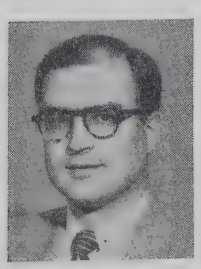

R. F. HARRINGTON

From 1945 to 1946 he served as an instructor at the Naval Radio Materiel School, Dearborne, Mich. From 1948 to 1950, he was employed as an instructor and research assistant at Syracuse University. While studying at The Ohio State University, he served as a Research Fellow in the Antenna Laboratory. Since 1952, he has been on the faculty of Syracuse University, currently as associate professor of electrical engineering.

Dr. Harrington is a member of Tau Beta Pi, Sigma Xi, and the American Association of University Professors.

❖

Hermann A. Haus (S'50–A'55) was born in Ljubljana, Yugoslavia, in 1925. He attended the Technische Hochschule in Graz from 1946 to 1948, and studied for one term at the Technische Hochschule in Vienna, Austria. In 1949 he received the B.S. degree from Union College, Schenectady, N. Y., in 1951 the M.S. degree from Rensselaer Polytechnic Institute, Troy, N. Y.; and in 1954 the Sc.D. degree from Massachusetts Institute of Technology, Cambridge, Mass.

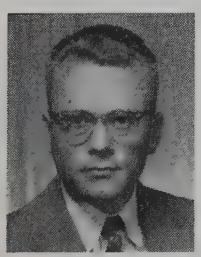

H. A. HAUS

He is now at M.I.T. as an associate professor of electrical engineering, and is also engaged in microwave tube research at the Research Laboratory of Electronics.

Dr. Haus is a member of Sigma Xi.

❖

Gedaliah Held was born in Warsaw, Poland, on January 4, 1926. He attended the Hebrew University in Jerusalem and received the M.S. degree in physics in 1950. Shortly thereafter he came to the United States as a graduate student at the University of California, Berkeley where he received the Ph.D. degree in electrical engineering in 1954.

G. HELD

From 1952 to 1954 he was a member of the technical staff of the University of California Antenna Laboratory and an instructor in the Department of Electrical Engineering.

In 1954 he joined the staff of the University of Washington in Seattle, where he is presently an associate professor in electrical engineering, specializing in microwave radiation and propagation.

❖

Edward S. Hensperger (S'52–A'53–M'56) was born on December 12, 1925, in New Brunswick, N. J. He received the B.S. degree in electrical engineering from Rutgers University in 1952. After graduation, he was employed by Airtron, Inc., Linden, N. J., where he became engaged in the design and development of microwave components. In 1955, Mr. Hensperger joined Stavid Engineering, Inc., Plainfield, N. J., as a senior design engineer.

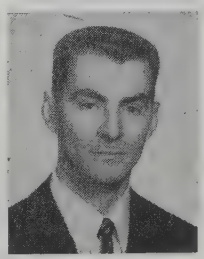

E. S. HENSPERGER

In 1956, he left Stavid and returned to Airtron, where he is presently Section Engineer in charge of the advanced microwave design group.

❖

D. D. King (M'46) was born on August 7, 1919, in Rochester, N. Y. He received the A.B. degree in engineering sciences in 1942 and the Ph.D. degree in physics in 1946, both from Harvard University. He was a teaching fellow in physics and communication engineering in 1943, serving as a staff member of the pre-radar Officer's Training School at Cruft Laboratory, Harvard University. He was a research associate there during 1945. In 1946 he was appointed research fellow in electronics, and in 1947, assistant professor of applied physics in Harvard.

D. D. KING

In 1948, he was appointed associate professor of physics in the Institute for Cooperative Research of Johns Hopkins University, Baltimore, Md., in 1950, assistant director, and in 1955, director of the Radiation Laboratory. He became vice-president, research, of Electronic Communications, Inc. in 1956.

Dr. King is a member of Sigma Xi and the American Physical Society.

P. D. Lomer was born in Cornwall, England, on May 17, 1928. He received the B.Sc. degree in physics from the University College of the South West, Exeter, in 1948 and the M.Sc. degree two years later. In 1950 he joined the Services Electronics Research Laboratory, Baldock, England, where he has been studying gas discharge devices with particular reference to microwave duplexers.

P. D. LOMER

Mr. Lomer is an associate member of the Institute of Physics.

❖

John W. McLaughlin (M'57) was born at Pocatello, Idaho, on December 2, 1925. He received the Bachelor of Science degree in electrical engineering from Utah State University in 1953. From 1953 to 1954 he held a research assistantship at Stanford University, and from 1954 to 1957 he was a research associate in the Stanford Electronics Laboratories doing research on traveling-wave tubes. In 1957 he received the Master of Science degree in electrical engineering from Stanford University. Since 1957 Mr. McLaughlin has been engaged in reflex klystron development at the Eitel-McCullough Microwave Tube Laboratory in Salt Lake City, Utah.

J. W. MCLAUGHLIN

❖

Murray R. Millet (M'56) was born in Newark, N. J., on November 10, 1924. He attended the University of Wisconsin and the Drexel Institute of Technology in Philadelphia, Pa., where he received the B.S. degree in 1955.

In 1950, Mr. Millet joined the Techrep Division of the Philco Corporation. In 1952 he transferred to the Government and Industrial Division of Philco, where he has been engaged in the design and development of microwave components used in radar and beacon systems.

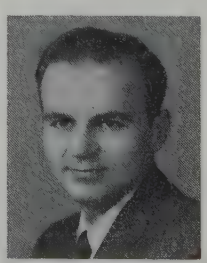

M. R. MILLET

Mr. Millet is currently a graduate student at the Moore School of Electrical Engineering, University of Pennsylvania.

R. M. O'Brien was born in Auckland, New Zealand, on September 23, 1924, and was educated in England. From 1943 to 1947 he served in the Royal Air Force, working on airborne radar equipment. In 1947 he joined the Services Electronics Research Laboratory, Baldock, England, to work on the design of new forms of duplexing systems.

R. M. O'Brien

He specialized in microwave gas discharge attenuators for use in these systems.

Recently he joined the Watton Engineering Co., Welwyn Garden City, England, to form a new department to investigate the application of electronics to metrology in precision mechanical engineering.

❖

S. Perry Schlesinger (M'55) was born in New York, N. Y., on October 9, 1918. He received the B.S. degree from Michigan State in 1941, the M.S.E. degree from Union College in 1950, and a Doctorate from Johns Hopkins University in 1957.

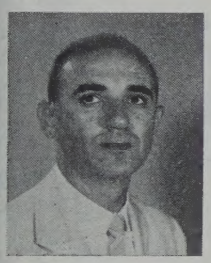

S. P. Schlesinger

In 1946, following war service as a destroyer engineer officer, he joined the General Electric Company, subsequently serving as an assistant professor of electrical engineering on the faculties of Union College and the U. S. Naval Academy. From 1953 through 1956 he was a research associate at the Radiation Laboratory of Johns Hopkins University working on back-scattering studies, millimeter techniques, and problems in dielectric image line transmission. He is now on the faculty of electrical engineering at Columbia University.

Dr. Schlesinger is a member of Sigma Xi, Phi Kappa Phi, and Pi Mu Epsilon.

❖

Herbert J. Shaw (M'55) was born in Seattle, Wash., on June 2, 1918. He received the B.S. degree from the University of Washington, Seattle, in 1941, and the M.A. and Ph.D. degrees in 1942 and 1948, respectively, from Stanford University, Stanford, Calif.

In 1941 he was a test engineer at the General Electric Company in Schenectady, N. Y. Since then he has been at Stanford University, where he is presently a senior research associate in the Microwave Laboratory and a lecturer in the Physics Department. He is engaged in research in microwave tubes and microwave physics.

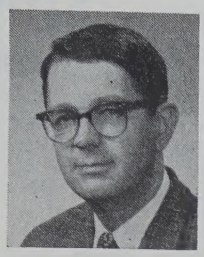

H. J. Shaw

Dr. Shaw is a member of Tau Beta Pi and Sigma Xi.

❖

Edward H. Turner (SM'55) was born December 21, 1920, in Cleveland, Ohio. He received the Bachelor of Science degree in 1942 from Harvard University, Cambridge, Mass.

E. H. Turner

From 1942 to the latter part of 1945 he was a staff member of the Radiation Laboratory at Massachusetts Institute of Technology, Cambridge, where he was with the Airborne Division. He also spent some time at the British Branch of the Laboratory.

After leaving M.I.T. he returned to Harvard to do graduate work in physics and received the A.M. degree in 1947 and the Ph.D. in 1950.

Since 1949, Dr. Turner has been a member of the technical staff in the Radio Research Department of Bell Telephone Laboratories, where his primary interest has been in waveguides and the use of ferrites at microwave frequencies.

He is a member of Sigma Xi and the American Physical Society.

❖

George Tyras (M'57) was born in Czestochowa, Poland, on November 26, 1920. He received the B.S.E.E. degree from Newark College of Engineering, Newark, N. J., in 1954 and the M.S.E.E. degree from the University of Washington, Seattle, in 1957.

From 1952 to 1954 he was affiliated with Charles Engelhard, Inc., where he was engaged in research and development of industrial instruments. In 1954 he joined the Boeing Airplane Company, Seattle, Wash., and became engaged in the analysis of fire control systems and radar detection.

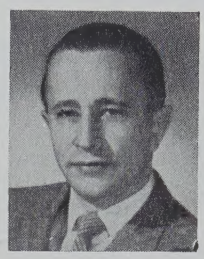

G. Tyras

He is presently involved in research on microwave propagation through anisotropic media and is doing further graduate work in electrical engineering at the University of Washington under the Boeing Graduate Study Program.

❖

A. T. Villeneuve (S'52–A'53) was born on March 14, 1930, in Syracuse, N. Y. He received the B.E.E. degree from Manhattan College, New York, N. Y., in June, 1952. From 1952 until 1955 he served as a research assistant at Syracuse University, where he received the M.E.E. degree in February, 1955. Since 1955 he has been an instructor at Syracuse, where he is continuing graduate work. His experience includes work on antennas and microwave devices as well as theoretical research in electromagnetic problems.

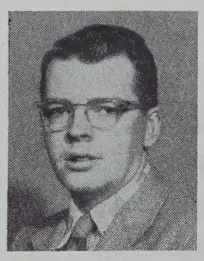

A. T. Villeneuve

He is an associate member of Sigma Xi and a member of Eta Kappa Nu.

❖

Lester M. Winslow was born in Los Angeles, Calif. on September 5, 1927. He served in the U. S. Navy from 1945 to 1948 and from 1951 to 1952. He received the B.E.E.E. degree from the University of Southern California, Los Angeles in 1953, the M.S.E.E. degree in 1955, and the Degree of Engineer in 1956, both from Stanford University, Stanford, Calif.

L. M. Winslow

From April, 1954 to March, 1958 he held an appointment as a research assistant at the Stanford Microwave Laboratory. In March, 1958, he joined the Raytheon Manufacturing Company in Santa Barbara, Calif.

Mr. Winslow is a member of Sigma Xi, Tau Beta Pi, and Eta Kappa Nu.

INSTITUTIONAL LISTINGS

The IRE Professional Group on Microwave Theory and Techniques is grateful for the assistance given by the firms listed below, and invites application for Institutional Listing from other firms interested in the Microwave field.

AIRTON, INC., 1101 W. Elizabeth Ave., Linden, N.J.
Designers and Producers of Complete Line of Microwave, Electronic and Aircraft Components.

COLLINS RADIO CO., Cedar Rapids, Iowa
Complete Industrial Microwave, Communication, Navigation and Flight Control Systems

HUGHES AIRCRAFT COMPANY, Culver City, Calif.
Radar Systems, Guided Missiles, Antennas, Radomes, Tubes, Solid State Physics, Computers

MARYLAND ELECTRONIC MANUFACTURING CORPORATION, College Park, Md.
Development and Production of Microwave Antennas and Waveguide Components

MICRODOT, INC., South Pasadena, Calif.
Microminiature Coaxial Connectors, Cables, and Assemblies

MICROWAVE DEVELOPMENT LABS., INC., 92 Broad St., Babson Park 57, Mass.
Design, Development & Production of Waveguide Components & Complete RF Assemblies

MICROWAVE TUBE LAB., SYLVANIA ELECTRIC PRODUCTS, INC., 500 Evelyn Ave., Mountain View, Calif.
Traveling-Wave Tubes, Backward-Wave Oscillators (Helix and Oscillators), Klystrons

RADAR DESIGN CORP., 3309 James St., Syracuse 6, N.Y.
Specializing in approximately 10-day "crash" delivery of special microwave components

WEINSCHEL ENGINEERING CO., INC., Kensington, Md.
Attenuation Standards, Coaxial Attenuators and Insertion Loss Test Sets

WHEELER LABORATORIES, INC., 122 Cutter Mill Road, Great Neck, N. Y.
Consulting Services, Research & Development, Microwave Antennas & Waveguide Components

The charge for an Institutional Listing is $50.00 per issue or $140.00 for four consecutive issues. Applications for Institutional Listings and checks (made out to the Institute of Radio Engineers) should be sent to Mr. L. G. Cumming, Technical Secretary, Institute of Radio Engineers, 1 East 79th Street, New York 21, N. Y.

FILED IN

1 for 2

with the ***New...***

UNIVERSAL RATIOMETER

model **B811A**

NOW IN ONE COMPACT PACKAGE TWO INSTRUMENTS

FXR's — B811A Universal Ratiometer, combines, at less cost, the many features of a separate ratiometer and standing wave amplifier.

- Compact package—printed wiring construction
- Increased sensitivity for more accurate reflectometer measurements
- Two cycle precision log meter—VSWR reflectometer readings of 1.02 to ∞ on only two scales
- VSWR, DB and Γ scales eliminate conversion tables
- Built-in input transformers—no accessories required
- Expanded VSWR scales and full 70 DB standing wave amplifier operation
- Crystal and bolometer operation

REPRESENTATIVE

WASHINGTON, D.

A & M ASSOC.
1145 19th ST., N.W
WASHINGTON, D. C.

WASHINGTON OREGON

AHMCO
BOEING FIELD
KING CITY AIRPORT
SEATTLE 8, WASH.

COLORADO NEW MEXICO UTAH WYOMING

HYTRONIC
MEASUREMENTS INC
1295 S. BANNOCK S
DENVER 23, COLORA

ILLINOIS INDIANA WISCONSIN

KADELL SALES ASSO
5875 N. LINCOLN ST
CHICAGO 45, ILLINO

FLORIDA GEORGIA ALABAMA

J. NEAL CO.
1941 S.W. 33rd AVE.
MIAMI, FLA.

CANADA

RADIONICS LTD.
8230 MAYRAND STRE
MONTREAL, CANADA

EXPORT

SZUCS INT'L CORP.
50 BROAD STREET
NEW YORK 4, N. Y.

CALIFORNIA ARIZONA

VAN GROOS CO.
21051 COSTANSO ST.
WOODLAND HILLS, CA

Precision Microwave Equipment

F-R MACHINE WORKS, Inc.
WOODSIDE 77. N. Y. AStoria 8-2800

FXR

TEST EQUIPMENT • RADAR COMPONENTS • HIGH-POWER MODULATORS

Write today for yo complete catalog.